Synthesis and Characterization of Amine-Functionalized Linkers for Zr-based Metal-Organic Frameworks

Karolina Magdalena Filipowicz

Thesis for the master's
Degree in Chemistry

60 study points

Department of Chemistry
Faculty of Mathematics and Natural Sciences
UNIVERSITY OF OSLO

July 2020

Preface

The work presented in this master thesis was done in the research group of Mats Tilset, at the Chemistry Department at the University of Oslo. It has been two challenging years which allowed me to explore chemistry and develop myself.

I would like to thank my supervisor Mats Tilset for giving me the opportunity to work on this project, and for always finding time to discuss chemistry.

I would like to thank Frode Rise and Dirk Pedersen for the work they do with the NMR lab, and helpful discussions. Thanks to Osamu for recording all the MS spectra.

Being a member of the Tilset group allowed me to meet so many people. Vladimir, you have been a patient co-supervisor! It has been so much fun to work with you. Knut, I admire your knowledge. I am thankful for all of your valuable help with the thesis and in the lab!

Thanks to Erlend for guiding me through the MOF-part of the project, and his valuable comments on the thesis. Isabelle, thank you for all of your support! Cristano, Inga and Stefan, I value our conversations! I am happy to have met you all!

I would also like to thank Madelen for all the fun that we had! Further, I want to thank my family for their support, and my dear friend, Ragnhild for everything you do for me, everyday.

Last but not least, I want to thank my high school sweetheart (and university sweetheart) Jeroen. for his endless love and support.

Abstract

Over the last years, Metal-Organic Frameworks have gained a lot of interest in the research world due to their extending list of applications including among others gas adsorption, gas storage, gas purification, gas separation and heterogeneous catalysis. In 2008, members of the Catalysis group at University of Oslo discovered a unique series of Zr-based MOFs, which are among the thermally and chemically most robust MOFs known today. The physical and chemical properties of MOFs are strongly dependent on the nature of the organic linker. Introduction of organic functional groups or transition-metal centers at the linkers make the corresponding MOFs interesting with respect to catalysis, adsorption, and other applications. Examples of such linkers are well known aniline derivatives where the amino group is aromatic. In this project, new amine-substituted linkers for Zr-based UiO-67 MOFs were synthesized. Such modified linkers are attractive for different purposes including CO_2 adsorption in MOFs and amine-coordination to metal centers in MOF-anchored catalysts.

Abbreviations

AIBN	Azobisisobutyronitril
b.s	broad singlet
d	doublet
"d"	a doublet by *o*-coupling with fine structure caused by additional *m*-, *p*-couplings and higher order splitting pattern
dba	dibenzylidenaceton
dd	doublet of doublets
DEPT	Distortionless Enhancement by Polarization Transfer
δ	chemical shift
DMF	*N*,*N*-dimethylformamide
DMSO	dimetylsulfoksid
dppf	1,1'-bis(diphenylphosphine)ferrocene
EA	Elemental analysis
EI	Electron ionization
ESI-MS	Electron spray ionization
Equiv.	equivalent(s))
Et	ethyl
HMBC	Heteronuclear Multiple Bond Correlation
HMQC	Heteronuclear Multiple Quantum Correlation
HRMS	High resolution mass spectrometry
HSQC	Heteronuclear Single Quantum Correlation
i	*iso*
IUPAC	International Union of Pure and Applied Chemistry
J	coupling constant
m	multiplet
m/z	mass-to-charge ratio
Me	methyl
m	*meta*
min	minutes
MOF	metal-organic framework
M_p	melting point
MS	mass spectrometry
NBS	*N*-bromosuccinimide
NMR	Nuclear magnetic resonance
o	*ortho*
p	*para*
ppm	parts per million
Ph	phenyl
Pin	pinacolato
PXRD	Powder X-Ray Diffraction

q	quartet
R. t.	room temperature
s	siglet
t	*tert*
THF	tetrahydrofurane
TGA	thermogravimetric analysis
TLC	Thin-layer chromatography
UiO	University of Oslo
v	frequency (IR)

Overview of compounds

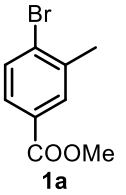

1a

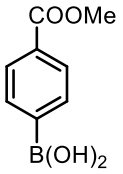

1b

comercially available

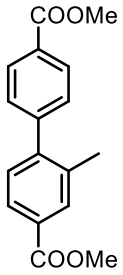

1c

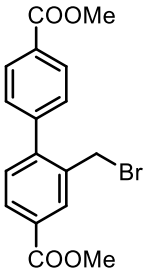

2

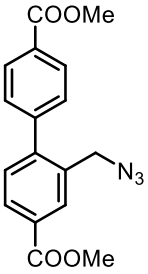

3a

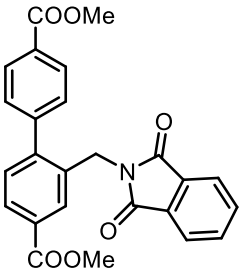

3b

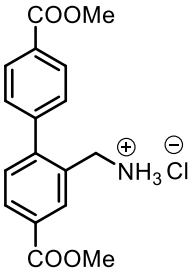

4a

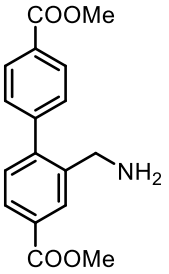

4b

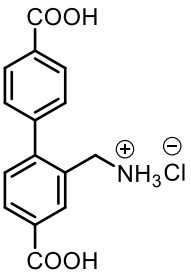

5

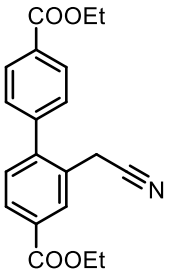

6

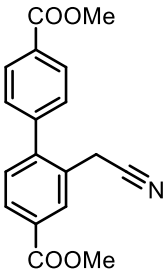

7

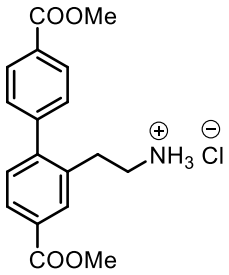

8a

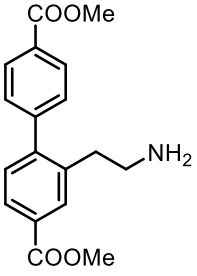

8b

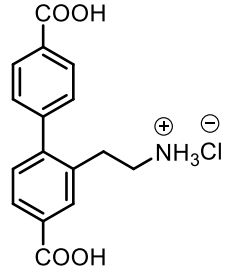

9

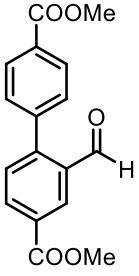

10

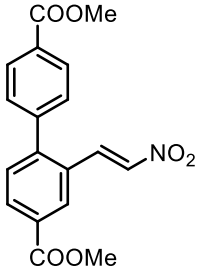

11

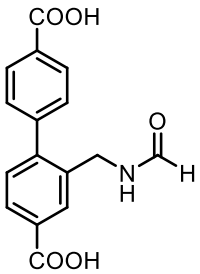

12

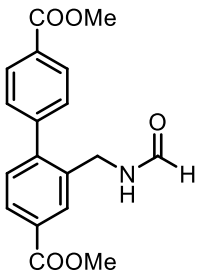

13

The aim of the project

Over the last decade, the Catalysis group at the University of Oslo has developed and studied a series of metal-organic frameworks (MOFs). The series consists of UiO-66, UiO-67 and UiO-68 MOFs, which received a lot of attention due to their thermal, chemical and physical stability.[1] The physical and chemical properties of MOFs are strongly dependent on the nature of the organic linker. Hence, a lot of research is directed towards the development of new functionalized linkers for UiO-series.

The aim of this MSc project is the synthesis of new and functionalized linkers for UiO-67 type MOFs. The two target linkers for this project are amine-functionalized, where one of the linkers has the amine in benzylic position, and the other carries an ethylamine substituent **Figure 1**. The amino groups have an increased basicity compared to the more common aniline-substituted linkers, as the lone pair of the nitrogens is not captured in resonance with the aromatic ring.[2] The increased basicity of these amines might be beneficial for CO_2 adsorption. Amine-based linkers are also attractive for other purposes, such as amine-coordination to metal centres in MOF-anchored catalysts.

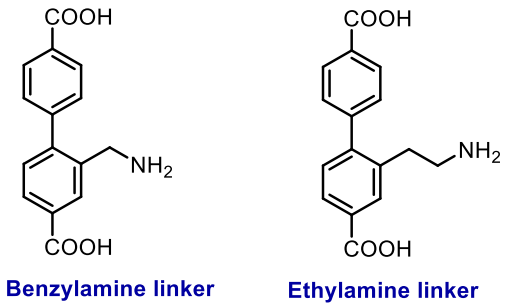

Figure 1: Target compounds of this project

The primary goal is to synthesize and characterize these new, functionalized UiO-67 linkers. The secondary goal of the project is to implement them into a UiO-67 metal-organic framework.

Contents

CHAPTER 1

Introduction

1.1 Metal-Organic Frameworks

Metal-organic frameworks (MOFs) consist of metal ions or cationic metal clusters and organic ligands, often referred to as *linkers*. IUPAC defines MOFs as coordination polymers whose structure extends in 2 or 3 dimensions via repeating coordination entities.[3] These coordination polymers have an open framework, which contains potential voids. "Voids" or "pores" are volumes of empty space in the material. MOFs are therefore classified as porous materials. It is also common that MOFs exhibit a high degree of crystallinity, although it is not one of the criteria.

The inorganic building blocks in MOFs are surrounded by organic ligands. These metal ions or clusters serve as cornerstones. Historically important metals which are utilized as cornerstones in many MOFs are Zn,[4] Fe,[5] Cu,[6] and Zr[1, 7]. The cornerstones are bridged by organic linkers, which are often dicarboxylic acids.[8, 9] It is most common that these linkers are prepared and utilized as carboxylic acids in the MOF synthesis. However, in MOFs they are almost exclusively deprotonated, present as carboxylates. The carboxylate groups are anionic and form strong metal-carboxylate bonds with the cationic metal centers. It is also common that the linkers have other coordinating functional groups in addition, such as imidazolates[10, 11] and amines[12]. A simplified schematic representation of a MOF structure is given in **Scheme 1**.

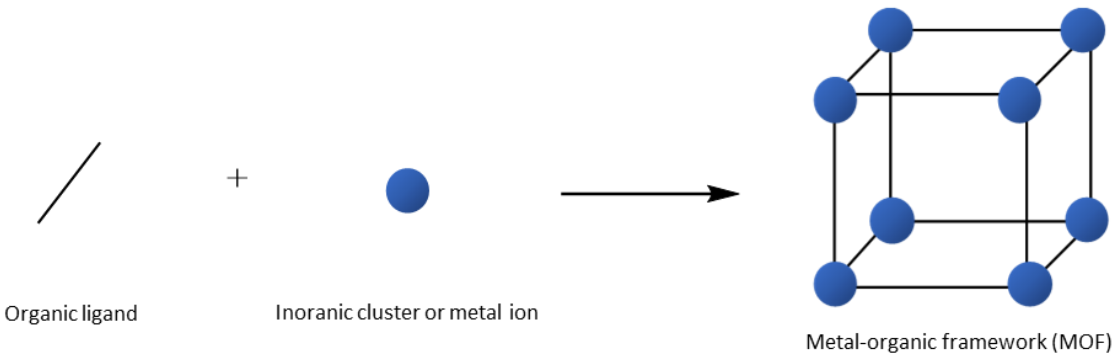

Scheme 1: Schematic representation of the construction of a metal-organic framework.

The term "metal-organic framework" was first introduced by Yaghi *et al.*, in 1995, where the structure of a 4,4'-bipyridine-based metal-organic framework was reported.[13] Although the term itself is relatively new, the concept behind metal-organic frameworks is not. There are reported structures dating back to 1959, which can fit the definition of a MOF.[14] However, a groundbreaking discovery in the MOF research first occurred in 1999, when MOF-5[4] and HKUST-1[15] were reported. Both materials were found to be significantly more robust than any of the previously reported MOFs. Their stability allowed for the complete removal of guest molecules (e.g. solvent molecules) from the pores of the material. Before this discovery, a thorough investigation of the material porosity could not be conducted, as the MOFs nearly invariably collapsed upon the removal of solvent molecules.[16]

The discovery of the unprecedented porosity of MOF-5 (surface area of ca. 3000 m^2g^{-1}) escalated the MOF research.[17, 18] It was soon realized that the MOFs could be "structurally designed" prior to the synthesis. This laid ground for *reticular synthesis*, a concept allowing to design porous structures with targeted geometry.[9] A series of materials with the same network topology is called an *isoreticular series*. Isoreticular MOFs can vary in functionalization or size, depending on the linker, but their topology remains unchanged.[13] Important examples of isoreticular MOFs are IRMOF (IsoReticular Metal-Organic Framework) series[4, 19] which includes MOF-5[4], and UiO (University of Oslo) series[1, 7]. The IRMOF series is presented in **Figure 2**.

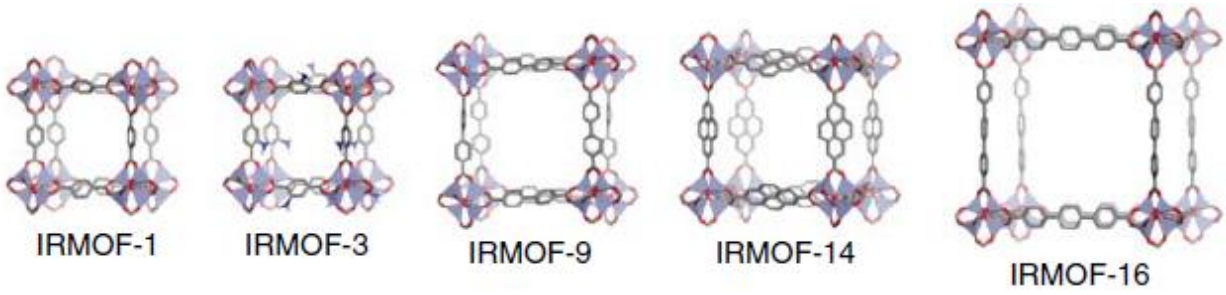

Figure 2: A selection of IRMOFs reported by Yaghi and coworkers.[19] Zinc, carbon, oxygen, and nitrogen atoms are shown in blue/gray, gray, red, and blue, respectively. The coordination sphere of zinc is represented by a tetrahedron. In IRMOF-3, the hydrogen atoms of the amino groups are shown in white. Hydrogens have been omitted from all other structures for the sake of clarity. Figure reproduced from reference [12].

The IRMOFs are zinc-based metal-organic frameworks, which are widely used to explain the concept of isoreticular series. The series illustrates how the functionalization, broadness and length of incorporated linkers affects the final properties of the material:[17]

- The linkers in IRMOF-1 and IRMOF-3 are of the same length, but IRMOF-3 is in addition functionalized with an uncoordinated amino group. This provides functionality to the material.
- The linkers in IRMOF-9 and IRMOF-16 are extended with respect to the linker in IRMOF-1. This increases the pore size of the MOF.
- The linker in IRMOF-14 is broader that the one in IRMOF-9. This affects the shape of the pores in the framework, thereby allowing fine-tuning of adsorption properties.

The IRMOFs illustrate how reticular synthesis allows systematic control of important MOF properties. Functionality and porosity can be easily tuned by varying the organic ligand.[17]

1.2 The UiO-MOF series

The first zirconium-based MOFs were discovered in 2008 by the Catalysis group at the University of Oslo.[1] This isoreticular MOF series featured UiO-66, UiO-67 and UiO-68 (**Figure 3**) and made a breakthrough in the research of Zr-MOFs.

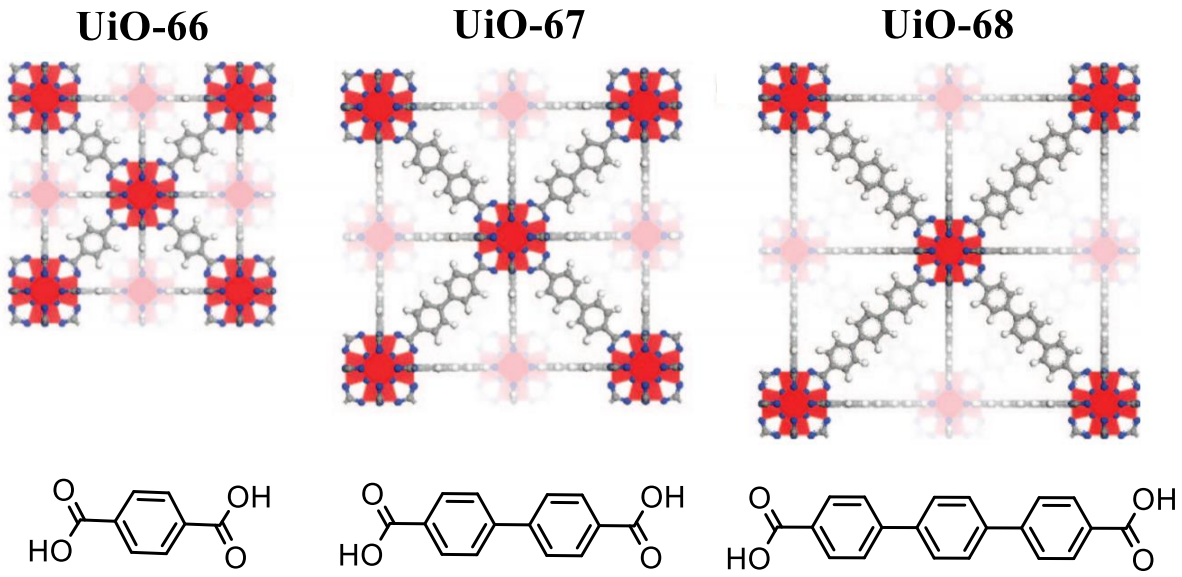

Figure 3: Top row: UiO-66, UiO-67 and UiO-68, respectively. Zirconium (red), oxygen (blue), carbon (gray), hydrogen (white). Bottom row: structures of the corresponding incorporated linkers, terephthalic acid (H_2BDC), biphenyl-4,4'-dicarboxylic acid (H_2BPDC) and pterphenyl-4,4''-dicarboxylic acid (H_2TPDC), respectively. Figure reproduced from reference [1].

The UiO-MOFs gained a lot of attention rapidly, thanks to their remarkable stability.[1] No other MOFs known at the time exhibited the same degree of thermal, mechanical, and chemical

stability. The stability of these Zr-based MOFs originates from the high connectivity number of the cluster, and the strong Zr-O bonds within the MOF.[1, 7] These bonds are not easily hydrolyzed, comparing to Zn-O bonds found in the IRMOF series.

The linkers bridging the inorganic building blocks in UiO-66, UiO-67 and UiO-68 are terephthalic acid, 4,4'-biphenyldicarboxylic acid and 4,4''-p-terphenyldicarboxylic acid, respectively (**Figure 3**). The theoretical surface area and the properties of pores depend on the dimensions of the linker, as it is illustrated with the IRMOF series.[19] The theoretical surface are of UiO-66 is 1187 m^2g^{-1}, followed by higher theoretical surface areas of UiO-67 (3000 m^2g^{-1}) and UiO-68 (4170 m^2g^{-1}). The increased surface areas are a direct result of the increased linker length.[1]

The UiO-MOFs consist of $Zr_6O_4(OH)_4$ clusters where 12 carboxylate groups of the linkers coordinate to each cluster. The cluster consists of six Zr^{4+} atoms, arranged in an octahedron.[1] The eight faces of the octahedron are capped by oxide and hydroxide. Additional 12 carboxylate groups (from the linker) complete the cluster to form $Zr_6O_4(OH)_4(CO_2)_{12}$, which gives a MOF composition $Zr_6O_4(OH)_4(CO_2)_{12}$.

1.3 Synthesis of UiO-MOFs

The synthesis of Zr-based UiO-MOFs has been thoroughly investigated over the last decade. Robust procedures have been designed to afford the Zr-based MOFs.[1, 20, 21] The ease at which these MOFs can be synthesized is another reason for their popularity. The idealized reaction equation for the synthesis of Zr-based MOFs with 12-coordinated Zr_6-clusters and linear ditopic linker is:

$$6ZrCl_4 + 8H_2O + 6H_2L \rightarrow Zr_6O_4(OH)_4L_6 + 24HCl \qquad (1)$$

The synthesis requires following reagents/conditions:

- Crystallization temperature (often 80-135°C)
- Appropriate solvent (e.g. DMF)
- Zirconium (IV) source (e.g. $ZrCl_4$)
- Modulators (optional, e.g. benzoic acid)

The crystallization of the product can be achieved at different temperatures. The synthesis requires also zirconium (IV) source, where $ZrCl_4$ is the most utilized source. It is however

hygroscopic and corrosive, making it unsuitable for industrial scale synthesis. [ref] Alternative zirconium (IV) sources are therefore desirable, and have been investigated.

The synthesis requires a solvent, which dissolves the organic linker and the zirconium source. The solubility issues associated with carboxylic acid linkers limit the choice for solvents. The most utilized solvent for the synthesis of UiO-MOF is DMF.[1]

Modulators are commonly utilized in the synthesis of UiO-MOFs, as they affect the properties of the product and/or the kinetics of its formation. In 2011, Behrens and co-workers documented the influence of monocarboxylic acid modulators in the synthesis of UiO MOFs.[22] They found that the size and morphology of Zr-based MOFs could be regulated by utilizing benzoic or acetic acid in the synthesis. Without modulation, the MOFs precipitated as microsized aggregates of nanocrystals or the synthesis led to products with a low surface area.

1.4 MOFs with amine-based linkers

Metal-organic frameworks bridge the fields of organic and inorganic chemistry, creating opportunities for various applications due to their physical and structural properties. MOFs have potential in the extending list of applications including catalysis,[7, 23, 24] gas adsorption,[21, 25, 26] gas storage,[21, 25, 27] gas purification and separation,[21, 26] and drug delivery[28, 29].

The increasing release of CO_2 into the atmosphere is a growing concern, which sparked the interest for utilizing MOFs for gas-based applications. [25, 30, 31] It is crucial to develop materials that selectively capture and adsorb CO_2. Extensive research has therefore been conducted to develop porous materials suitable for these applications. The high surface areas and tunable pores of MOFs, together with their good thermal stability, make them attractive for such applications.[24, 30, 32]

Reticular synthesis affords possibilities to target the desired structural and chemical features of MOFs by pre- and post-synthetic modification of their building units. The nature of the organic ligand influences the adsorptive properties of these materials. Incorporating linkers with functional groups which have strong interactions with CO_2 can therefore increase the adsorptive properties of the material.[33, 34] One of the most common functionalizations for this purpose involves amine-based linkers. The basicity of the amino group increases the materials affinity for CO_2.[35, 36] The capture of CO_2 is afforded through a nucleophilic attack on the carbonyl by

the lone pair on the nitrogen atom. A general reaction between an amine and CO_2 is shown in **Scheme 2**.

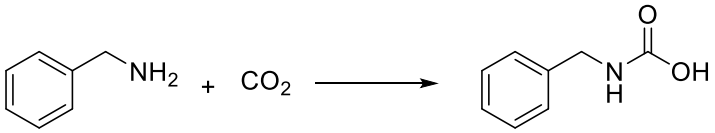

Scheme 2: Reaction between an amine and CO_2 resulting in a formation of a carbamic acid derivative.

The amine-functionalization was reported to increase the CO_2 adsorption of many MOFs.[25] To date, the most successful MOFs for CO_2 capture have alkylamine- functionalized linkers (R_1NHR_2 or RNH_2) incorporated into the MOF-structure.[33] These alkylamines have been shown to selectively react with CO_2, forming covalent C-N bonds. Several amine-based MOFs have been reported to increase the CO_2 adsorption compared to their analogs. UiO-66 analogs,[20] IRMOF-74-III,[33] and $[Zn_4(bpydb)_3(datz)_2(H_2O)]$[37] (bpydbH2 = 4,4'-(4,4'-bipyridine-2,6-diyl) dibenzoic acid; Hdatz = 3,5-diamino-1,2,4-triazole) are some of the examples.

The potential of UiO-66 for CO_2 adsorption has sparked interest for CO_2 adsorption study of different UiO-MOFs. The increased surface area by the linker length might give an indication that UiO-67 can store even larger amounts of CO_2 comparing to other analogs. This makes it interesting to explore the UiO-67 MOFs with a variety of incorporated functional groups (e.g amines and amides). Benzylic amines and other alkyl amines, such as the ones in **Scheme 2**, are of a particular interest for CO_2 adsorption due to their increased basicity. The increased basicity of the amino groups is due to the lone pair of the nitrogens not being captured in resonance with the aromatic ring. This amino groups are therefore more basic than these of the reported aniline-substituted linkers. Resonating structures of aniline illustrate the capture of the lone pair of nitrogen (**Scheme 3**).

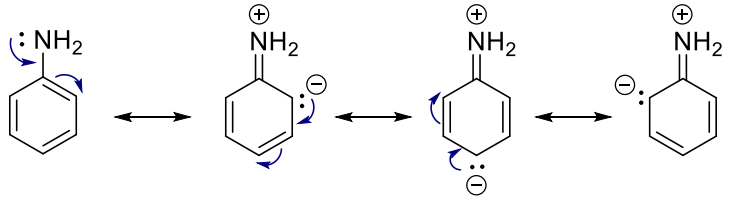

Scheme 3: Resonating structures of aniline illustrating how the lone pair on the nitrogen is captured in a resonance. This makes the lone pair less available for nucleophilic attacks, decreasing the basicity of the amine. Scheme adapted from reference [76].

There is however limited amount of studies conducted for UiO-67 MOFs with amine-based linkers for the CO_2 adsorption. This makes exploration and incorporation of new alkylamine liners into UiO-67 very attractive. Inspired by the studies conducted on amine-functionalized MOFs IRMOF-74-III and UiO-66, the goal of the thesis was therefore the synthesis of alkylamine linkers for UiO-67 MOF.

1.5 Cross-coupling reactions

Cross-coupling reactions are very important in organic chemistry.[38, 39] Cross-coupling is a wide term for coupling reactions such as Stille-, Sonogashira-, Negishi- and Suzuki.[40, 41] The Suzuki cross coupling (also called Suzuki-Miyaura reaction) has been one of the most exploited couplings in the last decade, as it is a powerful method which results in a direct formation of C-C bonds.[38-40, 42, 43] The reaction is a convenient approach for construction of aryl-aryl bonds to afford biaryl systems, which are coupled via sp^2–sp^2 linkages (**Scheme 4**). This coupling has been widely utilized in industrial processes[44], medicinal chemistry[45], materials science[46], and natural product synthesis[39], among other fields.

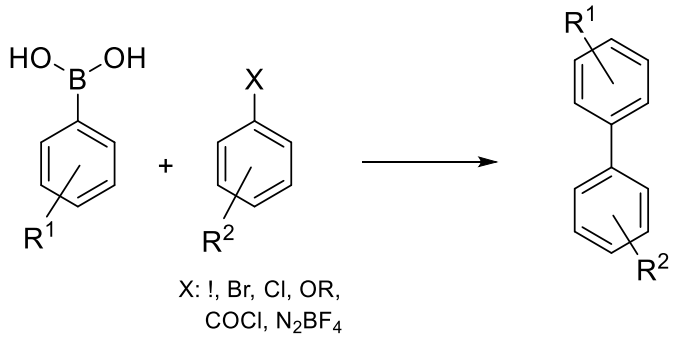

Scheme 4: A general schematic representation of Suzuki-Myaura reaction where two aryl systems are coupled together resulting in sp^2–sp^2 linkages.

The Suzuki-Miyaura cross-coupling has found several applications due to its high versatility. The advantage of this reaction is the commercial availability, low toxicity, and high stability of many attractive starting materials.[39, 43] The reaction also exhibits high compatibility with a variety of functional groups.[43]

The mechanism of the Suzuki-Miyaura cross coupling (**Figure 4**) has four distinct steps: 1) oxidative addition of an organic halide to the Pd(0)-species resulting in Pd(II); 2) *metathesis*, an exchange of the anion attached to the Pd(II)-species for the anion of the base; 3)

transmetallation between the Pd(II)-species and the borate complex; and 4) reductive elimination where C-C sigma bond is formed and Pd(0) is regenerated.

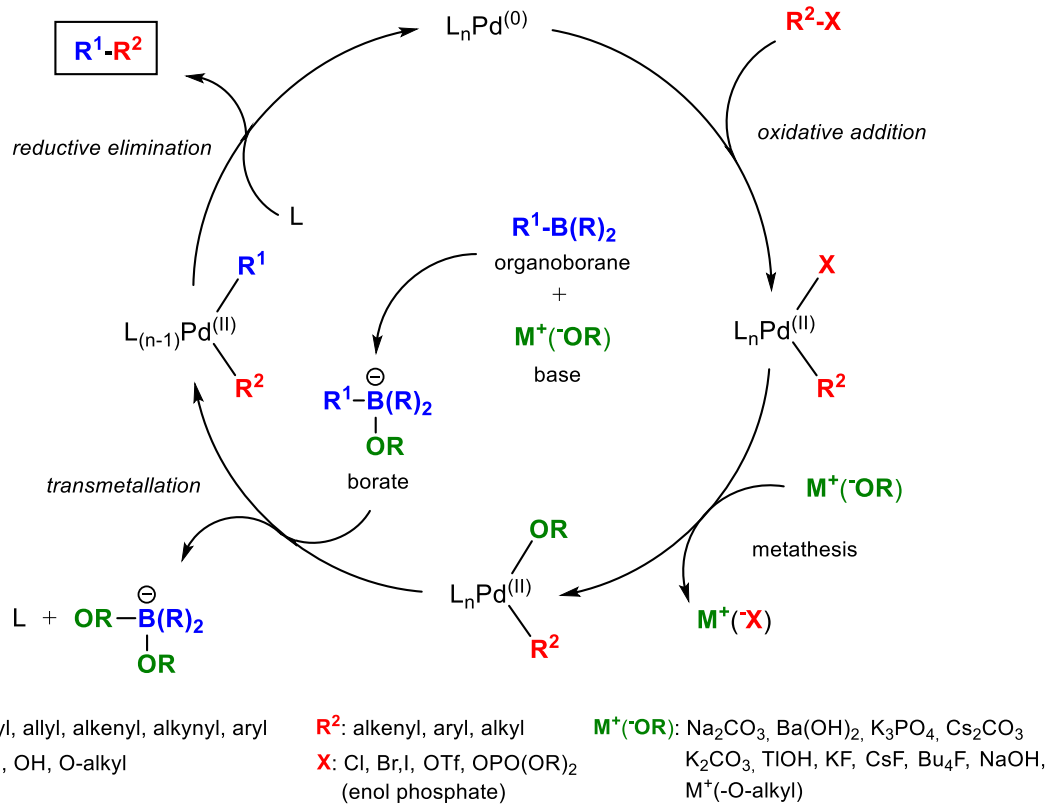

Figure 4: Schematic representation of the catalytic cycle of Suzuki-Miyaura coupling, which results in formation of C-C bonds. Figure adapted form reference [23].

This direct approach to obtain biaryl systems has been central for synthesis of many linkers for MOFs.[42] This coupling reaction can easily afford biphenyl systems, which are especially of interest for UiO-67 type of MOFs. A variety of functional groups can be incorporated in the product by coupling of functionalized aryls. The functionalization is however not always a result of a coupling reaction and might be required in following steps. The Suzuki-Miyaura cross-coupling was utilized in this project, and the results of the coupling will be discussed in Chapter 2.

1.6 Requirements for linkers

For the linkers to be suitable as building blocks for metal-organic frameworks and bring functionality to the material, there are requirements they have to fulfill. The stability of the linkers is perhaps the most important factor. The linker should be stable under the conditions for MOF synthesis, as well as further applications of MOFs. The syntheses of the UiO-type MOFs are carried out at high temperatures, often 120°C - 140°C, where generation of HCl results in a highly acidic reaction medium. For this reason, not all functionalized linkers are suitable for MOFs. For instance, linkers functionalized with esters and amides can show low resistance towards such conditions.

The stability of linkers based on the functional groups is important. Linkers might not only decompose under MOF syntheses and applications, but also undergo unexpected side reactions preventing the MOFs from working as they should. It is therefore important to have that in mind when potential linkers are designed. However, stability of the organic molecule does not limit itself to the functional groups. It is also important to consider the skeleton of the linker. Linkers are mostly aromatic, with a reason. Aromaticity is a strong driving force towards stable molecules. Compared to aliphatic systems, the aromatic systems exhibit a higher degree of rigidity, reducing the number of conformations the linkers might intake. This prevents the linkers from creating disordered structure. In addition, aromatic linkers are often easier to synthesize than the aliphatic linkers.[47]

Another requirement is that the linkers should be capable of coordinating to two or more metal clusters (cornerstones) at the same time when incorporated in MOFs. The coordination is most commonly achieved through nitrogens and oxygens. Examples of nitrogen and oxygen containing functional groups are N-heterocycles and carboxylic acids.[9]

In order for the linkers to be attractive for MOFs, they should be inexpensive. This condition is not directly related to the performance of the linkers in MOFs, but high costs have consequences for further applications.

CHAPTER 2

Introduction to the synthesis of new amine-based linkers

Promising results for CO_2 adsorption have been reported in the literature for MOFs containing amine-based linkers.[33, 34, 36, 48-50] This has sparked an interest for further development of new amine-based linkers where the methyl and ethylamine derivatives are of the highest importance. In this Chapter the general synthesis of these amine-based linkers is introduced. The syntheses of the important intermediates **1c** and **2** are discussed in detail.

2.1 Introduction to the synthesis of linker 5 and 9

The standard linker typically used for UiO-67 MOFs is biphenyl-4,4'-dicarboxylic acid. However, the development of new MOFs requires linkers with different features, and they are obtained through functionalization of the biphenyl skeleton. Biphenyl derivatives are commercially available, but the selection is limited. Thus, to obtain the desired functionalization, a multiple-step synthesis is often required, conveniently starting from coupling reactions.

In this thesis, benzyl bromide derivative **2** was chosen as the starting material for the synthesis of linkers **5** and **9**. The leaving group (Br) in the benzylic position provides a variety of options for the introduction of the amino group. Utilization of the same starting material **2** in syntheses of both linkers is also a favorable economic aspect that was considered (

Scheme 5).

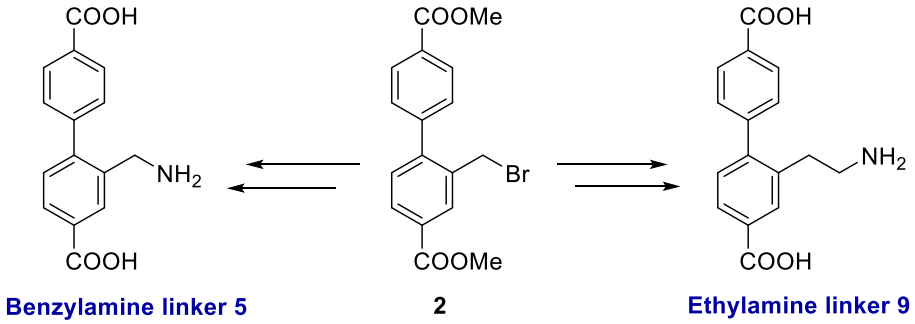

Scheme 5: The synthesis of the amine-based linkers from **2**.

2.2 Synthesis of the coupling reaction product 1

Compound **2** is not commercially available but could be synthesized through a two-step reaction sequence.[51-54] The first step is a synthesis of **1c**, where **1a** and **1b** are coupled via a palladium-catalyzed Suzuki-Miyuara cross-coupling reaction (**Scheme 6**).

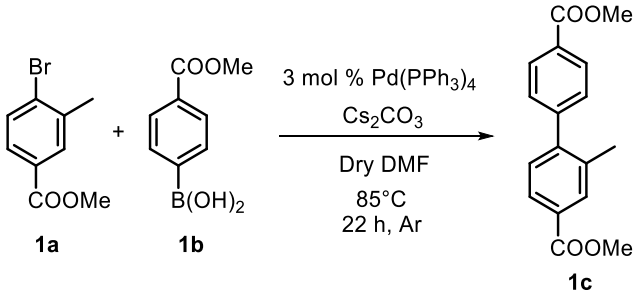

Scheme 6: Reaction conditions for the coupling reaction leading to **1.**

Upscaling of coupling reactions involves high amounts of the catalyst, which can lead to significant expenses. Thus, it was desired to reduce the cost of the synthesis without compromising the yields. It was therefore of interest to investigate a selection of Pd-based catalysts available in the laboratory. The mol. % of the catalyst was kept constant at 3 %, with an exception of P(tBu)2C(CH3)2CH2Pd(μ-Cl)]2 which was also tested at 6 mol %. The investigated catalysts are shown in Figure 5.

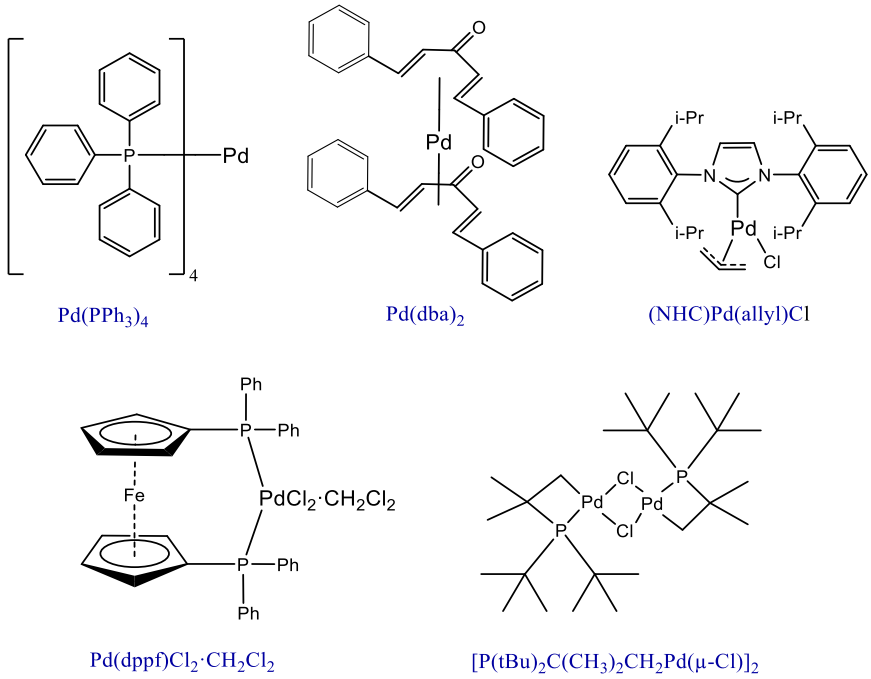

Figure 5: The various catalysts screened for the coupling reaction

All listed catalysts are commercially available expect for $[P(tBu)_2C(CH_3)_2CH_2Pd(\mu\text{-}Cl)]_2$, which was previously synthesized by Dr. Stefan Vanicek.[55] The rest of the catalysts are easily accessible from many suppliers, and an estimation of costs is given in **Table 1**.

Table 1: Prices for the Pd-catalysts or –precatalysts used in the cross-coupling reaction. Sigma-Aldrich 8/10-19

Catalyst	Price/gram (NOK)	Molecular weight (g/mol)	% Pd	Price/mmol (NOK)
$Pd(PPh_3)_4$	220	1155.56	9.2	254
$Pd(dba)_2$	290	575.00	18.5	167
$Pd(dppf)Cl_2{\cdot}CH_2Cl_2$	340	816.64	13	278
(NHC)Pd(allyl)Cl	2130	572.54	18.6	1217
$P(tBu)_2C(CH_3)_2CH_2Pd(\mu\text{-}Cl)]_2$	Commercially unavailable	686.37	31	-

When comparing the catalysts with respect to cost per gram, $Pd(PPh_3)_4$ is the most economical choice. However, for a better estimate, the prices were also calculated per mmol of the catalyst, indicating that $Pd(dba)_2$ is in fact the cheaper alternative. The calculated prices of $Pd(PPh_3)_4$

and $Pd(dppf)Cl_2 \cdot CH_2Cl_2$ per mmol are also reasonable. However, (NHC)Pd(allyl)Cl is by far the most expensive catalyst and is therefore not the best choice regarding cost.

All catalysts were screened by using 9.0 mmol of **1a,** and selected catalysts were also investigated at bigger scales (18 and 36 mmol). The calculated yields at 9.0 mmol of **1a** are based on one entry, and the results of the screening are given in **Table 2**.

Table 2: The results of screening the catalysts on various scale of starting material **a**.

Catalyst	1a (mmol)	Catalyst load (mol. %)	Yield (%)
$Pd(PPh_3)_4$	9.0	3	74
$Pd(dba)_2$	9.0	3	73
	36.0	3	71
	36.0	3	81
$Pd(dppf)Cl_2 \cdot CH_2Cl_2$	9.0	3	80
	18.0	3	75
	36.0	3	81
	36.0	3	85
(NHC)Pd(allyl)Cl	9.0	3	76
$P(tBu)_2C(CH_3)_2CH_2Pd(\mu\text{-}Cl)]_2$	9.0	3	47
	9.0	6	40

It can be concluded that there is no significant difference in yields obtained when using different commercially available catalysts at 9.0 mmol of the starting material. The yield is in a range of 73-80 %, which means that the performance of the catalysts under the same set of conditions is approximately equal. It was therefore reasonable to proceed with the cheapest catalyst, $Pd(dba)_2$, for the upscaling of the coupling reaction. Additionally, the catalyst that performed best on small scale, $Pd(dppf)Cl_2 \cdot CH_2Cl_2$, was also investigated further for the sake of comparison. The conclusion from the upscaling of the reaction is that there was no significant difference between the yields obtained when using $Pd(dba)_2$ (71% and 81%) and $Pd(dppf)Cl_2 \cdot CH_2Cl_2$ (81% and 85%). The yields were comparable and seemed to depend primary on the skills of the operator during the work up. Hence, the catalyst that was used for further reactions was the cheaper one, $Pd(dba)_2$.

Utilizing the catalyst $[P(tBu)_2C(CH_3)_2CH_2Pd(\mu\text{-}Cl)]_2$ in the coupling reaction resulted in significantly lower yield, compared to the other catalysts. The crude product contained

significant amounts of **1a**, indicating that the reaction did not run to completion. It is therefore evident that $[P(tBu)_2C(CH_3)_2CH_2Pd(\mu\text{-}Cl)]_2$ is not a suitable catalyst for the coupling reaction under the tested conditions.

2.3 Synthesis of the benzyl bromide 2

The benzyl bromide **2** is an important intermediate in the synthesis of the target molecules. The developed procedure was based in the previously reported protocols.[51, 52, 54] The intermediate **2** was afforded through bromination of **1c** with NBS (**Scheme 7**).

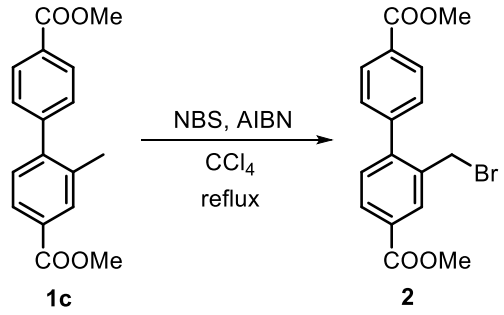

Scheme 7: Reaction conditions for the synthesis of **2**.

In the published procedure, CCl_4 was used as the solvent. However, given the environmental and safety concerns associated with CCl_4,[56, 57] an alternative solvent, MeCN, was investigated. A selection of performed bromination reactions at different scales is given in **Table 3**.

Table 3: A selection of bromination reactions at different scales with the corresponding yields and reaction conditions.

Entry	1c (mmol)	Solvent	Concentration[d] (mol/L)	Reaction time (h)	Yield (%)
1	5.29	CCl_4	0.18	4	66[e]
2	5.31	CCl_4	0.18	4	90
3	5.28	MeCN	0.18	4	85
4	14.1	MeCN	0.35	4	78
5	14.1	MeCN	0.35	5	56

[d] Concentration of **1** in the solvent;

[e] Reaction carried out without argon flow.

For the sake of comparison, the first bromination was run in CCl_4 (**Table 3**, **Entry 1**). The reaction mixture was refluxed for four hours resulting in a yield of 66%, which is slightly lower than the reported yield (73 %).[51] The crude product was purified by recrystallization from *i*PrOH, yielding **2** as colorless powder, which was pure by the ^{1}H NMR.

It was investigated whether the reaction could result in a higher yield under inert atmosphere. The reaction was repeated under argon flow (**Table 3**, **Entry 2**) and resulted in higher yield, indicating that the bromination might be sensitive towards oxygen.[58] From this point, the bromination reactions were carried out under argon flow.

Repeating the reaction in MeCN (**Table 3**, **Entry 3**), resulted in a somewhat lower yield than for reaction in CCl_4. However, **2** was successfully obtained when switching to the less toxic solvent with satisfactory yields. It can therefore be concluded that there are no apparent drawbacks related to the change of the solvent. The reaction was also successfully scaled up in MeCN with good yields.

When the reaction mixture was refluxed for four hours, the incomplete conversion of **1c** was observed. It was attempted to push the reaction to completion by refluxing for five hours, which resulted in minimal amount of **1c** present in the crude product. However, this led to the formation of a side product in greater extent than what was observed after four hours. The disappearance of **1c** has therefore compromised the purity of the crude product.

Both **1c** and side product were removed by recrystallization of the crude mixture. The yields are generally lower for the reactions carried out for five hours, with a yield range 55-57%. This might indicate that the side product was forming from the product. The presence of a molecular ion with m/z = 462.915 in ESI-MS, which corresponds to the sodium adduct of the over-brominated compound, indicates that the side product might be the dibrominated product. Another indication of dibromination is a singlet integrating for one at 6.56 ppm in the ^{1}H NMR spectrum of the crude product (**Figure 6**).

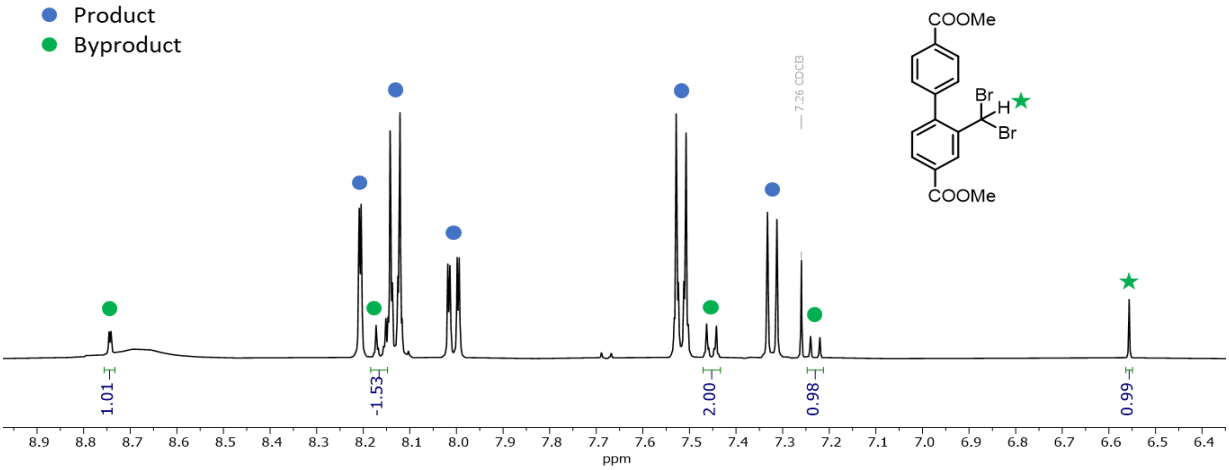

Figure 6: ^{1}H NMR (400MHz, $CDCl_3$) of the crude product from the five-hour reaction.

As an alternative to the purification by recrystallization from *i*PrOH, the crude product was purified by cooling down the reaction mixture to room temperature or in a freezer. This gave a product of high purity by ^{1}H NMR, with corresponding yields of 87% (four hours) and 55% (five hours). This is within the yield range obtained for the reactions at the same scale and reaction times in **Table 3**. The advantage of this alternative work-up is the lesser amounts of solvent used for the recrystallization, and less time-consuming purification.

In conclusion, the optimized reaction conditions resulted in higher yields than the one previously reported.[51] It was found that the reaction works well when carried out in an alternative, less environmentally hazardous solvent such as MeCN. Additionally, the product could be purified in an even easier manner than recrystallization from *i*PrOH, simply by normal precipitation on cooling of the reaction mixture.

CHAPTER 3

Synthesis and characterization of benzylamine-based linker

In this chapter, two syntheses of the benzylamine linker **5** are discussed. The first synthesis involves the reduction of an azide intermediate **3a** to the corresponding amine **4a**. The azide **3a** was successfully reduced in two ways, and multiple attempts of the reduction are briefly discussed. However, the explosive and toxic nature of sodium azide, which is required in significant amounts, makes it attractive to explore other synthesis routes. The second synthesis route utilizes the Gabriel reaction,[43] furnishing **5** through an intermediate **3b**. The synthesis of **5** and the important intermediates from both synthesis routes are covered in this chapter. Characterization of all the intermediates in this project has been done in a similar manner, and linker **9** will be used as an example for characterization in Chapter 4. The synthesis strategies to obtain **5** are given in **Scheme 8.**

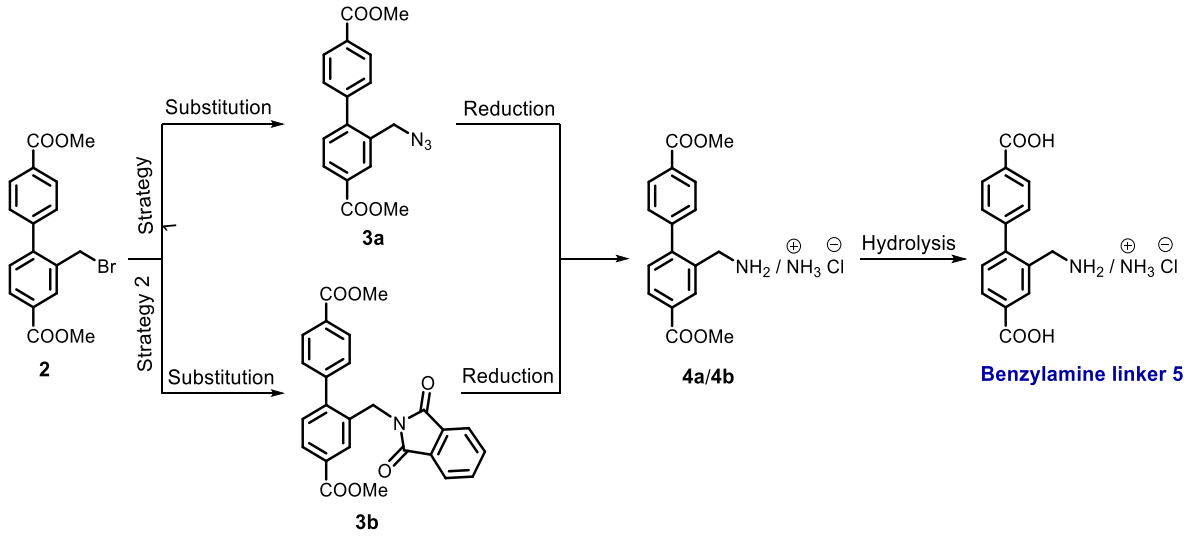

Scheme 8: Synthetic strategies to obtain the benzylamine linker **5**. The two main strategies involve reduction of the azide intermediate **3a** and Gabriel synthesis with **3b** as an intermediate. In addition, **5** can potentially be obtained by a substitution reaction between **2** and NH_3.

3.1 Synthesis of the benzylamines 4a/4b through the reduction of benzylazide 3a

Azides are widely used in the synthesis of the primary amines.[41] They can be obtained through a nucleophilic substitution reaction between organic halides and sodium azide. The azides can further be reduced to the corresponding amines with $LiAlH_4$, catalytic hydrogenation or Staudinger reaction, among others.[41] Because the desired amine also contains ester groups, $LiAlH_4$ is not a suitable reducing agent, as it is known to reduce ester groups.[2] The Staudinger reaction was therefore explored in this project. A general schematic representation of the reaction sequence from halides to amines is given in **Scheme 9**.

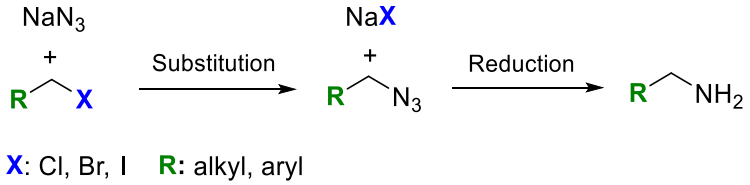

Scheme 9: A general reaction sequence to obtain amines from halides. The azide intermediate is obtained by a nucleophilic substitution reaction between a halide and NaN_3, followed by a reduction to yield the corresponding amine.

3.1.1 Synthesis of the benzylic azide 3a

The dominating solvents in the literature used for these reactions are DMSO, DMF and acetone/water mixtures. [59-62] Water may be used as a solvent or a co-solvent to increase the solubility of sodium azide.[63-67] Because the use of DMSO and DMF as solvents often leads to more tedious work-ups, these two solvents were not investigated. Attempts to find alternative solvent systems were made. The result of investigation of different solvent systems is given in **Table 4**.

Table 4: The investigated solvent systems and corresponding conditions for the synthesis of **3a**. The given time corresponds to time when full conversion of **2** was observed.

Entry	Solvent system	Temperature	Time (h)	Result
1	Acetone	Reflux	6	Mixture of products
2	Acetone/water (4:1)	Room temp.	24	Mixture of products
3	Ethanol	Reflux	2	Mixture of products
4	Ethanol	Reflux	0.5	Single product

The initial attempt to synthesize **3a** was carried out in acetone (**Table 4**, **Entry 1**). Refluxing the solution of **2** with sodium azide resulted in full consumption of **2** within 6 hours. Before full

conversion was achieved, significant amounts of a side product were formed together with **3a**. Because of poor selectivity at elevated temperature, the next reaction was performed at room temperature to seek a more selective reaction.

For the next attempt of synthesizing **3a**, an acetone/water solvent system was utilized (**Table 4**, **Entry 2**). The reaction was followed by TLC, and after 24 hours, **2** was no longer present. The reaction resulted in a mixture of products as observed with the previous reaction conditions. Later obtained spectra of **3a** confirmed that the desired product was the major product. However, due to the formation of large quantities of the side product, this solvent system was not investigated further.

For the next approach, ethanol was chosen as a solvent (**Table 4**, **Entry 3**). Sodium azide and **2** were refluxed in ethanol, and full conversion of **2** was observed within two hours. Changing the solvent system, from acetone to ethanol, resulted in a mixture of products. With increased reaction time more of the side products were formed. Thus, it was desired to investigate if shortening the reaction time might prevent formation of the side product, while keeping a full conversion of **2**. The reaction was therefore repeated under the same conditions, changing only the reaction time (**Table 4**, **Entry 4**). The ^{1}H NMR spectrum of the sample after 30 minutes showed the desired product of high NMR purity, with no organic side product formed. The product precipitated from the solution upon cooling and was isolated by filtration.

The identity of **3a** was confirmed by the ESI-MS, IR and NMR..[68] The IR spectrum of **3a** (**Figure 180** in Appendix) exhibited stretches which are characteristic for organic azides (1285 cm^{-1} and 2100 cm^{-1}). The reaction gives good yields in the range of 84-95% regardless of scale. The optimized reaction conditions are given in **Scheme 10**.

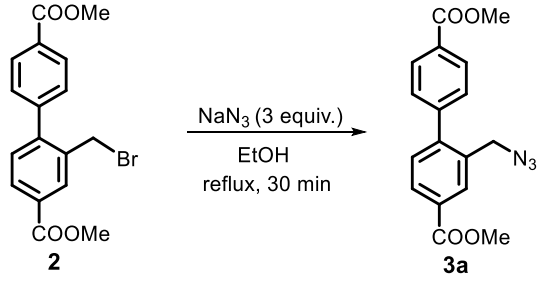

Scheme 10: The optimized reaction conditions for the synthesis of **3a**

The reaction conditions in **Scheme 10** successfully led to the desired product. It was also found that the amount of sodium azide could be decreased to 1.5 equivalents, which proved to work

well in the onepot synthesis of **4a** discussed in **Chapter X**.

3.1.2 Synthesis of 4a/4b through reduction of 3a by Staudinger reaction

One of the most popular reductions of azides to amines is the Staudinger reaction.[41] This reaction converts organic azides to primary amines by utilizing phosphines or phosphites and water. When the azide reacts with PPh_3, a phosphinimine intermediate is formed, and nitrogen gas is released. The free amine is subsequently obtained by addition of water, resulting in the formation of a byproduct, PPh_3O. The formation of PPh_3O is a drawback of this reaction because of the difficulties of its removal during the work-up. This proved to be the case in this project. The reaction mechanism is given in **Scheme 11**.

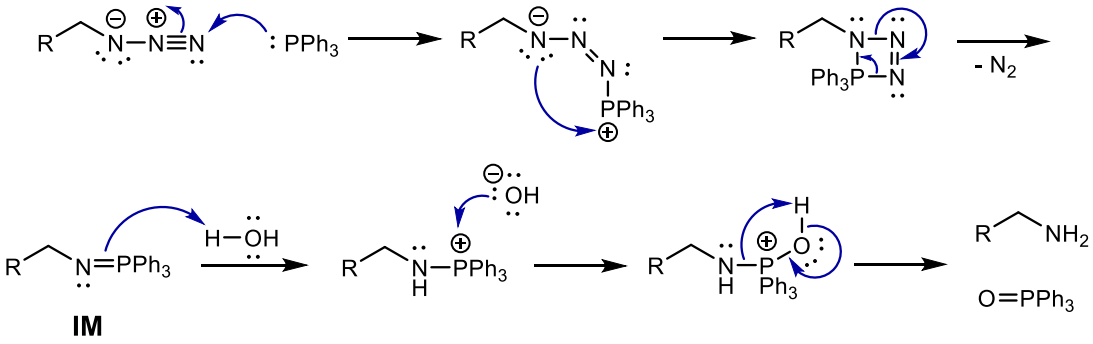

Scheme 11: The reaction mechanism of Staudinger reaction resulting in formation of primary amine and triphenylphosphine oxide. The phosphinimine intermediate is marked with "IM".

Popular solvent systems for the Staudinger reaction are THF/water[69, 70] and methanol[71]. The two solvent systems were investigated, and the formation of the desired product was observed in both reactions. The acquired ^1H NMR spectra of the reaction mixtures/crude products and authentic samples of the phosphines are given in **Figure 7**

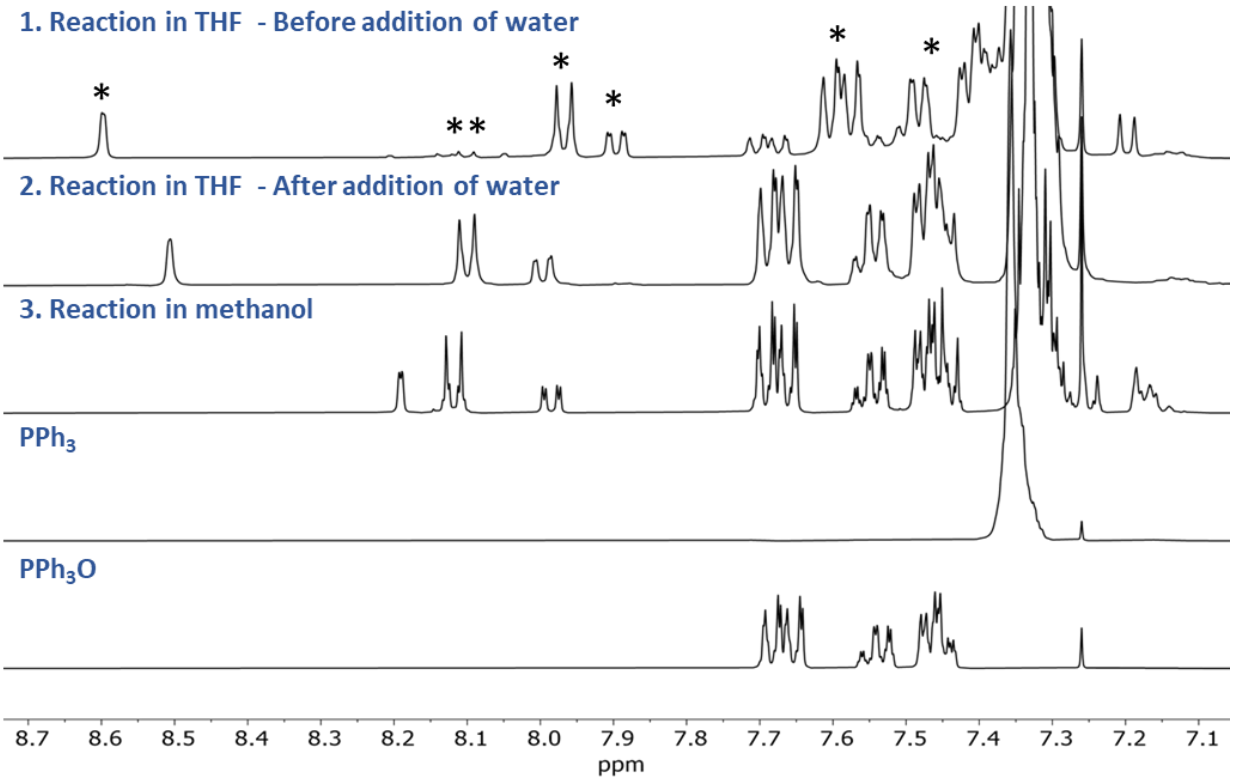

Figure 7: ^{1}H NMR (400MHz, $CDCl_3$) spectra of the crude mixtures from the Staudinger reactions in THF/water and methanol, and phosphines.

The first solvent system investigated was THF/water. Prior to the addition of water, PPh_3 and **3a** was refluxed in THF for 90 minutes, resulting in full conversion of **3a.** A new species was observed (* in 1, **Figure 7**) and was suspected to be the phosphinimine intermediate ("IM", **Scheme 11**). Because the new set of signals (1, **Figure 7**) did not match the signals of PPh_3O, it might have indicated that the desired intermediate had formed.

Water was subsequently added, and the reflux continued for another 90 minutes. The species suspected to be the intermediate disappeared, while a new species was formed together with PPh_3O (1, **Figure 7**). The presence of PPh_3O is confirmed upon comparison with an authentic sample of PPh_3O. This observation is consistent with the formation of the amine as depicted in **Scheme 11**.

The observed extra set of signals prior to the addition of water (** in 1, **Figure 7**) matched with the product signals (2, **Figure 7**). This indicated that the intermediate hydrolyzed to some extent before water was added. The reaction proceeded almost exclusively towards a single biphenyl product as the splitting pattern of the biphenyl system signals in ^{1}H NMR was maintained. This indicated that the reaction occurred in the benzylic position. Excess of PPh_3 is also observed in the ^{1}H NMR spectrum of the crude product.

The reaction in methanol was rapid, and full conversion of **3a** was observed already after one hour (3, **Figure 7**). The advantage of utilizing methanol is that the addition of water is not required, leading to a shorter reaction time. Because of this convenience, the Staudinger reactions were further carried out in methanol. The optimized reaction conditions are given in **Scheme 12**.

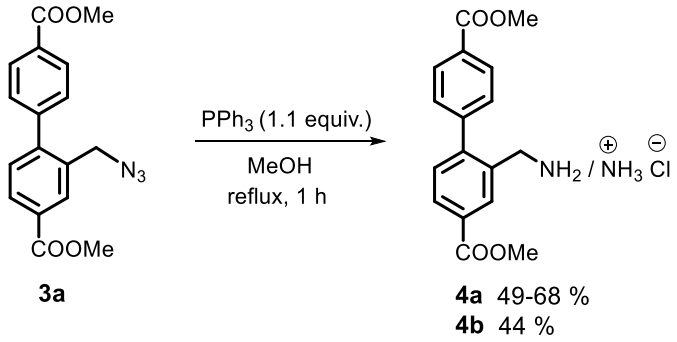

3a

4a 49-68 %
4b 44 %

Scheme 12: Reaction conditions for the Staudinger reaction.

The separation of the phosphines from the product proved to be challenging and different methods for the separation were investigated (**Table 5**).

Table 5: Different alternatives for work-up for attempted separation of the species.

Entry	Purification method	Separation of the species	Limitations of the work-up
1	addition of 35% HCl (excess) to the crude mixture	No	Limited precipitation
2	addition of 4.0 M HCl in dioxane to the crude	No	No precipitation
3	addition of 35% HCl (1.5 equiv.) to the crude mixture	Depending on the scale	Possible capture of impurities in the precipitation
4	acid-base extraction	Depending on the organic solvent	Varying consistency of the precipitation
5	addition of 1 M HCl to the toluene phase	Yes	Reproducibility issues of the precipitation

The first purification attempt involved the addition of conc. HCl (35 %, 0.4 mL) to the crude product dissolved in toluene (**Table 5**, **Entry 1**). This approach was inspired by a published procedure[71], where the hydrochloride salts of amines were obtained in a similar manner.

The free amine is soluble in toluene, whereas the phosphine and phosphine oxide are less soluble. Filtration of the toluene solution was necessary to remove the undissolved impurities before the addition of acid. It was expected that upon addition of HCl **4a** would precipitate leaving the phosphines in solution. Instead, the solution became cloudy with no evident precipitation. From this, one of two conclusions could be drawn. Either, **4a** was partially soluble in toluene resulting in weak precipitation, or the added portion of HCl contained too much water in which **4a** was soluble.

It was further investigated if the precipitation of **4a** was limited by the water content in HCl. If the solubility of **4a** in water caused the precipitation problem, it could be avoided by adding a water-free solution containing hydrochloric acid. The reaction was therefore repeated, and a portion of 4.0 M HCl in dioxane was added to the crude product (**Table 5**, **Entry 2**). Once again, no precipitation was observed and **4a** remained dissolved in the dioxane solution together with the phosphines.

Concentrated HCl was also investigated. The precipitation issue was approached by adding a much smaller volume of HCl (1.5 equiv.) to the toluene solution of the crude mixture (**Table 5**, **Entry 3**). The volume of the added water was thereby decreased, with HCl still in excess. This proved to be the solution to the problem, as the ammonium salt **4a** precipitated. The precipitate was extensively washed with toluene, effectively removing the phosphines embedded in the precipitation on small scales. The obtained product was of high NMR purity, with a yield of 52%.

Although the reaction was successful at smaller scales, the phosphines were still observed in the ^{1}H NMR spectrum of the product at bigger scales. The biggest concern of this work-up is that rapid precipitations can lead to co-precipitation of impurities. This was a motivation to explore other alternative work-ups such as acid-base extraction (**Table 5**, **Entry 4**).

In an acid-base extraction, organic compounds are separated from each other based on their acid-base properties. The product has an amine group which will be protonated upon addition of acid, resulting in an ammonium salt that will be soluble in the aqueous phase. This strategy assumes that the phosphines are not protonated to any significant degree, enabling the compounds to be separated. The crude product was dissolved in toluene and filtrated, resulting in a clear filtrate which was extracted with HCl (1 M). The acidic aqueous fractions were subsequently collected, and the pH was adjusted to 11-12 with sodium hydroxide (1 M) resulting in precipitation of **4a**. The product was pure by ^{1}H NMR with a yield of 44%.

The disadvantage of this work-up is the inconsistency in precipitation of the product. The reaction was repeated many times, and the precipitation varied from well-defined particles to cloudy solution where the free amine, **4b**, was not possible to isolate by filtration. The problems with obtaining the precipitation of **4b** might be caused by the diluted aqueous phase.

The reaction was scaled up (1.54 mmol and 3.07 mmol) and significantly smaller volumes of toluene and HCl (1 M) were used for the extraction to avoid precipitation problems. Upon extraction, the ammonium salt **4a** precipitated from the saturated aqueous phase (**Table 5**, **Entry 5**). The precipitation was obtained by filtration followed by extensive washing with toluene to ensure removal of the phosphines. The identity of the product was confirmed by ^{1}H NMR, and the product was of high NMR purity. The reaction was optimized, resulting in a yield range of 49-68%. There is however a drawback related to this method, as the precipitation was not always observed.

The method in **Entry 5** (**Table 5**) gave the purest product **4a**. The two-phase system of toluene and HCl prevented the impurities from precipitating together with **3a** into the aqueous phase. This was problematic for the work-up in **Entry 3** (**Table 5**), where addition of a small volume of HCl (35 %) to the toluene mixture could result in the capture of impurities.

3.1.3 One-pot synthesis of 4a from 2, through reduction of 3a

The reaction resulting in **3a** was rapid, but the drying of the product was time-consuming due to the large amount of water utilized in the work-up. Another disadvantage of the reaction is that the synthesis should preferably be performed at smaller scales due to safety issues. To facilitate the synthesis of **4a**, a one-pot reaction was investigated. The reaction conditions are given in **Scheme 13.**

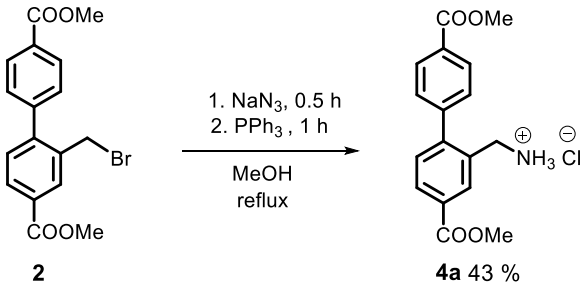

Scheme 13: Onepot synthesis of **4a** through reduction of **3a.**

In this reaction, **3a** was not isolated. Instead, **2** was refluxed with sodium azide for 30 minutes. PPh_3 was subsequently added, reducing **3a** to the corresponding amine within another hour. Prior to addition of HCl (35%), the reaction mixture was diluted with ethyl acetate and washed with water. This removed the excess of sodium azide. The precipitated product was filtrated and washed with CH_2Cl_2 which effectively removed trace amounts of captured impurities. The reaction resulted in a yield of 43%, which is comparable to the yields where **4a** was obtained through a direct reduction of **3a**. The advantage of this reaction is that the isolation of **3a** can be avoided, shortening the reaction sequence.

3.1.4 Synthesis of 4a/4b through reduction of 3a with Zn/NH_4Cl

Although the synthesis of **4a** in a Staudinger reaction proved to be successful, it was of interest to explore alternative ways of reducing the azide **3a**. The synthesis was inspired by a published procedure,[72] where a variety of azides were reduced to amines or amides under mild conditions. The method utilizes Zn as the reducing agent, and NH_4Cl as proton donor.

The reaction mixture was stirred in EtOH/H_2O (3:1) (r.t, 22h) to increase the solubility of NH_4Cl. However, no reaction occurred, which might be connected to solubility issues of **3a** in the solvent medium at this temperature. The reaction was repeated at reflux and was monitored by ^{1}H NMR, revealing that **3a** disappears within 9 hours. For practical reasons, the reaction was run overnight which did not affect the purity of the crude product. The reaction conditions are given in **Scheme 14**.

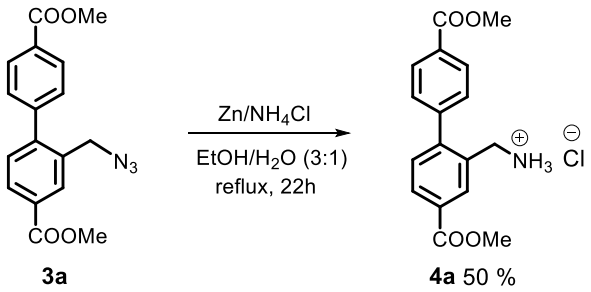

3a **4a** 50 %

Scheme 14: The reaction conditions for the reduction of **3a** with Zn/NH_4Cl.

The crude product was dissolved in ethyl acetate, and aqueous ammonia (28 %) was added to liberate the free amine. This was done to prevent the product loss upon addition of brine solution during the work-up, as the ammonium salt is water-soluble. The previously acquired ^{1}H NMR spectra of **4b** confirmed the formation of the desired product.

Further purification of **4b** was attempted by recrystallization but no appropriate recrystallization medium was identified. The product **4b** was instead obtained by dissolving the crude product in toluene, followed by addition of small amounts of HCl (35 %). Precipitation of the ammonium salt gave a product of increased purity, but not with the same quality as **4b** obtained from the Staudinger reaction. The reaction resulted in a yield of 47 %.

The hydrolysis of **3a** led successfully to the desired benzylamine linker **5**. The hydrolysis reaction will be discussed in **Chapter 3.3.**

3.1.5 Phosgenation of the free amine 4b

Determining the identity of the product obtained from the acid-base extraction discussed in X was initially problematic. The first ^{1}H NMR spectra of **4b** were difficult to interpret, because of unidentified products in the spectra. Yet, the ^{1}H NMR of the crude product indicated that only one species of a biphenyl structure was formed. It was therefore suspected that the product underwent a dynamic acid-base reaction, resulting in the presence of both the free amine and the amine salt. The ratio of the species would also vary for the different batches of **4b** synthesized in the same manner. Chloroform was suspected to be the origin of the problem as HCl can be formed in the solvent over time. In order to investigate if an acid-base reaction was the case, an excess of $NaHCO_3$ was added to the NMR tube containing **4b** in $CDCl_3$, followed by the heating of the sample. The potentially formed HCl should thereby be neutralized by the base, and possibly lead to a single product. This was based on the assumption that the observed product mixture consisted of **4a** and **4b**. The NMR spectra were acquired after one hour and the next day, and no change was observed. This indicated that the acid-base reaction was probably not the origin of the other species.

^{1}H NMR spectra were acquired in DMSO-d_6 and acetonitrile-d_3, and only one species was observed. This was another indication that $CDCl_3$ was causing the problem. The ^{1}H NMR spectrum of the product was therefore acquired with $CDCl_3$ from a new bottle, which revealed only one set of signals. This strengthens the suspicion of chloroform decomposition over time.

Chloroform can be oxidized resulting in the formation of phosgene and HCl (equation 1).[73] Primary amines can further react with phosgene, forming isocyanates (equation 2).[74] The reaction sequence is as follows:

$$CHCl_3 + \frac{1}{2}O_2 \rightarrow COCl_2 + HCl \qquad (1)$$

$$RNH_2 + COCl_2 \rightarrow RNHCOCl \rightarrow RN = C = O + HCl \qquad (2)$$

It was suspected that this might have been the reason for the observed mixture of products in the ^{1}H NMR spectrum. The other product in the spectrum could be isocyanate. However, upon comparison of the ^{1}H NMR spectrum of the single product **4b** with the previously obtained ^{1}H NMR spectra of the product mixture, none of the sets of signals matched these of **4b**. This might have been a result of **4b** being consumed in the reaction with phosgene, resulting in a mixture of chloroformamide (CA) and isocyanide (IC). This was investigated by Dirk Petersen, where the NMR tube with the sample was heated with hair drier under stirring for 10 minutes. This resulted in full conversion to one product, presumably isocyanate. The spectra obtained by Dirk Petersen are given in **Figure 8**.

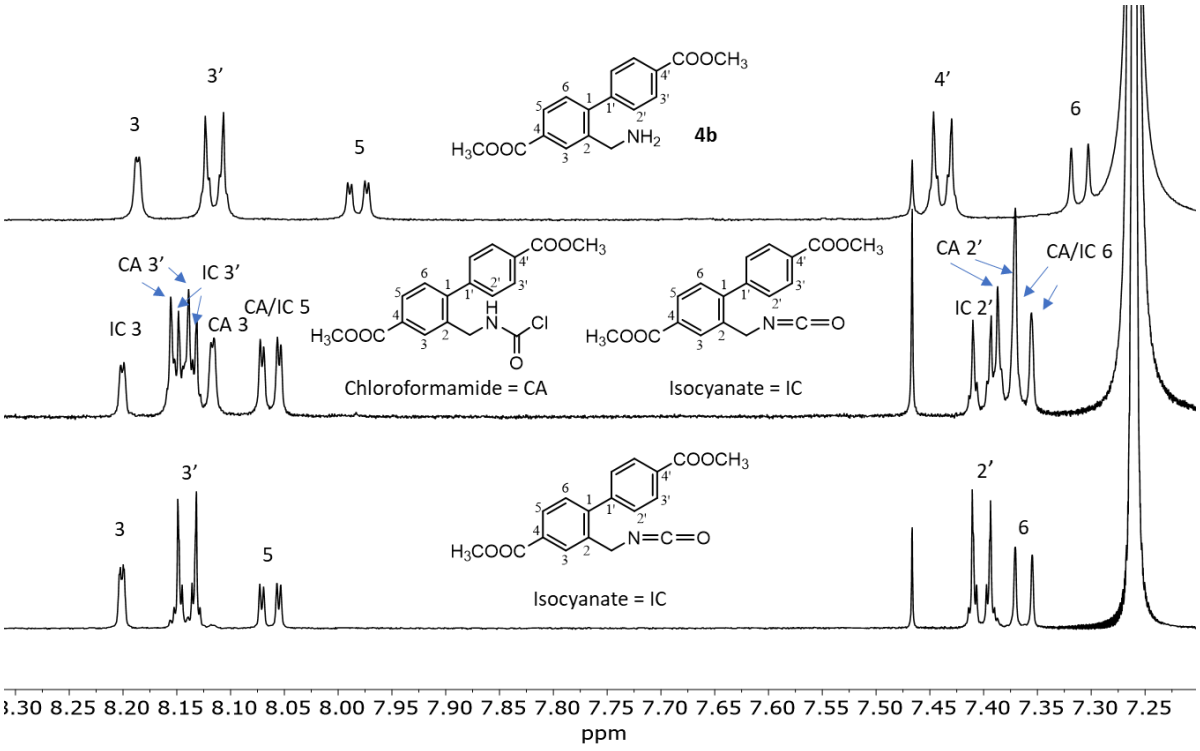

Figure 8: Aromatic region of the ^{1}H NMR of the product run in new chloroform (top), product run in old chloroform, before heating (middle) and product run in old $CDCl_3$ after heating of the sample (bottom) ($CDCl_3$, 500MHz). The spectra were obtained by Dirk Petersen.

Based on the ^{1}H NMR spectra in **Figure 8**, the reaction with phosgene seems to be a reasonable explanation for this phenomenon. It is also an interesting outcome that the product mixture is not a result of any acid-base interactions caused by the generated hydrochloric acid as originally suspected. Instead, the generated phosgene turned out to play a major role.

3.2 Synthesis of the benzylamine 3a through Gabriel synthesis

The synthesis of the benzylamine linker **5** through the reduction of the azide intermediate **3a**, proved to successfully lead to the desired product. However, alternative synthesis routes became attractive due to the safety issues related to sodium azide. Starting from benzyl bromide **2**, obtaining the targeted benzylamine requires the introduction of a nitrogen atom to the benzylic position. The functionalization often involves reduction of nitro groups, nitriles and as previously discussed, azides.[58] However, the nitrogen source might come in many other forms than the mentioned. One common example is a Gabriel reaction where phthalimide is used as a nitrogen source.

Gabriel synthesis is a well-established approach to synthesize primary amines starting from primary halides.[43, 58, 75] The reaction involves an alkylated phthalimide as an intermediate, which is obtained by the nucleophilic substitution reaction between phthalimide and **2** (**Scheme 15**). The intermediate **3b** can further be converted to the desired primary amine in a follow-up reaction. There are different alternatives for the follow-up reaction where the amine is released by a cleavage. The N-C bonds of the phthalimide-unit could be cleaved by hydrazine (Ing-Manske procedure[43, 58, 76]) or acid/base hydrolysis.[43, 75] The reaction conditions for the Ing-Manske procedure and base hydrolysis are given in **Scheme 15**.

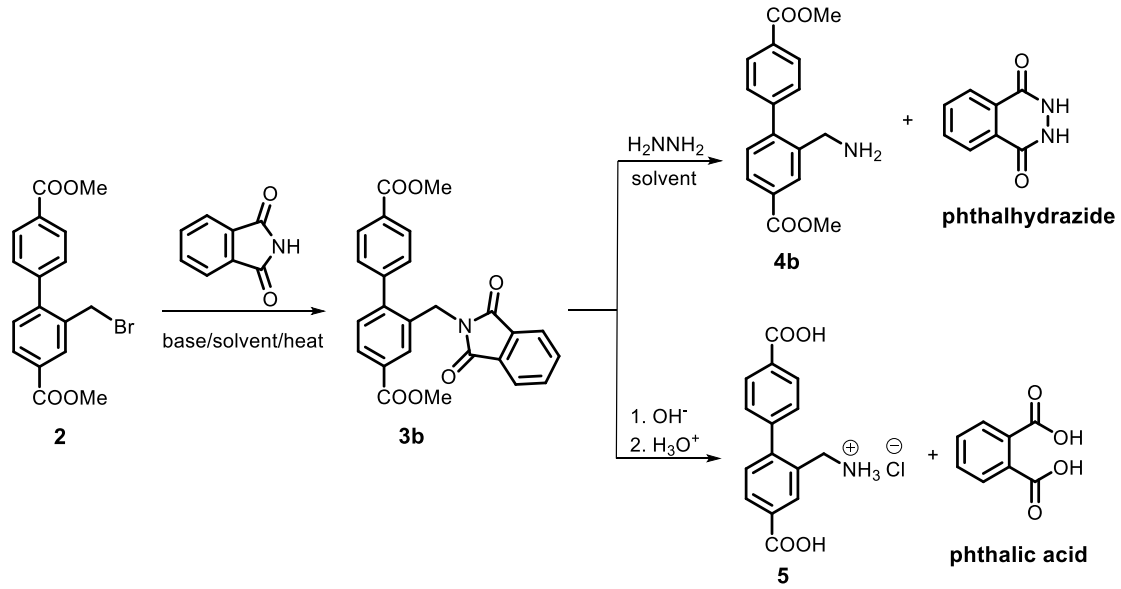

Scheme 15: Two alternative reaction conditions for cleaving of the C-N bonds in the phthalimide, resulting in a release the primary amine. Cleavage by hydrazine (top) and base hydrolysis (bottom).

The cleavage promoted with hydrazine leads to the primary amine product and phthalhydrazide. This is known as the Ing-Manske procedure, which is a hydrazinolysis. The cleavage by a base or acid affords the primary ammonium salt is obtained upon acidification. This reaction is a hydrolysis, which should lead to the hydrolysis of the methyl ester groups, as well as the ammonium salt and phthalic acid. Due to the ester groups and the amine group, the choice of conditions will lead to different forms of the amine-functionalized product; a free amine on ester form (**4b**) or the carboxylic acid **5**.

3.2.1 Synthesis of the phthalimide-substituted intermediate 3b

The synthesis of **3b** was inspired by a published procedure.[77] The conditions for the synthesis of the alkylated phthalimide **3b** from **2** are given in **Scheme 16**.

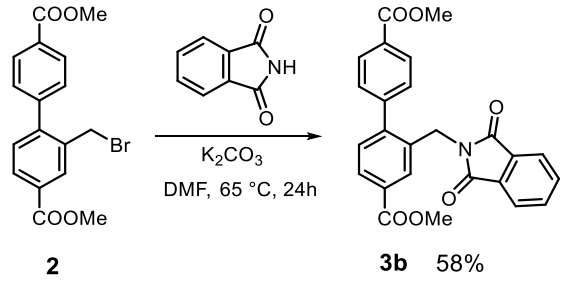

Scheme 16: Reaction conditions for synthesis of **3b**.

The reaction mixture was heated in DMF (65°C, 24 h) and resulted in the formation of the desired product **3b**. The reaction at 2.75 mmol scale resulted in a yield of 62%. Following the reaction progress by NMR, it was found that the full conversion of **2** was achieved after two hours, but overnight reactions were preferred for practical reasons.

3.2.2 Crystallographically determined structure of 3b

The crystals of **3b** were grown by slow diffusion of pentane into the saturated solution of **3b** in $CHCl_3$. The compound was characterized by using single crystal X-ray diffraction. Data collection and refinement were performed by Dr. David Wragg. The crystal data (cif-file) is given in Appendix (**Table 7**).

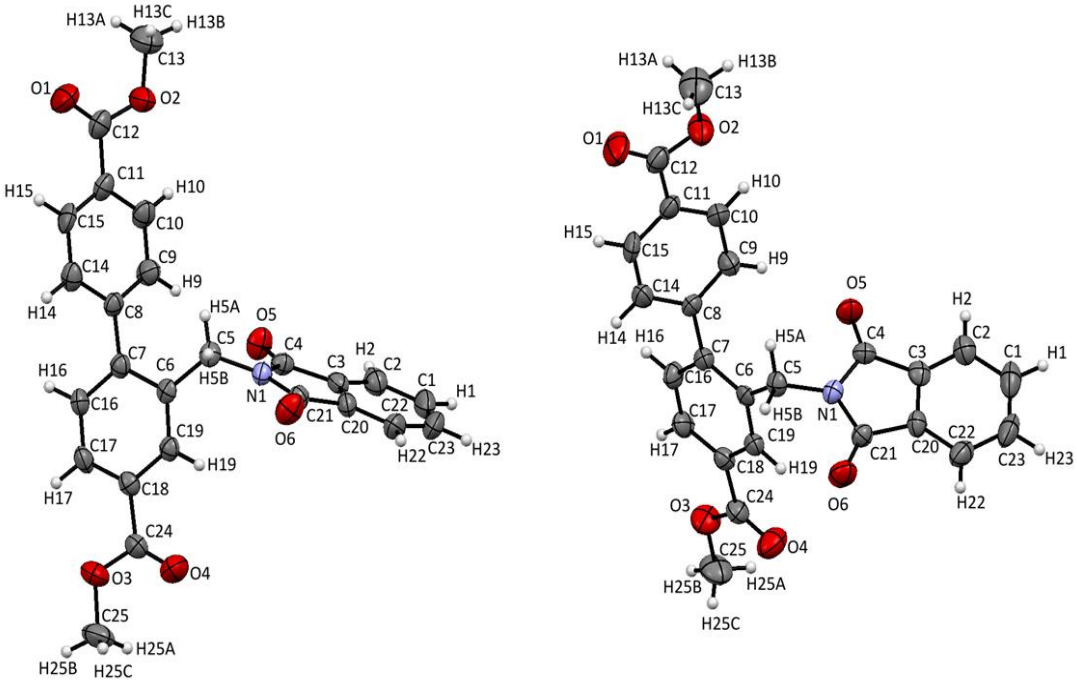

Figure 9: Crystallographically determined structure of **3b**. The structure is presented from two different angles.

The two phenyl rings of the biphenyl system are not coplanar. The rings are twisted with respect to each other by roughly 55° (**Table 6**). The torsion might be a result of the big phthalimide-substituent which forces the least substituted phenyl ring out of the plane. The phthalimide-substituent is clearly not coplanar with the axis through the biphenyl system. It is however not entirely perpendicular to the axis either, as it is slightly twisted. Further analysis of the structure revealed that each ester group is nearly in plane with the phenyl ring it is positioned at. This is evident from the small torsion angles (≈ 1°, **Table 6**) between the carbonyl carbon and aromatic carbon for each ester.

Table 6: A selection of torsion angles calculated for corresponding atoms in **3b**.

Atoms				**Torsion angle/°**
C6	C7	C8	C9	55.0 (10)
C19	C18	C24	O4	0.6 (11)

It was further investigated if there could be a possibility of π-π stacking in the packing diagram. The packing and relevant distances are shown in **Figure 10**.

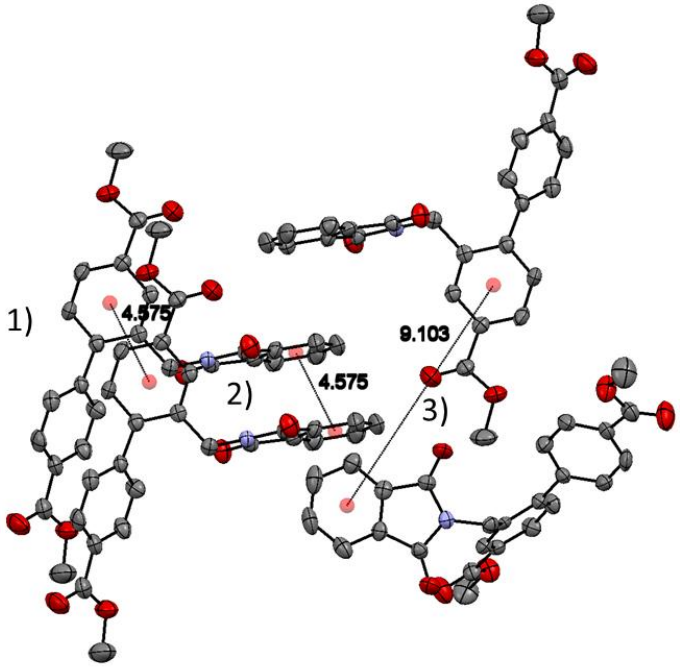

Figure 10: The packing of **3b** with measured distance between the centroids **1)** of two phenyl rings (4.575) **2)** of a phenyl ring and an aromatic ring of phthalimide-substituent (9.103) and **3)** the two aromatic rings of phthalimide-substituents (4.575).

The calculated distances between the centroids (**Figure 10**) indicate that the π-π stacking is not occurring in the packing structure, as the values are out of the reported range for π-π stacking.[78]

3.2.3 Attempted synthesis of 5 by cleavage with lithium hydroxide

The cleavage of the C-N bonds in the phthalimide substituent can be achieved by utilizing bases.[2] Due to the presence of esters, these reaction conditions not only cleave the phthalimide, but also hydrolyze the esters. The base-promoted cleavage should also result in formation of a byproduct, phthalic acid. If successful, this reaction would be a one-pot reaction leading directly to the target molecule **5**. This would shorten the reaction sequence by one step, avoiding hydrolysis of esters in the final step. However, separating the two carboxylic acid products might be challenging due to the solubility issues. The attempted cleavage with corresponding reaction conditions is shown in **Scheme 17**.

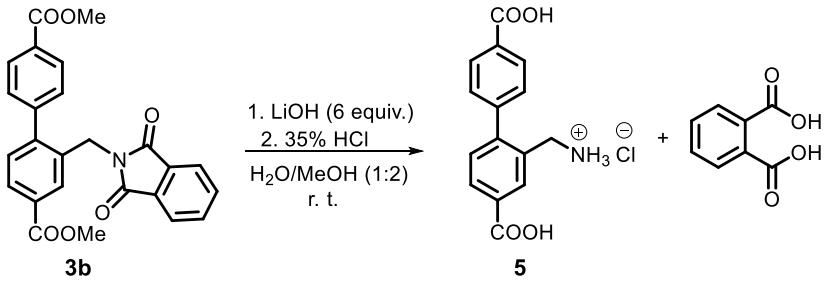

Scheme 17: The reaction conditions of cleavage-hydrolysis.

The reaction mixture was heated in H_2O/MeOH (r.t, 24 h) and the precipitation was obtained upon acidification. The aromatic regions of the spectra of the product mixture and authentic samples of **5** and phthalic acid are given in **Figure 11**.

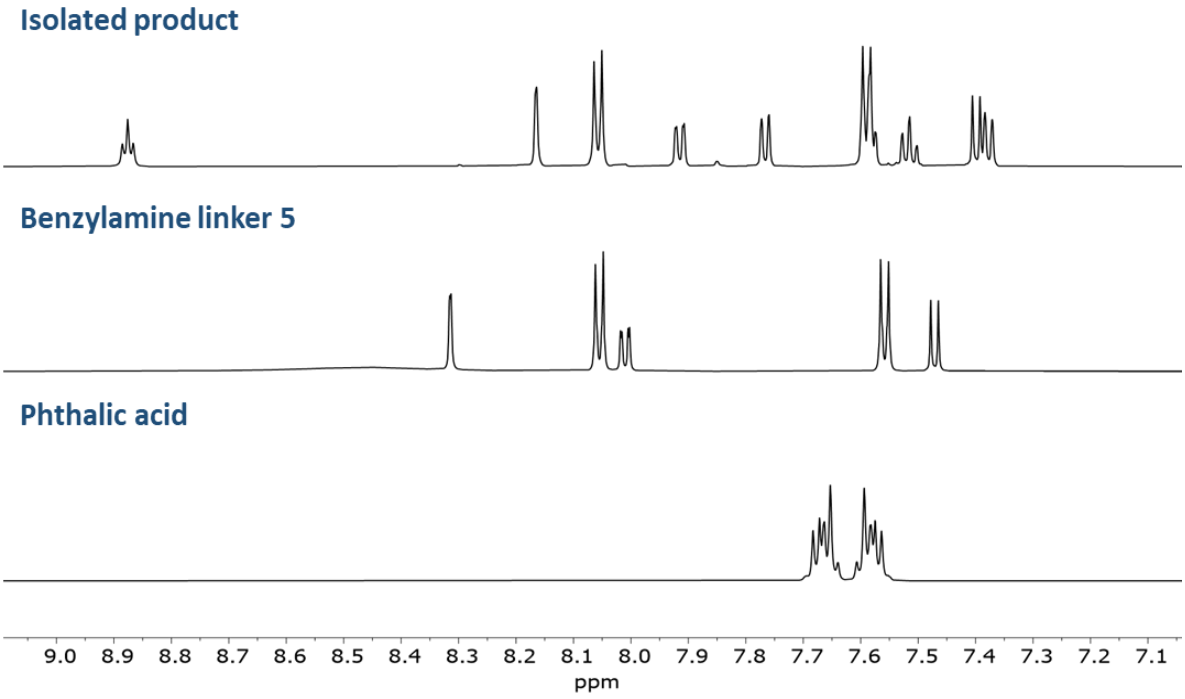

Figure 11: Stacked 1H NMR spectra of the isolated product (top, 600MHz), the benzylamine linker (middle, 600MHz) and phthalic acid (bottom, 300MHz) (DMSO-d_6)

The ^{1}H NMR signals of the isolated product did not match those of the linker **5**. The same observation was made for the phthalic acid. However, the signals of the isolated product had a typical splitting pattern expected for a compound with the same substituted biphenyl structure. This indicated that the change occurred in the benzylic position. The integration accounts for 11 protons in the aromatic region, where seven of these would be expected to come from **5**, and the remaining to come from phthalic acid (**Figure 12**).

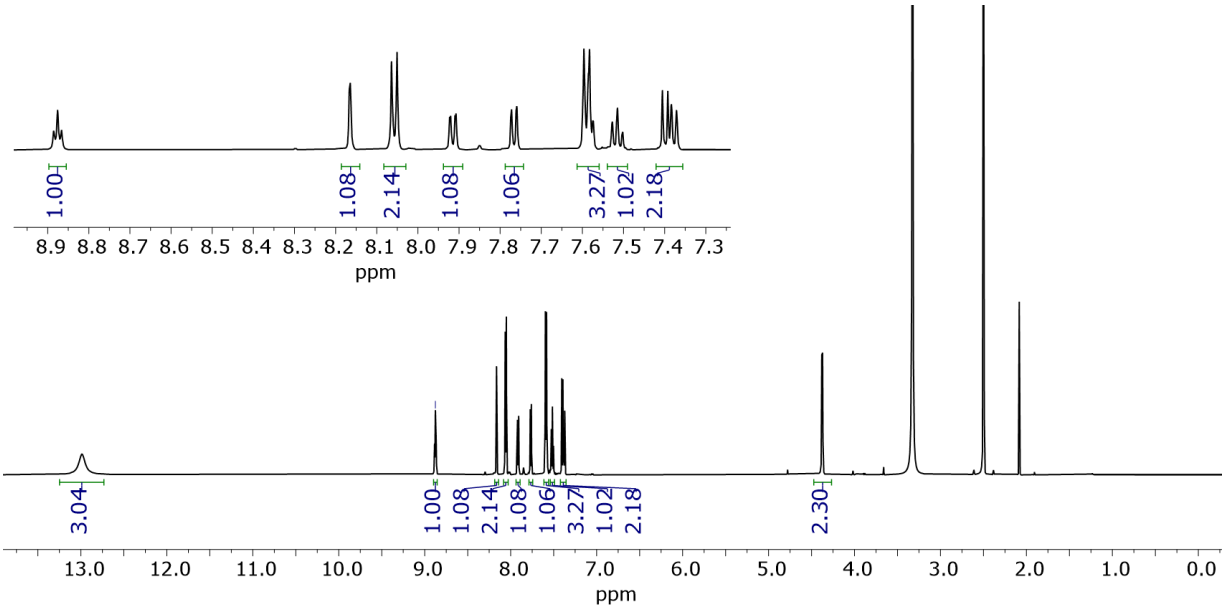

Figure 12: ^{1}H NMR (600MHz, DMSO-d_6,) spectrum of the isolated product from the cleavage with LiOH.

The broad peak at 12.99 ppm and disappearance of the ester signals indicated that the hydrolysis of the esters occurred. The signal integrates for 3H, where in total four carboxylic acid protons are expected to be present for **5** and phthalic acid. It is not uncommon that the integral of the signals corresponding to the carboxylic acid protons is inaccurate, due to the proton exchange with the solvent.[41] An interesting observation is that the signal of the methylene group now appears as a doublet, and another signal is observed at 8.88 ppm (t, 1H). From an acquired COSY spectrum, a correlation between these signals is observed (**Figure 183, Appendix**). Based on this, hydrolysis of **3b** without the cleavage can be excluded.

The isolated product was also characterized with other NMR experiment such as HSQC (**Figure 184, Appendix**) and HMBC (**Figure 13**). The signal at 8.88 ppm (t, 1H) showed no correlations to any carbon signals in HSQC. This indicated that the proton was directly attached to the nitrogen which remained in the benzylic position. From the HMBC spectrum, it was found that the signal in the aliphatic region (d, 2H) and the signal at 8.88 ppm (t, 1H) correlate to the same carbonyl carbon signal at 7.37 ppm. This indicated that the signals originate from one species, and not two as it was initially suspected.

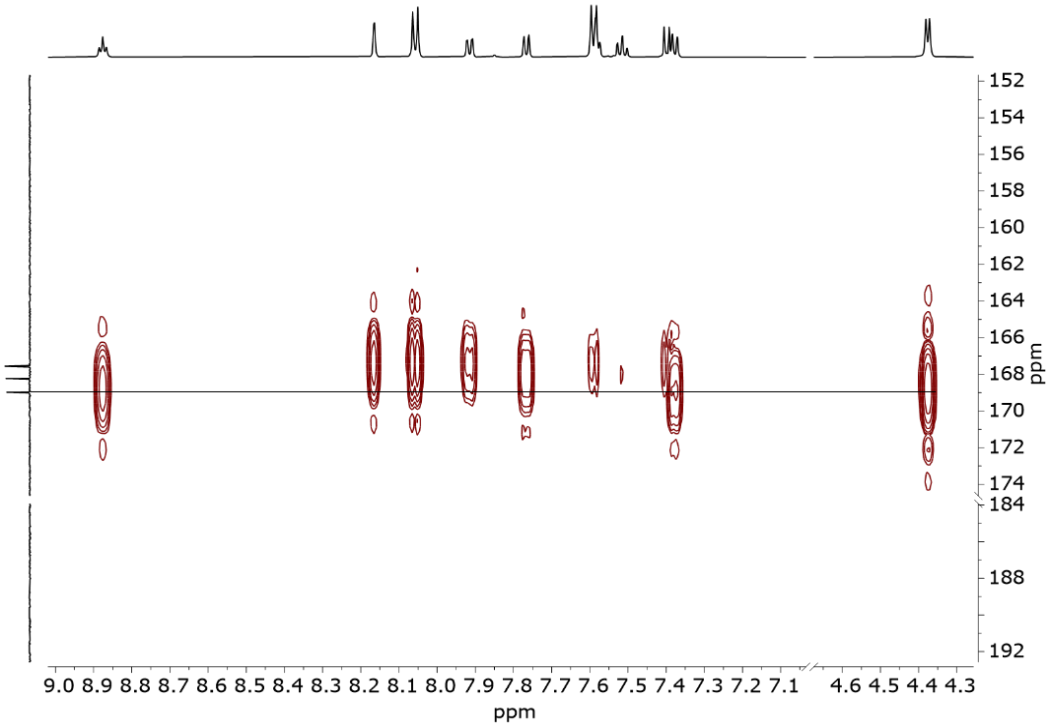

Figure 13: A selected region of the HMBC (600 MHz, DMSO-d_6), spectrum of the isolated product. Correlations between the signal at 169 ppm, and the discussed proton signals (t, 1H), 7.37 ppm (d, 2H) and (d, 2H .

Combining the knowledge from COSY, HSQC and HMBC it is reasonable to suspect that what occurred was in fact a "partial" cleavage of the C-N bonds, resulting in a formation of an amide. This explains not only the observed signals (and the doublet, but also the high ppm value of the triplet which is common for amide protons.[79] Additionally, this might be an explanation for why the broad signal of the carboxylic acid protons integrates for three. The expected product together with the suspected product of this reaction are given in **Scheme 18**.

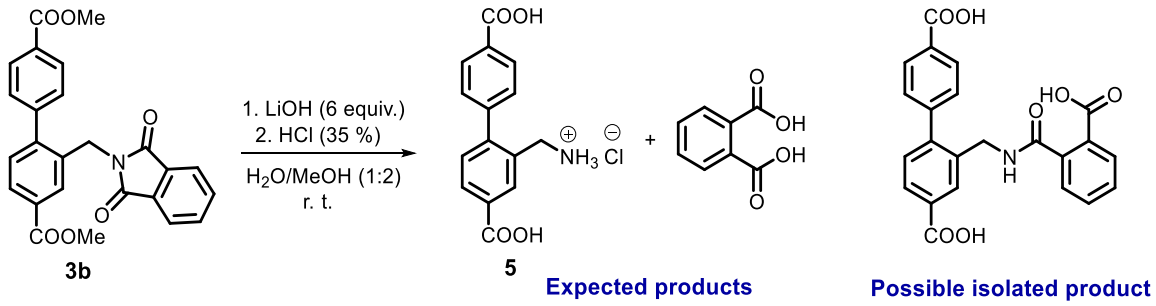

Scheme 18: The reaction with the expected and possible product

The assumption about the nature of the isolated product is strengthened by the observed m/z = 442.090 in the ESI-MS. Additionally, similar product is reported where a phthalimide-substituted compound was treated with potassium hydroxide in aqueous ethanolic solution, and the product was obtained upon acidification.[80] It was also attempted to perform the cleavage at reflux, but the reaction resulted in the same mixture.

3.2.4 Synthesis of the free benzylamine 3b by cleavage with hydrazine hydrate

The solvent which was found to be the most suitable for the cleavage with hydrazine hydrate was ethanol, which is by far the most popular solvent for this type of cleavage.[43] The reason behind it is the capability of ethanol to assist in proton transfers, which are crucial for the efficient cleavage of phthalimide. The reaction is given in **Scheme 19**.

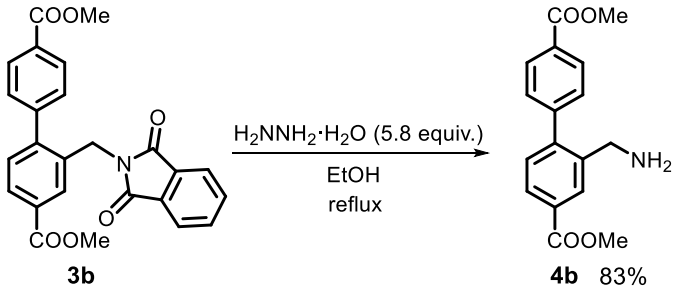

Scheme 19: The reaction conditions for the Ing-Manske procedure for the cleavage with hydrazine.

Compound **3b** was refluxed together with 5.8 equivalents of hydrazine hydrate. The progress of the reaction was monitored by ^{1}H NMR. Samples of the reaction mixture were taken out after one, two and three hours (**Figure 14**).

.

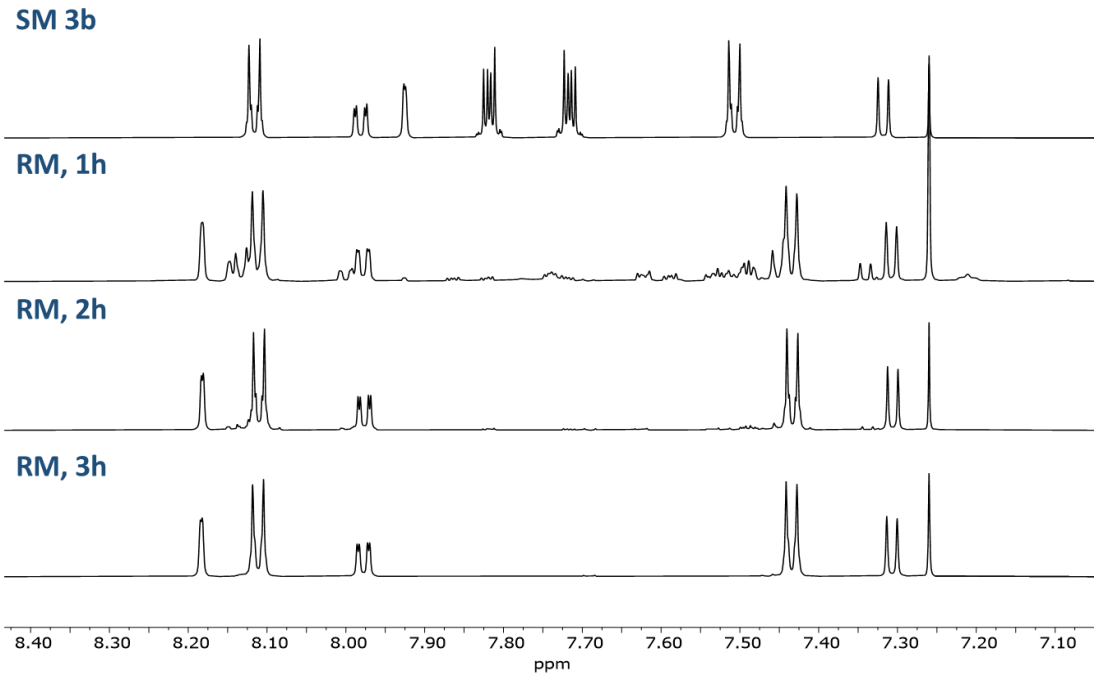

Figure 14: Aromatic region of the ^{1}HNMR (600MHz, $CDCl_3$) spectra belonging to **3b** and the reaction mixtures (RM) after one, two and three hours of reflux in ethanol.

The starting material **3b** was nearly consumed after one hour of reflux in ethanol. Formation of an unidentified species was observed simultaneously. The species disappeared within two hours, and the reaction proceeded selectively towards formation of a single product, **3b**. The observation might be the result of an intermediate being completely transformed to the product over time.

It was observed that when portions of the reaction mixture were taken out for NMR, white solid started to precipitate instantly upon cooling to room temperature. The solid was not soluble in $CDCl_3$, which was used as the NMR solvent for monitoring the reaction progress. The solid was suspected to be a byproduct, phthalhydrazide, which is inevitably forming in Gabriel hydrazinolysis. This cyclic byproduct is a known byproduct when the cleavage is promoted by hydrazine.[43] Stacked ^{1}H NMR spectra of phthalhydrazine and the reaction mixture is given in appendix (**Figure 185**).

Knowing that phthalhydrazide is precipitating in cooled ethanol, the two products could be separated by a simple filtration. The reaction mixture was therefore cooled with an ice bath, and the precipitated solid filtrated and washed with cold ethanol. However, the filtrate still contained the excess of hydrazine hydrate which should be removed from the product. To avoid removing the solvent under reduced pressure with hydrazine hydrate present, the best work-up seemed to be an extraction with water. This yielded **4b** which was pure (by NMR).

3.3 Synthesis of the benzylamine linker 5

The final reaction leading to the desired linker is a hydrolysis. These carboxylate linkers are further incorporated in MOFs. Because of the poor solubility of carboxylic acids in most of the common solvents, the free carboxylic acid is not released before the last step. Working with esters facilitates the syntheses, especially in means of work-up and purification.

The hydrolysis reaction is based on a procedure, developed in the Tilset group.[81] The reaction utilizes a base, often lithium hydroxide instead of other alkaline bases such as natrium hydroxide or potassium hydroxide. The reason for this preference is that the presence of sodium or potassium ions may interfere with the synthesis of MOFs The mechanism behind these problems has not been investigated, but it was observed that the problem was avoided when LiOH was used. The reaction conditions for the hydrolysis of **4a**/**4b** are given in **Scheme 20**.

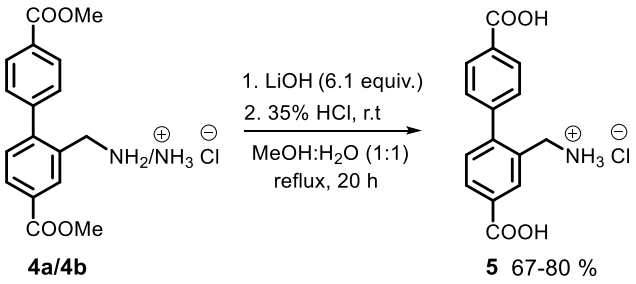

Scheme 20: Reaction conditions for hydrolysis of **4a** and **4b**

The hydrolysis proceeded in a straightforward manner. The solvent system chosen for this reaction is a mixture of methanol and water (1:1). Water was added to increase the solubility of LiOH, and the solvent system ensured solubility of **4a**/**4b** at higher temperatures. The reaction mixture was refluxed overnight, followed by filtration. The clear filtrate was then added hydrochloric acid to protonate the water-soluble carboxylates. The protonated linker becomes then insoluble in the water/methanol solution and precipitates out. The precipitated linker was subsequently isolated by filtration.

3.3 Comparison of the synthesis routes leading to 5

The two developed syntheses led successfully to the desired linker **5**. However, both syntheses are of low atom economy[82] (low atom efficiency), as they generate byproducts such as PPh_3O (synthesis involving azides) and phthalhydrazide (Gabriel synthesis with Ing-Manske procedure). These reactions are therefore not on the right path towards a "greener" chemistry.

A valid reason for utilizing the Gabriel reaction for obtaining the linker **5**, is the safety concern. The synthesis where the azide intermediate is utilized involves handling of the toxic and explosive sodium azide, which limits the interest in this synthesis route. Upscaling of this reaction should also be limited for this reason, preventing potential synthesis on multigram scale. Although the hydrazine hydrate utilized in the Gabriel synthesis is hazardous too, it is easier to handle compared to the sodium azide which should be handled with proper care. Additionally, the Gabriel synthesis does not involve the azide intermediate **3a**, which is connected to unknow risks as many other organic azides.[83]

CHAPTER 4

Synthesis and characterization of new ethylamine-based linker

Two synthetic strategies to extend the alkane chain on the linker are discussed in this chapter. Strategy 1 proceeds through the condensation of an aldehyde, resulting in an α, β-nitroalkene which upon reduction affords **9**. A second strategy was investigated, starting from nitrile **7**. The product is also in this case obtained through a reduction, followed by hydrolysis of **8a**/**8b.** (**Scheme 21**). The syntheses of the intermediates of both strategies are covered in this chapter. Their characterization is not discussed in depth, as it resembles the one for **9**, which is discussed and used as an example for characterization.

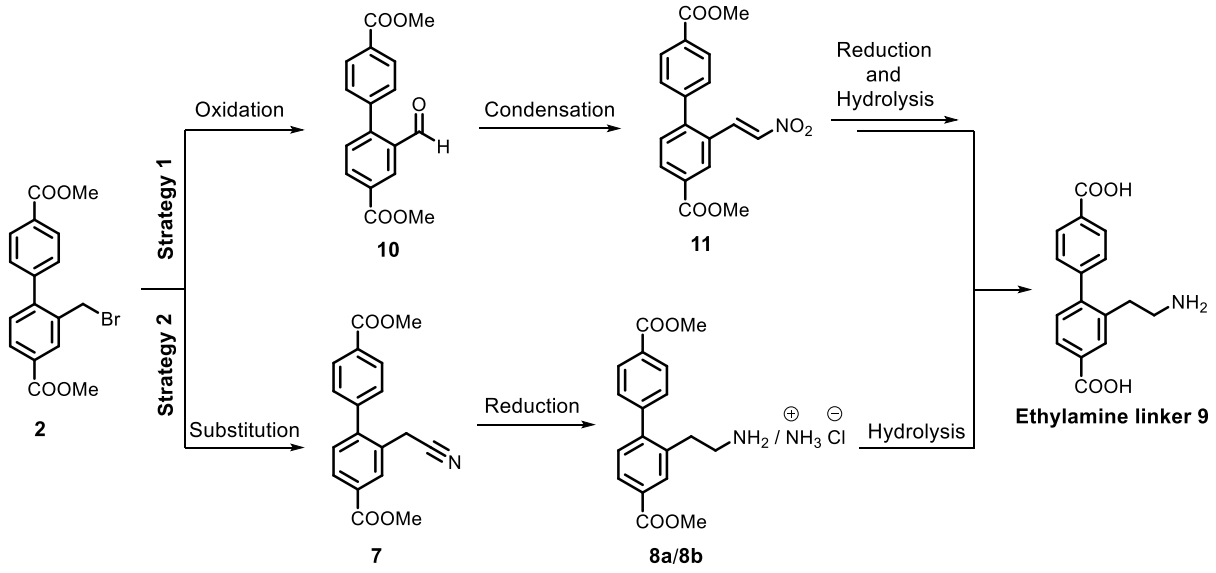

Scheme 21: Synthetic strategies to obtain the ethylamine linker **9**. In strategies 1 and 2 the corresponding amine is obtained by reduction of α, β-nitroalkene and a nitrile, respectively. The final step of both strategies is hydrolysis where **9** is obtained.

Alkyl halides are commonly used in synthesis and are oxidized in order to obtain aldehydes. Further treatment with CH_3NO_2 in condensation reactions is a convenient method for the synthesis of α, β-nitroalkenes.[84-88] Through the reduction of these, a variety of amines are accessible.

Compound **2** had to be converted to an aldehyde **10** to allow condensation with CH_3NO_2. Common methods to oxidize alkyl halides to aldehydes include Sommelet reaction,[89-91]

Kornblum oxidation,[92-94] and oxidation with H_2O_2[95, 96]. Successful oxidations with MnO_2[97] and pyridine *N*-oxide with Ag_2O[98] have also been reported. The two latter oxidations were attempted in this project.

After the condensation, the α, β-nitroalkenes are frequently reduced to the corresponding amines with $LiAlH_4$. This is however not a suitable reagent for reduction of **11,** as the esters are reduced to corresponding alcohols upon treatment with $LiAlH_4$.[2, 41] A milder reduction with a $NaBH_4$-transition metal salt system was therefore employed. However, reducing α, β-nitroalkenes to corresponding aliphatic amines under milder conditions can potentially require reduction over two steps.[99] This would inconveniently prolong the reaction sequence.

In strategy **2**, cyanide introduces the nitrogen source simultaneously to the carbon chain extension. The nucleophilic substitution reaction of 2 with cyanide forms nitrile **7**, which in turn can be reduced to the corresponding amine **8**. Some of the common approaches to reduce nitriles involve $LiAlH_4$, Pd/H_2 and $NaBH_4$-transition metal salt systems.[58] In this project, a $NaBH_4$-transition metal salt system has been utilized for the reduction of the nitrile **7**.

4.1 Attempted synthesis of the ethylamine 9 through α, β-nitroalkene 10

4.1.1 Synthesis of aldehyde 10

Aldehyde **10** has been reported in literature.[100-102] All published procedures for the synthesis of **10** include a coupling reaction. The simplest coupling reaction is given in **Scheme 22**.

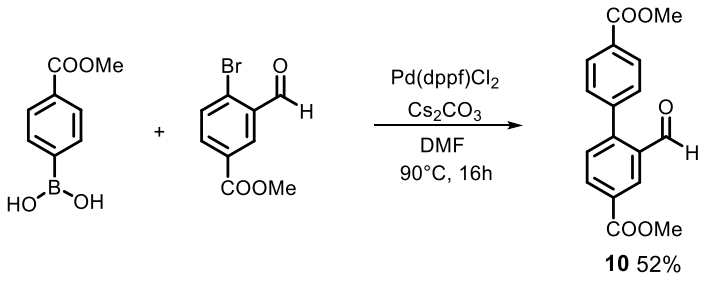

Scheme 22: A published coupling reaction yielding **10** with corresponding yield.[102]

The coupling conditions in **Scheme 22** are similar to those leading to **1c**. The literature procedure is an overnight reaction and requires DMF and Cs_2CO_2. However, proceeding with

this coupling requires a synthesis or purchase of methyl 4-bromo-3-formylbenzoate, which is very expensive (abcr: 9212 NOK/1 g, per 18.06.20).[103] This was the motivation to explore alternative synthesis of **10**.

Out of convenience, **2** was chosen as starting material. It would also demonstrate that **2** can be used in a wide range of reactions, as it was utilized in the syntheses of **3a**, **3b**, **6** and **7**.

The first attempt to oxidize **2** to **10** involved utilizing MnO_2 as oxidizing reagent. However, no reaction occurred. The next approach to synthesize **10** was inspired by a reported procedure, where a variety of benzylic alkyl halides was oxidized to corresponding aldehydes.[98] The optimized reaction conditions for the synthesis of **10** are given in **Scheme 23**.

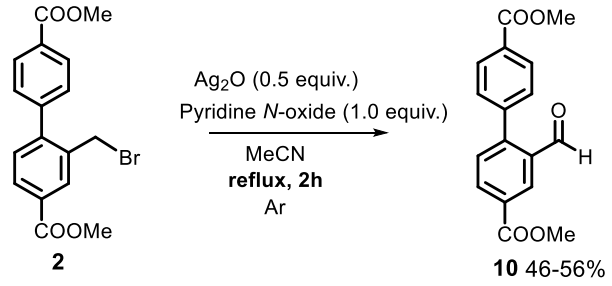

Scheme 23: Reaction conditions for synthesis of **10.**

The initial attempt to synthesize **10** by stirring of **2**, Ag_2O and pyridine *N*-oxide in MeCN at room temperature showed completion after two days. Repeating the reaction at reflux shortened the reaction time to two hours. From that point, the reflux was utilized for the synthesis of **10**. The crude product was purified by filtration and flash chromatography.

The drawback of this synthesis is the purification by flash chromatography, which proved to be time-consuming and demanding. A gradient eluent had to be used to balance retention and separation. The most suitable one was a gradual increase of ethyl acetate in hexane from 0 to 30 %. Monitoring the effect of gradient facilitated the separation of the species. However, mixed fractions could not be entirely prevented. This is the reason for the low to moderate yields. The reactions at 1.38 mmol scale resulted in **10** of high NMR purity with yields of 46-56 %.

Upon upscaling to 2.75 mmol, CH_2Cl_2 as eluent proved to be more efficient. This gave the product of high purity (by NMR), similar to the purity obtained by automatic flash chromatography. The corresponding yield of 42 % is comparable to the other yields.

Compared to the literature procedure for **10**, the herein reported reaction is cheap and fast. The aldehyde intermediate can be interesting for other reactions. For instance, target linker **5** might be accessible through reductive amination. This would avoid the use of the toxic sodium azide utilized in the synthesis of **3a**, in Chapter 3.

4.1.2 Synthesis of the α, β-nitroalkene 11

The condensation of **10** with CH_3NO_2 for the synthesis of **11** was inspired by a published procedure.[104] The optimized reaction conditions are given in **Scheme 24**.

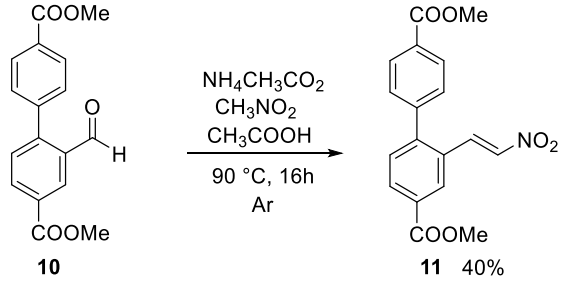

Scheme 24: The reaction conditions for the synthesis of **11**.

The purification of **11** proved to be challenging. Two side products were detected in the ^{1}H NMR spectrum of the crude product, in addition to **11**. Purification by flash chromatography with hexane/ethyl acetate eluent with gradient was therefore attempted. One of the side products was efficiently removed. The other side product was however not successfully separated from the product.

The purification of **11** proved to be challenging. Two side products were detected in the ^{1}H NMR spectrum of the crude product, in addition to **11**. One of the side products was efficiently removed by flash chromatography. The other side product was however not successfully separated from the product.

The product was recrystallized from *i*PrOH resulting in voluminous white solid. The two purification steps increased the purity of the product, but retained 7 % of the other species. The yield after two purification steps is 22 %. ^{1}H NMR spectra of the crude mixture, after flash chromatography and after recrystallization are given in **Figure 15**.

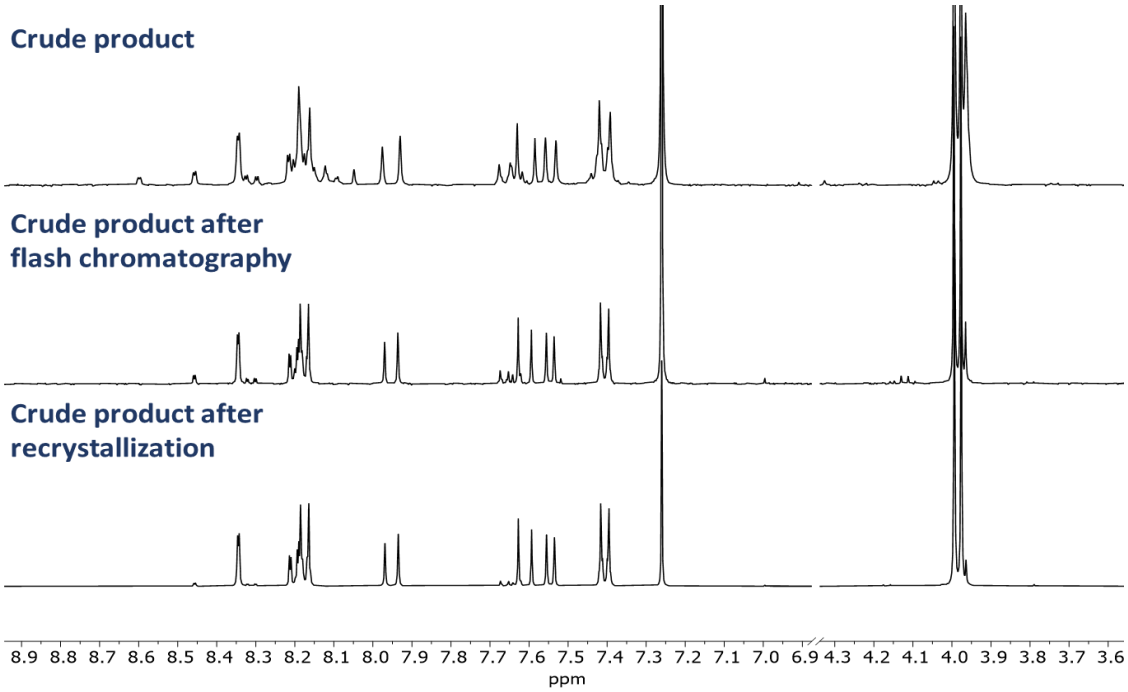

Figure 15: The crude product after extraction (top, 400 MHz), after flash chromatography (middle, 600 MHz) and after recrystallization (bottom, 600 MHz) ($CDCl_3$)

The aforementioned purification was time-consuming and resulted in low yield. It was therefore attempted to purify the crude product solely by recrystallization. Recrystallization from *i*PrOH gave the product in similar purity, but with a 40 % yield. Removal of the other species could clearly be achieved by recrystallization. No further purifications were attempted, and **11** was further utilized in the follow up reaction with the purity given in **Figure 15** (bottom spectrum).

4.1.3 Attempted reduction of α, β-nitroalkene 11 by catalytic hydrogenation

Both nitro groups and unsaturated compounds are commonly reduced by catalytic hydrogenation.[41] Hence, it was attempted to reduce both the carbon-carbon double bond and the nitro group of **11** in a one-pot reaction. The conditions for the attempted reduction of **11** are given in **Scheme 25**.

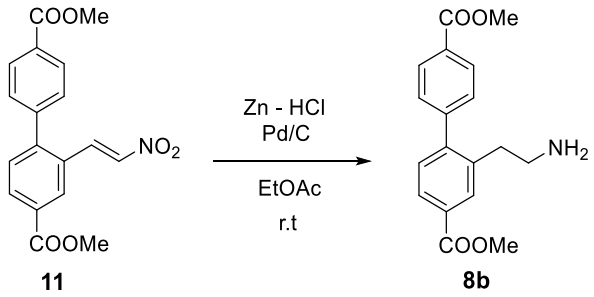

Scheme 25: Reaction conditions for reduction of 11 through catalytic hydrogenation.

The approach to reduce **11** to the corresponding amine was inspired by Winterton *et al*., where the reduction of another α, β-nitroalkene is achieved by introducing hydrogen gas through a balloon.[84] The setup utilized in this project consisted of two round bottomed flasks, where hydrogen gas was generated by addition of zinc powder to an aqueous solution of hydrochloric acid in one flask. The generated hydrogen gas was then bubbled through a solution of Pd/C and **11** in ethyl acetate (**Figure 16**).

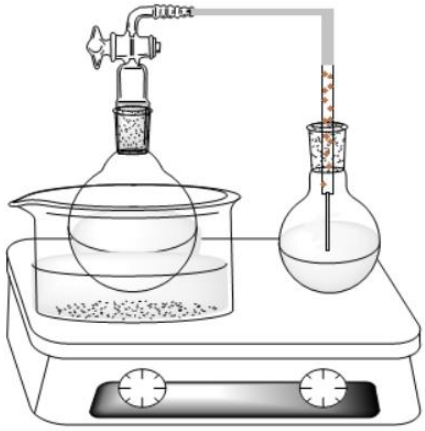

Figure 16: Setup for the attempted reduction of **11** by catalytic hydrogenation The left flask contains zinc powder and hydrochloric acid cooled with an ice bath. It is connected to a pipette filled with molecular sieves reaching into the reaction mixture.

The reaction mixture was saturated with hydrogen gas, followed by closing the system overnight and stirring at room temperature. The ^{1}H NMR spectrum of the reaction mixture taken after 24 hours revealed little conversion. The reaction resulted in formation of small amounts of an unidentified product. The ^{1}H NMR spectra of the reaction mixture and amine **8b**, known from the reduction of the **7,** did not match. Additionally, the m/z corresponding to **8a**/**8b** was not observed in ESI-MS of the reaction mixture. This indicated that the amine was most probably not formed. The identity of the formed product could not be determined.

4.1.4 Attempted reduction of α, β-nitroalkene 11 with $CoCl_2 \cdot 6H_2O$ and $NaBH_4$

The next attempt to reduce **11** was based on a published procedure utilizing sodium borohydride-transition metal salt system for selective reduction of nitriles and nitro compounds.[105] A suspension of **11**, $CoCl_2 \cdot 6H_2O$ and $NaBH_4$ in THF/methanol (1:1) was stirred overnight under argon atmosphere. The reaction resulted in a mixture of products (Appendix, **Figure 186**). Although ESI-MS confirmed the presence of the desired product, there seem to be selectivity problems. Hence, no further investigation of the reaction was conducted.

4.2 Synthesis of the ethylamine linker 9 by nitrile reduction

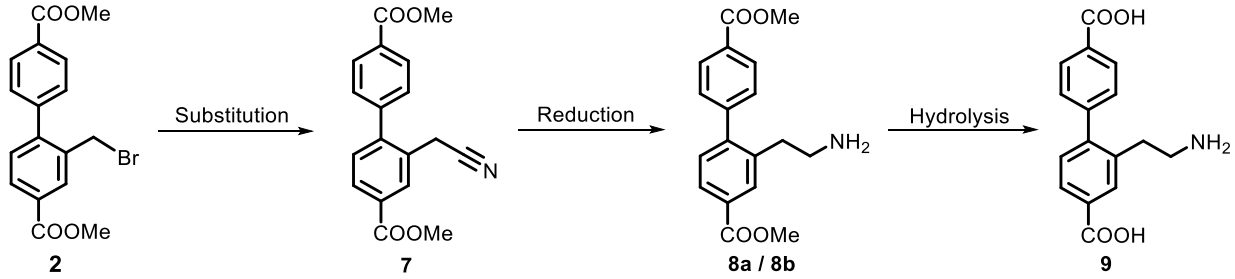

Scheme 26: Second synthesis route to **9**.

In the second synthesis route (depicted in **Scheme 26**), the chain prolongation and introduction of the nitrogen occur in one step.

4.2.1 Attempted synthesis of methyl ester nitrile 7

The initial attempt to synthesize **7** involved ethanol as a solvent, inspired by the efficient synthesis of the azide **3a** through a nucleophilic substitution reaction in the same solvent. The reaction conditions for attempted synthesis of 6 are given in **Scheme 27**.

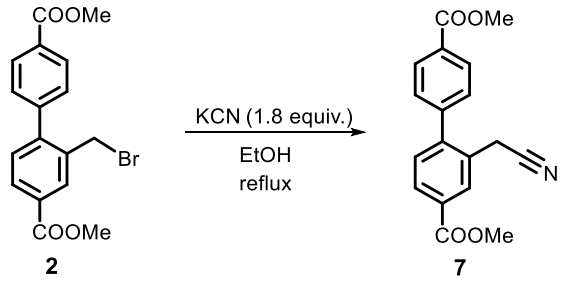

Scheme 27: Initial reaction conditions for the synthesis of **7**

The starting material **2** was refluxed with 1.8 equivalents of KCN, and the reaction was monitored by ^{1}H NMR. The reaction occurred in the benzylic position of **2**, as indicated by the maintained splitting pattern of the aromatic signals. Some unexplained signals were observed in the ^{1}H NMR spectra. Comparing the ^{1}H NMR spectra of the reaction mixture over time, significant differences in the aliphatic region were observed. The resonances corresponding to the methyl groups of the product (3.90 ppm) did not integrate for the expected six protons. This indicated a loss of methyl groups. On repeated runs, the ^{1}H NMR resonances corresponding to the methyl groups disappeared within 4-5 hours. At the same time, new signals appeared at 3.91 ppm and 3.89 ppm (**Figure 17**). The product was investigated by ^{13}C NMR and 2D NMR.

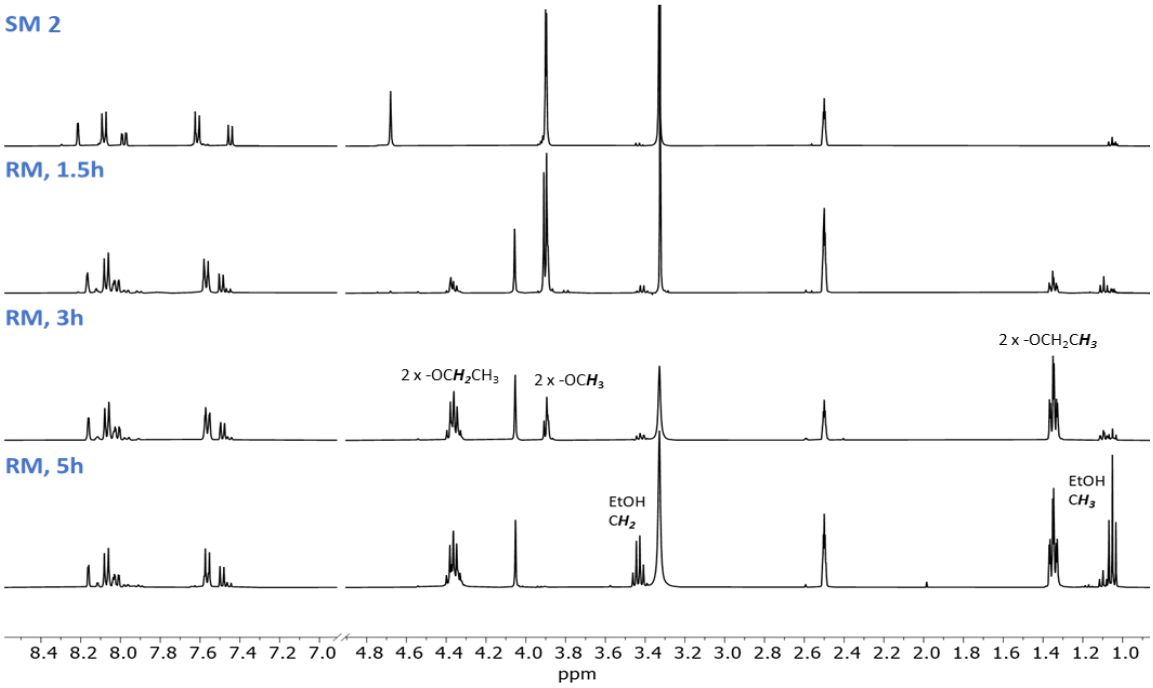

Figure 17: Stacked ^{1}H NMR (400MHz, DMSO-d_6) spectra of **2** and the reaction mixture after 1.5 hour, 3 and 5 hours.

In ^{13}C NMR, the first indication that a nitrile product has been formed is the extra signal at 118.5 ppm (red circle, **Figure 18**), which is in accordance with the literature.[79] The signal did not correlate to any ^{1}H signals, strengthening the assumption about the nitrile.

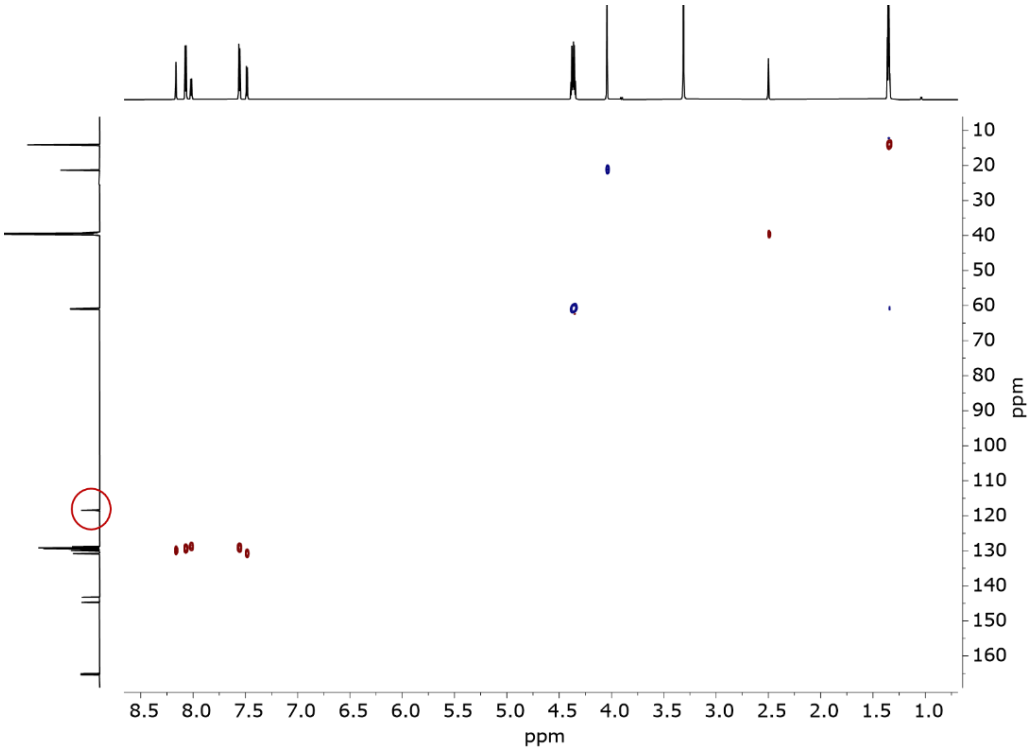

Figure 18: HSQC (800 MHz, DMSO-d_6) spectrum of the isolated product showing the carbon signal (red circle) of the nitrile.

The next step was to identify the new signals in the aliphatic region of the ^{1}H NMR. The signal at 4.37 ppm (m, 4H) correlated to the carbon signals at 61.1 ppm and 60.9 ppm, and the signaø at 1.35 ppm (m, 6H) correlated to the signal at 14.1 ppm (**Figure 19**). An additional DEPT experiment confirmed that the signals correspond to two methylene groups and two methyl groups (Appendix, **Figure 124**)

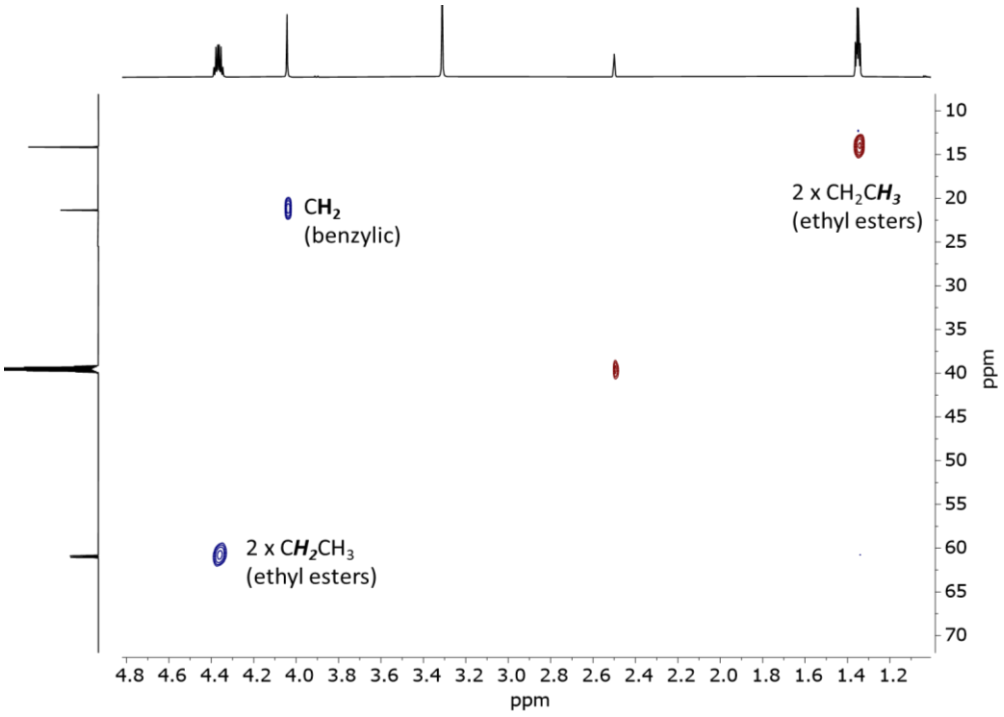

Figure 19: Zoom of HSQC (800 MHz, DMSO-d_6) spectrum of the isolated product showing the correlations between ^{1}H signals and ^{13}C signal in the aliphatic region.

A correlation between the two multiplets is observed in a COSY spectrum (Appendix, **Figure 125**). The observations from the NMR analysis indicates the presence of ethoxycarbonyl groups, suggesting that transesterification had occurred. NMR integration and ESI-MS show a gradual substitution of methoxy groups by ethoxy groups, resulting in ethyl esters. The signals found in the ESI-MS spectrum at m/z = 360.121 correspond to the transesterification product. Additionally, a signal at m/z = 346.205 is observed which corresponds to incomplete transesterification product where the substitution only occurred on one carbonyl. The desired dimethyl ester product with m/z = 309.100 is not observed (**Figure 20**). Based on the observed changes of the ^{1}H NMR resonances in the aromatic region, it can be concluded that the nucleophilic substitution happens prior to or simultaneously to the transesterification.

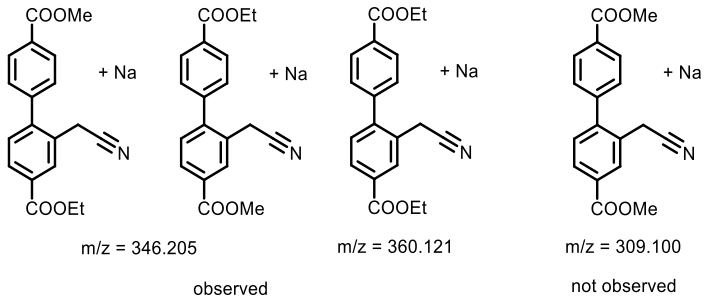

Figure 20: The compounds observed in the ESI-MS spectrum

Further, it was observed that the number of equivalents of KCN influenced the transesterification rate. It was observed that when 1.8 equivalents of KCN were used, the transesterification was complete after 4-5 hours. However, when 1.1 equivalents of KCN were used, the transesterification seems to be significantly slower. The transesterification was then nearly complete after 21 hours.

4.2.2 Investigation of transesterification from 7 to 6.

In order to investigate if KCN catalyzed the transesterification, two parallel reactions were run. In the first reaction, **7** was refluxed in ethanol together with 1.8 equivalents of KCN. The second reaction was carried out in similar manner, but no KCN was added to the reaction mixture. The two reactions were simultaneously followed by ^{1}H NMR, revealing that the transesterification from **7** to **6** occurred only in the reaction where KCN was present. This is in agreement with earlier reports of cyanide-catalyzed transesterfications in the literature.[106]

4.2.3 Synthesis of nitrile methyl ester 7

To prevent the transesterification from happening, the solvent was changed from ethanol to methanol. This proved to be efficient and the synthesis of **7** was successful. The reaction was complete within 15 minutes using 1.1 equivalents of KCN. The optimized reaction conditions are given in **Scheme 28**.

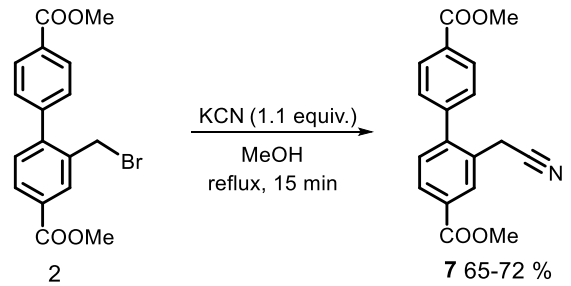

Scheme 28: Reaction conditions for the synthesis of the nitrile **7** from **2**.

4.2.4 Synthesis of 8a/8b through reduction of 7

The reduction of **7** was based on the published procedure[105] which utilized sodium borohydride-transition metal salts systems for selective reduction of nitriles. The reaction conditions are given in **Scheme 29**.

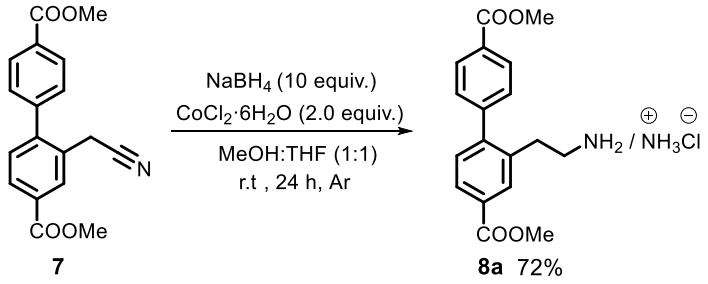

Scheme 29: Reaction conditions for the reduction of **7**.

To a cooled, crystal blue suspension of **7** and $CoCl_2 \cdot 6H_2O$ in THF/methanol (1:1) $NaBH_4$ was added within a course of few minutes. The reaction mixture was subsequently stirred overnight at room temperature under argon atmosphere. After the initial work-up (see Experimental section), an oil was obtained. The residue was partially dissolved in small amounts of toluene and the solution was filtered. Addition of concentrated hydrochloric acid to the clear toluene solution while stirring afforded **8b** as a thick yellow/white precipitation. The product was isolated by filtration and was of acceptable NMR purity, with a yield of 72 %.

The product was also isolated as free amine **8b** through an acid-base work-up, similar to the one discussed in Chapter 3. The purity of **8b** was acceptable, but the reaction resulted in a poor yield. Due to time limitations, the purifications of **8a**/**8b** and the upscaling of the reaction was not optimized.

4.2.5 Synthesis of ethylamine linker 9 by hydrolysis of 8b

The hydrolysis of **8b** (**Scheme 30**) was carried out under similar conditions[81] to the one of **4a** and **4b**, which is discussed more in detail in Chapter 3.

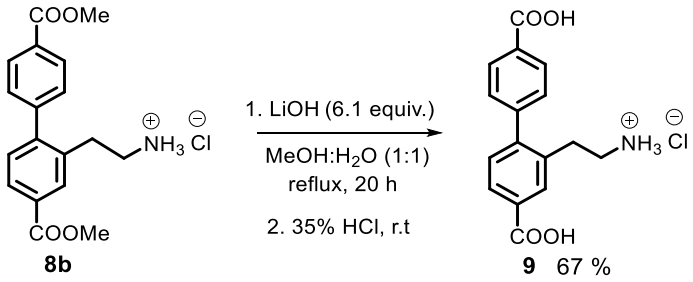

Scheme 30: Reaction conditions for the hydrolysis of **8b** leading to the ethylamine linker **9**.

The reaction mixture was refluxed in MeOH/H_2O (20 h) and precipitation of **9** was obtained by addition of HCl (35%). The protonated linker was isolated by vacuum filtration and dried at room temperature.

4.2.6 Characterization of ethylamine linker 9

The ethylamine linker **9** has been characterized by a wide range of NMR experiments. All of the intermediates discussed in the thesis have been characterized in the same manner, but linker **9** will be used as an example.

Upon studying of the ^{1}H NMR spectrum of **9**, a clear indication that **8b** has been hydrolyzed is the presence of a broad signal (13.10 ppm, 2H) which corresponds to the two carboxylic acid protons (**Figure 21**).

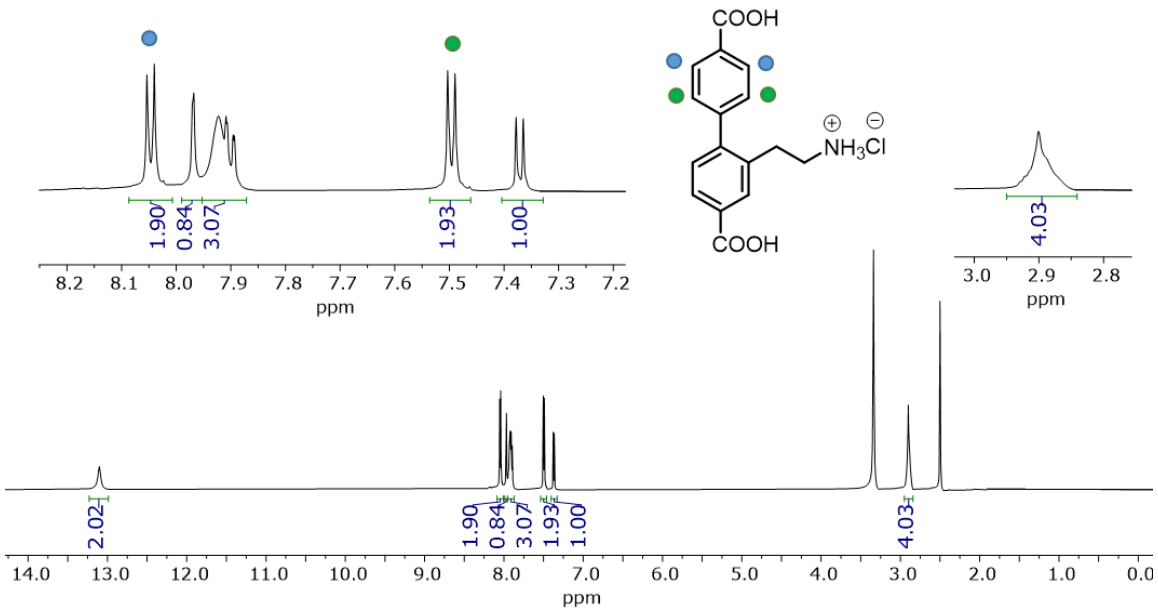

Figure 21: ^{1}H NMR spectrum of the ethylamine linker **9**. (600 MHz, DMSO-d_6)

The integration of the product signals accounts for 16 protons which is in accordance with what is expected. The phenyl rings of compound **9** are non-equivalent because of the ethylamine substituent, resulting in chemically inequivalent protons and carbons. Separate carbon and proton signals are therefore observed, except for the positions marked with green and blue circles. The proximity of some carbon signals complicated the assignment. This was especially challenging for quaternary carbons. The problem could in many cases be solved by acquiring selective HSQC and HMBC experiments. The experiments were however not acquired for all compounds, and assignment of the signals was based on elimination when selective HSQC and HMBC were not performed.

The major difference between the ^{1}H NMR spectra of the linkers **5** and **9** is the signal at 2.90 ppm (m, 4H). The signal corresponds to the methylene protons of **9**, which originally would be expected to appear as two independent triplets. However, the signals exhibit a high-order splitting pattern. The phenomenon is observed when the difference between the chemical shift of the two groups of protons has a similar magnitude (in Hertz) to the coupling constant *J* (in Hertz).[79] While the two outer peaks decrease in the intensity, the two inner peaks increase as the triplets emerge into each other resulting in a complex multiplet.

Another characteristic feature of **9** is the signal (br. s, 7.92 ppm) corresponding to the ammonium salt protons. The identity of this signal was confirmed by ^{1}H-^{15}N HMBC, where a clear correlation is observed (**Figure 22**).

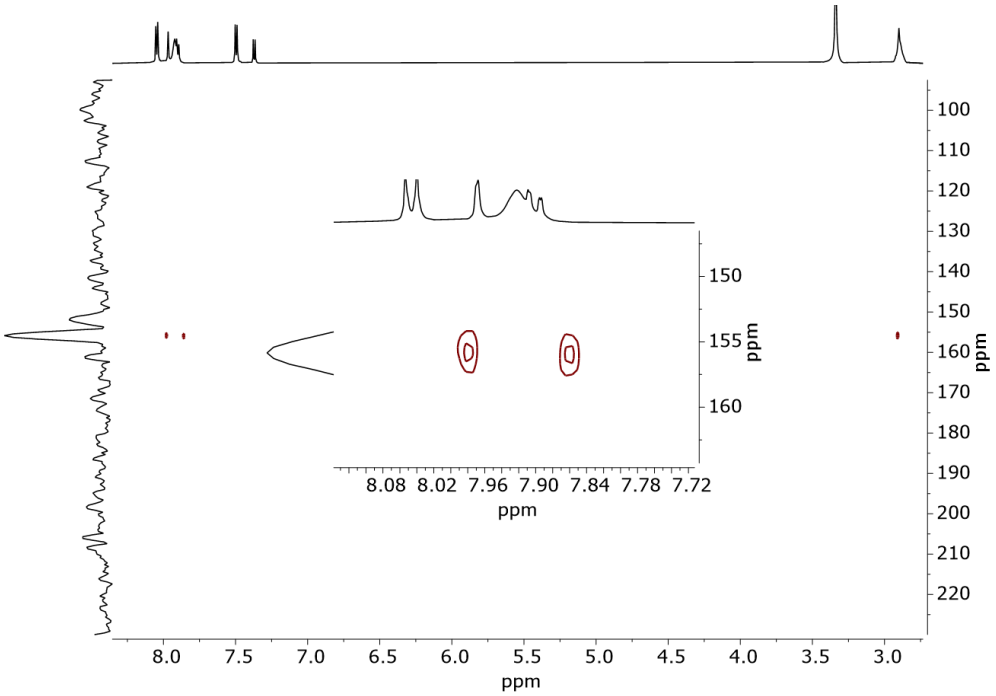

Figure 22: ^{15}N HMBC of **9** showing the correlation between the Broadened ^{1}H NMR resonance and the nitrogen signal, confirming the identity of the corresponding protons.

The 2D NMR experiment ^{1}H-^{15}N HMBC is a useful technique to determine if the molecule contains nitrogen atoms. The ^{15}N HMBC spectra have been acquired for many of the synthesized nitrogen-containing compounds.

4.3 Comparison of the synthesis routes leading to 9

The two discussed synthetic strategies to obtain **9** each proved to have their challenges. The syntheses of the aldehyde **10** and the α, β-nitroalkene **11** were time-consuming, with non-satisfactory yields. This strategy did not lead to the desired product. However, the synthesis of the aldehyde **10** from **2** was successfully developed, giving a potential for exploring an alternative synthesis route for the benzylamine linker **5**.

The ethylamine linker **9** was successfully obtained through the synthesis involving the nitrile intermediate. The desired product was afforded by the reduction of the nitrile, followed by hydrolysis. However, the purification and upscaling of the reduction and hydrolysis require further optimization.

CHAPTER 5

Syntheses of UiO-67 metal-organic frameworks

Since the breakthrough with the UiO-MOF series in 2008, the MOFs studied by the Catalysis group at the University of Oslo were mainly UiO-66 and UiO-67.

The synthesis of the standard UiO-67 metal-organic frameworks is still mainly based on the original synthesis procedure published in 2008,[1] which utilizes zirconium (IV) tetrachloride, biphenyl-4.4'-dicarboxylic acid (H_2BPDC) as the linker and DMF as the solvent. The synthesis is also often carried out with a modulator, often benzoic acid.

5.1 Synthesis and characterization of UiO-67 and UiO-67-benzylamine

The incorporation of functionalized linkers in UiO-67 can be done with varying ratios of the functionalized linker and biphenyl-4.4'-dicarboxylic acid, resulting in mixed-linker MOFs. For this project, the synthesis was attempted with 0.1 equivalents of 5 and 0.9 equivalents of the H_2BPDC. The idealized reaction equation for the synthesis of UiO-67-benzylamine where 10% of **5** is incorporated is given in equation 3.

$$6ZrCl_4 + 5.4H_2BPDC + 0.6BA + 8H_2O \xrightarrow{\text{benzoic acid}} Zr_6O_4(OH)_4(BPDC)_{5.4}(BA)_{0.6} + 24HCl \quad (3)$$

The first attempt to synthesize the UiO-67-benzylamine was carried out in a diluted system (300 equiv. of DMF). The synthesis resulted in amorphous solid as revealed by powder X-ray diffraction analysis (Appendix, **Figure 187**). In the next attempt, a concentrated system (50 equiv. of DMF) was utilized. The concentration of the reaction mixture was previously found to influence the MOF syntheses.[20] The synthesis of UiO-67-benzylamine was conducted in parallel with the synthesis of UiO-67, as a control experiment. In the UiO-67 MOF only the linker biphenyl-4.4'-dicarboxylic acid is incorporated. The reactions resulted in formation of two crystalline products. The crystallinity of the two materials was confirmed by powder XRD (**Figure 23**)

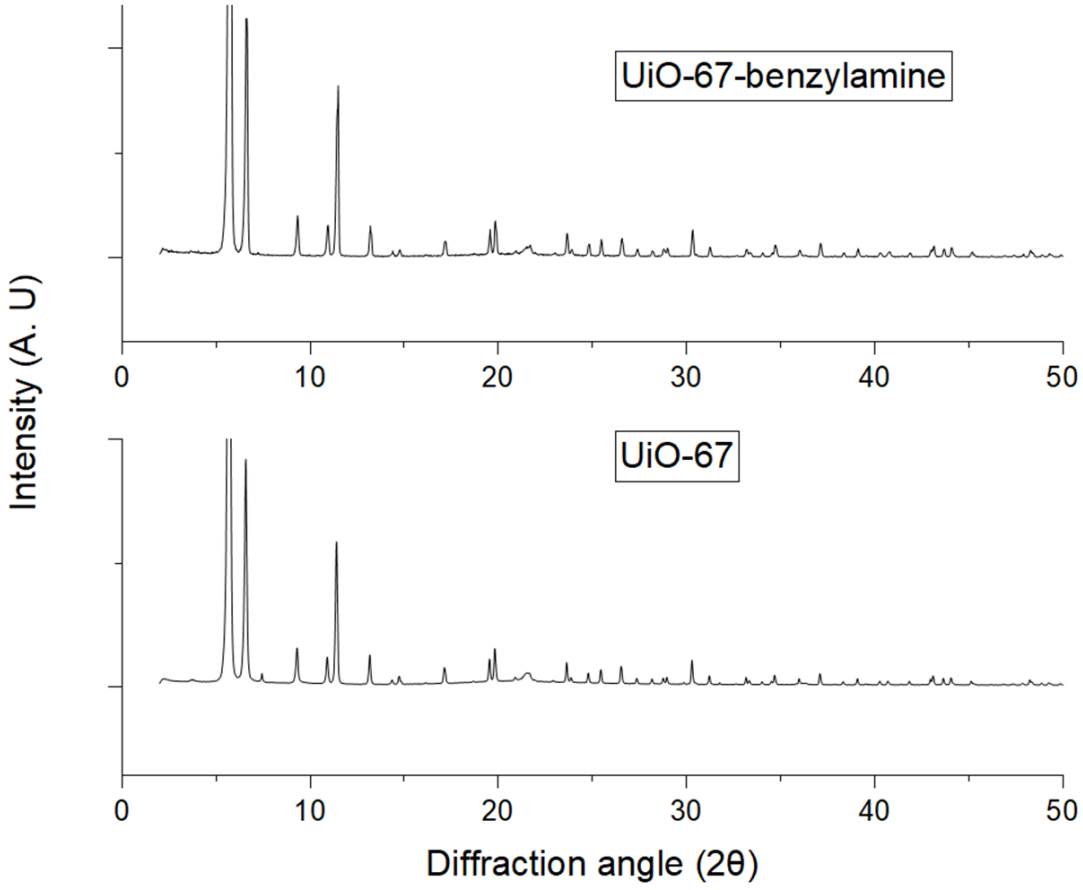

Figure 23: X-ray diffraction pattern of UiO-67-benzylamine and UiO-67.

From the X-ray diffraction pattern, it was evident that the syntheses of the MOFs resulted in crystalline materials with similar diffraction patterns. The two crystalline materials were subsequently characterized using thermogravimetric analysis (TGA). The acquired TGA plots are given in **Figure 24**.

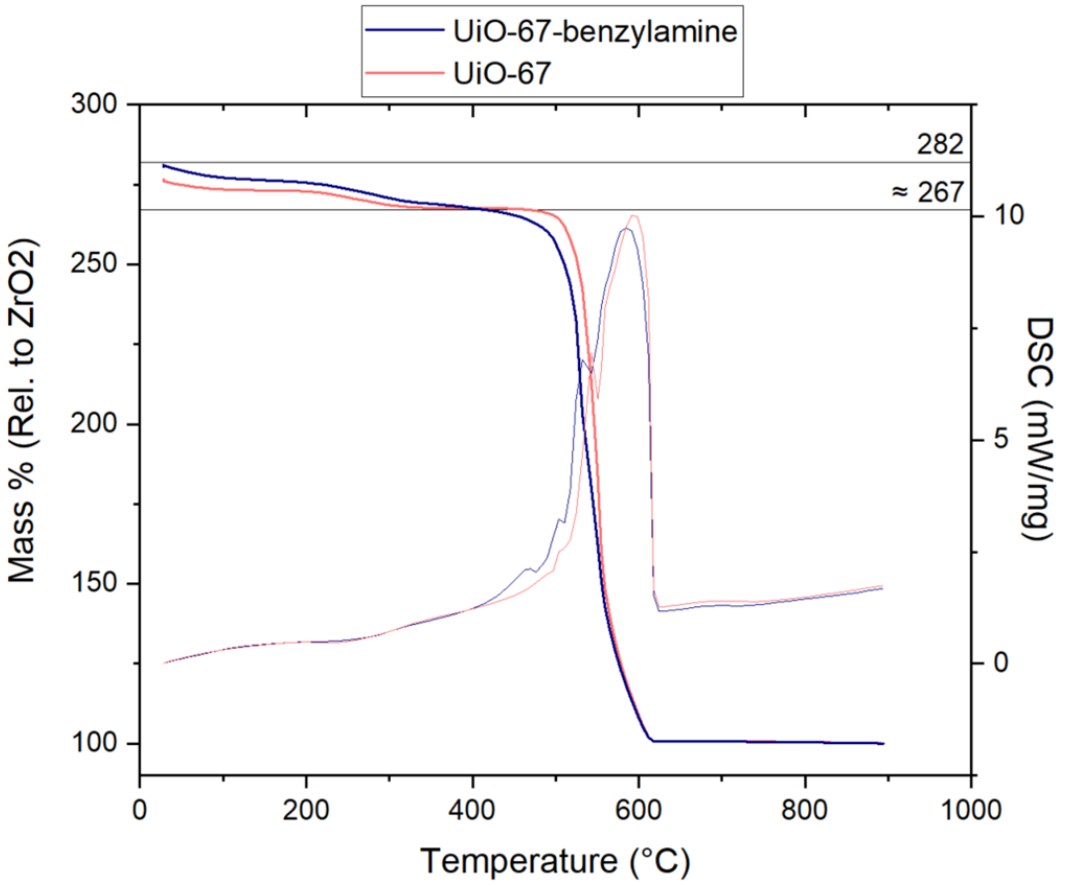

Figure 24: Thermogravimetric analysis of the synthesized UiO-67 (red curve) and UiO-67-benzylamine (blue curve), with corresponding curves for diffraction scan calorimetry (DSC). The mass % on the y-axis is normalized with respect to ZrO_2, where 100% corresponds to ZrO_2. The plateaus of ideal dehydrated UiO-67 and the synthesized UiO-67 are marked.

The plateau of the synthesized UiO-67 in **Figure 24** was lower than the reported plateau of a nearly ideal, defect-free UiO-67.[20] The synthesized UiO-67 began to decompose at approximately 430 °C, which is similar to the reported decomposition temperature of roughly 450 °C.[1] Additionally, the synthesized UiO-67 exhibited higher stability than UiO-67-benzylamine, which started to decompose close to 400 °C.

Further analysis of the MOF materials involved nitrogen adsorption measurements at -196.15 °C (77 K). Combined with BET theory, the approximate BET surface area of the MOFs was calculated. The adsorption/desorption diagram is given in **Figure 25.**

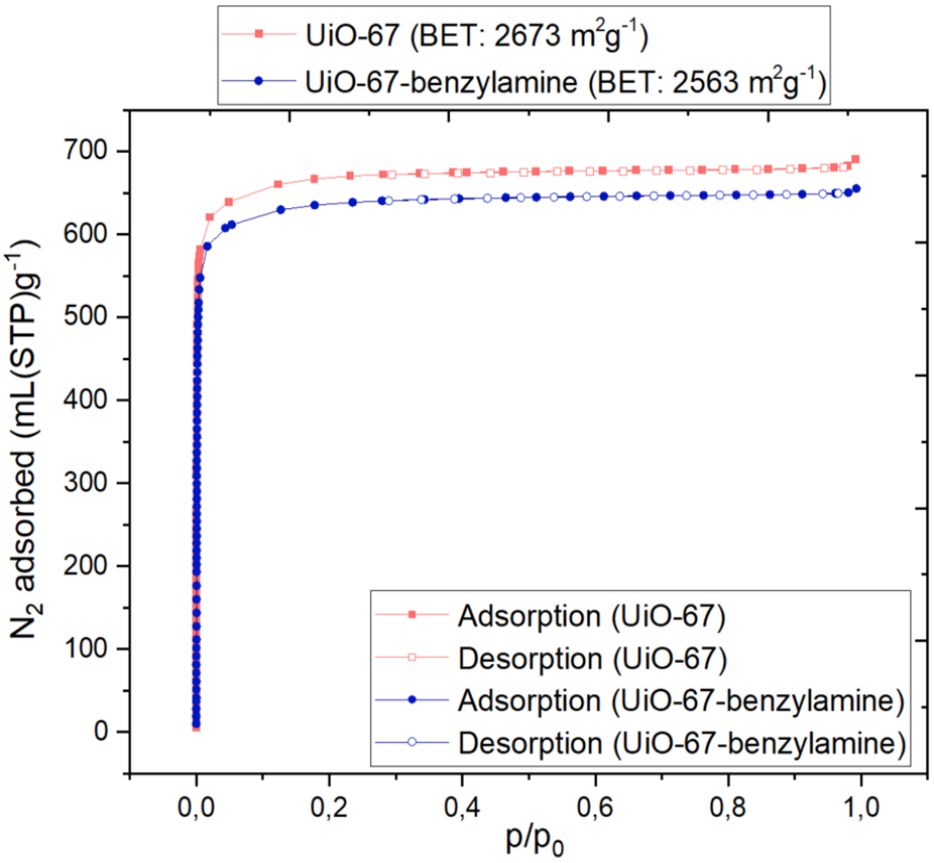

Figure 25: Nitrogen adsorption measurements of the synthesized UiO-67 and UiO-67-benzylamine, with corresponding calculated BET surfaces.

The measurements indicated that both MOFs exhibited high surface areas. The calculated specific surface areas for UiO-67 and UiO-67-benzylamine are 2673 m^2g^{-1} and 2563 m^2g^{-1}, respectively. Based on this it can be concluded that the surface areas of the synthesized MOFs are in accordance with what is reported in the literature (2579 m^2g^{-1}).[20] The high surface area of UiO-67-benzylamine indicates that the MOF can have potential in applications such as CO_2 adsorption.

The two MOFs were also investigated using scanning electron microscopy. The obtained images are given in **Figure 26**.

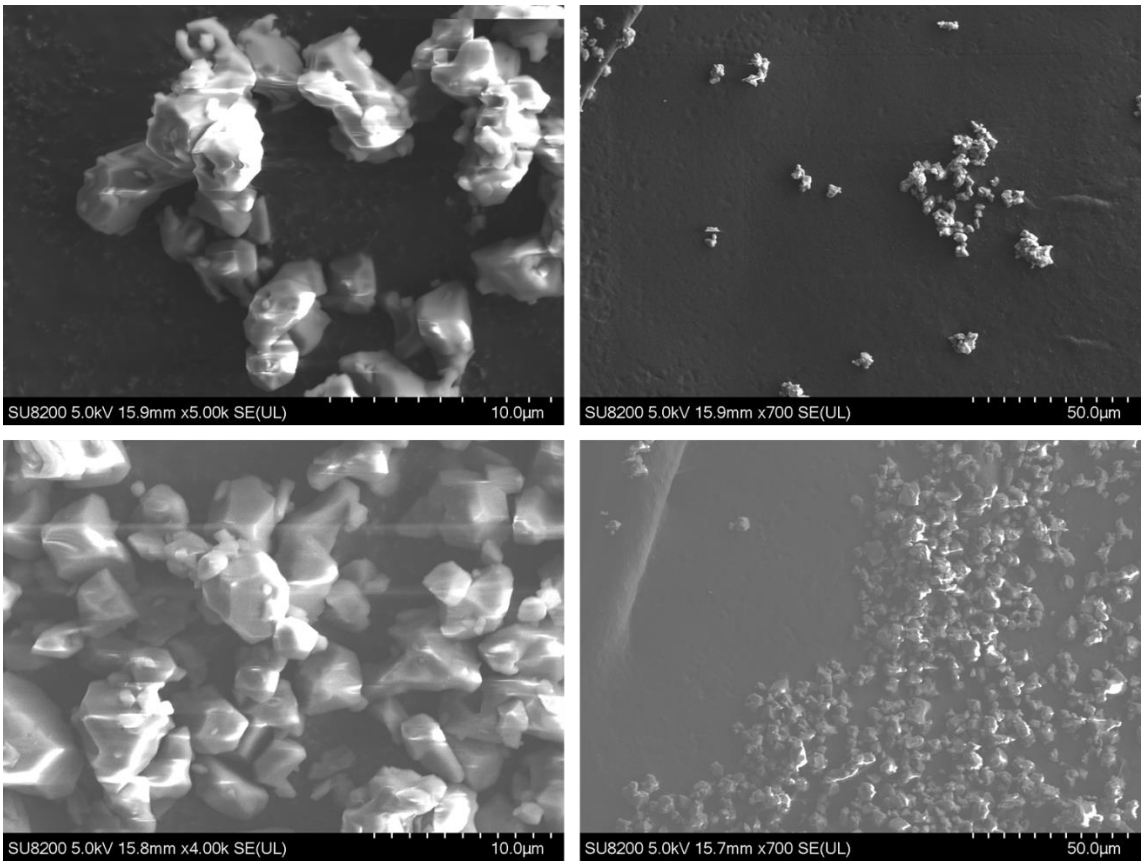

Figure 26: Micrographs of UiO-67 (top row) and UiO-67-benzylamine (bottom row) obtained with scanning electron microscopy.

The obtained SEM images are of poor quality, which makes it difficult to draw safe conclusions regarding the nature of the MOFs. However, there were signs of octahedral crystallites present in the sample of the synthesized UiO-67, which are associated with the UiO-67-structure. The crystallites were varying in size and shape. The crystallites of UiO-67-benzylamine also exhibit such irregularity in size and shape. However, the varying appearance of the crystallites can also indicate that other linkers than H_2BPDC have been incorporated in the MOF. As a result, crystallites different from these of non-functionalized UiO-67 can be observed.

Another feature of SEM is the option of obtaining a rough estimate over the elemental composition of the materials, by energy dispersive X-ray (EDX) microanalysis. The obtained results are given in (SEE APPENDIX).

Although the synthesis of the MOF material proved to be successful, it cannot be concluded that **5** was incorporated, or if only the standard linker (H_2BPDC) was incorporated. One of the ways to verify this is by MOF digestion, an NMR experiment. The UiO-67 and UiO-67-benzylamine MOFs were digested in 1M NaOD in D_2O, with sodium

trimethylsilylpropanesulfonate (DSS) as an internal standard at 0.0 ppm. The result of the digestions is given in **Figure 27**.

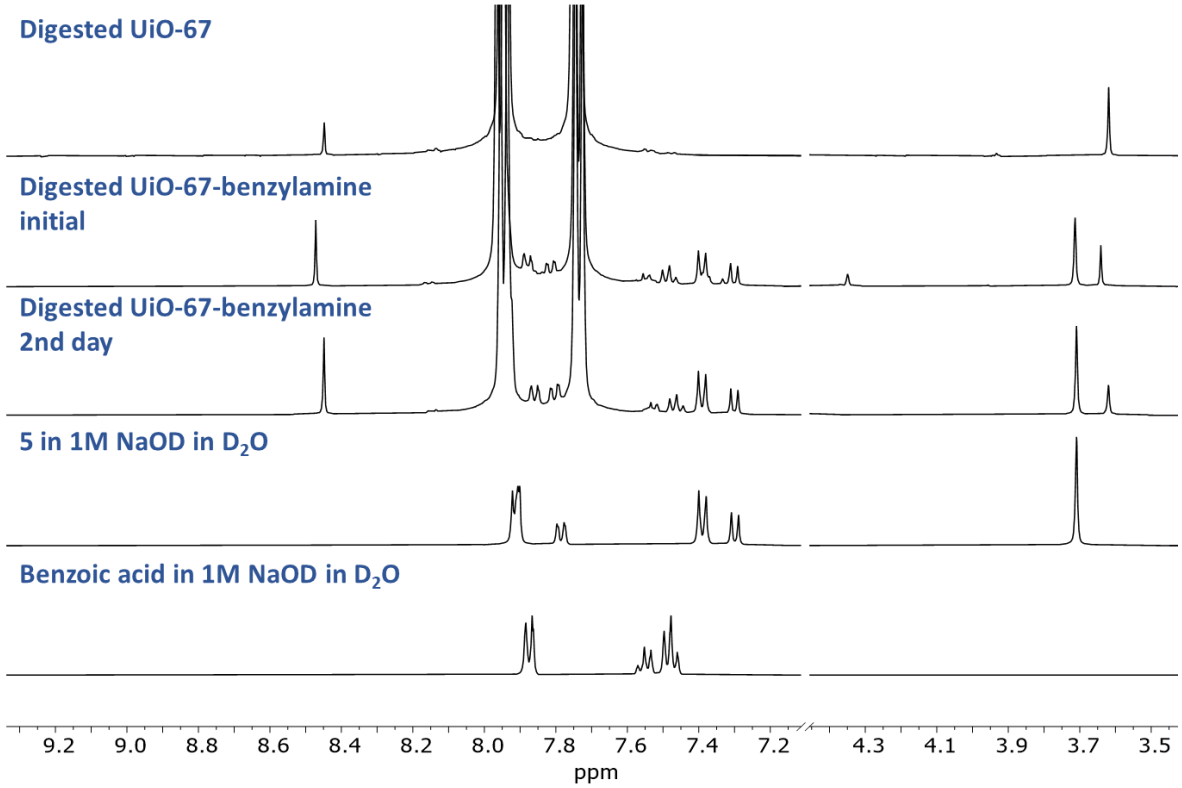

Figure 27: Stacked ^{1}H NMR (400 MHz, 1M NaOD in D_2O) spectra of digested UiO-67, UiO-67-benzylamine (initial), UiO-67-benzylamine (2nd day), **5** and benzoic acid.

The digestion of UiO-67-benzylamine revealed that the linker **5** has been successfully incorporated in the MOF. To verify the identity of the signals suspected to belong to **5**, the ^{1}H NMR sample was spiked with **5**. The intensity of these signals increased drastically, confirming the incorporation of **5** in the MOF.

From the ^{1}H NMR spectrum of digested UiO-67, it is apparent that only the linker biphenyl-4.4'-dicarboxylic acid was incorporated. No benzoic acid was present in the spectrum after the MOF was digested. Based on the ^{1}H NMR spectrum, the MOF exhibits a low degree of defectivity. Benzoate was however incorporated in the UiO-67-benzylamine MOF. This became apparent upon comparison of the ^{1}H NMR spectra of the digested MOF and the authentic sample of benzoate. Further studying of the ^{1}H NMR spectrum of the digested UiO-67-benzylamine revealed that there seemed to be an additional set of signals. These signals were overlapping with other signals and were not expected. It was therefore challenging to find out where they originated from. ^{1}H NMR spectra of the same sample was acquired the following day, at which point the additional set of signals was no longer present.

The disappearance of the additional set of signals with time in the basic media indicated that the unidentified species was unstable under basic conditions. At the same time, the intensity of the signals corresponding to **5** seemed to have increased slightly. It is therefore tempting to assume that the other species converts to **5** over time. The same seems to be the case for the increasing formate signal at 8.48 ppm, which might indicate that formate is formed together with **5**. This is however difficult to verify based on the MOF digestion only. Other experiments are needed to determine the origin of the second set of signals. This is investigated in **Chapter 5.2**

5.2 Synthesis of the formylated linker 12

The linker used for the MOF synthesis was of high NMR purity, supporting that the other species was formed during the MOF synthesis. To monitor the behavior of the linker during the MOF synthesis, it was attempted to recreate the MOF synthesis conditions in an NMR experiment. The linker was therefore subjected to treatment in DMF under acidic conditions. ^{1}H NMR spectra of **5** in DMF were initially obtained prior to addition of hydrochloric acid and right after the addition, all before heating. The next spectra were acquired after the NMR-tube was heated in oil bath at 130°C for 1h, 21h and two days, respectively (**Figure 28**).

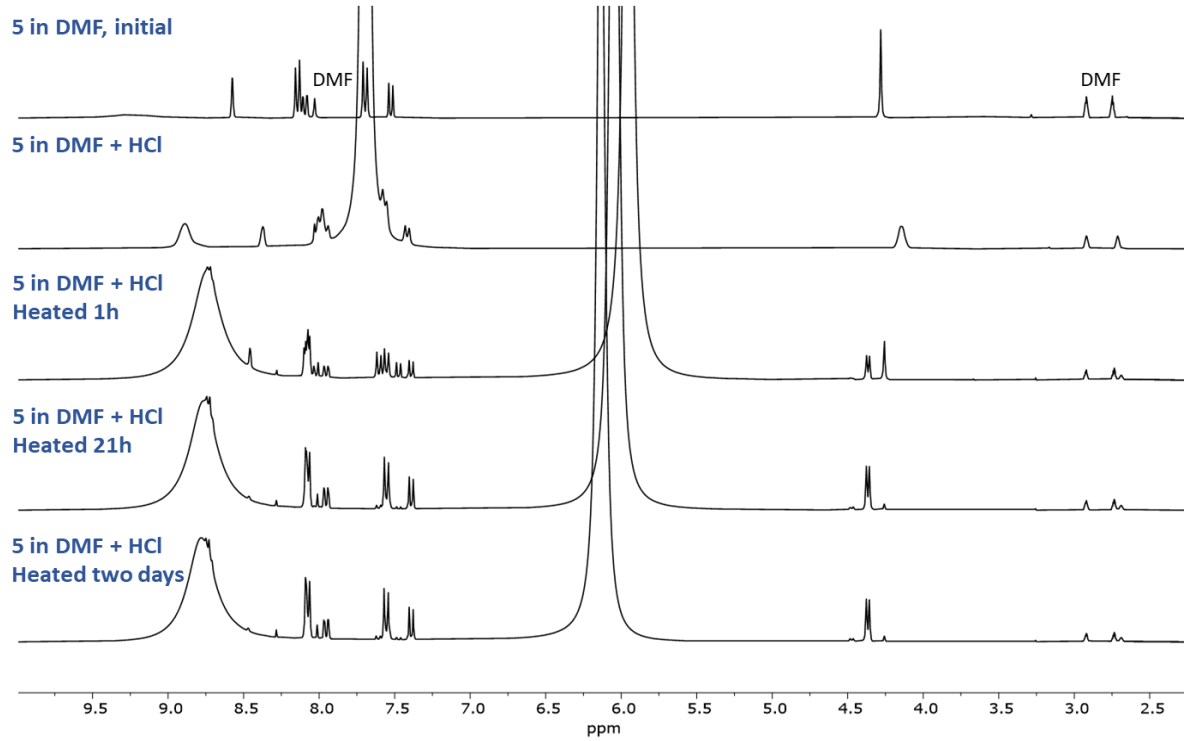

Figure 28: Stacked ^{1}H NMR (300MHz, DMF-d_7) spectra from the NMR experiment where the linker is submitted to acidic conditions with heating over time.

What is evident upon studying of the spectra from **Figure 28**, is that at least two sets of signals were present after heating the sample for one hour. The presence of **5** in trace amounts was confirmed by spiking with **5**. It was apparent that the reaction did not run to completion after two days of heating in an oil bath. Nevertheless, the purpose of this experiment was to determine if **5** undergoes unexpected reactions under conditions similar to those of MOF synthesis. This experiment confirmed formation of an unidentified species, which with high probability might be the one observed in **Figure 27** (Digested UiO-benzylamine initial).

Based on the NMR experiment, it was clear that another species was formed during the MOF synthesis. The next step was to find out what kind of a side reaction is taking place. In 2015 Zwolinski *et al*., reported a case where an unidentified species is observed in the UiO-66-NH_2 MOF.[107] The synthesis of the UiO-66-NH_2 MOF can be carried out based on several protocols that have been published. Most of these syntheses are based on the reaction between 2-amino-terephthalic acid and $ZrCl_4$ in DMF at elevated temperatures (80–120°C). The materials obtained from similar reactions have been reported to contain significant amounts of the same unidentified ligand.

Zwolinski *et al*. isolated the side product and identified it as 2-formamidoterephthalic acid (**Scheme 31**). The group stated that this side product could be formed in a transamidation reaction during the synthesis of UiO-66-NH_2, which occurred between the incorporated linker and DMF used as the solvent. This side reaction is difficult to avoid under the acidic conditions which are typical for the synthesis of many MOFs, and thus could easily occur in the synthesis of other amine-based MOFs.

Because of the similarity between 2-aminoterephthalic acid and **5**, it was suspected that the reactive amino group in **5** underwent the same formylation reaction as in the reported case.The suspected formylation and 2-formamidoterephthalic acid are shown in **Scheme 31**.

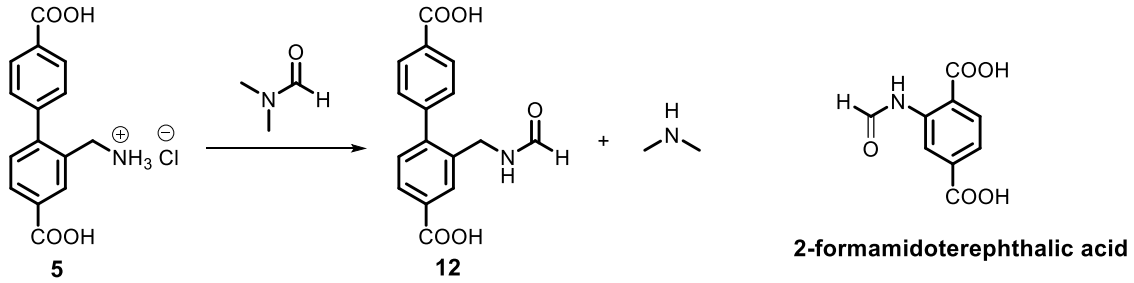

Scheme 31: The formylation of **5** in a reaction with DMF, and the side product isolated by Zwolinski *et al.*

The next step was to verify the formation of **12** by isolating and characterizing this compound. For this purpose, the conditions of MOF synthesis were mimicked shown in **Scheme 32**.

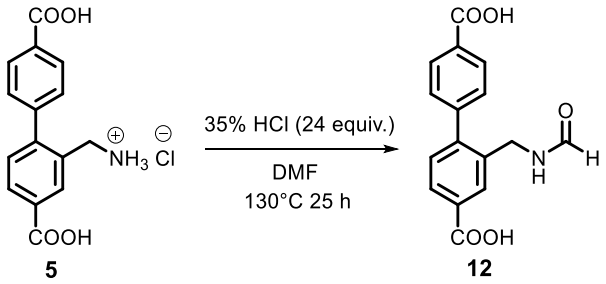

Scheme 32: The reaction conditions for formylation of **5**.

The formylation was carried out at 100 mg scale of **5**. The ^{1}H NMR spectra of the isolated product and **5** are given in **Figure 29**.

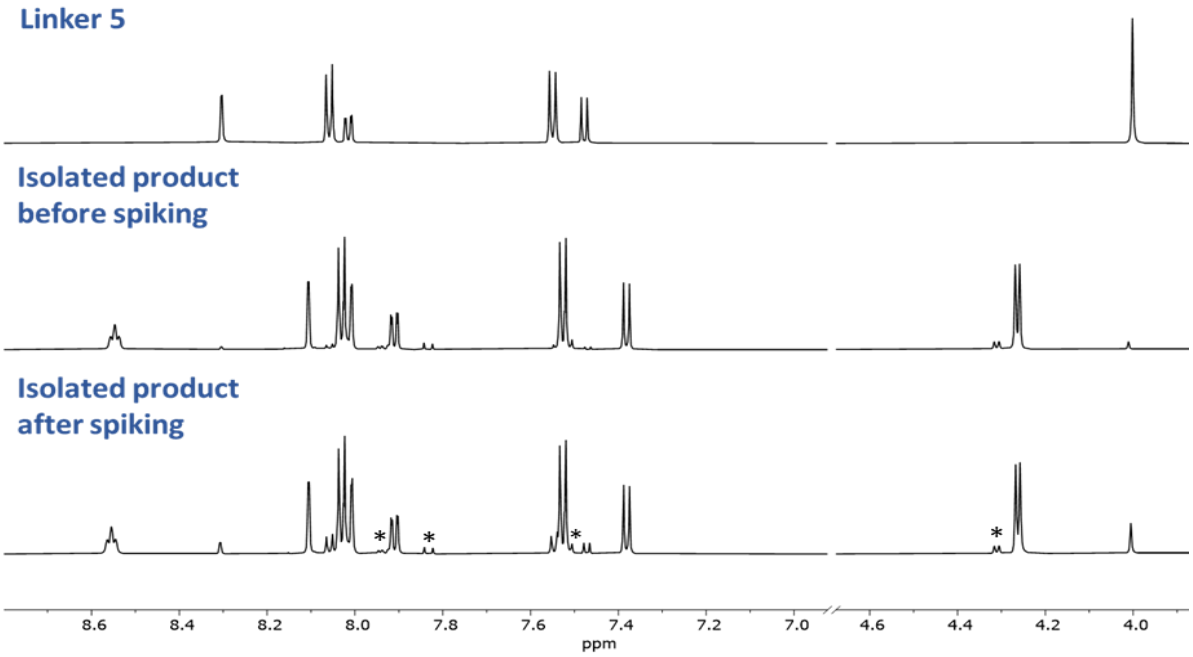

Figure 29: Selected regions of stacked ^{1}H NMR (600 MHz, DMSO-d_6) spectra of **5** (top), the isolated product before spiking with **5** (middle) and the isolated product after spiking (bottom). The signals of an unidentified side product are marked with "*".

As it is evident from **Figure 29**, **5** underwent a reaction under conditions similar to those employed in the MOF synthesis. This was already the conclusion after the NMR experiment, but this time the unidentified species was isolated. It was clear that full conversion of **5** was once again not achieved. The isolated product contained unreacted **5**, which was supported by the spiking of the sample with the linker. It was attempted to push the reaction to full conversion of **5** to **12** by doubling the equivalents of HCl and DMF. The reaction time was also increased from 25 hours to 72 hours. Full conversion was however not achieved, and there was no apparent difference in the ^{1}H NMR spectra of **12** obtained in these two reactions.

The identity of the formylated linker **12** was confirmed by ESI-MS, where the molecular ion of [**12**+Na]$^{+}$ was observed (m/z = 322.069). It is however difficult to determine the identity of the other side product (**Figure 29**, signals marked with "*" in the bottom spectrum). The set of signals resembles the major product in terms of the splitting pattern, especially the doublet in the aliphatic region. There is therefore a reason to believe that the other product resembles **12** in a high degree. The literature reports similar compounds isolated as mixtures of rotamers.[108, 109] The electrons of amides are delocalized, making the rotation around the amide bond slow enough to make the compound appear as two species, rotamers, in the ^{1}H NMR spectrum. It is therefore tempting to suspect that the side product is the minor rotamer. It is therefore tempting to suspect that the side product is the minor rotamer, although it was not investigated in detail.

After isolating **12**, its ^{1}H NMR spectrum was acquired in 1M NaOD in D_2O. The NMR sample was acquired immediately after the sample's preparation, followed by an NMR experiment the next day. The result is given in **Figure 30**.

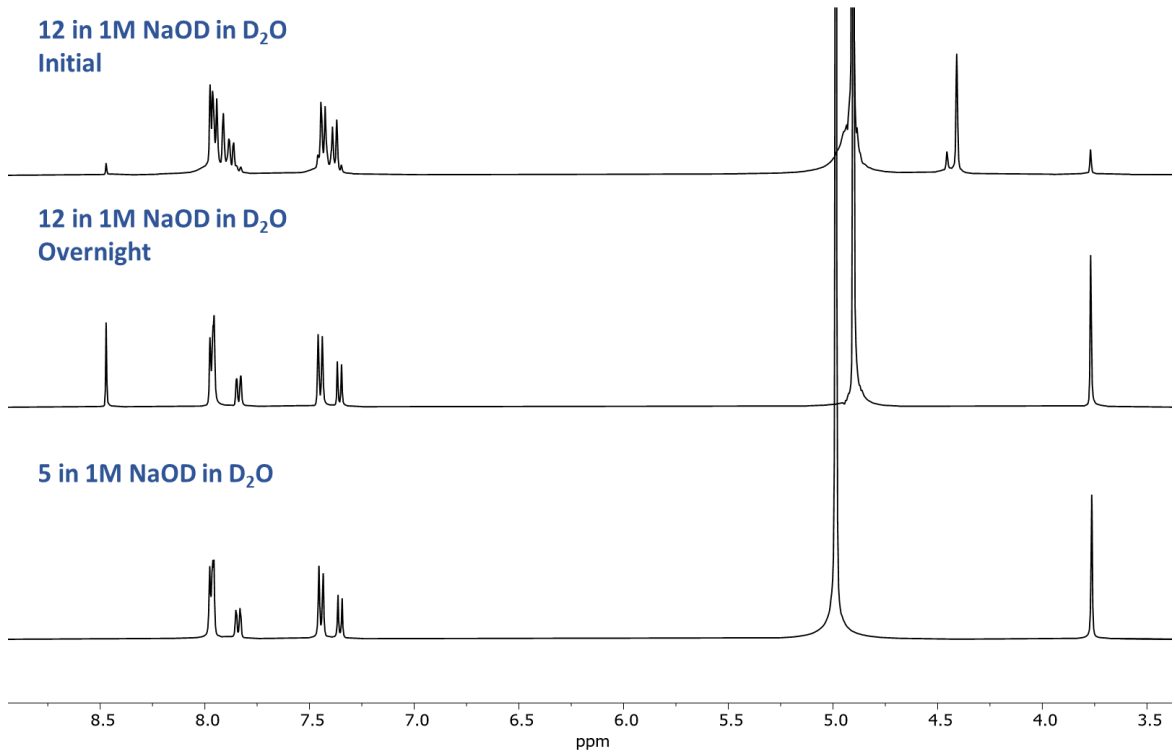

Figure 30: The ^{1}H NMR (1M NaOD in D_2O, 400 MHz) spectra of **12** digested overtime (top and middle) and digested **5 (**bottom**)**

The NMR experiment in **Scheme 32** verified the first assumption from the digestion of UiO-67-benzylamine: **12** converted to **5** over time in basic media. The NMR experiment revealed that **12** indeed converted to **5** over time**.** The hydrolysis of **12** to **5** was already observed in the initial spectrum of **12** in 1M NaOD in D_2O. When another spectrum of the same NMR sample was acquired the next day, **12** was fully converted to **5**. The formate signal was then the only difference between the spectrum of digested **5** and **12**. The observation made earlier about increasing signals of **5** and formate overtime was therefore confirmed to be true. The hydrolysis of **12** is given in **Scheme 33**.

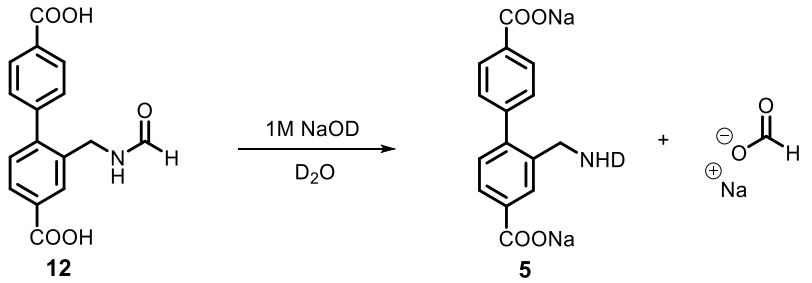

Scheme 33: Hydrolysis of **12** to **5.**

The attempted purification of **12** by recrystallization was not successful, as the product was found to be only partly soluble in DMSO. The product was therefore characterized with traces of the starting material and the side product present. The characterization of **12** is discussed in Chapter 4.4.

The ester derivative of **12**, **13**, was synthesized in the same manner. The idea behind **13** was to grow crystals, as the ester derivatives tend to be more soluble in most the solvents. However, no crystals were obtained. The compound **13** was further hydrolyzed resulting in deformylation and hydrolysis of the ester groups, leading to **5**. The reaction sequence from **4a** to **5** is given in **Scheme 34** with corresponding reaction conditions.

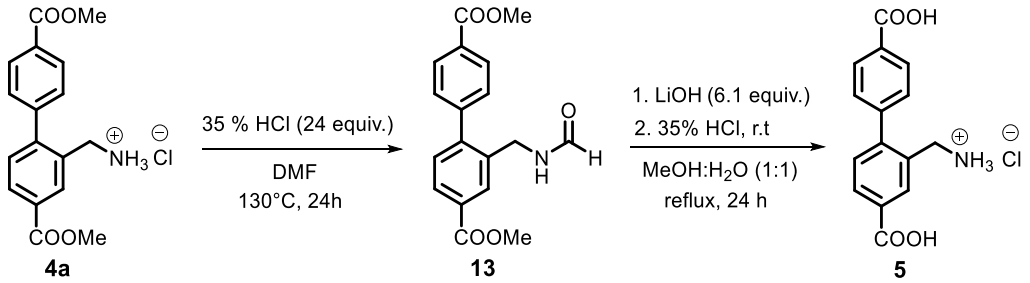

Scheme 34: Synthesis of **5** through hydrolysis of **13**, obtained by formylation of **4a**.

The isolated compound **13** appeared as a mixture of products in ^{1}H NMR spectrum, yet only one species was observed in the GC-MS spectrum (). Based on this, it was suspected that **13** appeared as two rotamers in the ^{1}H NMR, which is also suspected for **12**.

Combining the information from TGA, NMR and EDS the organic content of the UiO-67 MOF could be estimated. The organic content calculated for the synthesized UiO-67 and an ideal UiO-67 is given in **Figure 31**.

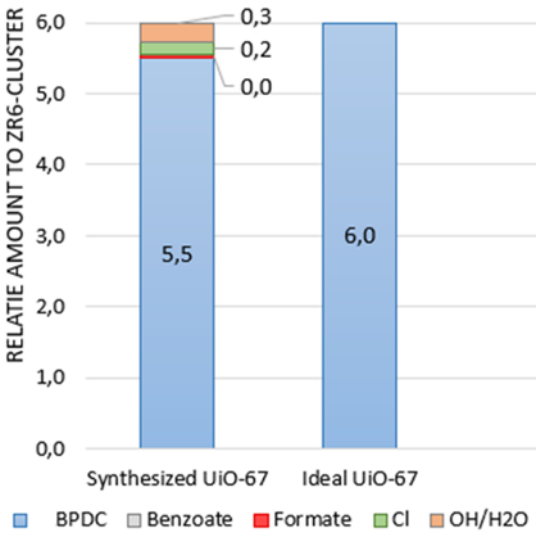

Figure 31: Composition of the constituents in the synthesized UiO-67 and UiO-67-benzylamine relative to Zr_6-cluster.

The calculation indicated that the synthesized UiO-67 was not defect-free, as hydroxide anions and water were present in the MOF. Their presence might be due to the charge compensation upon defectivity. Based on the ^{1}H NMR spectrum of the digested UiO-67, it was also found that negligible amounts of formate have been incorporated into the MOF, resulting in a 0.0% content per zirconium cluster. However, this is a rough estimate of the MOF content. The ideal UiO-67 exhibits no defectivity, with 100% incorporation of BPDC.

Estimating the organic content of UiO-67-benzylamine was also attempted in similar manner, but the overlapping signals in the ^{1}H NMR spectrum of the MOF disabled the calculations. The organic composition of UiO-67-benzylamine was therefore not estimated.

5.3 Attempted removal of the “protecting group” in UiO-67-benzylamine

The synthesized UiO-67-benzylamine MOF was characterized using various techniques such as powder XRD, TGA, SEM, EDX, nitrogen adsorption and NMR. Another interesting characterization method of the MOF would be testing of its CO_2 adsorption capabilities. Attempts were therefore made to enable this investigation.

As previously described, the increased basicity of the amino group of **5** might be beneficial for CO_2 adsorption. In order to investigate its potential, the amine should be present on its free form in the MOF. The linker **5** has been incorporated into the MOF as a hydrochloride salt. However, because the acidic conditions are a direct consequence of HCl being generated under the MOF synthesis, the linker would inevitably undergo protonation.

The inevitable amine protonation is not the only problem which has to be resolved in order to measure CO_2 adsorption. It has been shown that UiO-67-benzylamine contained formylated linker **12**, which means that the "protecting group" must be removed for the same reason. Because of the decomposition of **12** to **5** under the digestion conditions, it is difficult to determine their ratio in the formed MOF (UiO-67-benzylamine) It is also not clear how fast the hydrolysis happens. To estimate the amount of the formylated linker present in the MOF, digestion had to be performed in a medium where **12** was stable. UiO-67-benzylamine was therefore digested in 1 M D_3PO_4 (in DMSO-d_6) which revealed that the linker was mostly present as **12** in the MOF, with trace amounts of **5** (top spectrum)).

5.3.1 Attempted deformylation of UiO-67-benzylamine with methanol

The first attempt of deformylation of UiO-67-benzylamine was inspired by Zwolinski *et. al*., where removal of the discussed "protecting group" in UiO-66-NH_2 was explored.[107] The formylated linker could be deformylated post-synthetically upon treatment with methanol. Deformylation could be achieved by refluxing the MOF in methanol. The UiO-67-benzylamine was therefore refluxed in methanol for 24 hours. Digestion of the MOF in D_3PO_4 revealed that no evident deformylation occurred. This conclusion was based on the comparison of the UiO-67-benzylamine digested before and after reflux in methanol (**Appendix, Figure 190**). This indicated that the deformylation was unsuccessful.

5.3.2 Attempted deformylation of UiO-67-benzylamine with sodium sulfide

The next approach of deformylation was inspired by Wei *et al.*, where deformylation of similar organic compounds has been investigated.[110] However, the procedure is not developed for post-synthetic deformylation of MOFs. The deformylation is achieved by treatment with sodium sulfide in an aqueous solution. The drawback of utilizing such conditions on MOFs is that the framework tends to lose its crystallinity in basic aqueous solutions.[111] This happens because Zr

(IV) has higher affinity towards OH^- than oxygens from the carboxylates of the linkers.[111] Having this in mind, the deformylation has been attempted. The reaction conditions are given in **Scheme 35**.

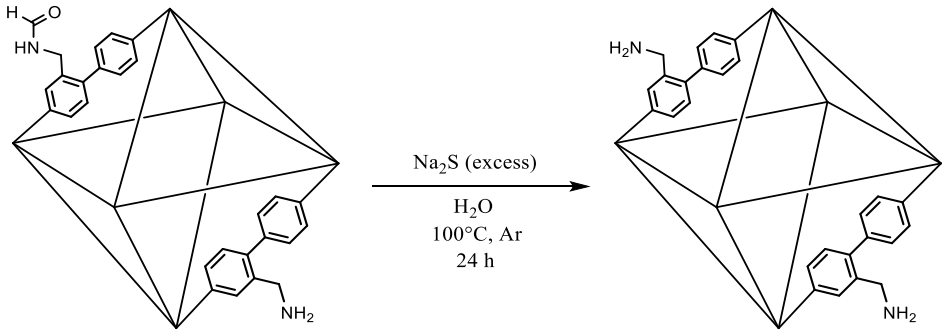

Scheme 35: Reaction conditions for attempted deformylation of UiO-67-benzylamine.

A suspension of UiO-67-benzylamine in water was heated at 100°C with an excess of sodium sulfide. After isolation, the solid was digested in 1 M D_3PO_4 (in DMSO-d_6). (**Figure 32**).

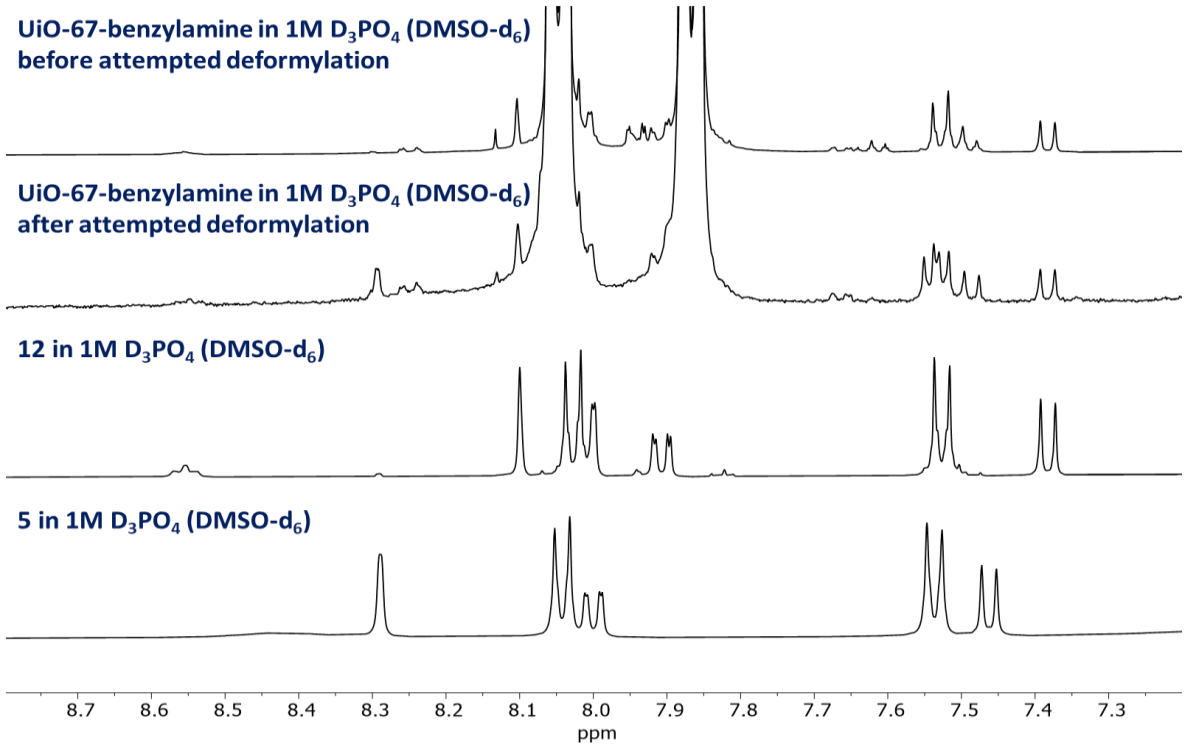

Figure 32: Stacked ^1H NMR (400 MHz, 1M D_3PO_4 in DMSO-d_6) spectra of the digested UiO-67-benzylamine before and after attempted deformylation, **12** and **5**.

The conclusion that can be drawn from this experiment is that the deformylation occurred to some extent. It is clear from **Figure 32** that the signals of **5** increased after the attempted deformylation, comparing to the spectrum of the MOF obtained before the attempt. It is however evident that more than 50 % of **12** is still present, suggesting that the deformylation was inefficient. It is possible that longer reaction time or larger amounts of sodium sulfide would push the reaction towards deformylation. It was however not investigated further due to time limitations.

Although the partial deformylation was observed, the basic media of aqueous Na2S could lead to decomposition of the MOF's framework. Analyzing the deformylated MOF by powder XRD was therefore required. Powder XRD revealed that UiO-67-benzylamine sustained its crystallinity. (**Appendix**, **Figure 192**) The porosity of the MOF could be evaluated by nitrogen adsorption measurements, which were not conducted due to time limitations.

5.4 Characterization of the formylated linker 12

The characterization of **12** was performed in a similar manner to the previously discussed compounds. Assignment of the aromatic and aliphatic signals was therefore mostly straightforward and based on the 2D NMR correlations and the splitting pattern of the signals. The quaternary carbons have been assigned based on HMBC. The ^{1}H NMR spectrum of **12** is given in **Figure 33**.

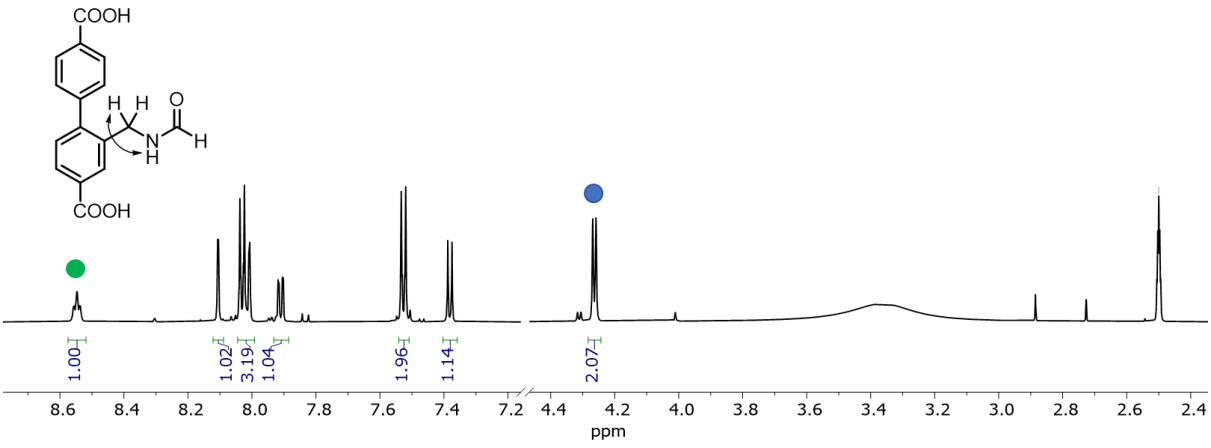

Figure 33: The ^{1}H NMR (600 MHz, DMSO-d_6) spectrum of **12**.

What is different for **12** comparing to the other discussed compounds is the methylene group which appears as a doublet (blue circle). For the other amine-based compounds (**4a**, **4b** and **5**) the methylene protons gave rise to a sharp or a broad singlet. This can be a result of the amine

protons taking part in proton exchange process with the solvent molecules, which is more rapid than the exchange of a formamide proton. The splitting is a clear indication that the methylene protons are coupling to another single proton. It is reasonable to assume that this single proton is the proton on the nitrogen atom, a neighbor to the methylene group. This is supported by the presence of a triplet at 8.55 ppm (green circle) which integrates for one proton, and the fact that there is a correlation between the doublet and the triplet in the COSY spectrum (marked with a black ring). The correlation in the COSY spectrum is marked with a black ring (**Figure 34**).

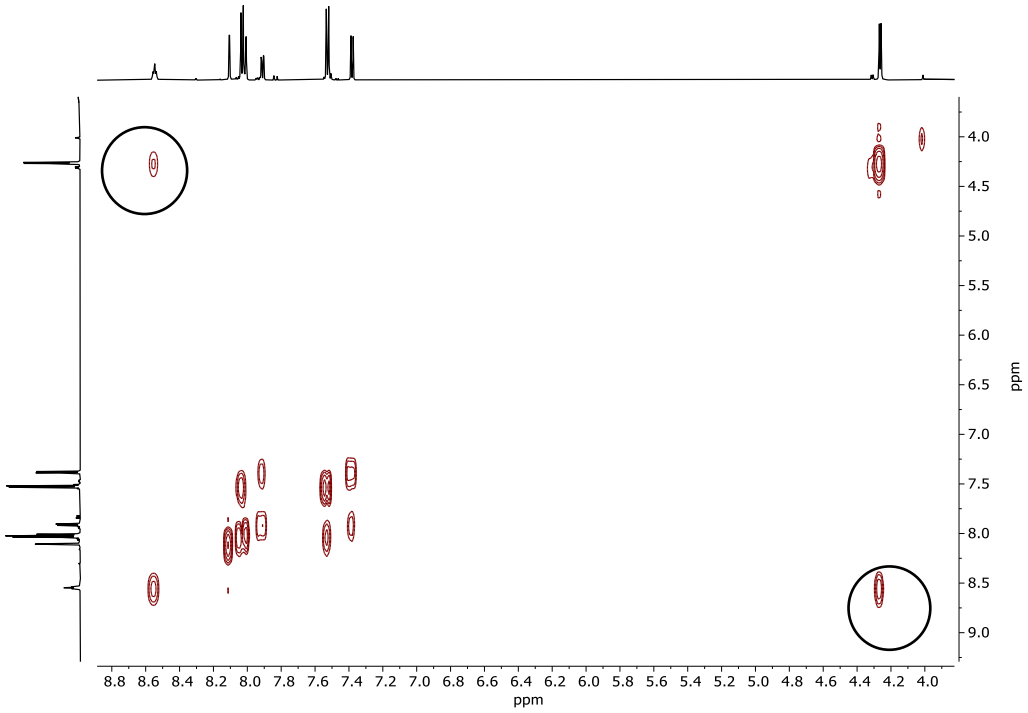

Figure 34: COSY spectrum of **12** (DMSO-d_6)

Furthermore, the triplet does not correlate to any carbon in HSQC, indicating that this proton must be the one on the nitrogen atom. This is in accordance with what is expected from the NMR data of **12**. The HSQC spectrum is given in **Figure 35**.

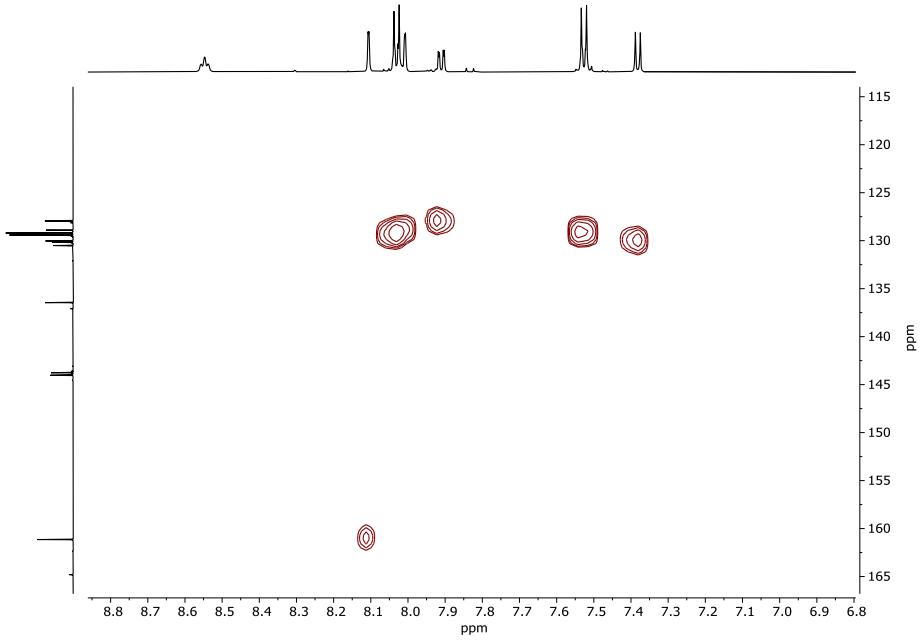

Figure 35: HSQC spectrum of **12** (DMSO-d_6)

The next step is to identify which of the two doublets (blue circles) that correspond to which of the two protons (in blue) in

Figure 36.

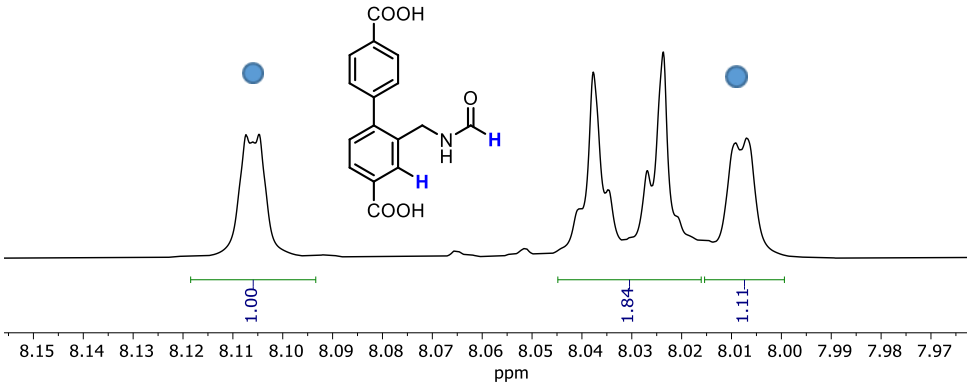

Figure 36: The two doublets

The signals cannot be accurately assigned based on the ^{1}H NMR spectrum only, as their splitting pattern and chemical shift is similar. However, the signals can be easily differentiated by HSQC. The carbon signal corresponding to the aromatic proton should come at a much lower ppm value comparing to the carbonyl. This was also observed in the HSQC spectrum in **Figure**

35. The structural information gained from analyzing the 2D spectra is also verified by a NOESY experiment, which shows the important correlations **Figure 37**

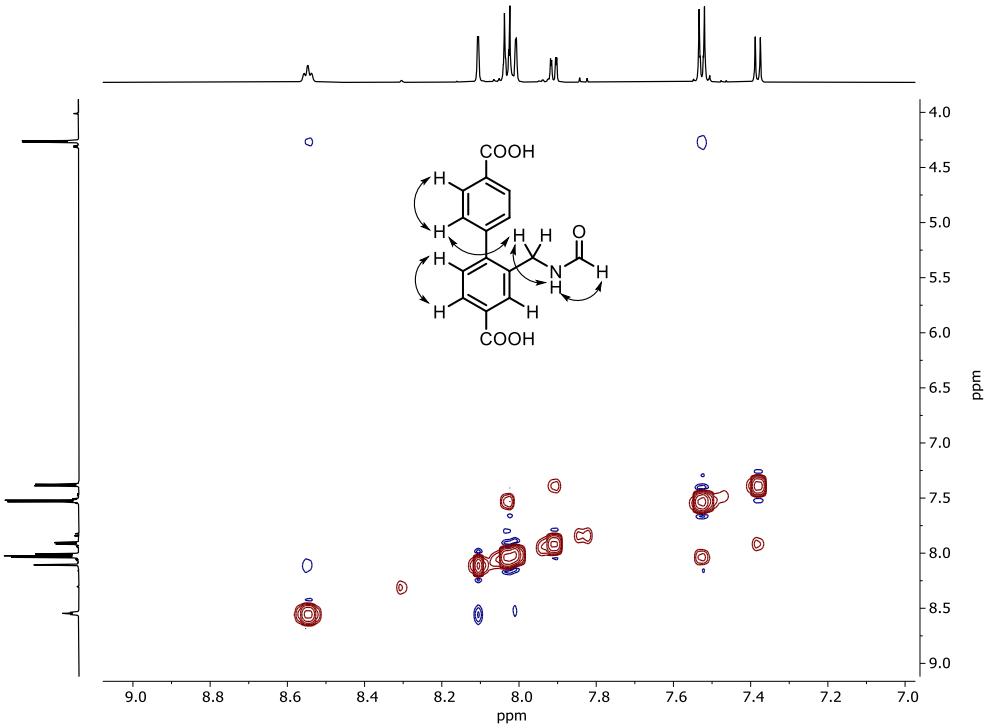

Figure 37: NOESY (600 MHz, DMSO-d6) spectrum of 12.

Another interesting experiment that can give valuable information about the splitting pattern is ^{1}H-^{15}N HMBC. This 2D experiment gives information about what protons are close to the nitrogen atom, in similar fashion to HMBC where long-range correlations between protons and carbons are observed. Additionally, the experiment can often show which proton is sitting on the nitrogen itself. ^{1}H-^{15}N HMBC is given in **Figure 38.**

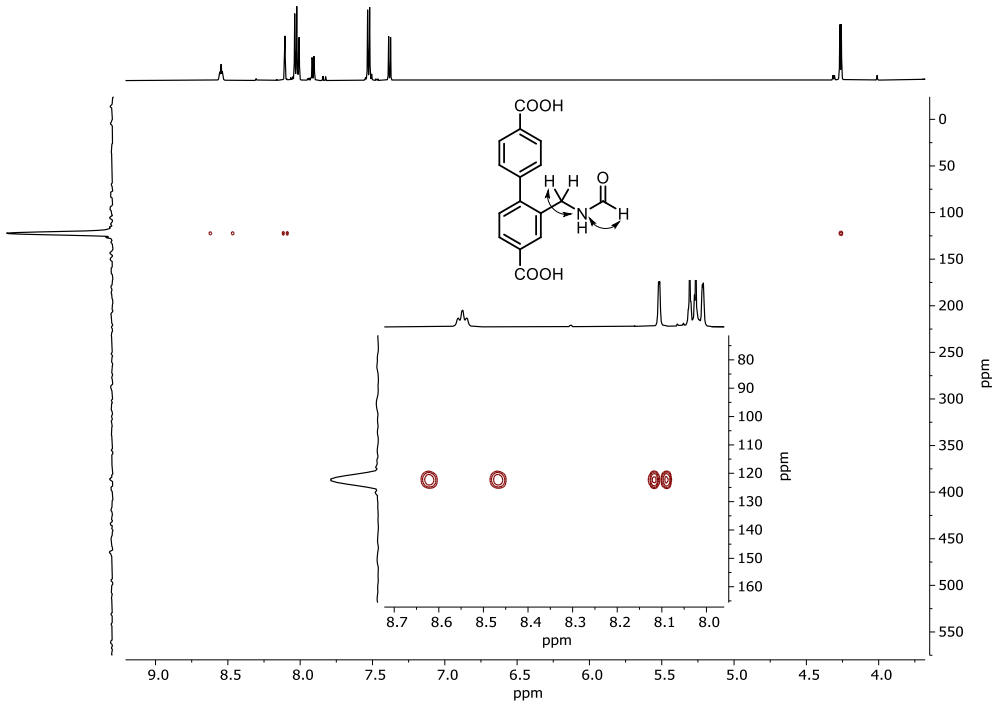

Figure 38: ^{1}H-^{15}N HMBC spectrum of **12** which shows a clear correlation between the nitrogen signal and the methylene protons, as well as the proton on the nitrogen itself.

The correlations given in **Figure 38** confirm that the methylene protons (doublet at 4.27 ppm) correlate to the nitrogen. It is also possible to see that the single proton directly attached to the carbonyl (doublet at 8.11 ppm) correlates to the nitrogen as well. This is in accordance with what was established about the structure of the isolated compound. Finally, the correlation between the triplet and the nitrogen signal indicates that this proton is in fact the one directly attached to the nitrogen.

2D NMR spectroscopy combined with the knowledge gained from ESI-MS enabled identifying the structure of **12**.

CHAPTER 6

Conclusion and further work

Two amine-based linkers, **5** and **9,** have been successfully synthesized and characterized with various characterization techniques, such as NMR, melting point measurements and elemental analysis. Some of the intermediates have also been characterized with IR.

It was demonstrated that the benzylamine linker **5** can be synthesized by two methods pathways, through the reduction of an azide intermediate and by Gabriel synthesis. The reduction of the azide intermediate could be achieved by Staudinger reaction as well as reduction with Zn/NH_4Cl. The linker 5 has been successfully incorporated into a UiO-67 type of MOF, which has been characterized with a range of techniques. It was found that the UiO-67-benzylamine has high surface area, which is promising for potential applications such as CO_2 adsorption and gas storage.

In addition, two synthetic strategies for the ethylamine linker **9** have been investigated. The synthesis route through the α, β-nitroalkene **11** did not lead to the desired product. However, the aldehyde **10** was successfully obtained from the benzyl bromide **2**, introducing possibilities for an alternative synthesis of linker **5**. The linker **9** was however successfully obtained through the reduction of 7, However, the reduction step requires further optimalization.

6.1 Further work

The developed syntheses of the linkers allow for further incorporation of them into MOFs and further investigation of the materials. Although the benzylamine linker **5** has been successfully incorporated into a UiO-67 type of MOF, there are other interesting characterization techniques which can still be utilized to characterize the MOF, such as CO_2-adsorption measurements. This requires further investigation of the deformylation of the MOF, where the reaction Na2S is a good starting point, which can possibly be to optimized. Incorporation of the ethylamine linker into a UiO-67 MOF, has not been investigated in this project. Synthesizing UiO-67-ethylamine and comparing its performance to the one of the benzylamine linker can give insight into how increased alkane chain influences adsorption of CO_2.

CHAPTER 7

Experimental

All chemicals were used as received from the commercial suppliers. Dry DMF and MeCN used in reactions were obtained from an MB SPS-800 Solvent Purification system from MBraun. NMR solvents were used as delivered from Cambridge Isotope and Sigma Aldrich Laboratories. Hexanes were distilled before use. Type 2 water was utilized in reactions. Thin layer chromatography was performed on 60 F_{254} silica coated aluminum plates from Merck. Flash chromatography was performed on silica gel from Merck (Silicagel 60, 0.040-0.063 mm) either manually or with an Isco Inc. CombiFlash Companion with PeakTrack software (v.1.4.10)

The NMR spectra were recorded with Bruker DPX200, DPX300, AVII400, AVIII400, AV600 and AVII600 spectrometers at ambient temperature, with residual solvent peaks as references. Chemical shift values (δ) are given in parts per million (ppm) relative to the utilized solvent. Reference peaks: $CDCl_3$: 7.26 ppm (^{1}H NMR), 77.0 ppm (^{13}C NMR). DMSO-d_6: 2.50 ppm (^{1}H NMR) and 39.5 ppm (^{13}C NMR), DMF-d_7: 2.94 ppm, 35.2 ppm (^{13}C NMR) and D_2O: 4.79 ppm (^{1}H NMR).

Mass spectra were obtained by Osamu Sekiguchi, using MicroMass Prospec Q (EI) and MicroMass QTOF 2W (ESI). All ESI-spectra were run in positive ion mode. IR spectra were obtained using the instrument Schimadzu IRAffinity-1. All melting points are uncorrected and were obtained with a Stuart SMP10 melting point apparatus. Elemental analysis was performed by Mikroanalytisches Laboratorium Kolbe, Oberhausen, Germany. PXRD patterns were collected with Bruker D8 Discovery diffractometer equipped with a focusing Ge-monochromator and a Bruker LYNXEYE detector. TGA analyses were performed on a NetzschSTA 449 F3-Jupiter instrument. Flow of a mixture of 5 mL/min O_2 and 20 mL/min of N_2 was utilized, with a ramp rate of 10 °C/min. The samples were transferred into an Al_2O_3 sample holder, and the data was collected for the temperature range of 30°C – 900 °C. SEM images were taken on a Hitachi SU8230 Field Emission Scanning Electron Microscope (FE-SEM). Nitrogen adsorption were performed with a BelSorp mini II instrument. In each measurement, the sample was pretreated at 150 °C for two hours under vacuum.

7.1 Synthesis of 1c

A solution solution of methyl-4-bromo-3-methylbenzoate (8.25 g, 36.0 mmol, 1.0 equiv.), 4-methoxycarbonylphenylboronic acid (6.48 g, 36 mmol, 1.0 equiv.), $Pd(dppf)Cl_2{\cdot}CH_2Cl_2$ (0.882 g, 1.08 mmol, 0.03 equiv.) and Cs_2CO_3 (17.6 g, 54 mmol, 1.5 equiv.) in dry DMF (170 mL) was stirred at 85 °C under argon flow for 22 h. The mixture was then cooled to room temperature followed by addition of water (ca. 100 mL) and stirred for 1h. The precipitation was isolated by vacuum filtration. The solids were dissolved in CH_2Cl_2, filtered through a silica plug and evaporated. The obtained crude was recrystallized from EtOH to give **1c** as a white-pinkish powder (8.69 g, 30.6 mmol, 85 %).

^{1}H NMR (600 MHz, $CDCl_3$): δ 8.10 ("d", *J* = 8.4 Hz, 2H, **3'-H**), 7.96 (s, 1H, **3-H**), 7.90 (dd, *J* = 8.0, 1.1 Hz, 1H, **5-H**), 7.39 ("d", *J* = 8.4, 2H, **2'-H**), 7.29 (d, *J* = 7.9 Hz, 1H, **6-H**), 3.95 (s, 3H, **8'-H**) 3.94 (s, 3H. **8-H**), 2.30 (s, 3H, **9-H**).

^{13}C NMR (151 MHz, $CDCl_3$): δ 167.14 (**7**), 167.02 (**7'**), 145.80 (**1'**), 145.56 (**1**), 135.69 (**2**), 131.77 (**3**), 129.81 (**6**), 129.70 (**4**), 129.63 (**3'**), 129.33 (**4'**), 129.14 (**2'**), 127.23 (**5**), 52.35 (**8'**), 52.31 (**8**), 20.49 (**9**).

MS (ESI, MeCN): 307.094 ($[M+Na]^+$, 100), 308.097 (16), 325.105 ($[M+Na+H_2O]^+$, 49)
HRMS (ESI, MeCN): 307.0946 calculated for $C_{17}H_{16}O_4Na$, found: 307.0941 (0.0 ppm)

M_p: 119-120 °C

The spectroscopic data[112] and melting point[113] are in coherence with what is previously reported in the literature.

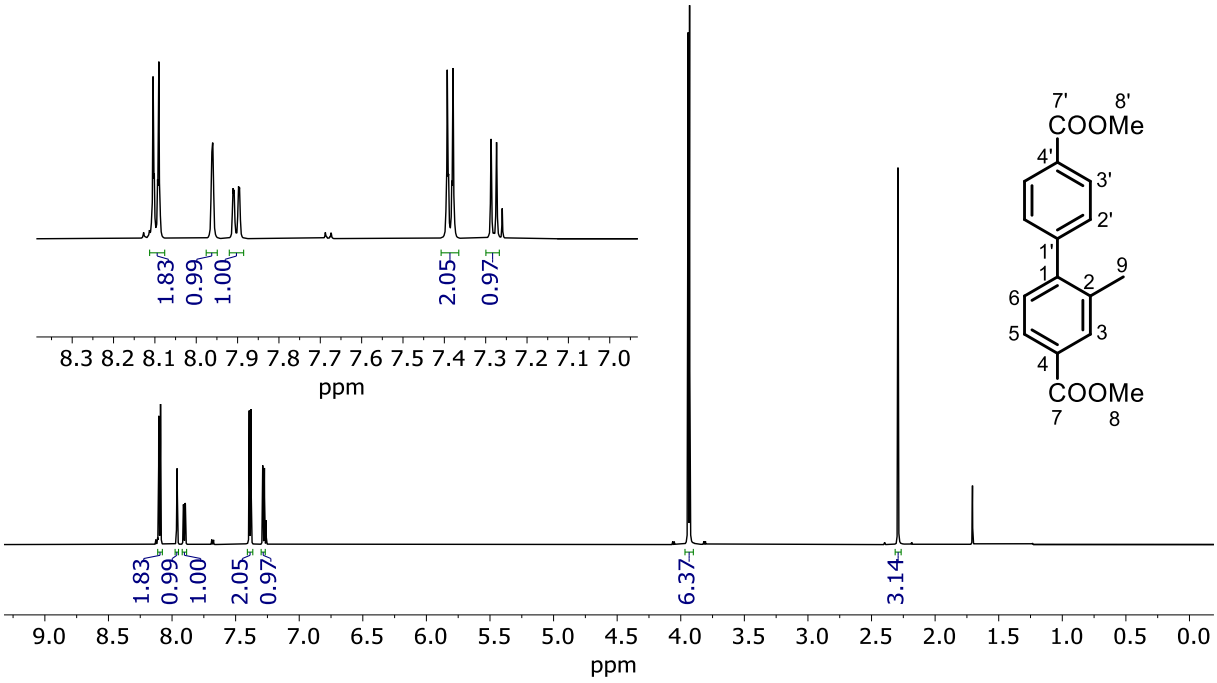

Figure 39: ^{1}H NMR (600 MHz, $CDCl_3$) spectrum of **1c**.

7.2 Synthesis of 2

A solution of **1c** (4.00 g, 14.1 mmol, 1.0 equiv.), NBS (3.01 g, 16.9 mmol, 1.2 equiv.) and AIBN (0.231 g, 1.41 mmol, 0.1 equiv.) in acetonitrile (40 mL) was refluxed for 4 h under argon flow. Cooling the solution in a freezer resulted in the precipitation of **2**, which was isolated by filtration in a Buchner funnel. The solids were washed with *i*PrOH yielding **2** as a yellow powder (4.42 g, 12.2 mmol, 87%).

^{1}H NMR (600 MHz, $CDCl_3$): δ 8.22 (d, *J* = 1.8 Hz, 1H, **3-H**), 8.14 ("d", *J* = 8.3 Hz, 2H, **3'-H**), 8.02 (dd, *J* = 8.0, 1.8 Hz, 1H, **5-H**), 7.53 ("d", *J* = 8.2 Hz, 2H, **2'-H**), 7.33 (d, *J* = 8.0 Hz, 1H, **6-H**), 4.42 (s, 2H, **9-H**), 3.96 (s, 6H, **8-H** and **8'-H**)

^{13}C NMR (151 MHz, $CDCl_3$): δ 166.8 (**7'**), 166.4 (**7**), 145.5 (**1**), 144.0 (**1'**), 135.8 (**2**), 132.5 (**3**), 130.6 (**6**), 130.5 (**4**), 130.0 (**4'**), 129.9 (**3'**), 129.7 (**5**), 129.0 (**2'**), 52.5 (**8'** or **8**), 52.4 (**8'** or **8**), 30.9 (**9**).

MS (ESI, MeCN) (rel. %): 385.005 ($[M+Na]^+$, 100), 387.003 ($[M+Na]^+$, 99.5), 386.007 (20)

HRMS (ESI, MeCN): 385.0051 calculated for $C_{17}H_{15}BrNaO_4$, found: 385.0046 (0.1 ppm)

Mp: 123-124 °C

The spectroscopic data is in coherence with what is previously reported in the literature.[112] The melting point was not previously reported.

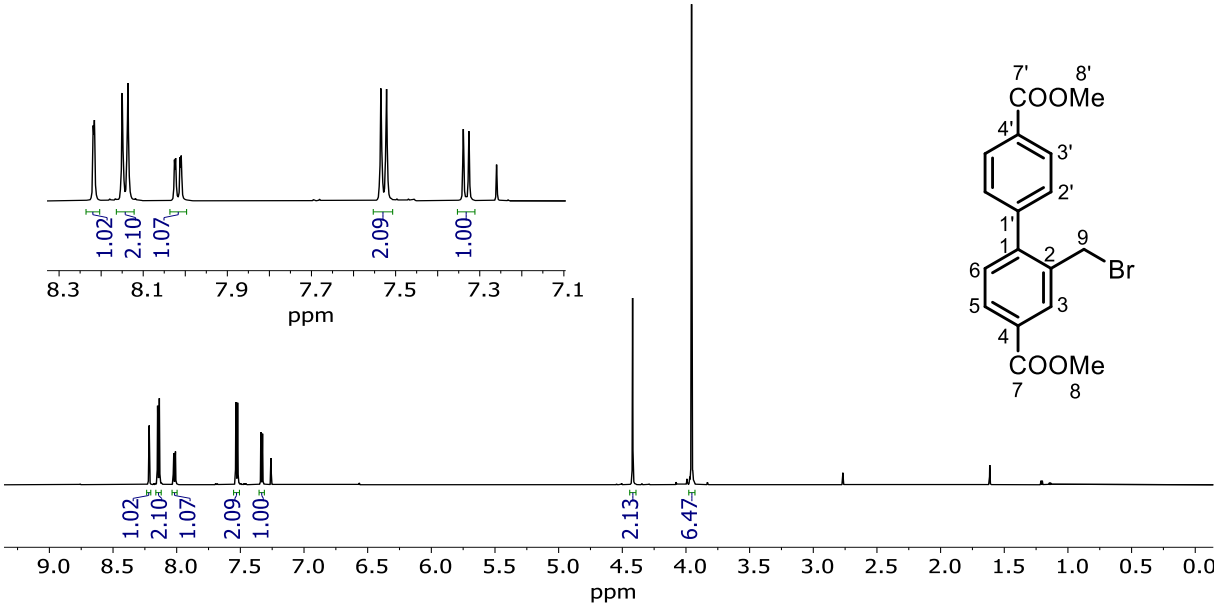

Figure 40: ^{1}H NMR (600 MHz, $CDCl_3$) spectrum of **2**.

7.3 Synthesis of 3a

A solution of **2** (2.00 g, 5.51 mmol. 1.0 equiv.) and NaN_3 (1.07 g, 16.5 mmol, 3.0 equiv.) was refluxed in EtOH (50 mL) for 30 min. The precipitation from the hot solution was isolated by filtration and the product was extensively washed with water, yielding **3a** as a white solid (1.70 g, 5.24 mmol, 95 %).

^{1}H NMR (600 MHz, $CDCl_3$) δ 8.15 (d, *J* = 1.8 Hz, 1H, **3-H**), 8.13 ("d", *J* = 8.3 Hz, 2H, **3'-H**), 8.08 (dd, *J* = 7.9, 1.8 Hz, 1H, **5-H**), 7.43 ("d", *J* = 8.3 Hz, 2H, **2'-H**), 7.40 (d, J = 8.0 Hz, 1H, **6-H**), 4.32 (s, 2H, **9-H**), 3.97 (s, 3H, **8-H**), 3.96 (s, 3H, **8'-H**).

^{13}C NMR (151 MHz, $CDCl_3$): δ 166.8 (**7'**), 166.5 (**7**), 145.7 (**1**), 144.1 (**1'**), 133.4 (**2**), 131.1 (**3**), 130.6 (**6**), 130.3 (**4**), 130.0 (**4'**), 129.9 (**3'**), 129.7 (**5**), 129.2 (**2'**), 52.5 (**8** or **8'**), 52.5 (**8** or **8'**), 52.4 (**9**).

MS (ESI, MeCN) (rel. %): 348.096 ($[M+Na]^+$, 100), 349.099 (19)

HRMS (ESI, MeCN): 348.0960 calculated for: $C_{17}H_{15}N_3O_4Na$, found: 348.0955 (-0.1 ppm)

IR (KBr): *ν*(N=N=N): 2100 cm^{-1}, *ν*(C=O): 1726 cm^{-1}, *ν*: 1285 cm^{-1}

This compound has not been previously reported.

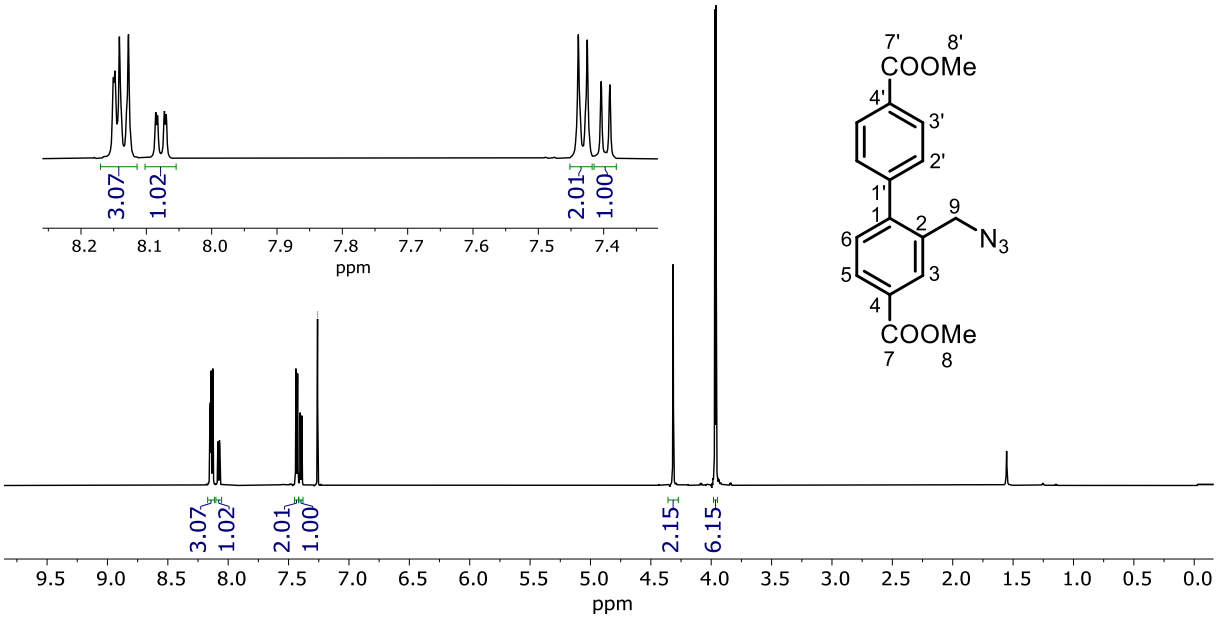

Figure 41: ^{1}H NMR (600 MHz, $CDCl_3$) spectrum of **3a**.

7.4 Synthesis of 4a by Staudinger reaction

A solution of **3a** (0.500 g, 1.54 mmol, 1.0 equiv.) and PPh_3 (0.443 g, 1.68 mmol, 1.1 equiv.) was refluxed in MeOH (50 mL) for 1.5 h. After cooling to room temperature, the solvent was removed under reduced pressure. The yellow oil was dissolved in toluene (30 mL) and filtrated. The clear filtrate was transferred to a separatory funnel and shaken with 1M HCl (15 mL). The precipitation in the aqueous phase was filtrated and washed with toluene yielding **4a** as a white solid (0.350 g, 1.04 mmol, 68 %).

^{1}H NMR (600 MHz, DMSO-d_6): δ 8.55 (br. s, 3H, -N**H**$_3$), 8.35 (d, *J* = 1.7 Hz, 1H, **3-H**), 8.08 ("d", *J* = 8.3 Hz, 2H, **3'-H**), 8.03 (dd, *J* = 8.0, 1.8 Hz, 1H, **5-H**), 7.60 ("d", *J* = 8.3 Hz, 2H, **2'-H**), 7.50 (d, *J* = 8.0 Hz, 1H, **6-H**), 3.99 (s, 2H, **9-H**), 3.91 (s, 3H, 12-H), 3.89 (s, 3Hz, 1-H).

^{13}C NMR (151 MHz, DMSO-d_6): δ 166.0 (**7'**), 165.8 (**7**), 145.0 (**1**), 143.4 (**1'**), 132.2 (**2**), 130.6 (**6**), 129.8 (**3**), 129.7 (**2'**), 129.6 (**4**), 129.4 (**3'**), 129.3 (**4'**), 129.0 (**5**), 52.5 (**12** or **1**), 52.4 (**1** or **12**), 39.2 (**9**).

MS (ESI, MeCN): 300.123 ($[M+H]^+$, 100), 301.126 (18), 283.096 ($[M-NH_2]^+$, 14),

HRMS (ESI, MeCN): 300.1235 calculated for: $C_{17}H_{18}NO_4$, found: 300.1230 (0.1 ppm)

M_p: 210-211 °C

This compound has not been previously reported.

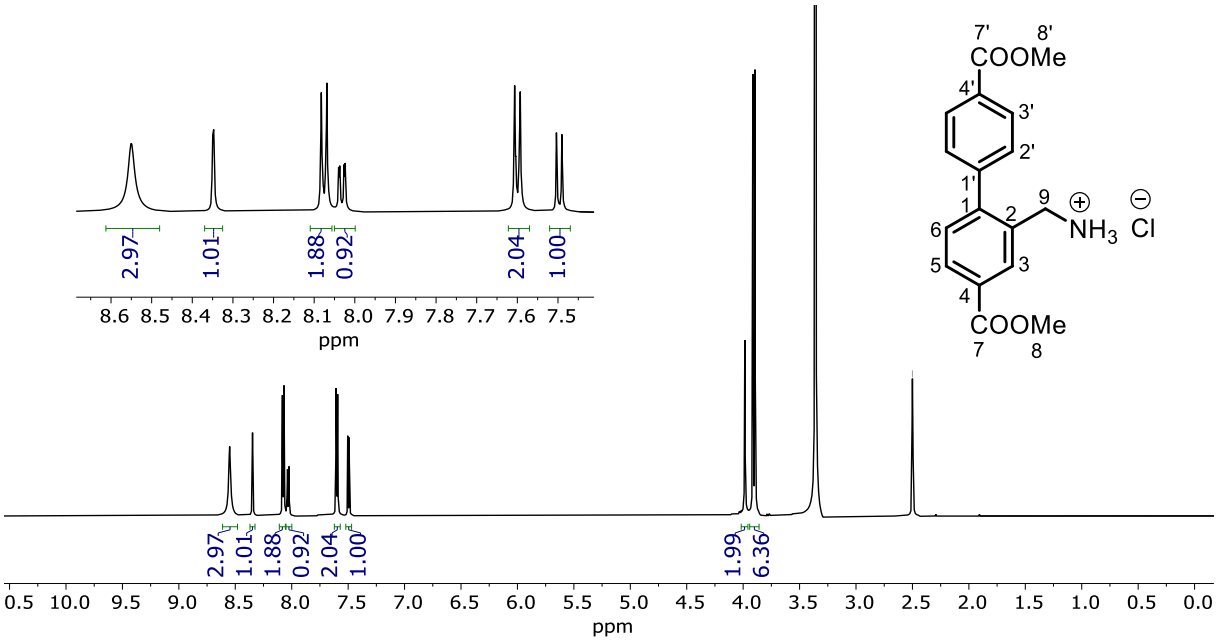

Figure 42: ^{1}H NMR (600 MHz, DMSO-d_6) spectrum of **3a**.

7.5 Synthesis of 4a by reduction with Zn/NH_4Cl

Zn (0.0323 g, 0.494 mmol, 1.6 equiv.) was added to a solution of **3a** (0.101 g, 0.309 mmol, 1.0 equiv.) and NH_4Cl (0.0428 g, 0.798 mmol, 2.6 equiv.) in EtOH/H_2O (3:1) (10 mL) and refluxed for 22 h. After the reaction was complete, the solvent was removed under reduced pressure. The crude product was dissolved in EtOAc (40 mL) and added 28% NH_4OH (4 mL), and the solution was stirred for 30 min. The phases were separated, and the organic phase was washed with brine (25 mL) and dried with Na_2SO_4 followed by filtration. The solvent was removed under reduced pressure. The crude product was dissolved in toluene (8 mL) and 35% HCl (40.9 µL, 1.5 equiv.) was added, resulting in the precipitation of white solid over the course of one hour of stirring. The product was then isolated by filtration with a glass frit filter, yielding **4a** (0.0510 g, 0.153 mmol, 50 %) as a white solid. The product was pure by ^1H NMR with minor solvent residues and other small impurities.

7.6 Synthesis of 4a from 2 by reduction of 3a in a one-pot reaction

A solution of **2** (0.500 g, 1.38 mmol, 1.0 equiv.) and NaN_3 (0.134 g, 2.06 mmol, 1.5 equiv.) in MeOH (20 mL) was refluxed for 30 min, followed by addition of PPh_3 (1.44 g, 5.49 mmol, 4.0 equiv.). The reaction mixture was refluxed for another 1.5 h. After cooling to room temperature, the reaction mixture was diluted with EtOAc (80 mL) and washed with water (3x80mL). The organic phase was dried with Na_2SO_4, filtered and the solvent was removed under reduced pressure. The yellow crude oil was dissolved in toluene (15 mL) and 35% HCl (183 µL, 1.5 equiv.) was added resulting in precipitation of white solid. The solution was stirred for 1h, before the white precipitation was obtained by filtration. The solids were extensively washed with toluene, followed by washing with CH_2Cl_2 yielding **4a** as a white solid (0.197 g, 0.587 mmol, 43 %).

7.7 Synthesis of 5

A solution of **4a** (0.500 g, 1.49 mmol, 1.0 equiv.) and LiOH (0.218 g, 9.09 mmol, 6.1 equiv.) in MeOH (20 mL) and water (20 mL) was refluxed for 20 h. After cooling to room temperature, the reaction mixture was filtrated. The pH of the filtrate was then adjusted with 35% HCl until pH = 1, and precipitation was observed. The precipitation was filtrated and washed with water, before drying at room temperature for four days yielding **5** as a white solid (0.365 g, 1.19 mmol, 80 %).

^{1}H NMR (600 MHz, DMSO-d_6): δ 8.31 (d, *J* = 1.7 Hz, 1H, **3-H**), 8.05 ("d", *J* = 8.3, 2H, **3'-H**), 8.01 (dd, *J* = 7.9, 1.7 Hz, 1H, **5-H**), 7.56 ("d", *J* = 8.2, 2H, **2'-H**), 7.47 (d, *J* = 7.9 Hz, 1H, **6-H**), 3.99 (s, 2H, **8-H**).

^{13}C NMR (151 MHz, DMSO-d_6): δ 167.0 (**7'**), 166.8 (**7**), 144.7 (1), 143.1 (**1'**), 131.9 (**2**), 130.8 (**4**), 130.5 (**6**), 130.4 (**4'**), 129.8 (**3**), 129.5 (**2'**), 129.5 (**3'**), 129.1 (**5**), 39.3 (**8**).

^{15}N(^{1}H) NMR (600 MHz, DMSO-d_6): δ 228 (**N**H_3).

MS (ESI, MeCN): 272.092 ($[M+H]^+$, 100), 273.095 (17)

HRMS (ESI, MeCN): 272.0922 calculated for: $C_{15}H_{14}NO_4$, found: 272.0917 (0.2 ppm)

EA: calculated for $C_{15}H_{14}ClNO_4$: C: 58.55, H: 4.59, N: 4.55. Found: C: 59.01, H: 4.72, N: 4.59.

M_p: > 300°C

This compound has not been previously reported.

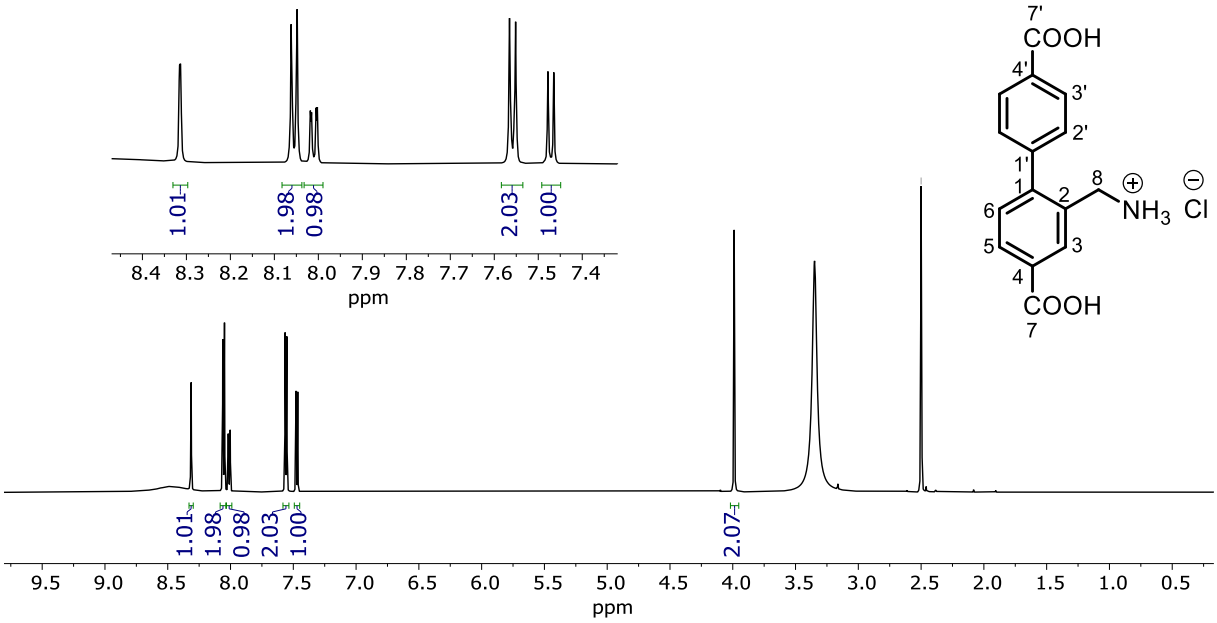

Figure 43: ^{1}H NMR (600 MHz, DMSO-d_6) spectrum of **5**.

7.8 Synthesis of 3b

A solution of **2** (1.00 g, 2.76 mmol, 1.0 equiv.), phthalimide (0.447 g, 3.03 mmol, 1.1 equiv.) and K_2CO_3 (0.762 g, 5.51 mmol, 2.0 equiv.) was heated in DMF mL) at 65 °C for 24 h. To the cooled reaction mixture water (100 mL) was added and the solution was allowed to stir for 30 min. The precipitation was isolated by filtration and was washed with water. Recrystallization from EtOH yielded **3b** as a white solid (0.693 g, 1.61 mmol, 58 %).

^{1}H NMR (600 MHz, $CDCl_3$) δ 8.5 ("d", *J* = 8.5 Hz 2H, **3'-H**), 7.98 (dd, *J* = 8.0, 1.7 Hz, 1H, **5-H**), 7.93 (d, 1H, *J* = 1.1 Hz, **3'-H**), 7.84 – 7.78 (m, 2H, **12-H**), 7.74 – 7.69 (m, 2H, **13-H**), 7.51 ("d", *J* = 8.5 Hz, 2H, **2'-H**), 7.32 (d, *J* = 7.9 Hz, 1H, **6-H**), 4.82 (s, 2H, **9-H**), 3.95 (s, 3H, **8'-H**), 3.87 (s, 3H, **8-H**).

^{13}C NMR (151 MHz, $CDCl_3$): δ 168.0 (**10**), 166.9 (**7'**), 166.6 (**7**), 145.1 (**1**), 144.5 (**1'**), 134.3 (**13**) , 134.2 (**2**), 132.1 (**11**), 130.4 (**6**), 130.3 (**4**) , 129.9 (**3'**), 129.8 (**4'**), 129.3 (**2'**), 128.7 (**3**), 128.7 (**5**), 123.6 (**12**), 52.4 (**8, 8'**), 39.3 (**9**).

MS (ESI, MeCN) (rel. %): 452.110 ($[M + Na]^+$, 100), 453.114 (28), 486.084 ($[M+K]^+$, 36)

HRMS (ESI, MeCN): 452.1110 calculated for: $C_{25}H_{19}NO_6Na$, found: 452.1104 (0.0 ppm)

M_p: 172-173 °C

This compound has not been previously reported.

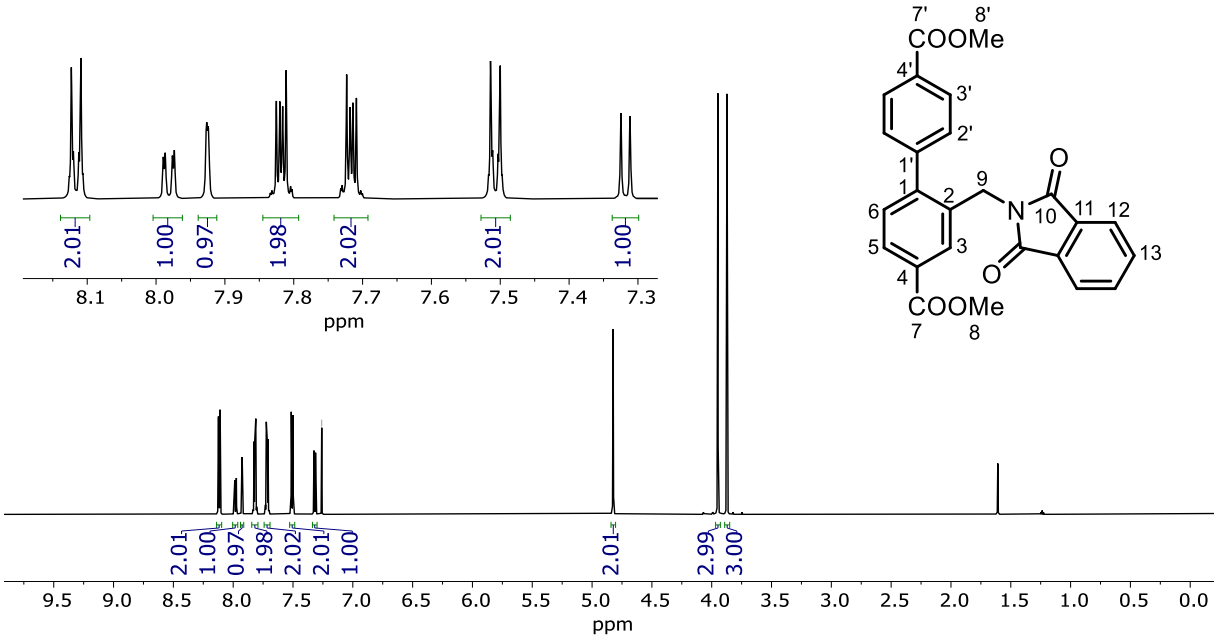

Figure 44: ^{1}H NMR (600 MHz, $CDCl_3$) spectrum of **3b**.

7.9 Synthesis of 4b

Hydrazine hydrate (330 µL, 6.80 mmol, 5.8 equiv.) was added to a solution of **3b** (0.500 g, 1.16 mmol, 1.0 equiv.) in EtOH (60 mL). The solution was heated at reflux for 2 h. The solution was cooled with an ice bath, and precipitation of phthalhydrazide was observed. The solid was filtrated and washed with cold EtOH (10-15 mL). The filtrate was diluted with CH_2Cl_2 (125 mL) and washed with water (3x100 mL). The organic phase was then dried with Na_2SO_4 and filtrated. The solvent was removed under reduced pressure, yielding **4b** as a white solid (0.291 g, 0.972 mmol, 83 %).

^{1}H NMR (600 MHz, $CDCl_3$): 8.18 (d, *J* = 1.7 Hz, 1H, **3-H**), 8.11 ("d", *J* = 8.3, 2H, **3'-H**), 7.98 (dd, J = 7.9, 1.8 Hz, 1H, **5-H**), 7.43 ("d", *J* = 8.3, 2H, **2'-H**), 7.30 (d, J = 7.9 Hz, 1H, **6-H**), 3.95 (s, 3H, **8'-H**), 3.94 (s, 3H, **8-H**), 3.83 (s, 2H, **9-H**).

^{13}C NMR (151 MHz, $CDCl_3$): δ 167.0 (**7**), 166.9 (**7'**), 145.1 (**1'**), 144.9 (**1**), 140.9 (**2**), 130.2 (**6**), 130.1 (**4**), 129.8 (**3'**), 129.6 (**4'**), 129.5 (**3**), 129.1 (**2'**), 128.1 (**5**), 52.38 (8' or 8), 52.36 (8' or 8), 43.9 (**9**).

MS (ESI, MeCN) (rel. %): 300.1230 ($[M+H]^+$, 100), 301.1264 (19), 283.0965 (17)

HRMS (ESI, MeCN): 300.1230, calculated for $C_{17}H_{18}NO_4$, found: 300.1230 (0.0 ppm)

M_p: 111-112 °C

This compound has not been previously reported.

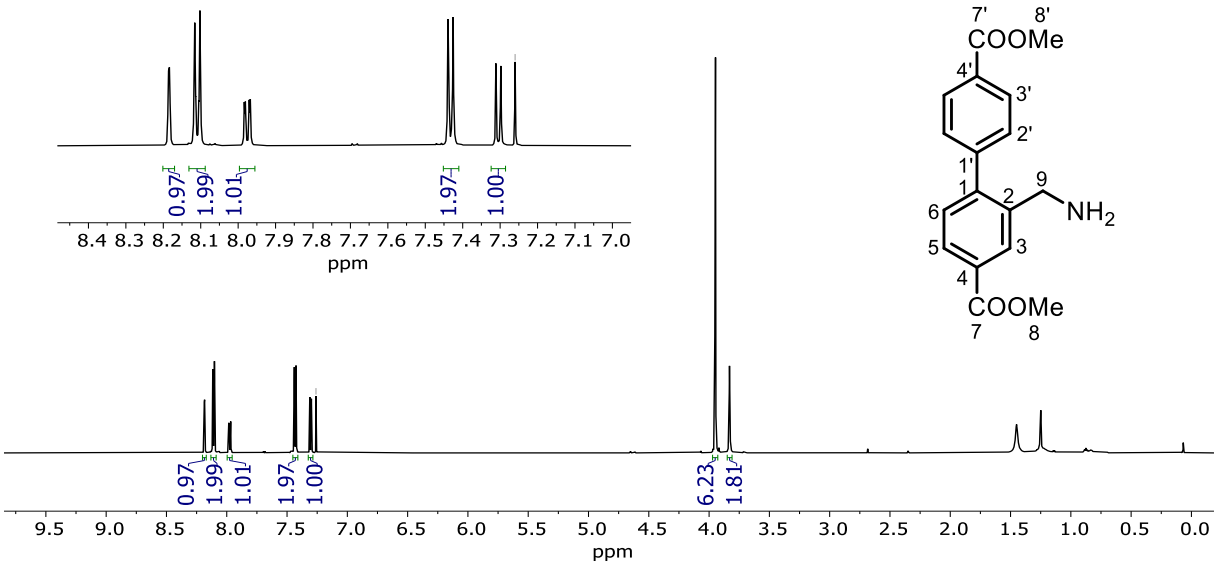

Figure 45: ^{1}H NMR (600 MHz, $CDCl_3$) spectrum of **4b**.

7.10 Synthesis of 7

A solution of **2** (4.00 g, 11.0 mmol, 1.0 equiv.) and KCN (0.789 g, 12.1 mmol, 1.1 equiv.) in MeOH (100 mL) was refluxed for 15 min, and a white precipitation was observed during this time. After cooling to room temperature, water (100 mL) was added, and the mixture was stirred for 30 min. The precipitate was isolated by vacuum filtration and extensively washed with water and diethyl ether, followed by air drying, yielding **7** as a white solid (2.44 g, 7.90 mmol, 72 %).

^{1}H NMR (600 MHz, DMSO-d_6): δ 8.17 (d, *J* = 1.8 Hz, 1H, **3-H**), 8.07 ("d", *J* = 8.3, 2H, **3'-H**), 8.02 (dd, J = 7.9, 1.8 Hz, 1H, **5-H**), 7.57 ("d", *J* = 8.3, 2H, **2'-H**), 7.49 (d, *J* = 8.0 Hz, 1H, **6-H**), 4.05 (s, 2H, **9-H**), 3.91 (s, 3H, **8-H**), 3.89 (s, 3H, **8'-H**)

^{13}C NMR (151 MHz, DMSO-d_6): δ 165.9 (**7'**), 165.6 (**7**), 144.8 (**1**), 143.3 (**1'**), 130.9 (**6**), 130.1 (**3**), 129.7 (**4**), 129.49 (**3'**), 129.46 (**4'**), 129.3 (**14**), 129.2 (**2'**), 128.9 (**5**), 118.5 (**10**), 52.4 (**8**), 52.3 (**8'**), 21.4 (**9**).

MS (ESI, MeCN) (rel. %): 332.089 ($[M+Na]^+$, 100), 333.093 (20)

HRMS (ESI, MeCN): 332.0899 calculated for $C_{18}H_{15}NO_4Na$, found: 332.0893 (0.2 ppm)

IR (KBr): *ν*(C≡N): 2245.07 cm^{-1}, *ν*(C=O): 1720.50 cm^{-1}

Mp: 157-158 °C

This compound has not been previously reported.

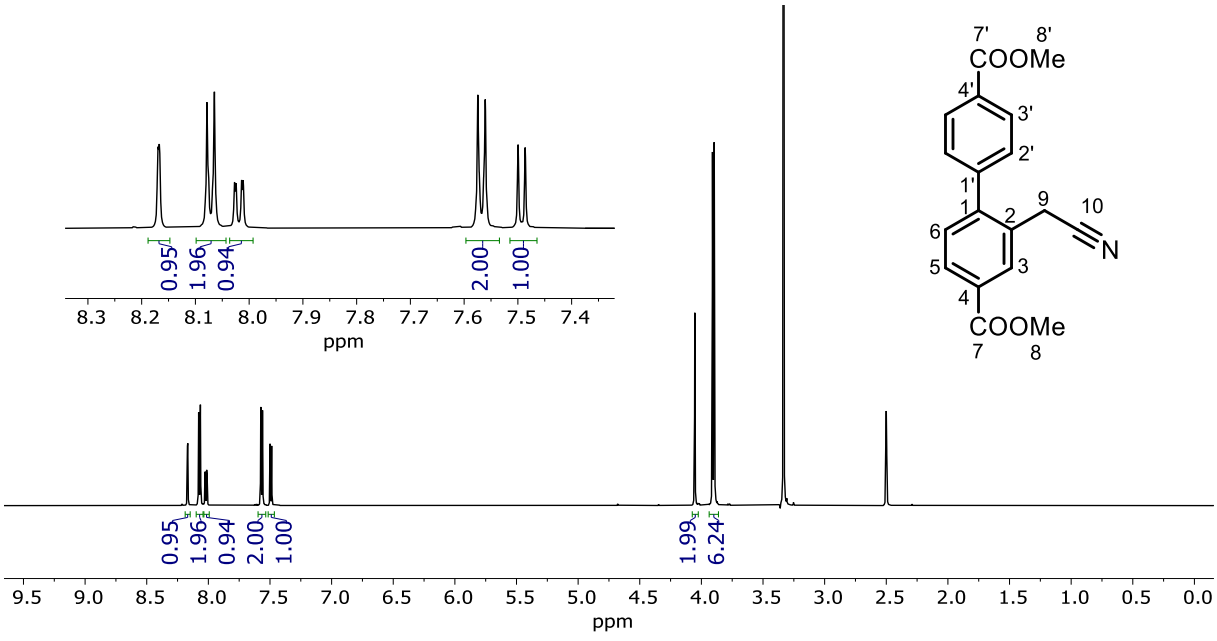

Figure 46: ^{1}H NMR (600 MHz, DMSO-d_6) spectrum of **7**.

7.11 Synthesis of 6 from 7

A solution of **7** (0.101 g, 0.325 mmol, 1.0 equiv.) and KCN (0.0180 g, 0.276 mmol, 0.9 equiv.) in EtOH (3 mL) was refluxed for 2.5 h. After cooling to room temperature, water (ca. 2 mL) was added and white precipitation was observed. The solution was allowed to stir for 30 min followed by vacuum filtration. Recrystallization from *i*PrOH yielded **6** as a white solid (0.0620 g, 0.183 mmol, 56 %).

^{1}H NMR (800 MHz, DMSO-d_6): δ 8.16 (d, *J* = 1.8 Hz, 1H, **3-H**), 8.07 ("d", *J* = 8.3 Hz, 2H, **3'-H**), 8.02 (dd, *J* = 7.9, 1.8 Hz, 1H, **5-H**), 7.58 – 7.54 ("d", *J* = 8.3 Hz, 2H, **2'-H**), 7.49 (d, *J* = 7.9 Hz, 1H, **6-H**), 4.39 - 4.35 (m, 4H, **8, 8'-H**), 4.04 (s, 2H, **10-H**), 1.36 – 1.34 (m, 6H, **9, 9'-H**).

^{13}C NMR (201 MHz, DMSO-d_6): δ 165.4 (**7'**), 165.0 (**7**), 144.7 (**1**), 143.3 (**1'**), 130.8 (**6**), 130.0 (**4**), 129.9 (**3**), 129.6 (**4'**), 129.4 (**3'**), 129.4 (**2**), 129.1 (**2'**), 128.8 (**5**), 118.4 (**11**), 61.1 (**8** or **8'**), 60.9 (**8** or **8'**), 21.4 (**10**), 14.1 (**9, 9'**).

MS (ESI, MeCN) (rel. %): 360 ($[M+Na]^+$, 100), 361.121 (22), 379.152 (12)

HRMS (ESI, MeCN): 360.1212 calculated for $C_{20}H_{19}NO_4Na$, found: 360.1206 (0.1 ppm)

M_p: 75-76 °C

This compound has not been previously reported.

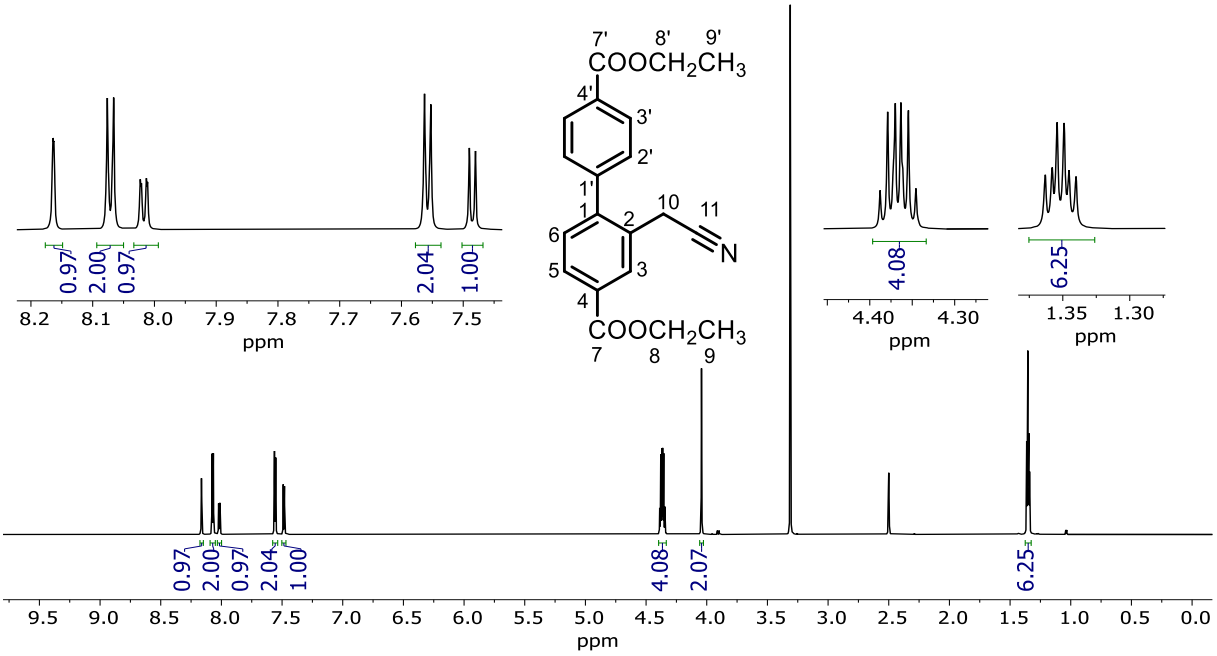

Figure 47: ^{1}H NMR (800 MHz, DMSO-d_6) spectrum of **6**.

7.12 Synthesis of 7 from 2 in a one-pot reaction

A solution of **2** (0.100 g, 0.275 mmol, 1.0 equiv.) and KCN (0.0328 g, 0.507 mmol, 1.8 equiv.) in EtOH (3 mL) was refluxed for 4 h. After cooling to room temperature, water (ca. 2 mL) was added and white precipitation was observed. The solution was allowed to stir for 30 min followed by vacuum filtration. Recrystallization from EtOH yielded **7** as a white solid (0.0232 g, 0.0688 mmol, 25 %).

7.13 Synthesis of 8a

$NaBH_4$ (0.612 g, 16.2 mmol, 10 equiv.) was added to a solution of **6** (0.500 g, 1.62 mmol, 1.0 equiv.) and $CoCl_2 \cdot 6H_2O$ (0.769 g, 3.23 mmol, 2.0 equiv.) in MeOH (12.5 mL) and THF (12.5 mL). The reaction mixture was stirred for 24 h at room temperature. Argon flow was utilized during the first hour of stirring. After 24 hours, 3 M HCl (25 mL) was added to the black solution until the solution became clear and pink. The pH of the solution was subsequently adjusted to pH =11-12 with 28% NH_4OH (~ 30 mL). The solution was then extracted with EtOAc (3x50 mL). The collected organic phases were washed with brine (150 mL), dried with Na_2SO_4 and filtered. The solvent was removed under reduced pressure yielding a yellow oil. Isolation of **8a**; the crude product was dissolved in toluene (ca 8 mL) and 35 % HCl (208 µL) was added to the clear solution resulting in a precipitation. The reaction mixture was allowed to stir for 1 h. The precipitation was isolated by vacuum filtration yielding **8a** as a light brown solid (0.397 g, 1.14 mmol, 72 %).

^{1}H NMR (600 MHz, DMSO-d_6): δ 8.07 ("d", *J* = 8.2 Hz, 2H, **3'-H**), 7.99 (d, *J* = 1.9 Hz, 1H, **3-H**), 7.98 (br. s, 3H, -N**H**$_3$), 7.92 (dd, J = 8.0, 1.8 Hz, 1H, **5-H**), 7.53 ("d", *J* = 8.2 Hz, 2H, **2'-H**), 7.40 (d, *J* = 8.0 Hz, 1H, **6-H**), 3.89 (s, 3H, **8'** or **8**), 3.89 (s, 3H, **8'** or **8**), 2.95 – 2.83 (m, 4H, **9, 10-H**).

^{13}C NMR (151 MHz, DMSO-d_6): δ 166.1 (**7'**), 166.0 (**7**), 145.4 (**1**), 144.5 (**1'**), 135.4 (**4**), 130.5 (**6**), 130.4 (**3**), 129.5 (**2**), 129.5 (**3'**), 129.3 (**2'**), 129.0 (**4'**), 127.7 (**5**), 52.4 (**8**, **8'**), 39.3 (**9** or **10**), 30.2 (**9** or **10**).

^{15}N(^{1}H) NMR (600 MHz, DMSO-d_6): δ 156 (**N**H_3).

MS (ESI, MeCN) (rel. %): 297.112 (16), 314.139 ($[M+H]^+$, 100), 315.142 (20)

HRMS (ESI, MeCN): 314.1392 calculated for $C_{18}H_{20}NO_4$, found: 314.1386 (0.2 ppm)

M_p: 147-148°C

This compound has not been previously reported.

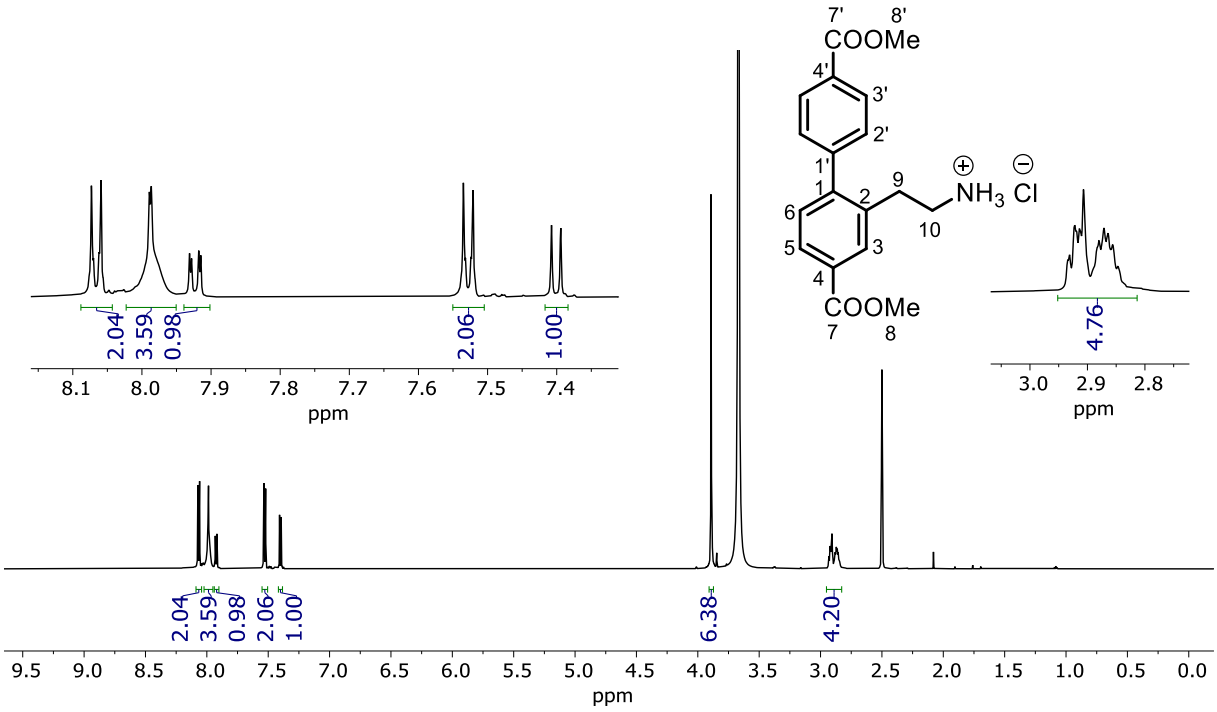

Figure 48: ^{1}H NMR (600 MHz, DMSO-d_6) spectrum of **8a**.

7.14 Synthesis of 8b

The compound **8b** was synthesized in the same manner as **8a** at 3.23 mmol scale. The utilized amounts of the reagents are: **6** (1.00 g, 3.23 mmol, 1.0 equiv.) and $CoCl_2 \cdot 6H_2O$ (1.54 g, 6.46 mmol, 2.0 equiv.) and $NaBH_4$ (1.22 g, 32.3 mmol, 10.0 equiv.). The crude product was dissolved in ethyl acetate (10 mL) and extracted with 1M HCl (2x5 mL). The solution was pH-adjusted to pH = 12 with 1M NaOH affording **8b** as a pale yellow solid (0.124 g, 0.396 mmol, 12 %).

^{1}H NMR (600 MHz, DMSO-d_6): δ 8.05 ("d", *J* = 8.3, 2H, **3'-H**), 7.96 (d, *J* = 1.8 Hz, 1H, **3-H**), 7.87 (dd, *J* = 7.9, 1.8 Hz, 1H, **5-H**), 7.51 ("d", *J* = 8.3, 2H, **2'-H**), 7.36 (d, J = 7.9 Hz, 1H, **6-H**), 2.88 (s, 3H, **8'-** or **8-H**), 3.89 (s, 3H, **8'-** or **8-H**), 2.76 – 2.63 (m, 4H, **9-, 10-H**).

^{13}C NMR (151 MHz, DMSO-d_6): δ 166.1 (**8**), 166.0 (**8'**), 145.2 (**1**), 145.0 (**1'**), 138.0 (**2**), 130.5 (**3**), 130.2 (**6**), 129.29 (**2'**), 129.26 (**3'**), 129.2 (**4**), 128.8 (**4'**), 127.0 (**5**), 52.3 (**8'** or **8**), 52.2 (**8'** or **8**), 42.1 (**9** or **10**), 35.1 (**9** or **10**).

^{15}N(^{1}H) NMR (600 MHz, DMSO-d_6): δ 25 (**N**H_3)

MS (ESI, MeCN) (rel. %): 297.112 (16), 314.139 ($[M+H]^+$, 100), 315.142 (20)

HRMS (ESI, MeCN): 314.1392 calculated for $C_{18}H_{20}NO_4$, found: 314.1387 (0.1 ppm)

M_p: 79-80 °C

This compound has not been previously reported.

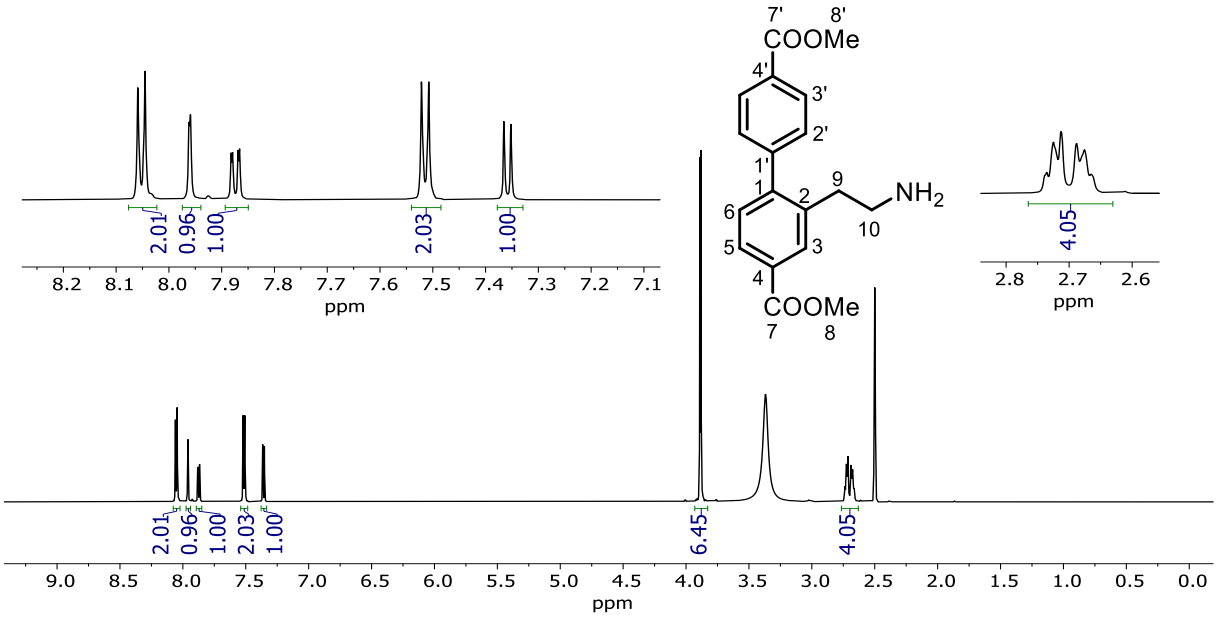

Figure 49: ^{1}H NMR (600 MHz, DMSO-d_6) spectrum of **8b**.

7.15 Synthesis of 9

A solution of **8b** (0.100 g, 0.290 mmol, 1.00 equiv.) and LiOH (0.0424 g, 1.77 mmol, 6.2 equiv.) in MeOH (2.5 mL) and water (2.5 mL) was refluxed for 20 h. The reaction mixture was cooled and filtrated through a paper filter. The paper filter was subsequently washed with water (ca. 3 mL). The product was precipitated from the solution by adding HCl (35 %) until the pH was 1-2. The precipitation was collected by vacuum filtration in a glass filter and extensively washed with water, followed by washing with diethyl ether, yielding **9** as a light brown solid (0.0620 g, 0.193 mmol, 68 %).

^{1}H NMR (600 MHz, DMSO-d_6): δ 13.10 (b. s, 2H, COO**H**), 8.05 (“d”, *J* = 8.1 Hz, 2H, **3’-H**), 7.97 (d, *J* = 1.8 Hz, 1H, **3-H**), 7.92 (br. s, 2H, -N**H**), 7.91 (dd, *J* = 8.0 Hz, 1.8 Hz, 1H, **5-H**), 7.50 (“d”, *J* = 8.2 Hz, 2H, **2’-H**), 7.37 (d, *J* = 7.9 Hz, 1H, **6-H**), 2.89 (m, 4H, **8, 9-H**).

^{13}C NMR (151 MHz, DMSO-d_6) δ 167.1 (**7’**), 167.0 (**7**), 145.1 (**1**), 144.2 (**1’**), 135.1 (**2**), 130.6 (**4**), 130.5 (**3**), 130.3 (**6**), 130.1 (**4’**), 129.5 (**3’**), 129.1 (**2’**), 127.8 (**5**), 39.3 (**8** or **9**), 30.2 (**8** or **9**).

^{15}N(^{1}H) NMR (600 MHz, DMSO-d_6): δ 35 (**N**H_3)

MS (ESI, MeCN) (rel. %): 286.107 ($[M+H]^+$, 40), 290.895 (100), 292.892 (63)

HRMS (ESI, MeCN): 286.1079 calculated for $C_{16}H_{16}NO_4$, found: 286.1073 (0.2 ppm)

M_p: 288-289 °C:

EA: calculated for $C_{16}H_{16}ClNO_4$: C: 59.73, H: 5.01, N: 4.35. Found: C: 55.19, H: 5.46, N: 3.99

This compound has not been previously reported.

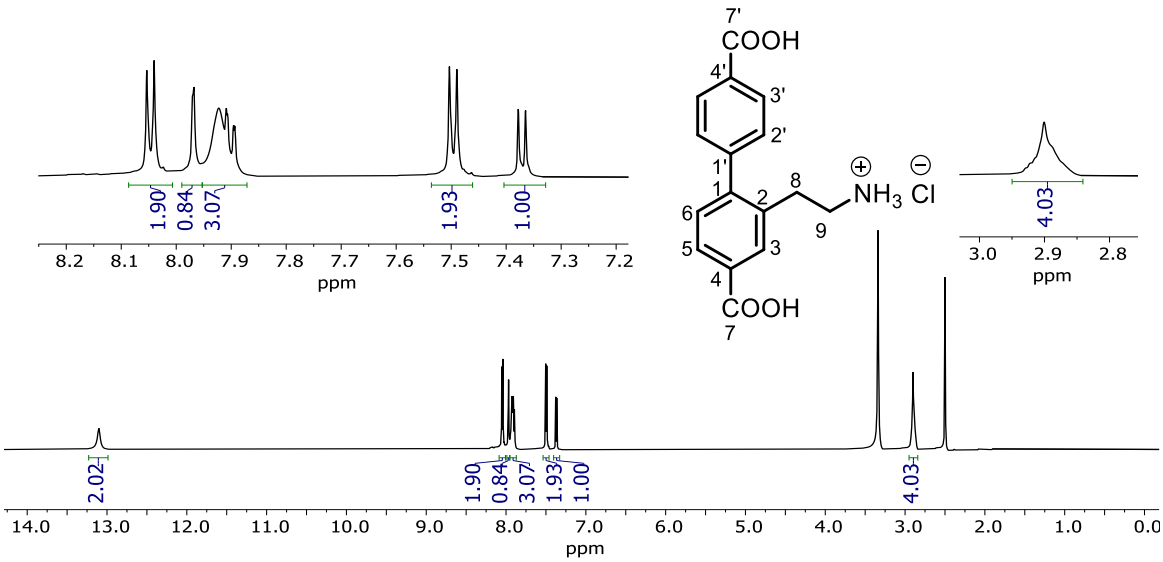

Figure 50: ^{1}H NMR (600 MHz, DMSO-d_6) spectrum of **9**.

7.16 Synthesis of 10

Silver oxide (0.160 g, 0.688 mmol, 0.5 equiv.) was added to a solution of **2** (0.500 g, 1.38 mmol, 1.0 equiv.) and pyridine N-oxide (0.131 g, 1.38 mmol, 1.0 equiv.) in acetonitrile (25 mL). The reaction mixture was refluxed for 2 h under argon atmosphere. The reaction was followed by ^{1}H NMR or TLC. After completed reaction, the reaction mixture was filtered and the solvent was removed under reduced pressure. The crude product was purified by flash chromatography using EtOAc: Hexane (0- 30 % gradient) as eluent yielding **10** as white solid (0.233 g, 0.782 mmol, 57 %).

^{1}H NMR (600 MHz, $CDCl_3$): δ 9.98 (s, 1H, **9-H**), 8.69 ("d", *J* = 1.9 Hz, 1H, **3'-H**), 8.31 (dd, *J* = 8.0, 1.9 Hz, 1H, **5-H**), 8.17 ("d", *J* = 8.5 Hz, 2H, **2'-H**), 7.55 (d, *J* = 8.0 Hz, 1H, **6-H**), 7.48 ("d", *J* = 8.3 Hz , 2H, **2'-H**), 3.99 (s, 3H, **8-H**), 3.97 (s, 3H, 1-H, **8'-H**).

^{13}C NMR (151 MHz, $CDCl_3$): δ 190.9 (**9**), 166.6 (**7'**), 166.0 (**7**), 148.5 (**1**), 141.6 (**1'**), 134.3 (**5**), 133.9 (**2**), 131.2 (**6**), 130.6 (**4'**), 130.6 (**4**), 130.1 (**2'**), 130.0 (**3'**), 129.7 (**3**), 52.7 (**8**), 52.6 (**8'**).

MS (ESI, MeCN) 321.073 ([M+Na]$^{+}$, 100), 322.077 (20), 353.100 (47)
HRMS (ESI, MeCN): 321.0739 calculated for $C_{17}H_{14}O_5Na$, found: 321.0733 (0.1 ppm)

Mp: 145-146 °C

The spectroscopic data are in coherence with what is previously reported in the literature.[102] The melting point was not previously reported.

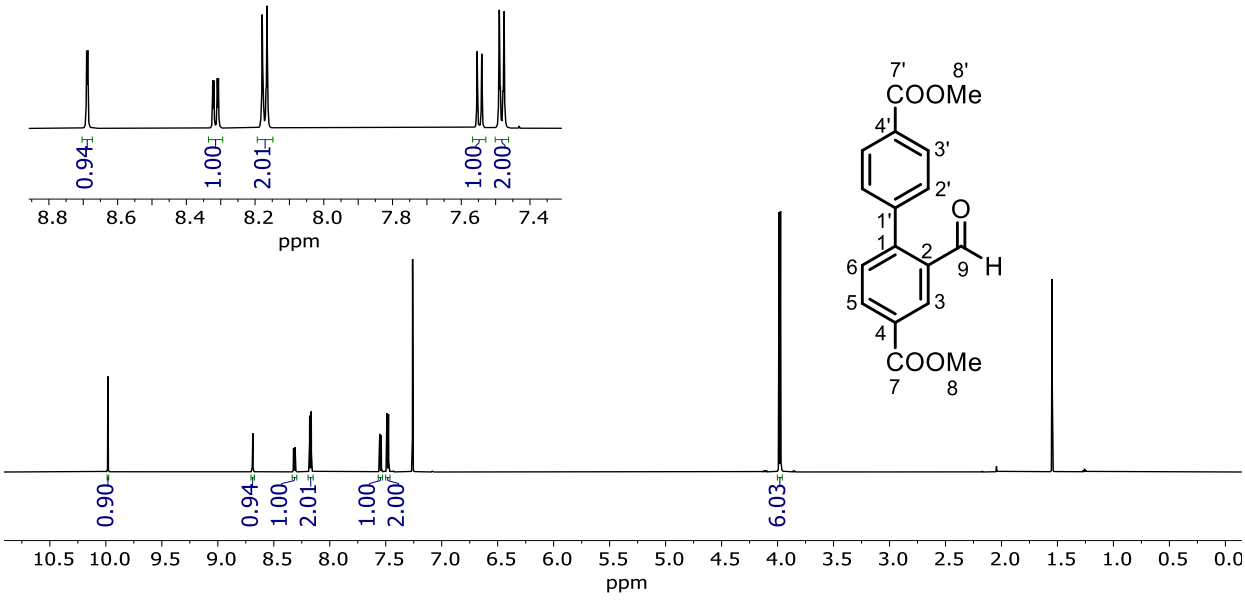

Figure 51: ^{1}H NMR (600 MHz, $CDCl_3$) spectrum of **10**.

7.17 Synthesis of 11

A solution of **10** (0.100 g, 0.34 mmol, 1.0 equiv.) and ammonium acetate (0.0620 g, 0.804 mmol, 2.4 equiv.) in CH_3NO_2 (4.00 mL, 59 mmol, 75 equiv.) and CH_3COOH (8 mL) was heated at 90 °C under argon flow for 20 h. The solution was cooled and diluted with water (20 mL). The aqueous phase was extracted with EtOAc (3x30 mL). The collected organic phases were washed with brine (100 mL), dried with Na_2SO_4 and filtrated. The solvent was removed under reduced pressure. Recrystallization from *i*PrOH yielded **11** as a white/yellow solid (0.0459 g, 0.134 mmol, 40 %). The isolated product contained approximately 4 % of an unidentified impurity according to ^{1}H NMR.

^{1}H NMR (600 MHz, $CDCl_3$): δ 8.34 (d, *J* = 1.7 Hz, 1H, **3-H**), 8.20 (dd, *J* = 8.1, 1.7 Hz, 1H, **5-H**), 8.17 (“d”, *J* = 8.2, 2H, **3’-H**), 7.95 (d, *J* = 13.6 Hz, 1H,), 7.61 (d, *J* = 13.6 Hz, 1H,), 7.54 (d, *J* = 8.0 Hz, 1H, **6-H**), 7.41 (“d”, *J* = 8.2, 2H, **2’-H**), 3.99 (s, 3H, **8-H**), 3.98 (s, 3H, **8’-H**).

^{13}C NMR (151 MHz, $CDCl_3$): δ 166.6 (**7’**), 165.9 (**7**), 147.1 (**1**), 142.8 (**1’**), 139.0 (9 or 10), 136.7 (9 or 10), 132.3 (**5**), 131.2 (**6**), 130.7 (**4’**), 130.6 (**4**), 130.2 (**3’**), 129.8 (**2’**), 129.1 (**3**), 128.7 (**2**), 52.8 (**8**), 52.5 (**8’**).

^{15}N(^{1}H) NMR (600 MHz, DMSO-d_6): δ 371 (**N**O_2).

MS (ESI, MeCN): 364.079 ($[M+Na]^+$, 100), 365.082 (19)

HRMS (ESI, MeCN): 364.0797 calculated for $C_{18}H_{15}NO_6Na$, found: 364.0792 (0.0 ppm)

M_p: 178-179 °C

This compound has not been previously reported.

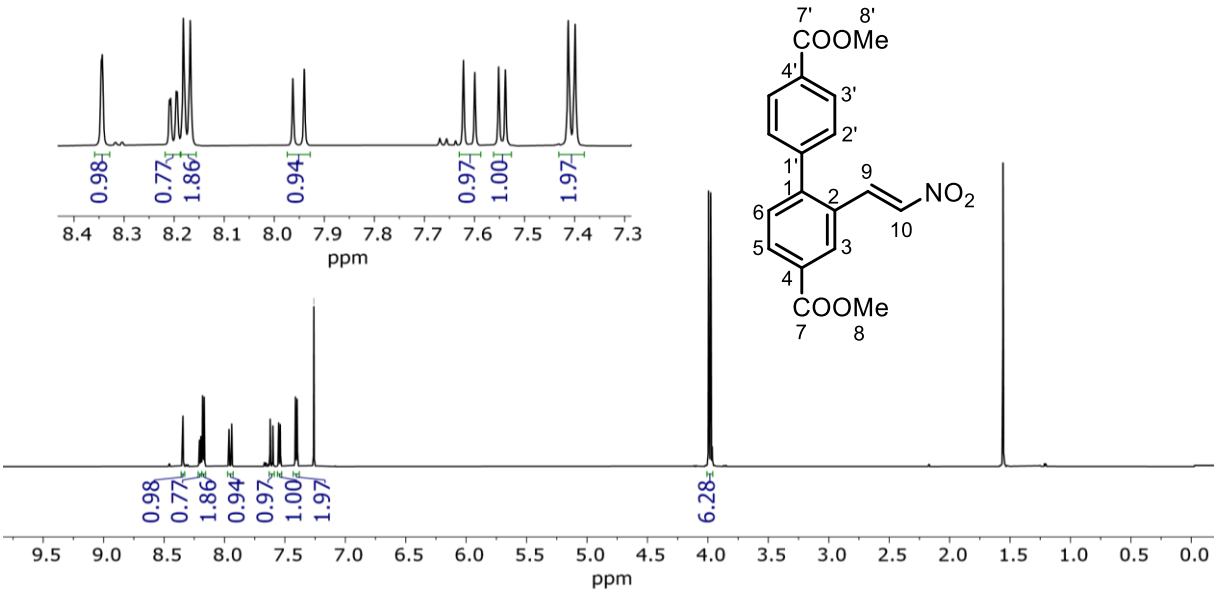

Figure 52: ^{1}H NMR (600 MHz, $CDCl_3$) spectrum of **11**.

7.18 Synthesis of 12

A solution of **5** (0.100 g, 0.325 mmol, 1.0 equiv.) and 35% HCl (0.687 mL, 7.78 mmol, 24 equiv.) was heated in DMF (2 mL) at 130 °C for 25h. The solution was cooled and water (ca. 0.5 mL) was added resulting in precipitation of a white product. The precipitation was isolated by vacuum filtration in a glass frit yielding **12** as a white solid (0.0496 g, 0.166 mmol, 51 %). The isolated product contained approximately 4 % of **5**, and approximately 8 % of an unidentified side product by ^{1}H NMR.

^{1}H NMR (600 MHz, DMSO-d_6): δ 8.55 (t, *J* = 5.8 Hz, 1H, N**H**), 8.11 (d, *J* = 1.8 Hz, 1H, **9-H**), 8.03 ("d", *J* = 8.3, 2H, **3'-H**), 8.01 (d, *J* = 1.7, 1H, **3-H**), 7.91 (dd, *J* = 7.9, 1.8 Hz, 1H, **5-H**), 7.53 ("d", *J* = 8.4, 2H, **2'-H**), 7.38 (d, *J* = 8.0 Hz, 1H, **6-H**), 4.26 (d, *J* = 6.0 Hz, 2H, **8-H**).

^{13}C NMR (151 MHz, DMSO-d_6): δ 167.1 (**7'** or **7**), 167.1 (**7'** or **7**), 161.2 (**9**), 144.0 (**1**), 143.8 (**1'**), 136.46 (**2**), 130.51 (**4**), 130.2 (**4'**), 130.0 (**6**), 129.4 (**3'**), 129.2 (**2'**), 128.9 (**3**), 128.0 (**5**), 38.6 (**8**).

^{15}N(^{1}H) NMR (600 MHz, DMSO-d_6): δ 122 (**N**H_3)

IR (KBr): *v*: 3336.85 cm^{-1}, *v*(C=O): 1693.50 cm^{-1} ,1641.42 cm^{-1}
MS (ESI, MeCN) (rel. %): 322.069 ([M+Na]$^{+}$, 100), 323.072 (18)
HRMS (ESI, MeCN): 322.0691 calculated for $C_{16}H_{13}NO_5Na$, found: 322.0686 (-0.1 ppm)

M_p: > 300 °C

This compound has not been previously reported.

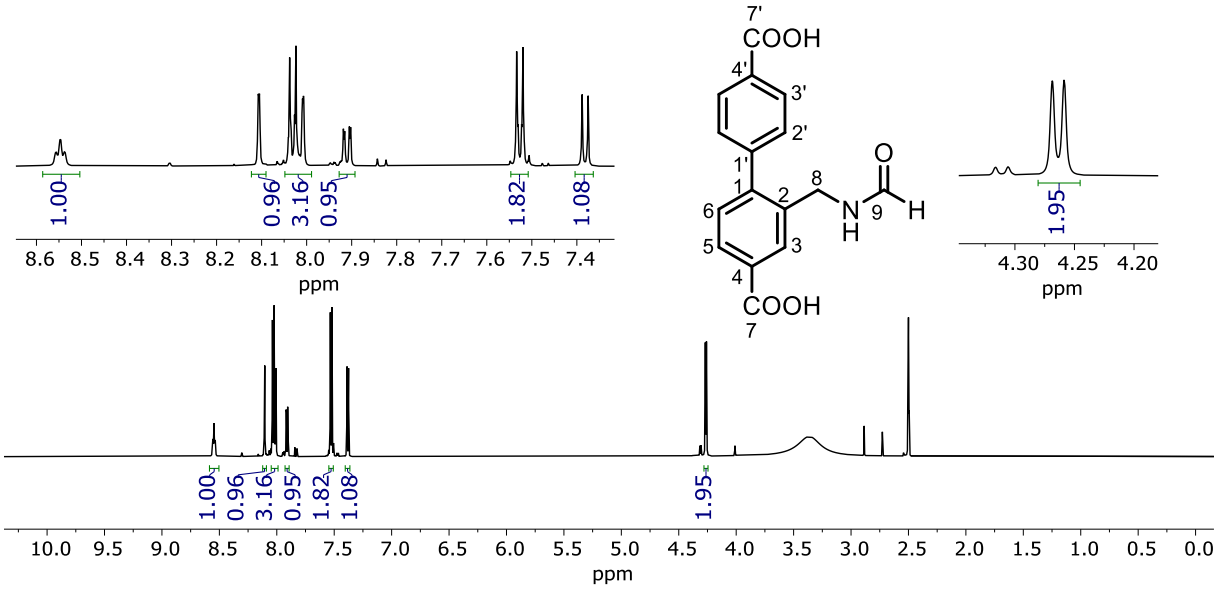

Figure 53: ^{1}H NMR (600 MHz, DMSO-d_6) spectrum of **12**

7.19 Synthesis of 13

A solution of **4a** (0.101 g, 0.310 mmol, 1.0 equiv.) and 35% HCl (0.630 mL, 7.35 mmol, 24 equiv.) was heated in DMF (2 mL) at 130 °C for 24 h. The solution was cooled and water (ca. 1.5 mL) was added resulting in precipitation of a white product. The precipitation was isolated by vacuum filtration in a glass frit yielding **13** as a white solid (0.0629 g, 0.192 mmol, 64 %). The isolated product contained approximately 10 % of an unidentified side product by ^{1}H NMR.

^{1}H NMR (600 MHz, DMSO-d_6) δ 8.56 (m, 1H, -N**H**), 8.10 (d, *J* = 1.7 Hz, 1H, **10**-**H**), 8.05 ("d", *J* = 8.3 Hz, 2H, **3'-H**), 8.02 (d, *J* = 1.8 Hz, 1H), 7.94 (dd, *J* = 8.0, 1.9 Hz, 1H, **5**-**H**), 7.57 ("d", *J* = 8.3 Hz, 2H, **2'-H**), 7.42 (d, *J* = 8.0 Hz, 1H, **6**-**H**), 4.27 (d, *J* = 5.9 Hz, 2H, **9**-**H**), 3.89 (s, 3H, **8**'- or **8**-**H**), 3.89 (s, 3H, , **8**'- or **8**-**H**).

^{13}C NMR (151 MHz, DMSO-d_6) δ 166.0 (**8'**), 165.9 (**8**), 161.1 (**10**), 144.3 (**1**), 144.0 (**1'**), 136.8 (**2**), 130.2 (**6**), 129.4 (**2'**), 129.29 (**3'**), 129.27 (**4**), 129.0 (**4'**), 128.7 (**3**), 127.8 (**5**), 52.31 (**8'** or **8**), 52.28 (**8'** or **8**), 38.51 (**9**).

^{15}N(^{1}H) NMR (600 MHz, DMSO-d_6): δ 122 (**N**H_3)

MS (ESI, MeCN) (rel. %): 350.100 ($[M+Na]^+$, 100), 351.103 (20), 366.074 (13)

HRMS (ESI, MeCN): 350.10044 calculated for $C_{18}H_{17}NO_5Na$, found: 350.0999 (0.1 ppm)

M_p: 123-124 °C

This compound has not been previously reported.

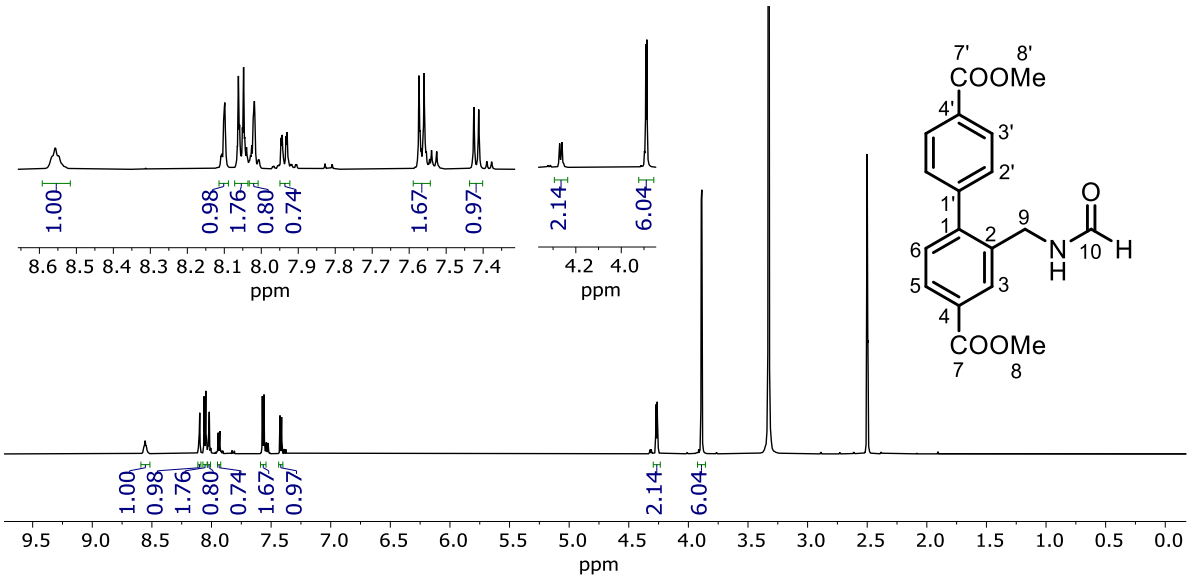

Figure 54: ^{1}H NMR (600 MHz, DMSO-d_6) spectrum of **13**.

7.20 Synthesis of UiO-67 MOF

Zirconium chloride (0.507 g, 2.18 mmol, 1.0 equiv.) and water (0.460 mL, 26.0 mmol, 3.0 equiv.) was dissolved in DMF (8.30 mL) at room temperature. The clear solution was then heated close to the boiling point before adding benzoic acid (2.36 g, 19.3 mmol, 9.0 equiv.). The clear solution was subsequently transferred to a round bottomed flask containing the H_2BPDC linker (0.528 g, 2.18 mmol, 1.0 equiv.). The flask was put in an oil bath and heated at 130 °C for 24 h in a reflux setup. The resulting white precipitate was isolated the following day, and washed with warm DMF, followed by washing with acetone. The precipitate was then dried in an oven at 150 °C overnight, yielding a crystalline solid confirmed by power XRD analysis.

7.21 Synthesis of UiO-67-benzylamine

Zirconium chloride (0.505 g, 2.17 mmol, 1.0 equiv.) and water (0.460 mL, 26.0 mmol, 3.0 equiv.) was dissolved in DMF (8.30 mL) at room temperature. The clear solution was then heated close to the boiling point before adding benzoic acid (2.36 g, 19.3 mmol, 9.0 equiv.). The clear solution was subsequently transferred to a round bottomed flask containing the H_2BPDC linker (0.469 g, 1.94 mmol, 0.9 equiv.) and **5** (0.0670 g, 1.92 mmol, 0.1 equiv.). The flask was put in an oil bath and heated at 130 °C for 24 h in a reflux setup. The resulting white precipitate was isolated the following day, and washed with warm DMF, followed by washing with acetone. The precipitate was then dried in an oven at 150 °C overnight, yielding a crystalline solid confirmed by powder XRD analysis.

7.22 Attempted deformylation of UiO-67-benzylamine with methanol

A suspension of UiO-67-benzylamine (0.101 g) was refluxed in methanol (50 mL) for 22 h. The solid was isolated by filtration and was washed with room-tempered methanol, before dying in the oven at 100 °C overnight. The MOF was digested in 1 M D_3PO4 (in DMSO-d_6) which revealed that the attempted deformylation was unsuccessful (APPENDIX).

7.23 Attempted deformylation of UiO-67-benzylamine with Na_2S

A suspension of UiO-67-benzylamine (0.0504 g) and sodium sulfide (0.00540 g) in water (20 mL) was heated at 100 °C under argon flow for 24 h. The solid was subsequently washed with water and acetone, and centrifuged. The liquids were removed with a pipette and the MOF was dried at 65 °C before digestion in 1 M D_3PO4 (in DMSO-d_6). The digestion revealed partial deformylation, with more than 50% of **12** still present. (APPENDIX)

CHAPTER 8

Appendix

8.1 Compound 1c

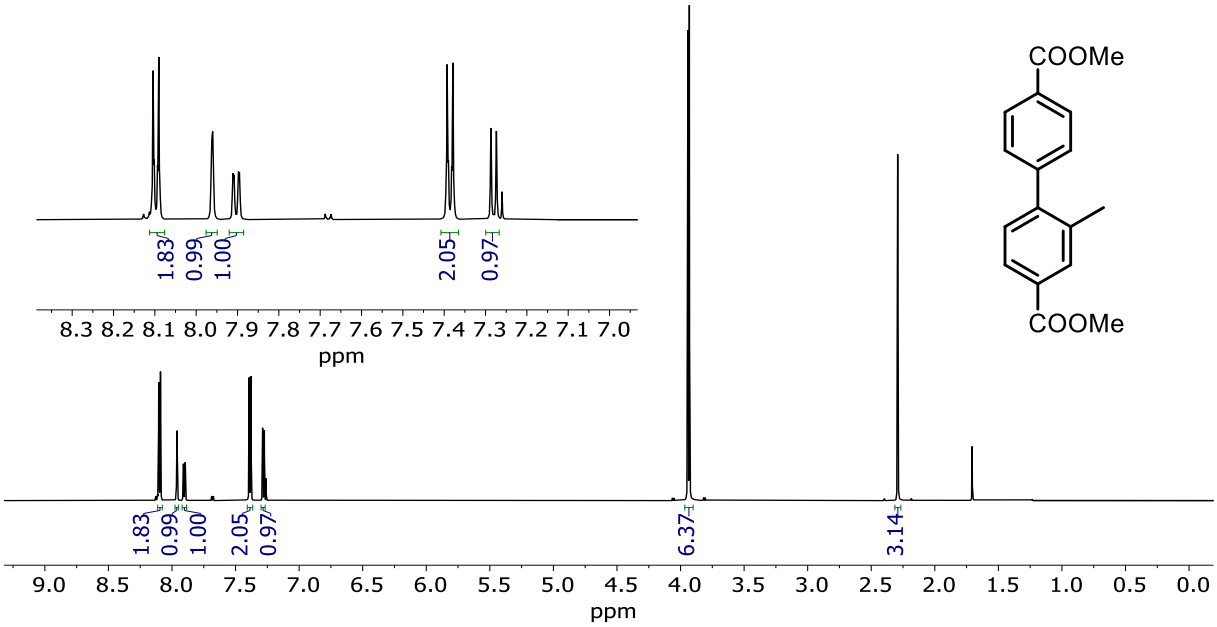

Figure 55: ^{1}H NMR (600 MHz, $CDCl_3$) spectrum of **1c**.

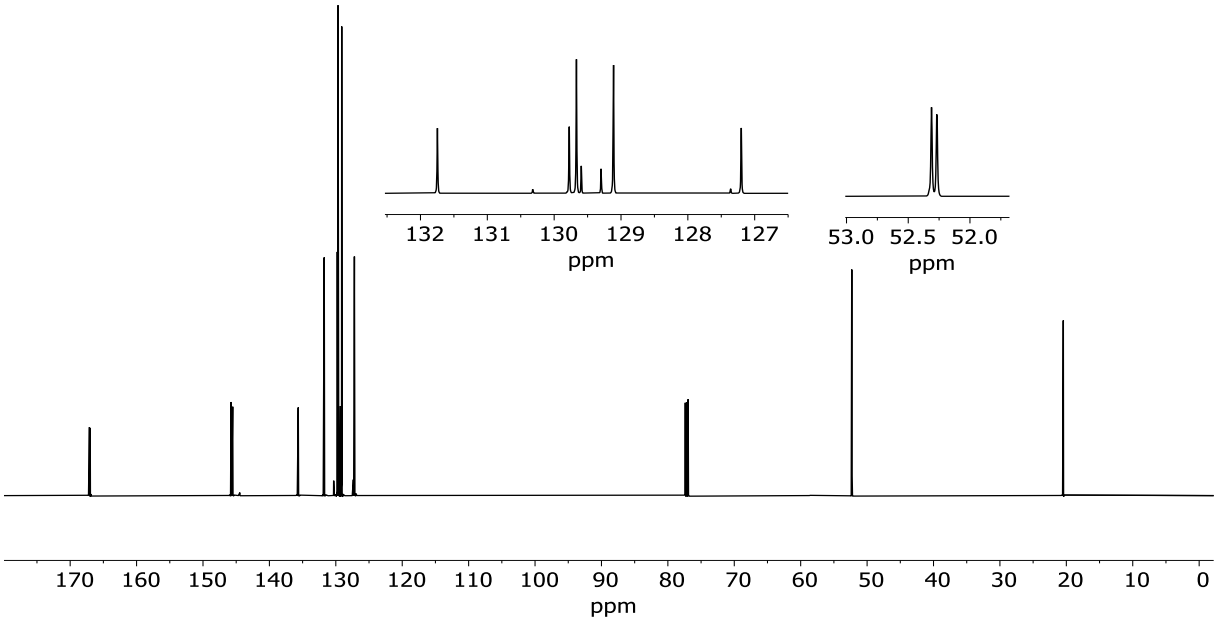

Figure 56: ^{13}C NMR (151 MHz, $CDCl_3$) spectrum of **1c.**

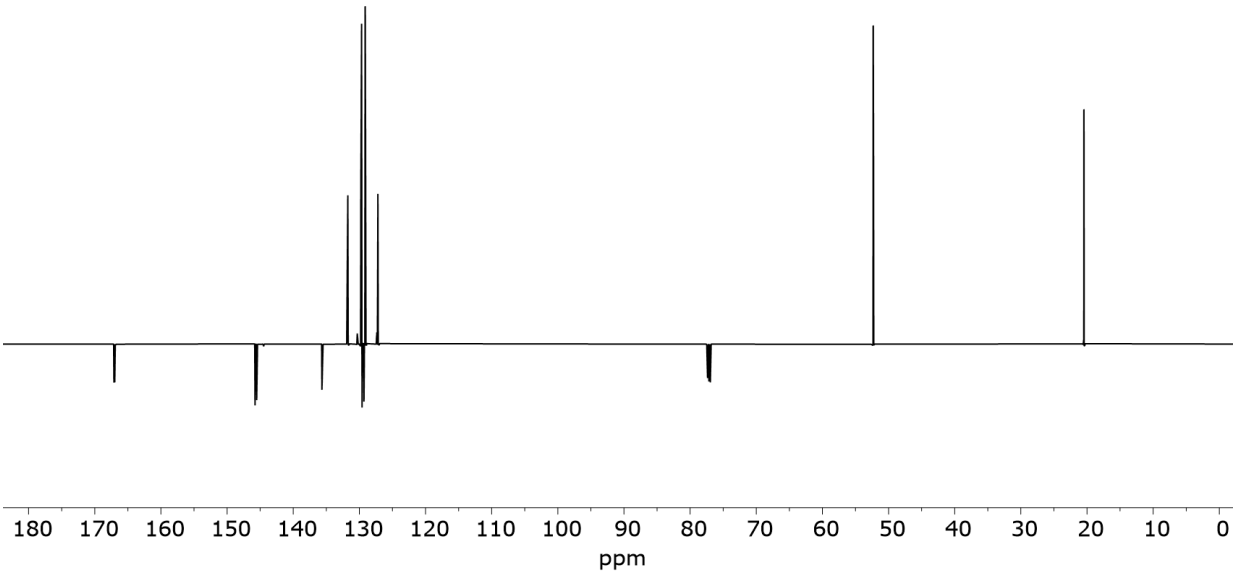

Figure 57: DEPT135Q (151 MHz, $CDCl_3$) spectrum of **1c.**

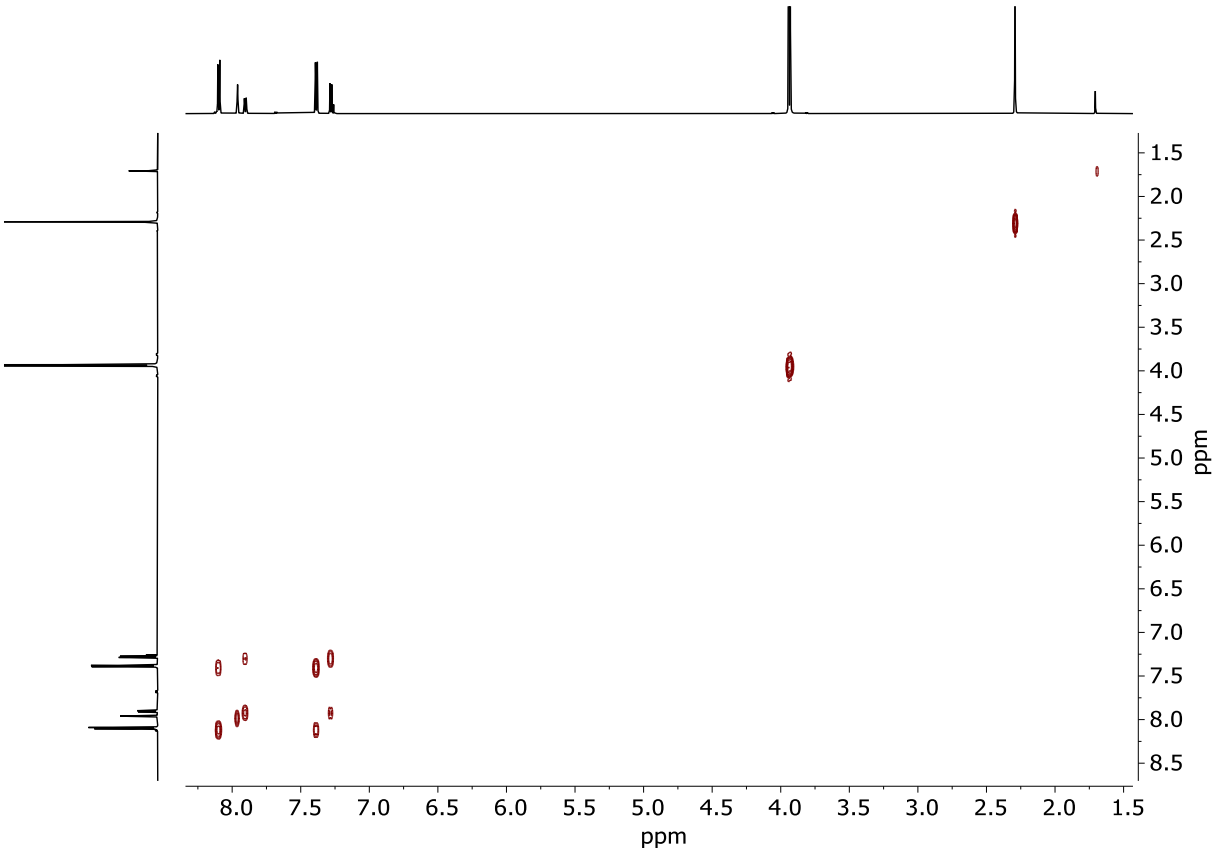

Figure 58: COSY (600 MHz, $CDCl_3$) spectrum of **1c.**

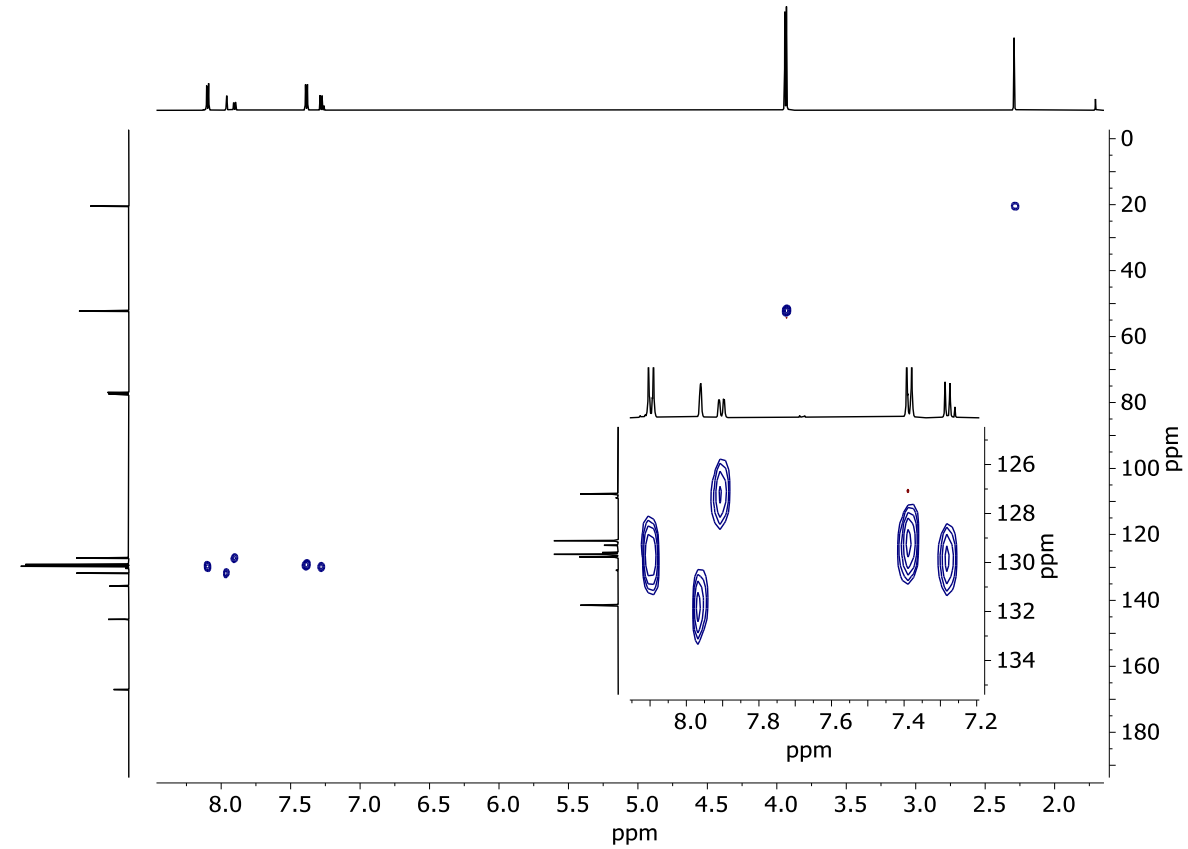

Figure 59: HSQC (600 MHz, $CDCl_3$) spectrum of **1c.**

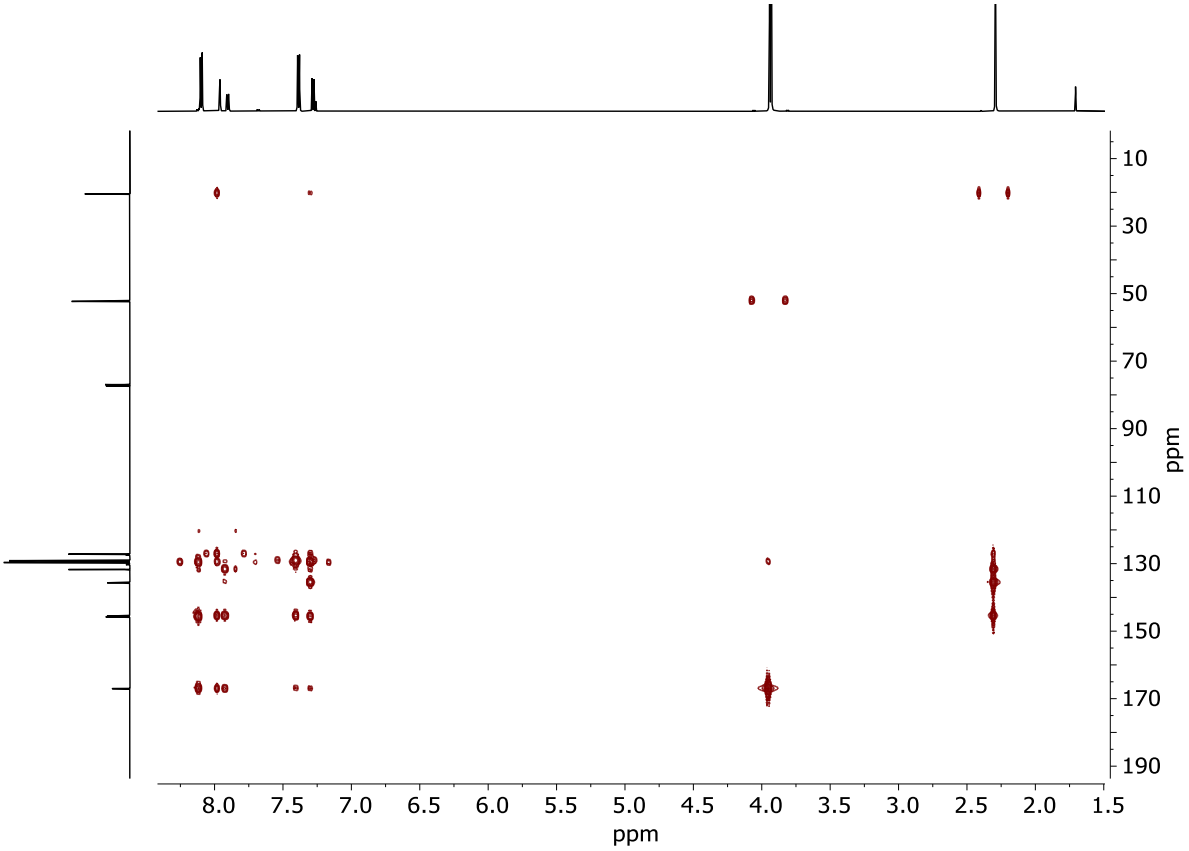

Figure 60: HMBC (600 MHz, $CDCl_3$) spectrum of **1c**.

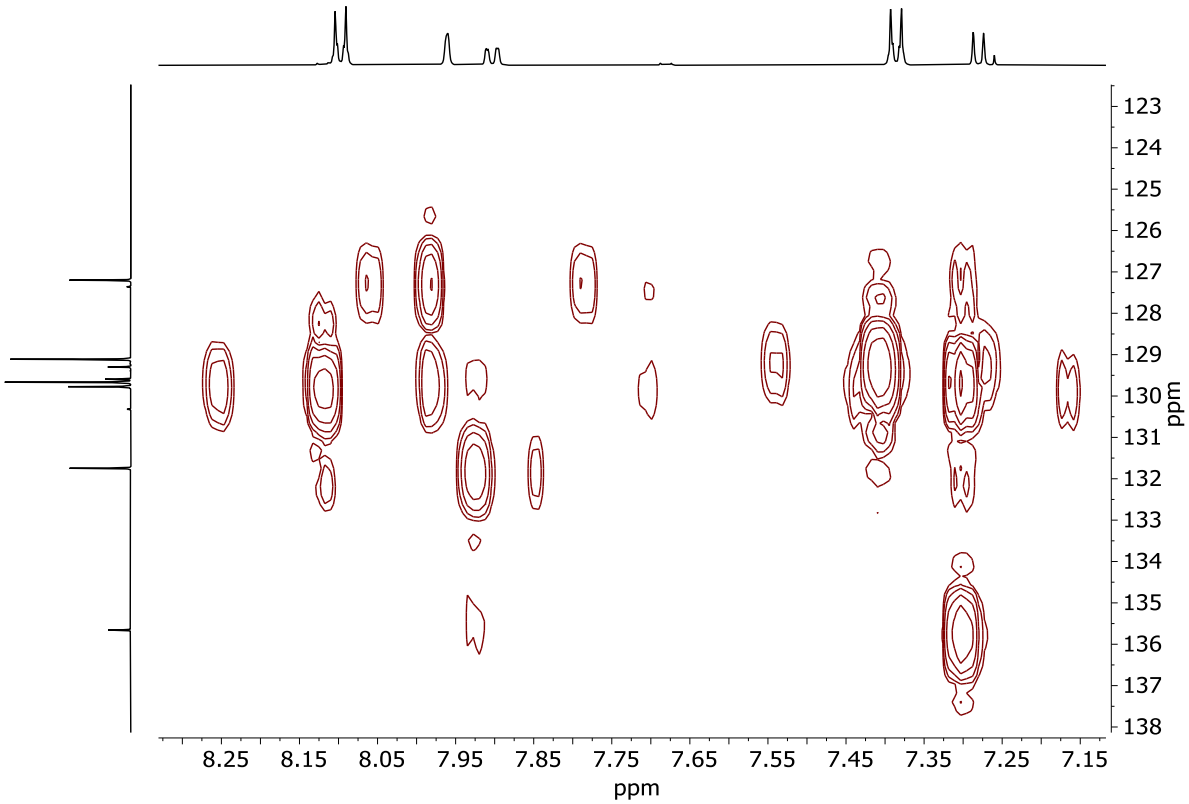

Figure 61: Zoom of HSQC (600 MHz, $CDCl_3$) spectrum of **1c**.

8.2 Compound 2

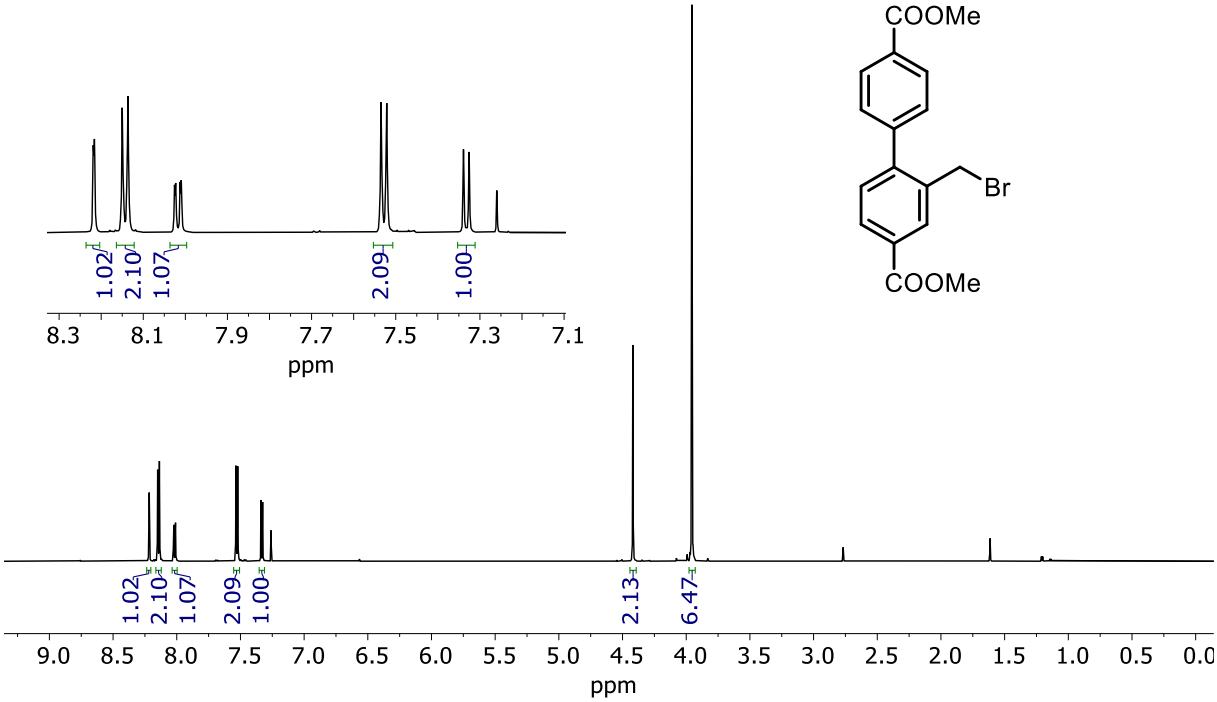

Figure 62: ^{1}H NMR (600 MHz, $CDCl_3$) spectrum of **2**.

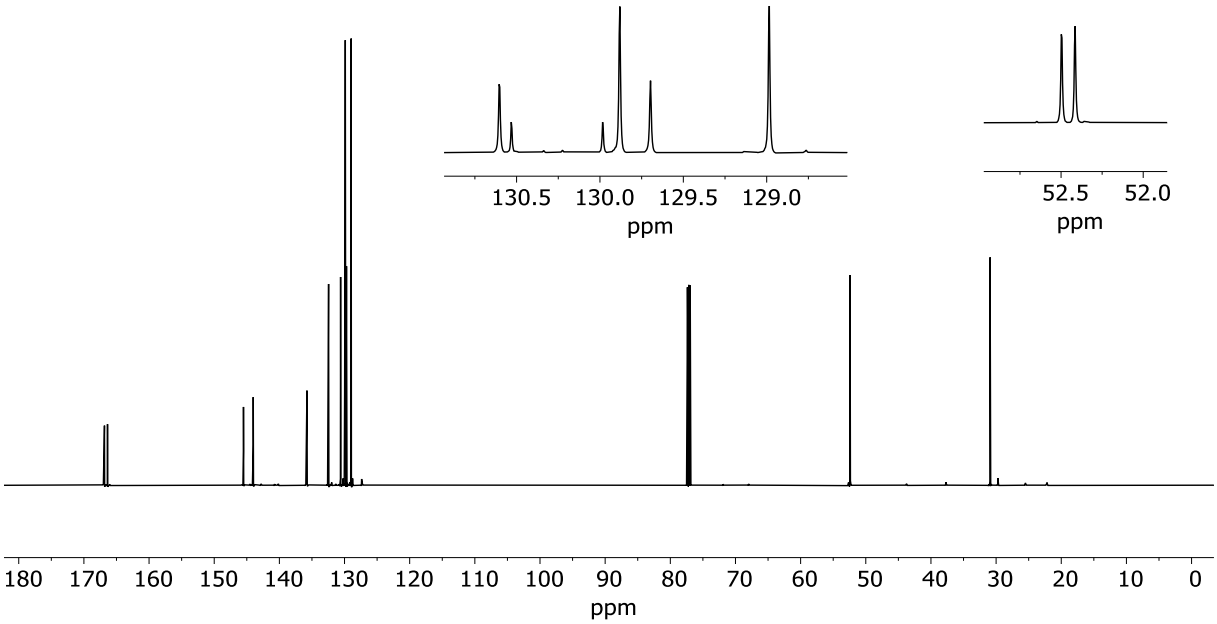

Figure 63: ^{13}C NMR (151 MHz, $CDCl_3$) spectrum of **2.**

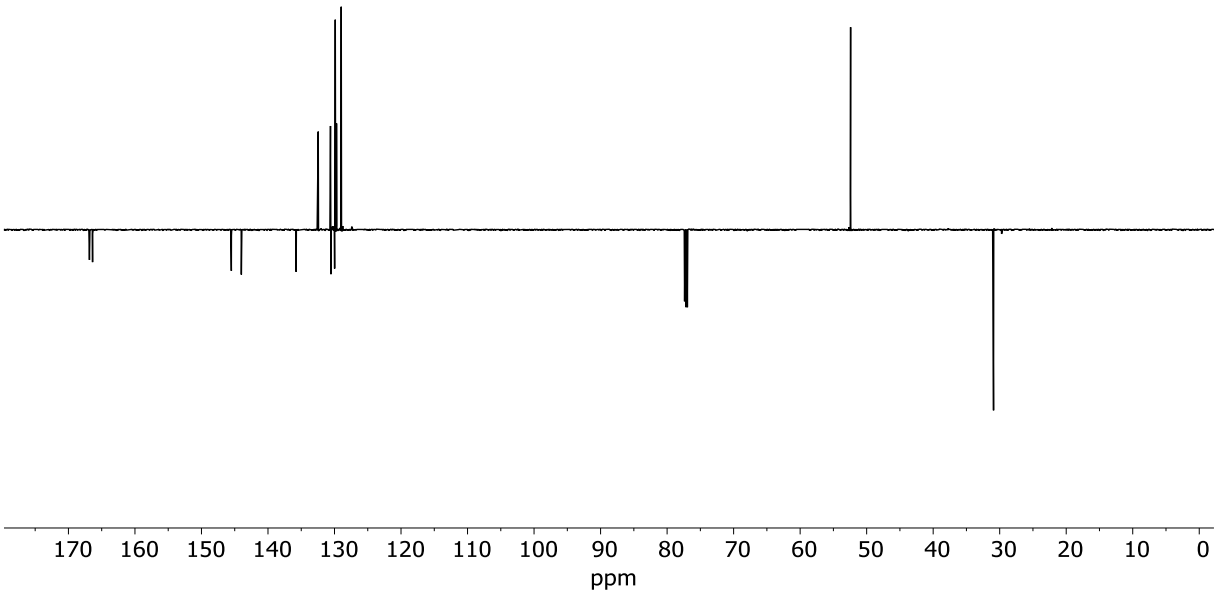

Figure 64: DEPT135Q (151 MHz, $CDCl_3$) spectrum of **2.**

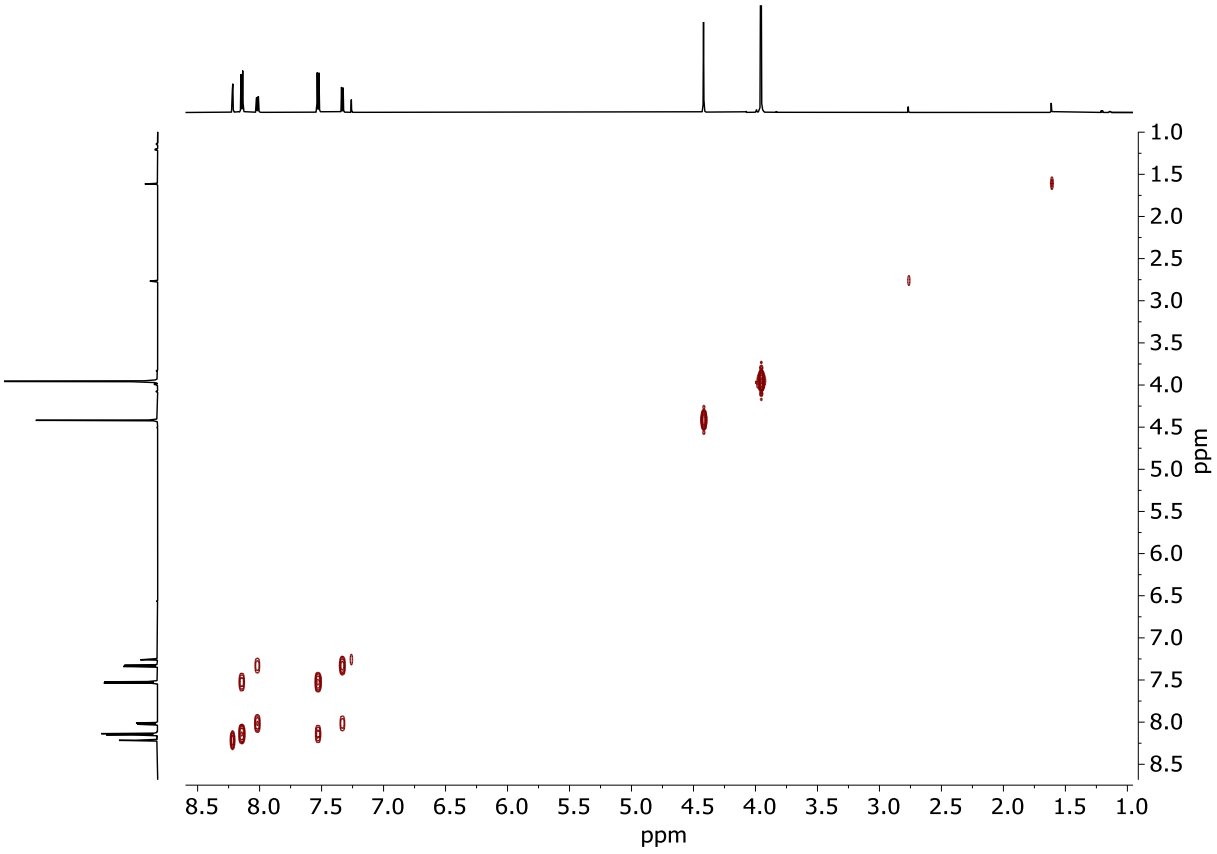

Figure 65: COSY (600 MHz, $CDCl_3$) spectrum of **2.**

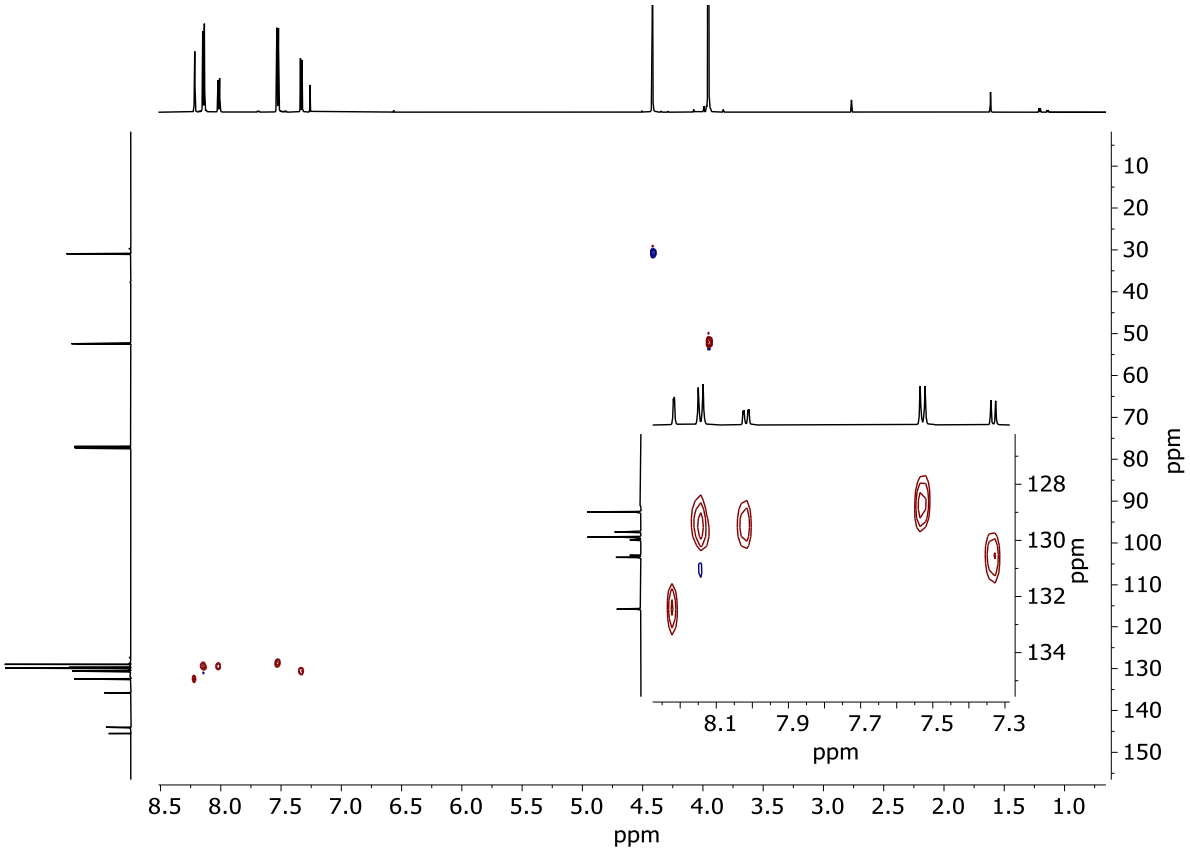

Figure 66: HSQC (600 MHz, $CDCl_3$) spectrum of **2.**

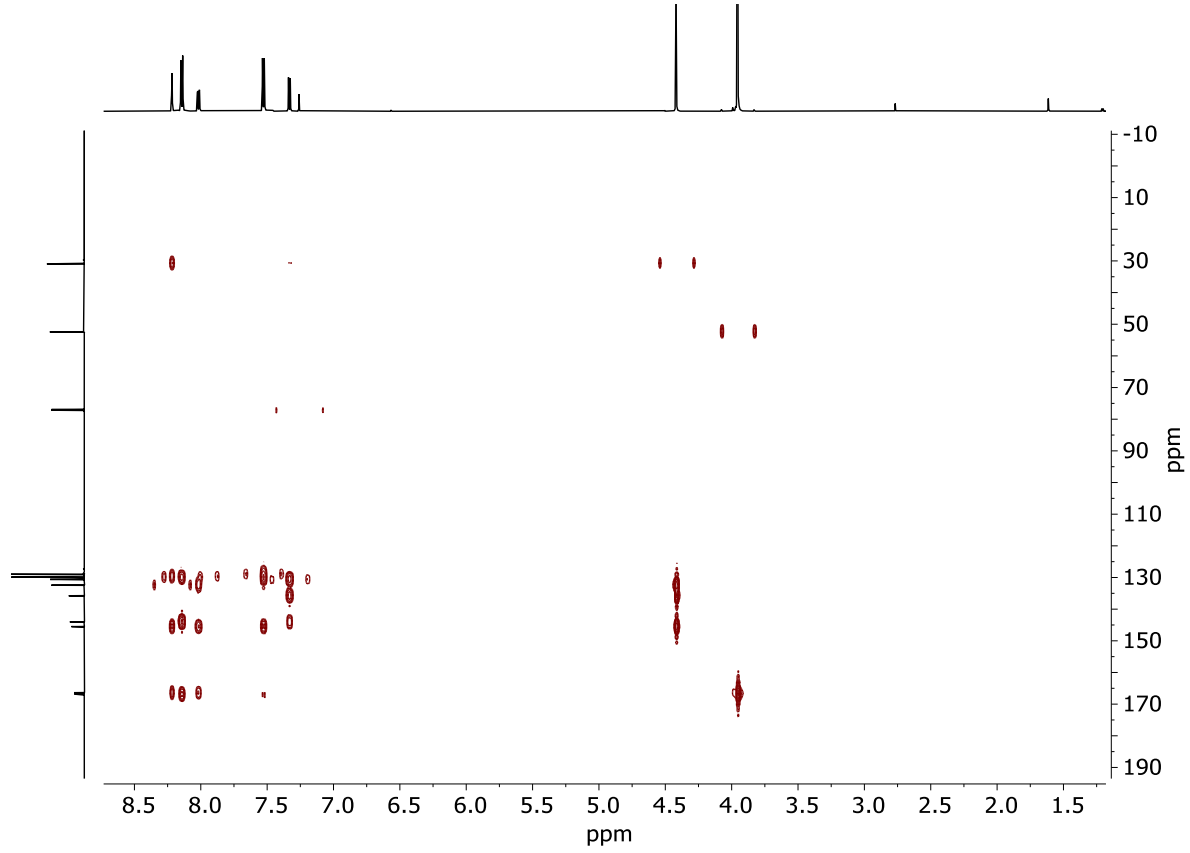

Figure 67: HMBC (600 MHz, $CDCl_3$) spectrum of **2**.

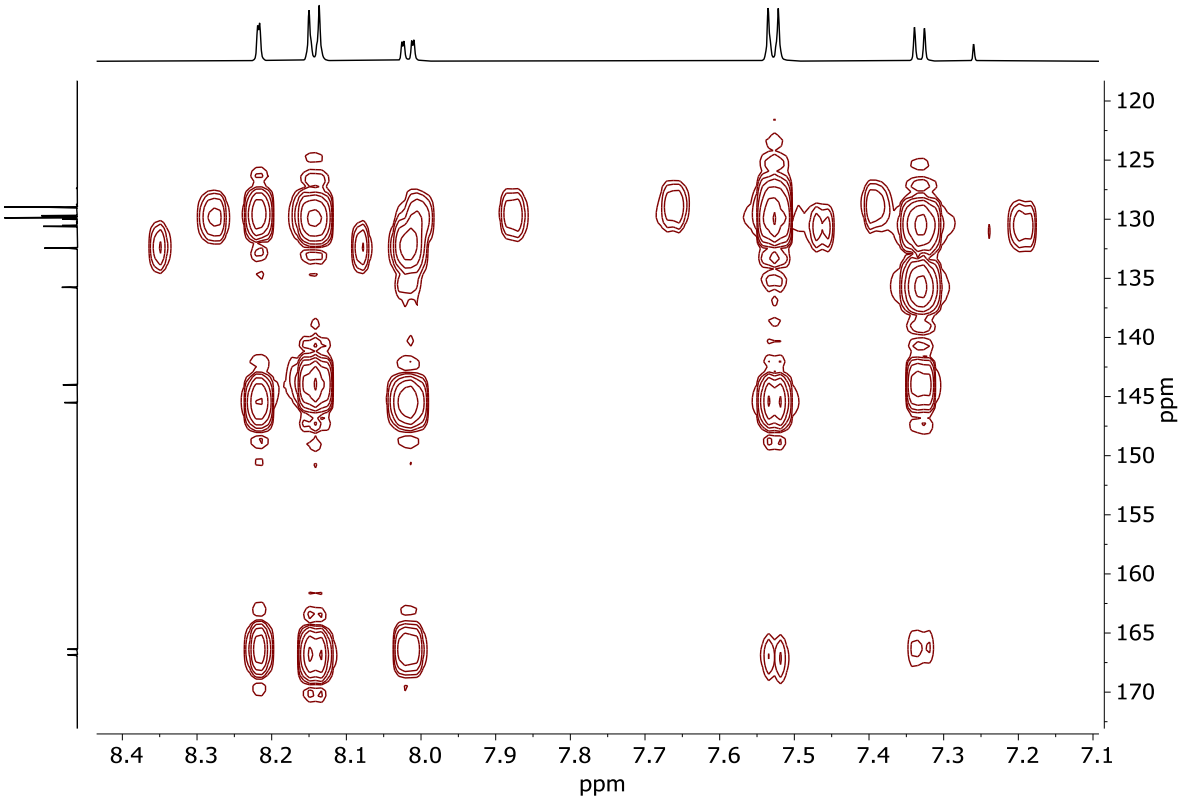

Figure 68: Zoom **of** HMBC (600 MHz, $CDCl_3$) spectrum of **2**.

8.3 Compound 3a

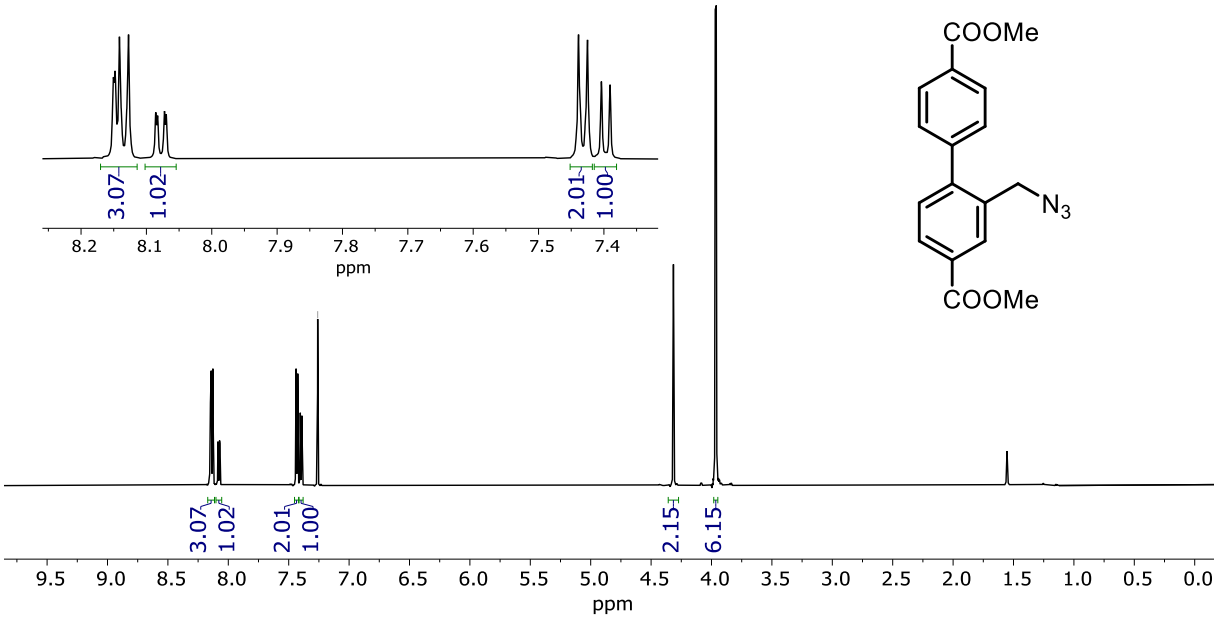

Figure 69: ^{1}H NMR (600 MHz, $CDCl_3$) spectrum of **3a**.

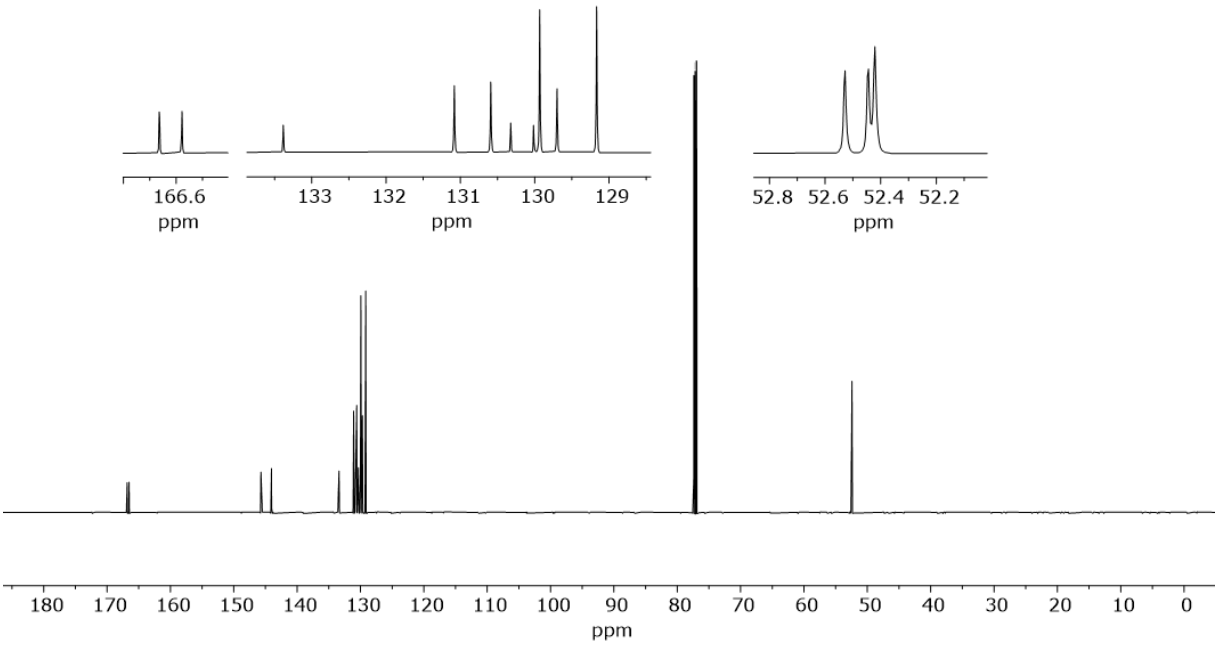

Figure 70: ^{13}C NMR (151 MHz, $CDCl_3$) spectrum of **3a.**

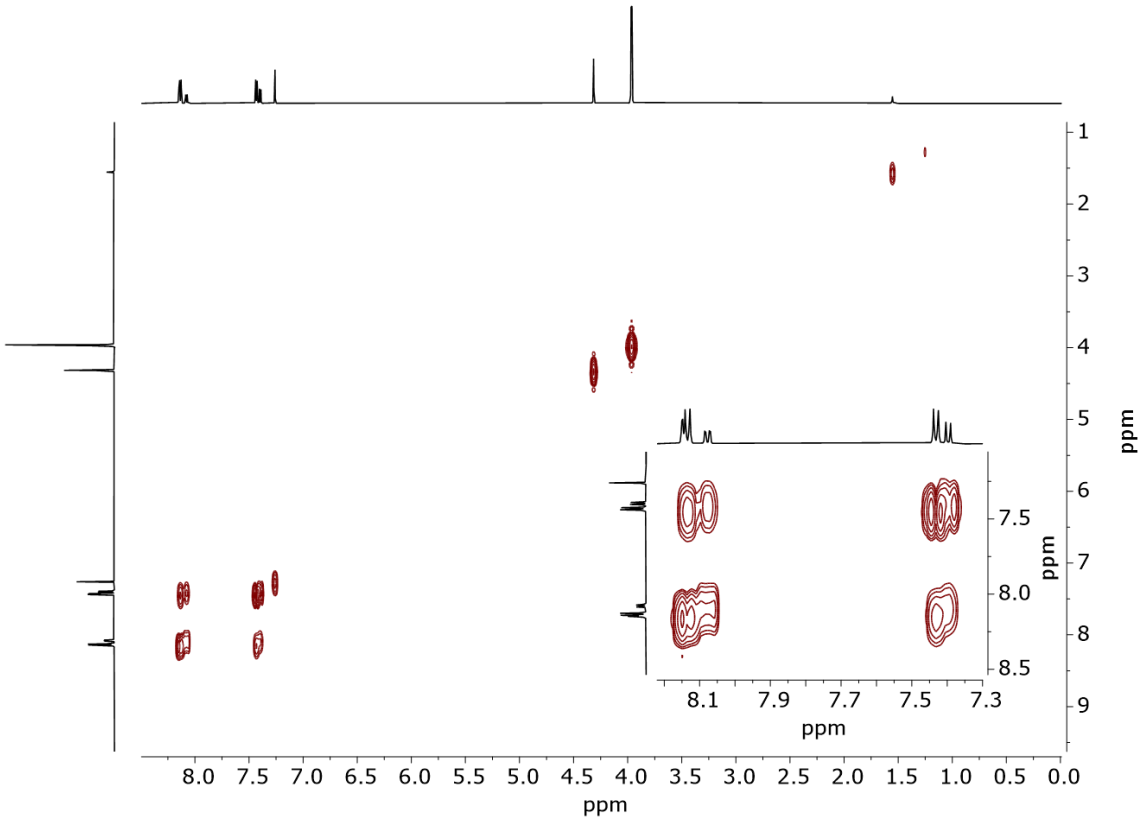

Figure 71: COSY (600 MHz, $CDCl_3$) spectrum of **3a**.

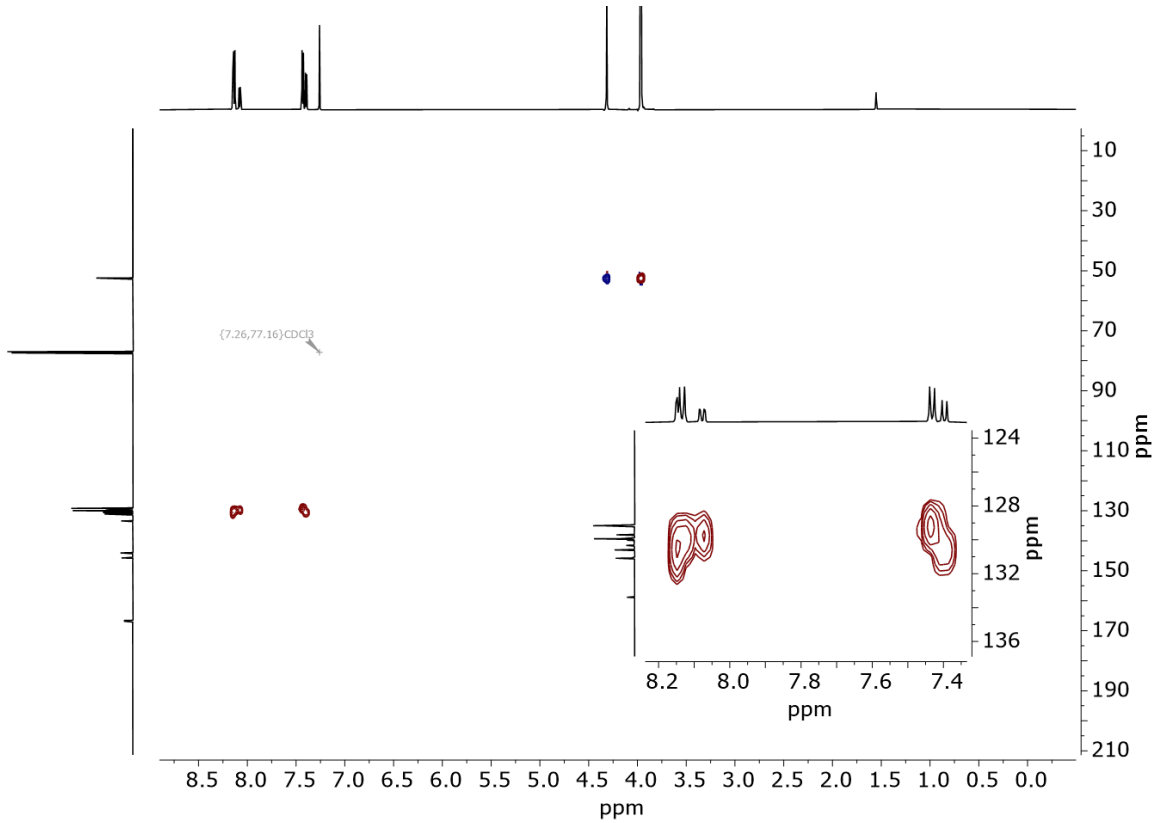

Figure 72: HSQC (600 MHz, $CDCl_3$) spectrum of **3a**.

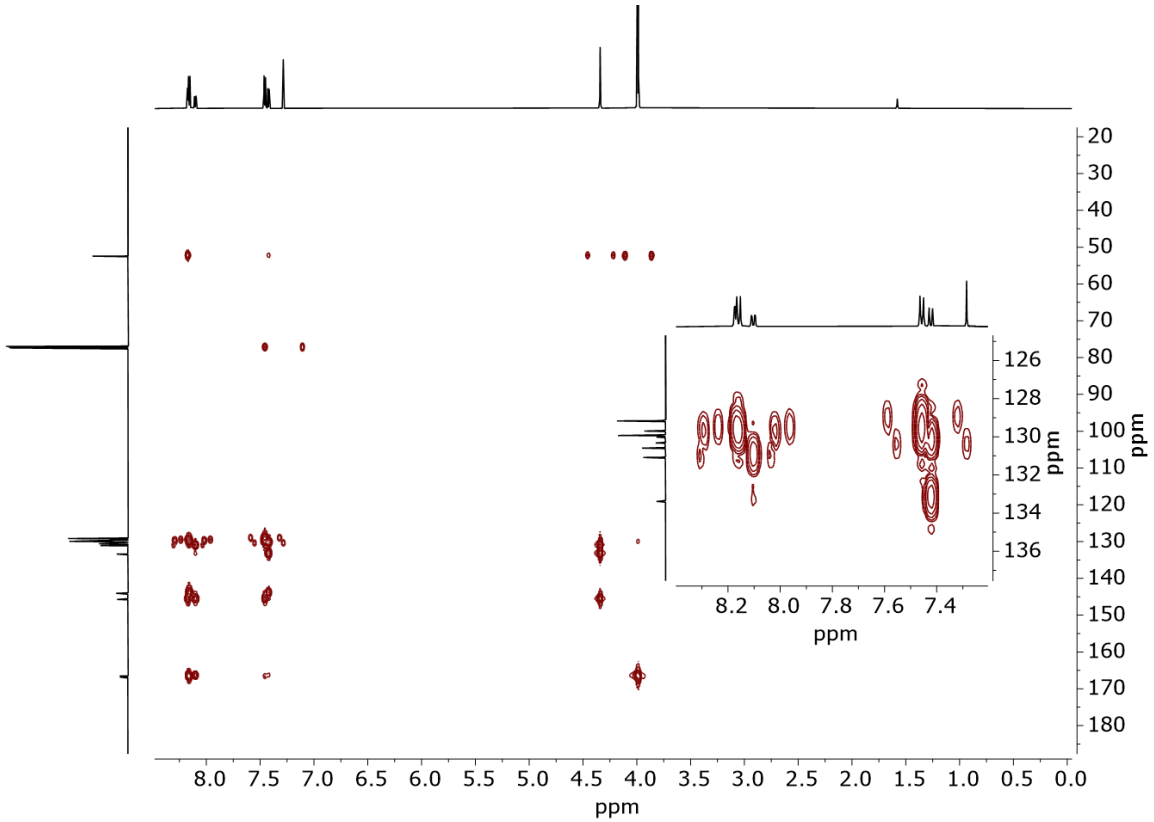

Figure 73: HMBC (600 MHz, $CDCl_3$) spectrum of **3a**.

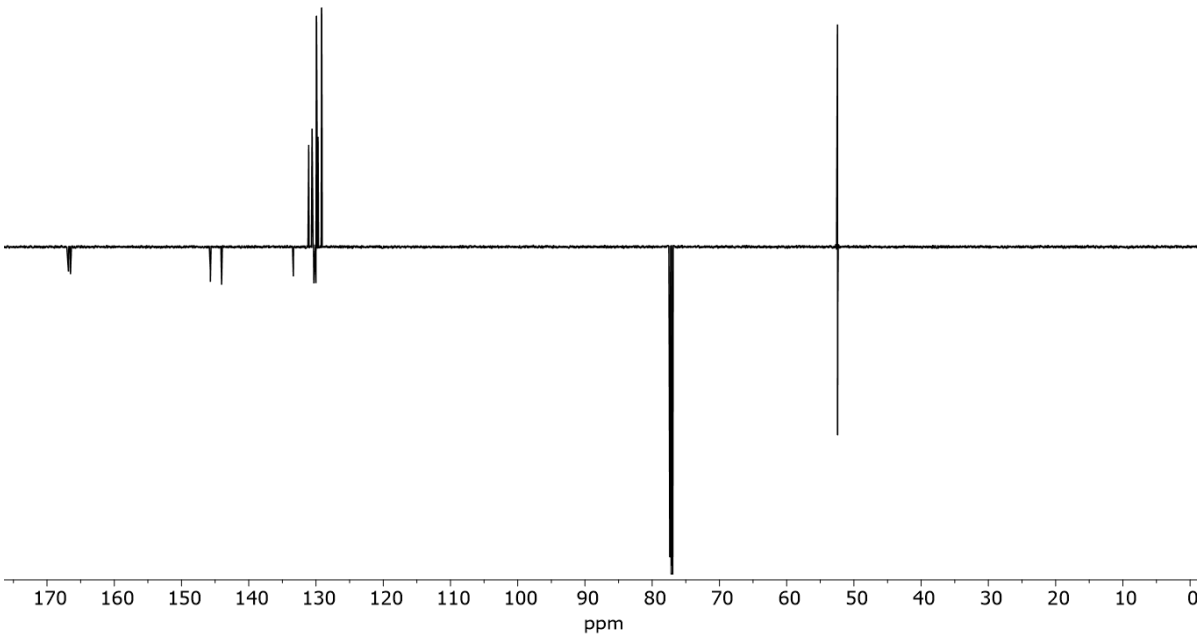

Figure 74: DEPT135Q (151 MHz, $CDCl_3$) spectrum of **3a**.

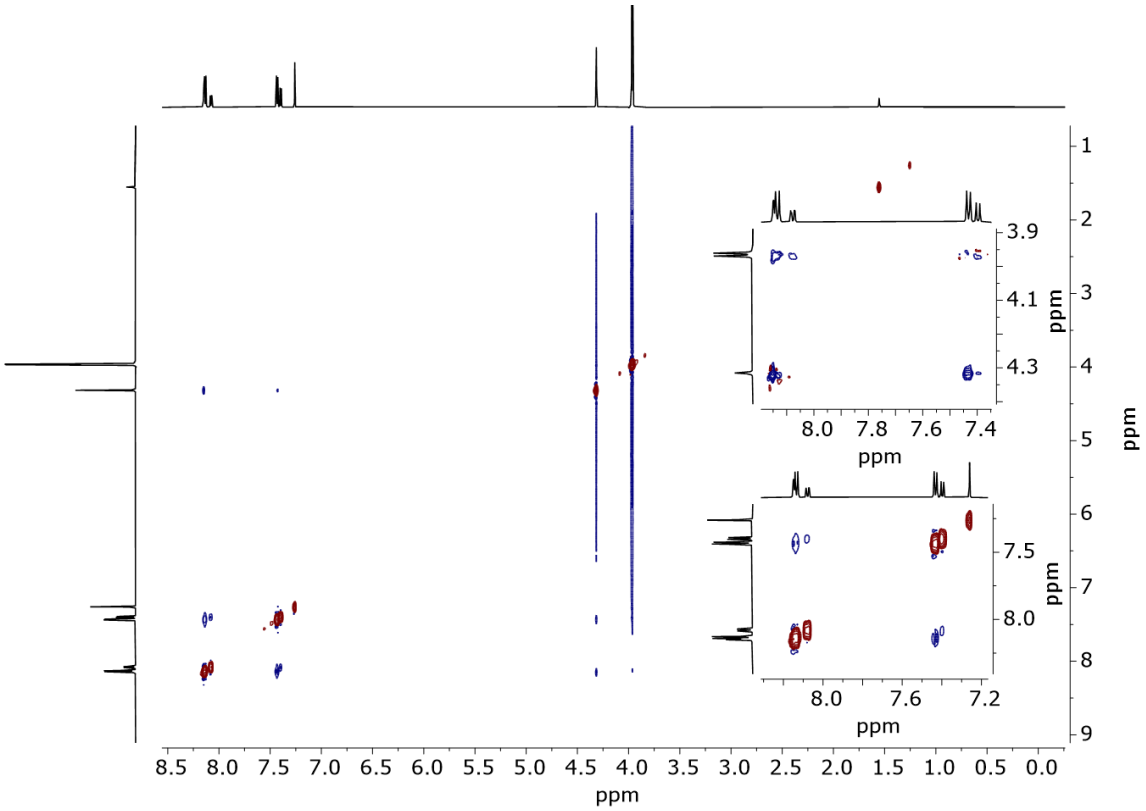

Figure 75: NOESY (600 MHz, $CDCl_3$) of **3a**.

8.4 Compound 4a

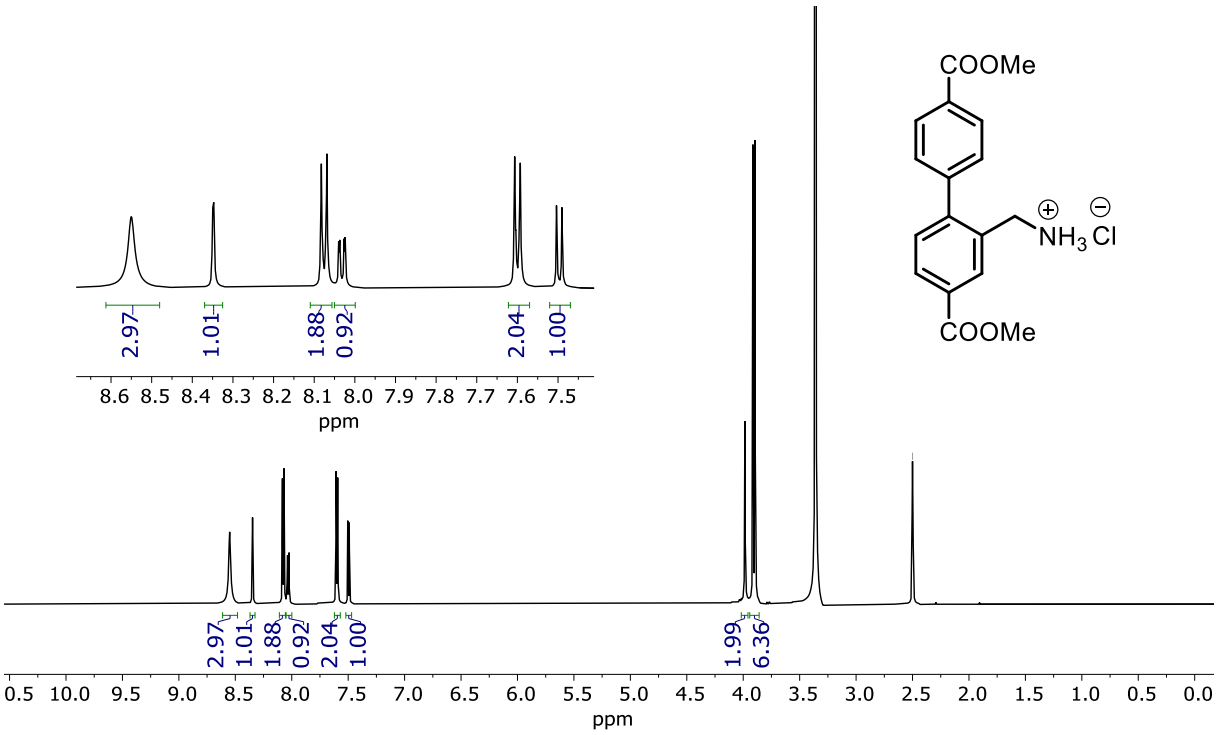

Figure 76: ^{1}H NMR (600 MHz, DMSO-d_6) spectrum of **4a**.

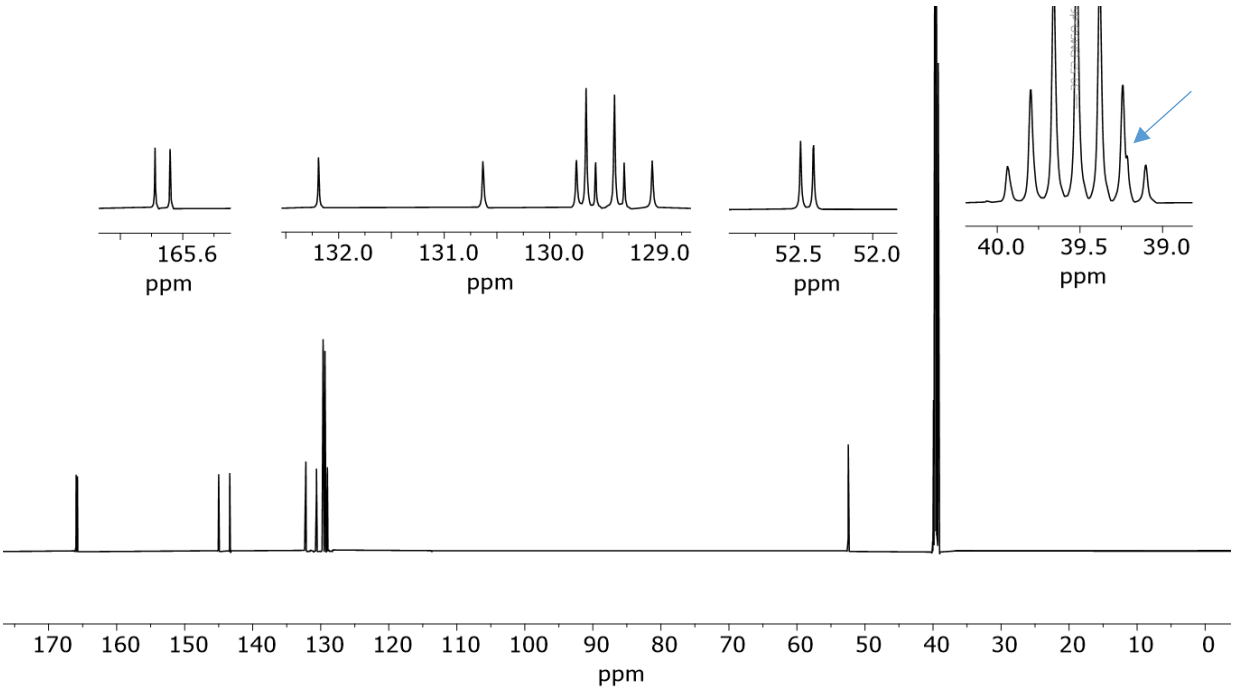

Figure 77: ^{13}C NMR (151 MHz, DMSO-d_6) spectrum of **4a**. Methylene carbon is marked with a blue arrow.

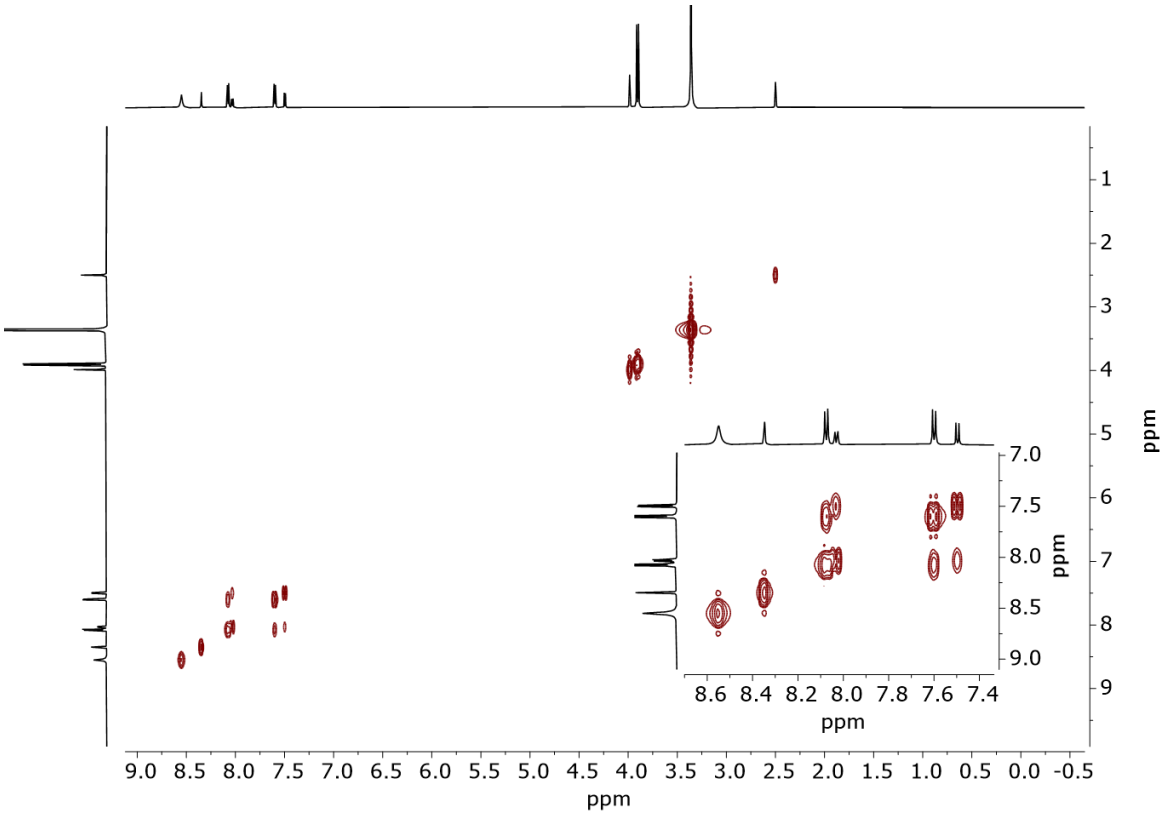

Figure 78: COSY (600 MHz, DMSO-d_6) spectrum of **4a**.

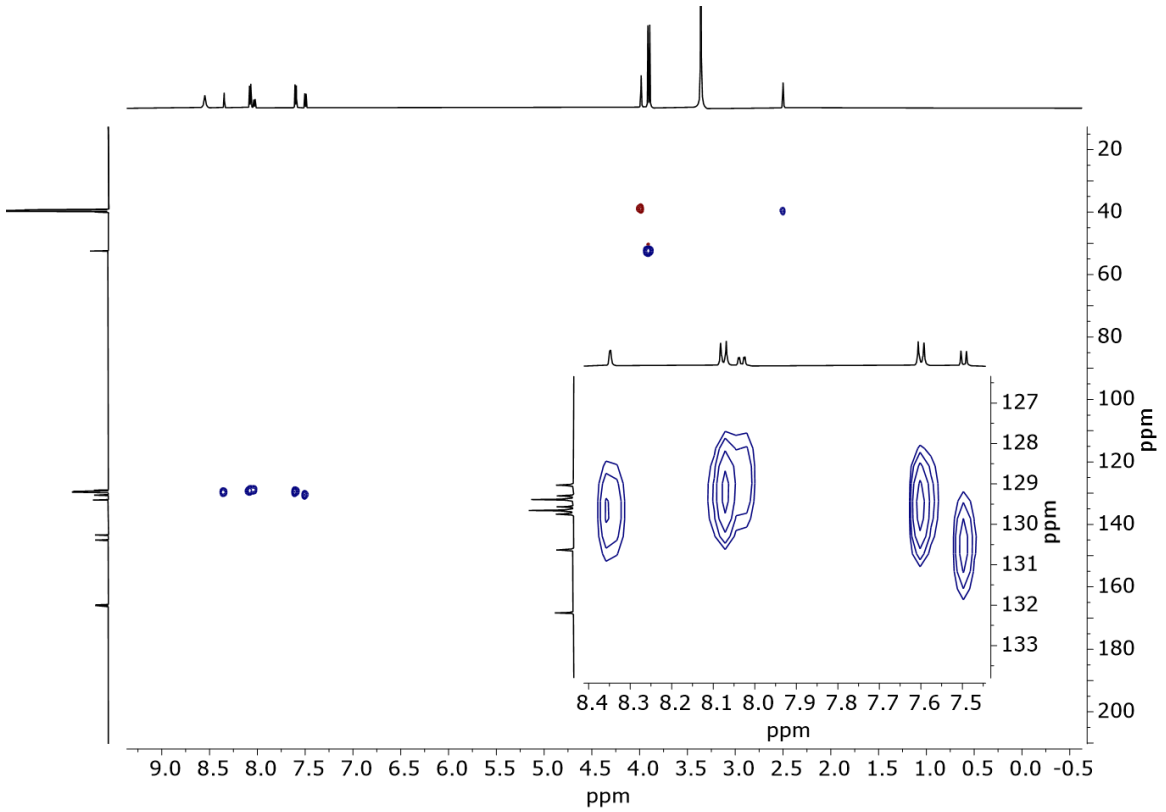

Figure 79: HSQC (600 MHz, DMSO-d_6,) spectrum of **4a**.

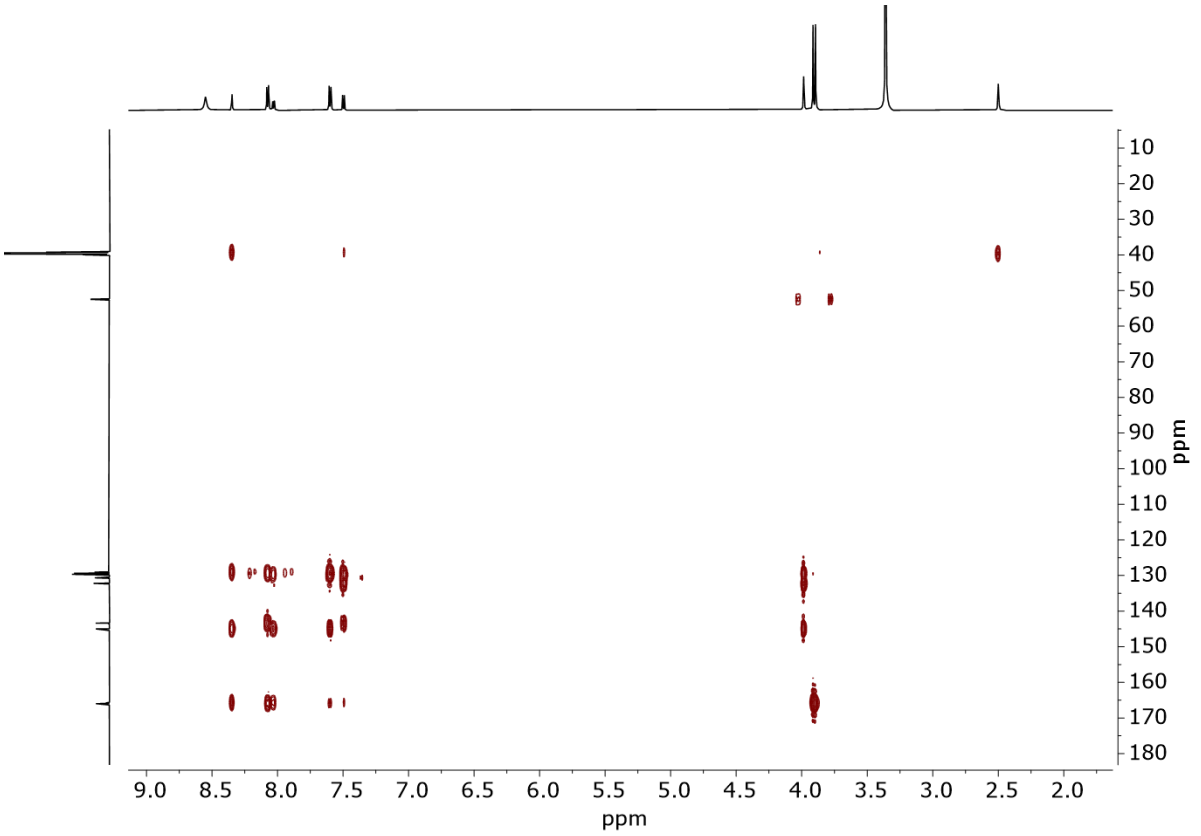

Figure 80: HMBC (600 MHz, DMSO-d_6,) spectrum of **4a**

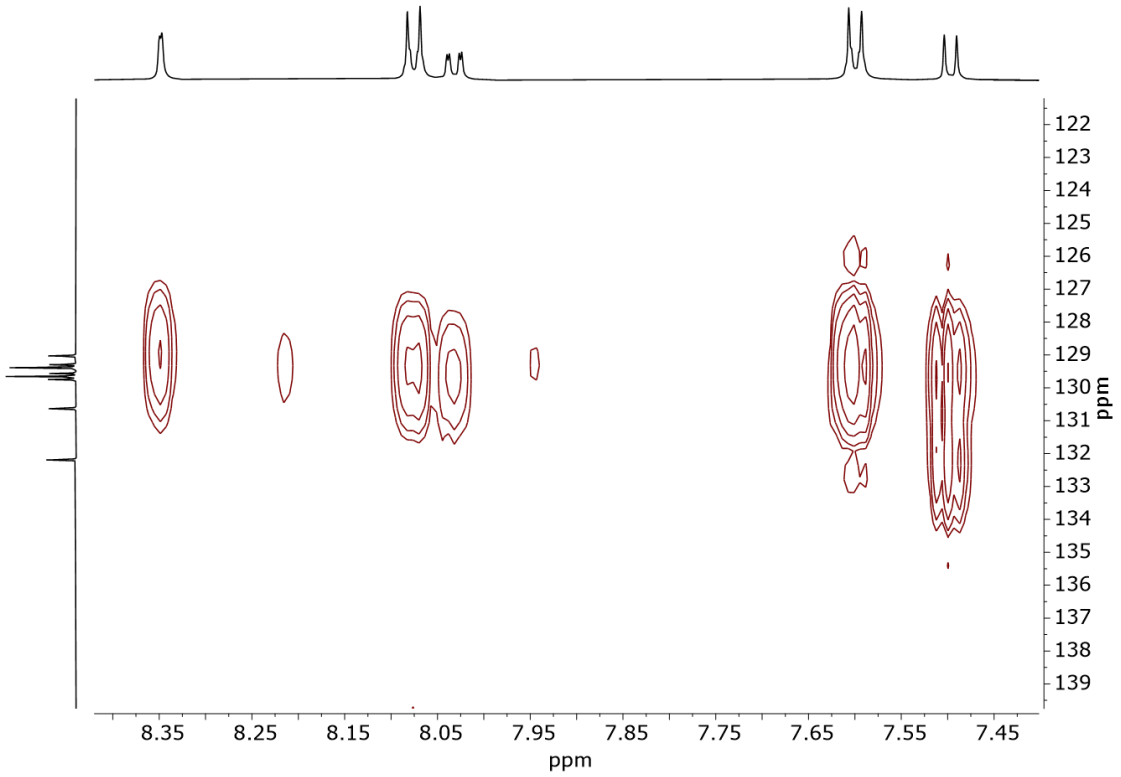

Figure 81: Zoom of HMBC (600 MHz, DMSO-d_6,) spectrum of **4a.**

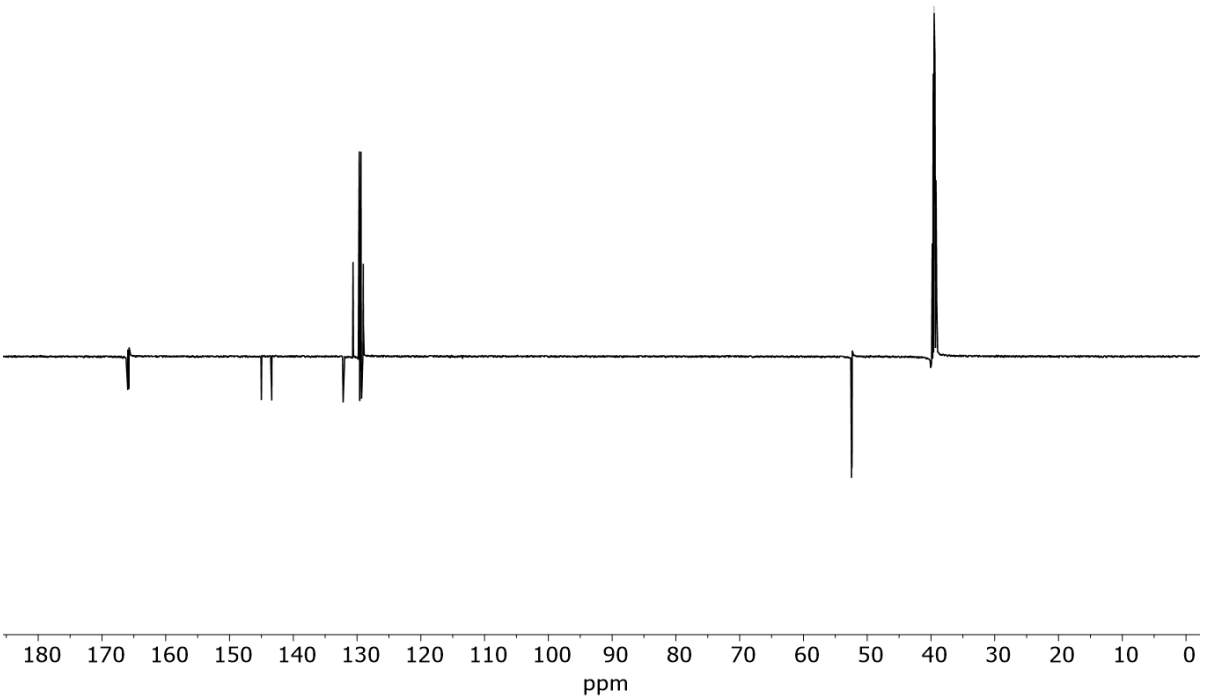

Figure 82: DEPT135Q (151 MHz, DMSO-d_6) spectrum of **4a**.

8.5 Compound 5

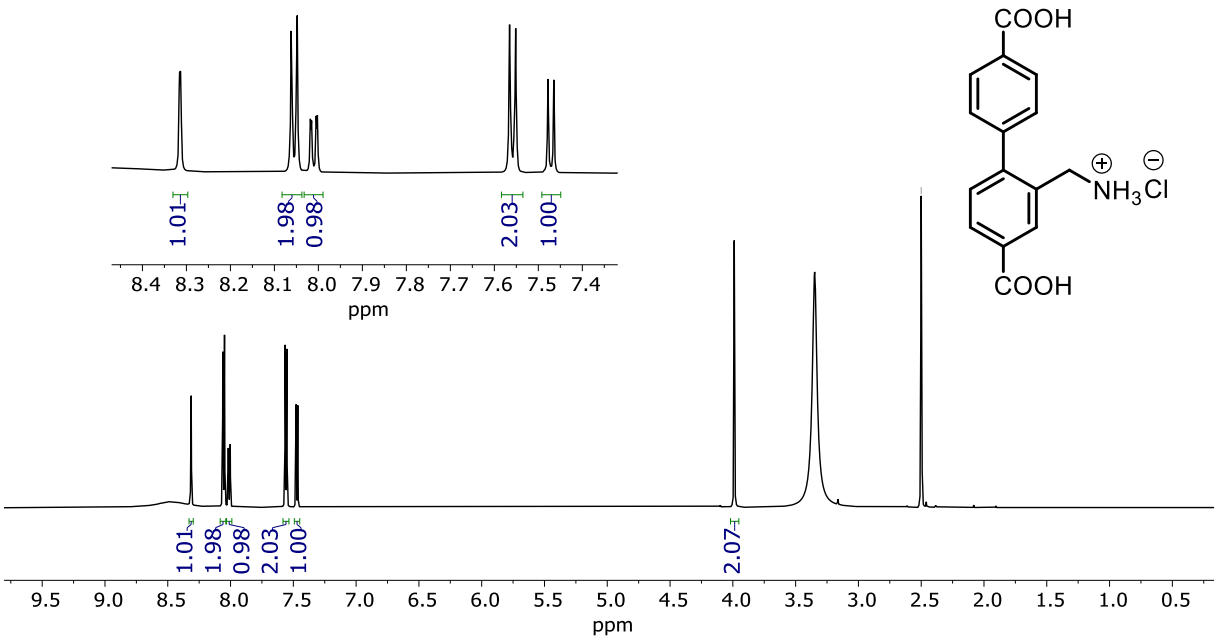

Figure 83: ^{1}H NMR (600 MHz, DMSO-d_6) spectrum of **5.**

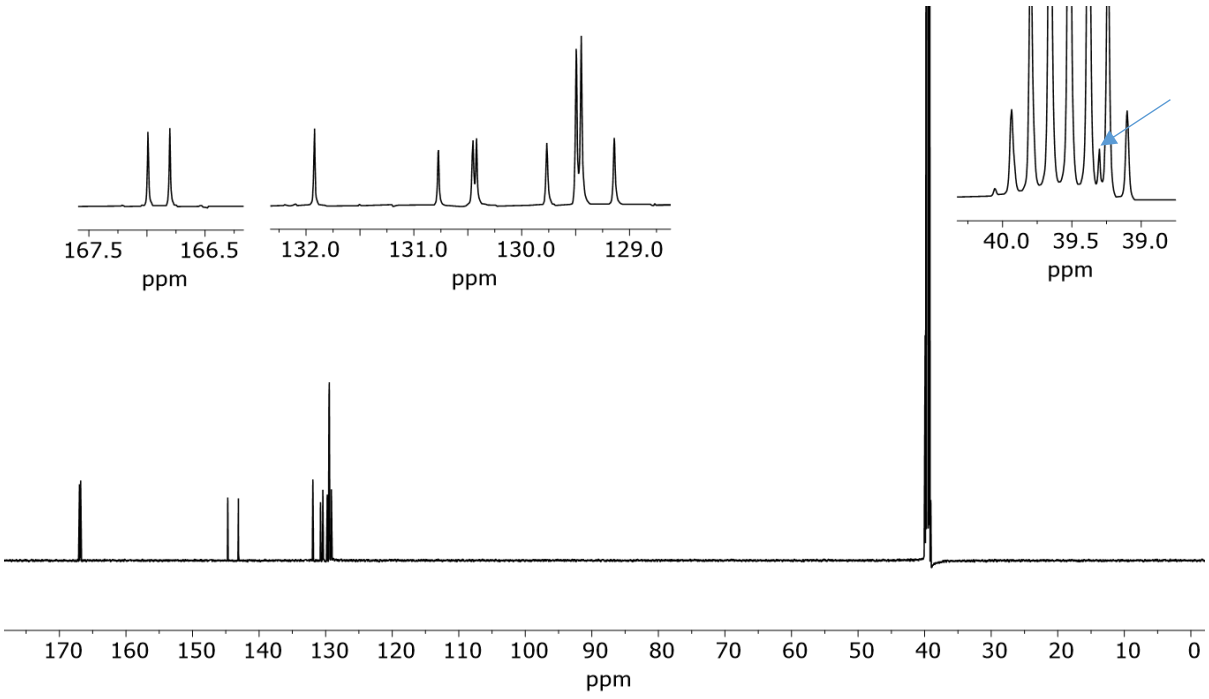

Figure 84: ^{13}C NMR (151 MHz, DMSO-d_6) spectrum of **5**. Methylene carbon is marked with a blue arrow.

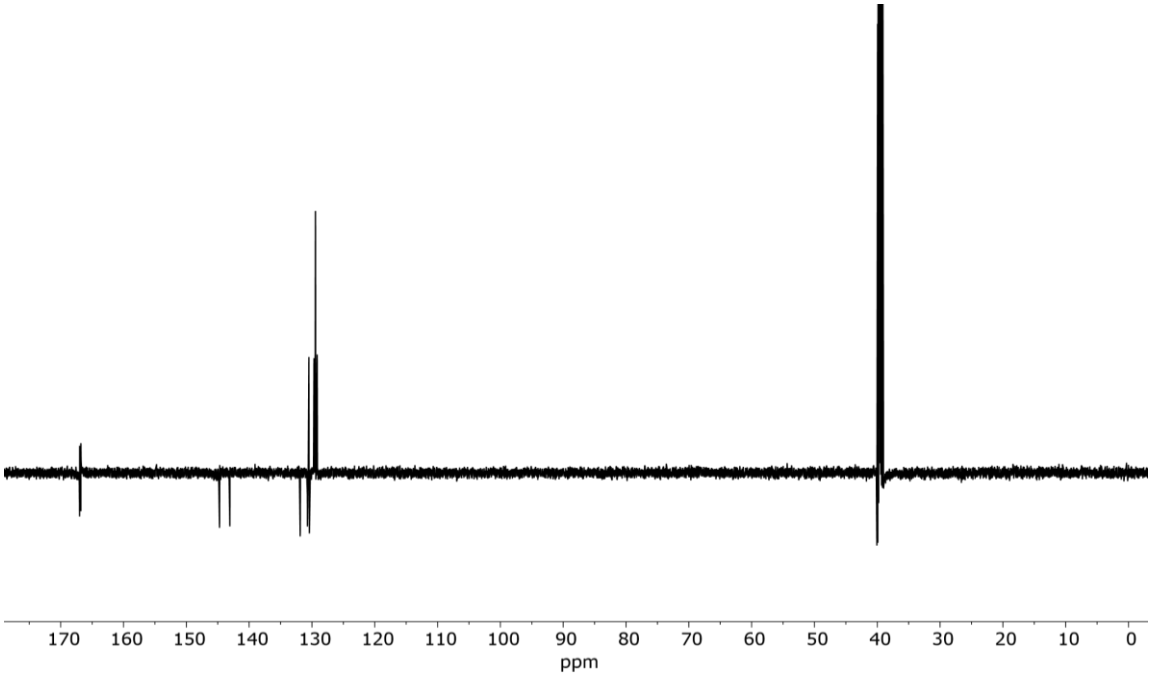

Figure 85: DEPT135Q (151 MHz, DMSO-d_6) spectrum of **5**.

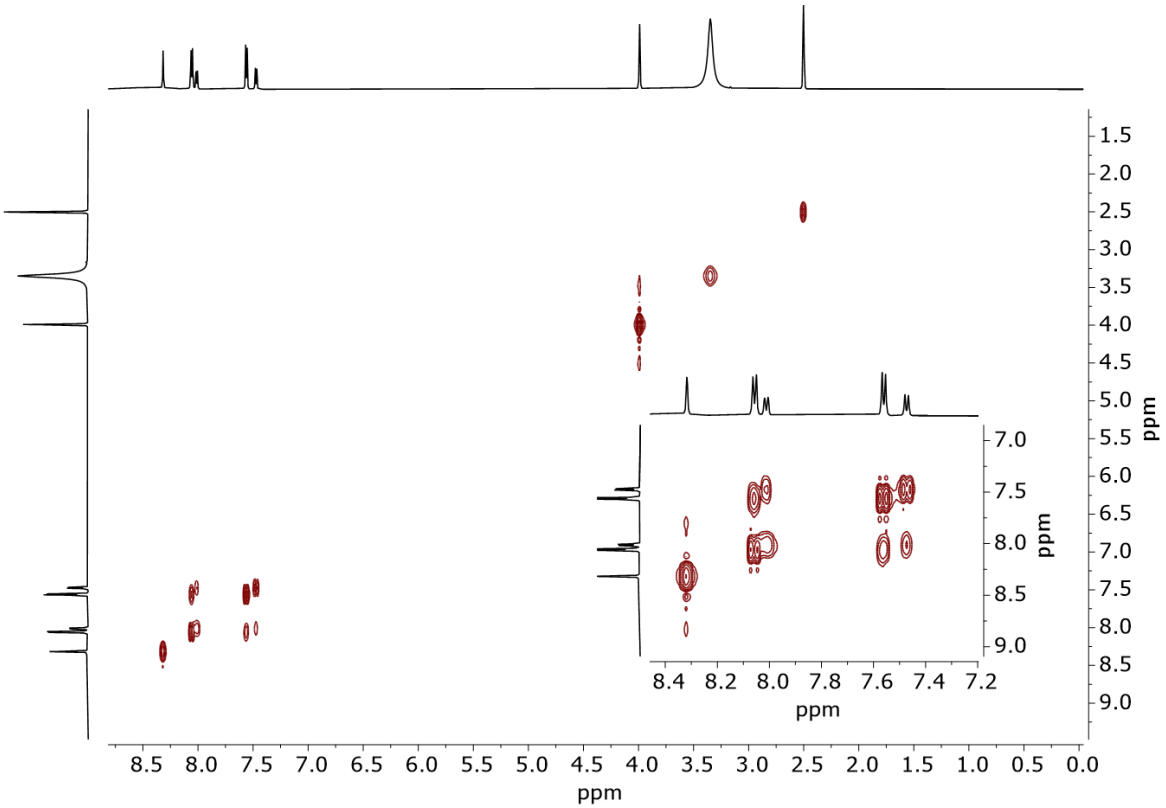

Figure 86: COSY (600 MHz, DMSO-d_6,) of **5**.

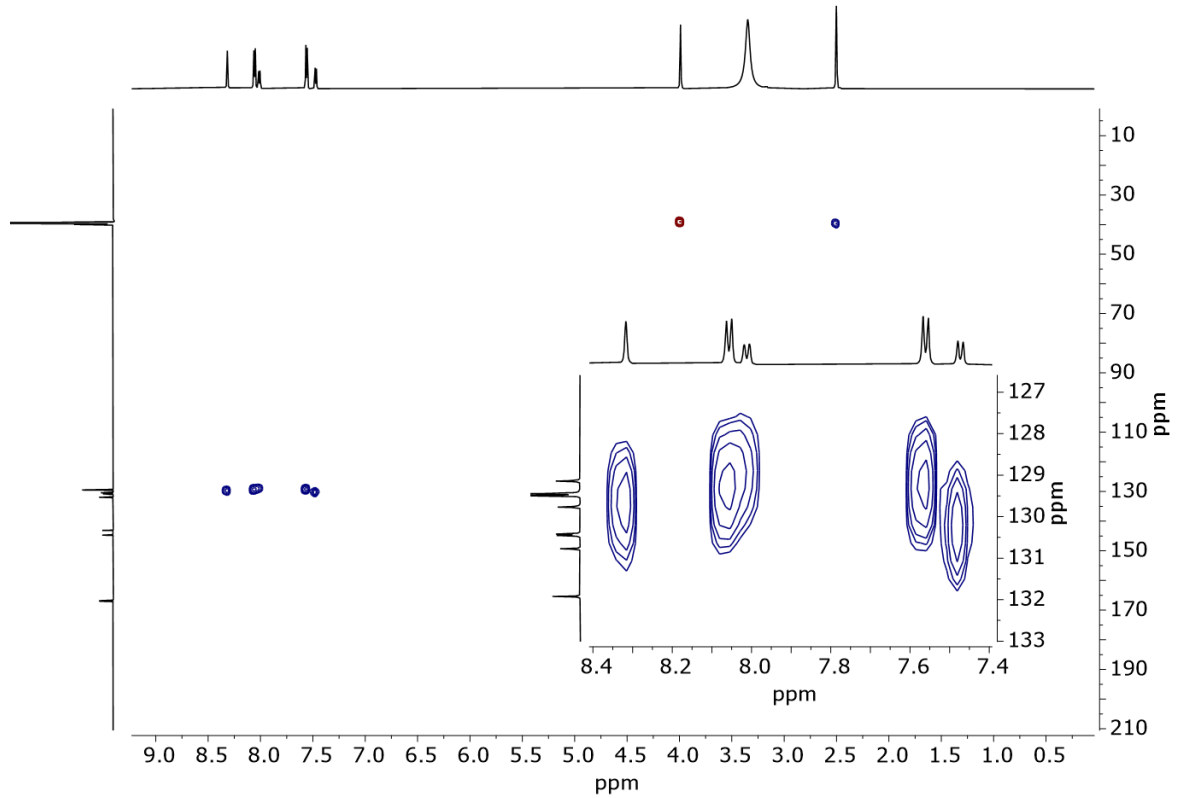

Figure 87: HSQC (600 MHz, DMSO-d_6) spectrum of **5**.

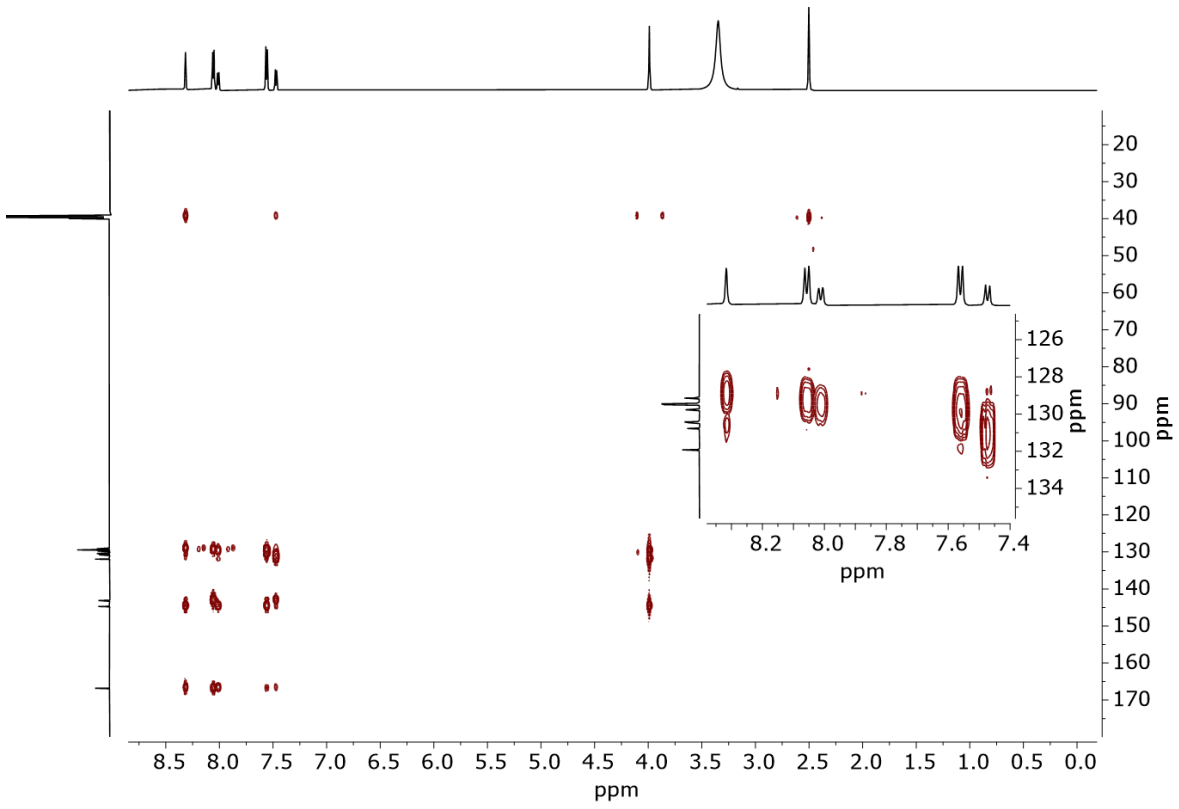

Figure 88: HMBC (600 MHz, DMSO-d_6) spectrum of **5**.

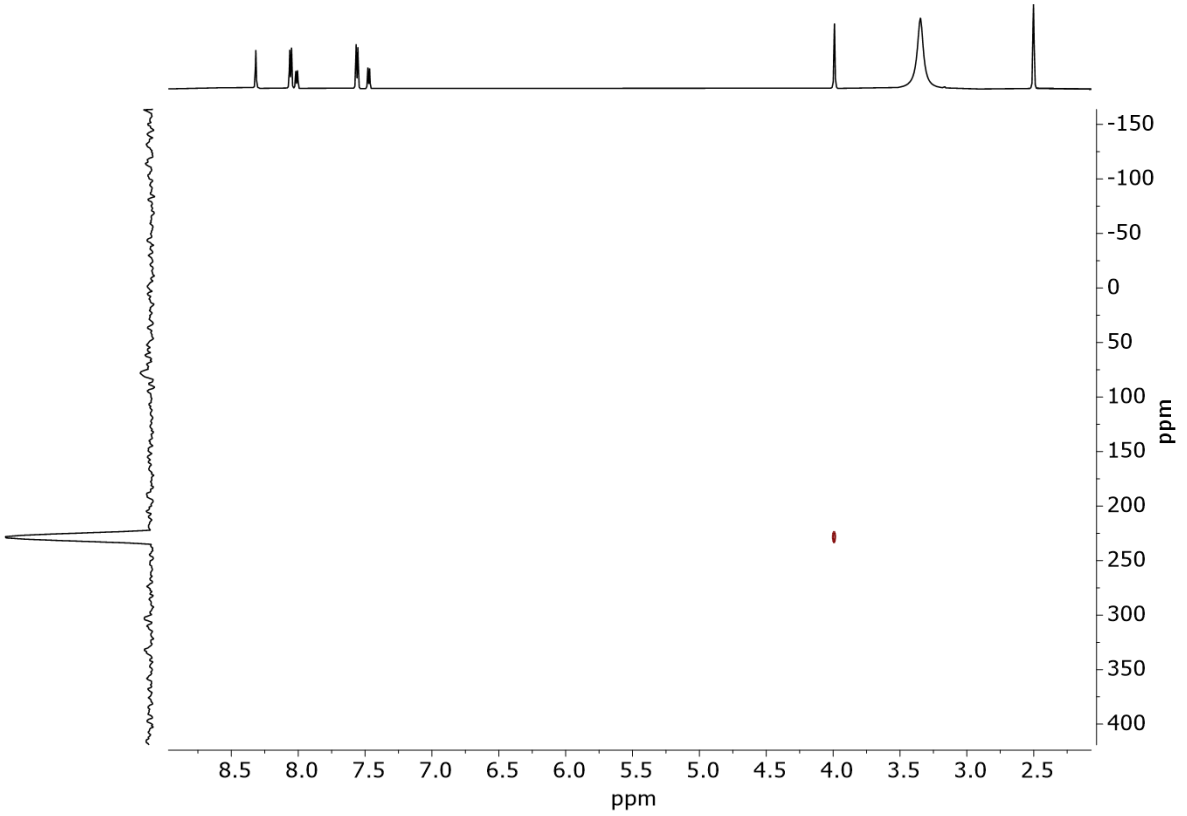

Figure 89: ^{1}H-^{15}N HMBC (600 MHz, DMSO-d_6) spectrum of **5**.

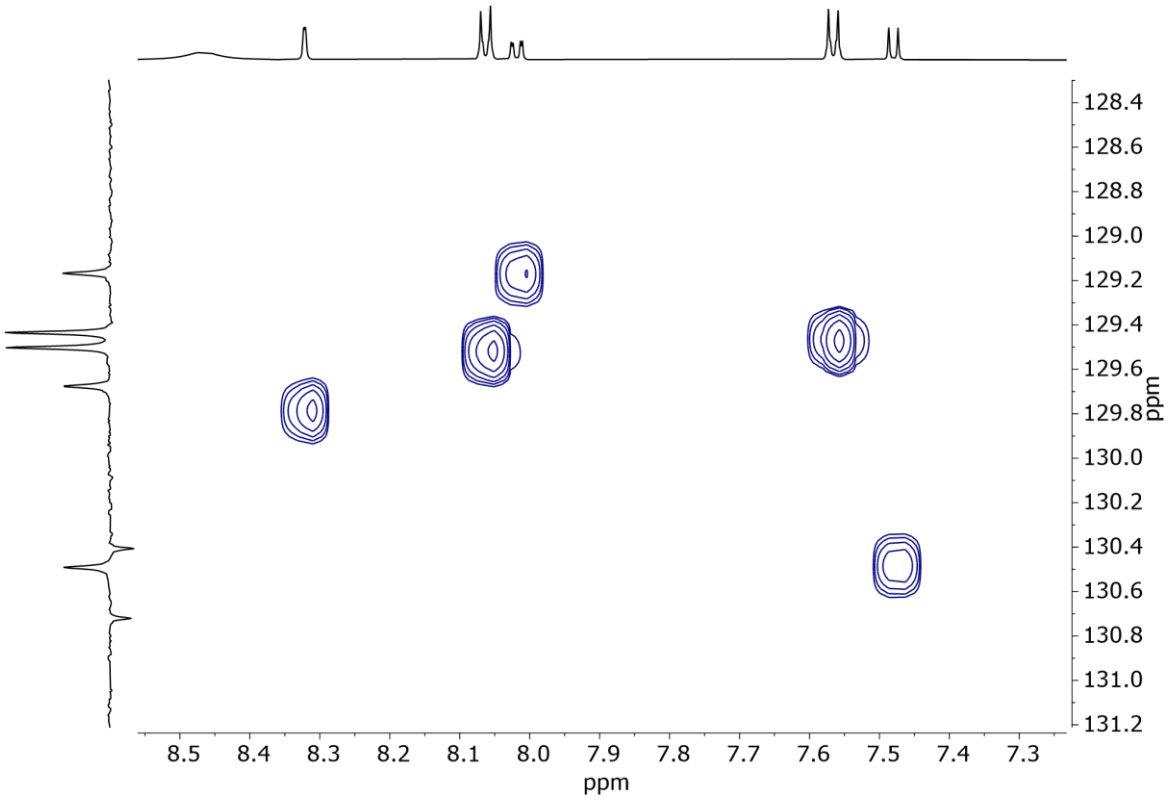

Figure 90: S HSQC (600 MHz, DMSO-d_6) spectrum of **5**.

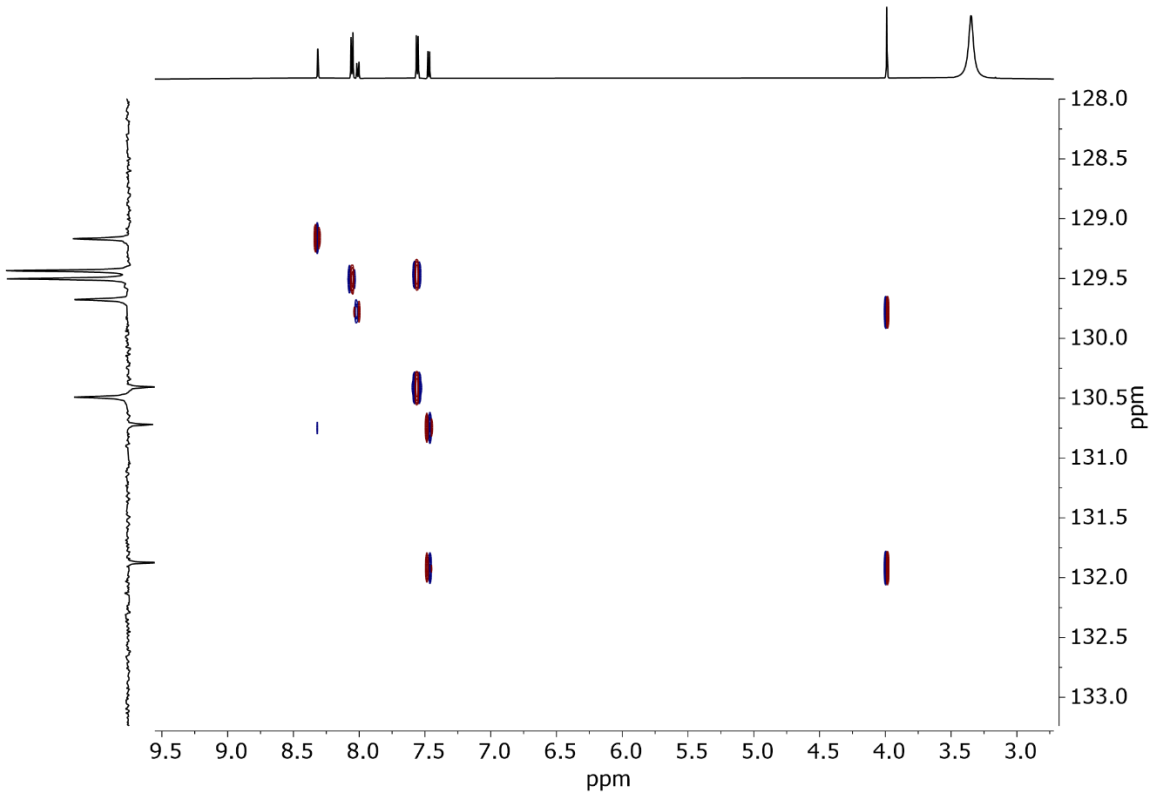

Figure 91: S HMBC (600 MHz, DMSO-d_6) spectrum of **5**.

8.6 Compound 3b

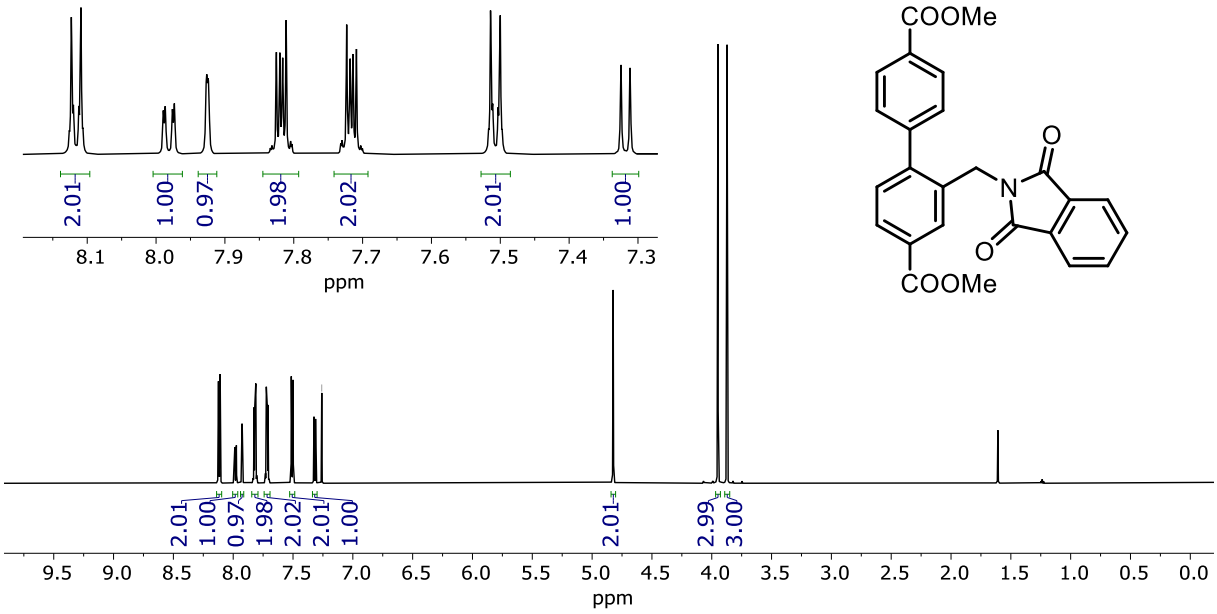

Figure 92: ^{1}H NMR (600 MHz, $CDCl_3$) spectrum of **3b**.

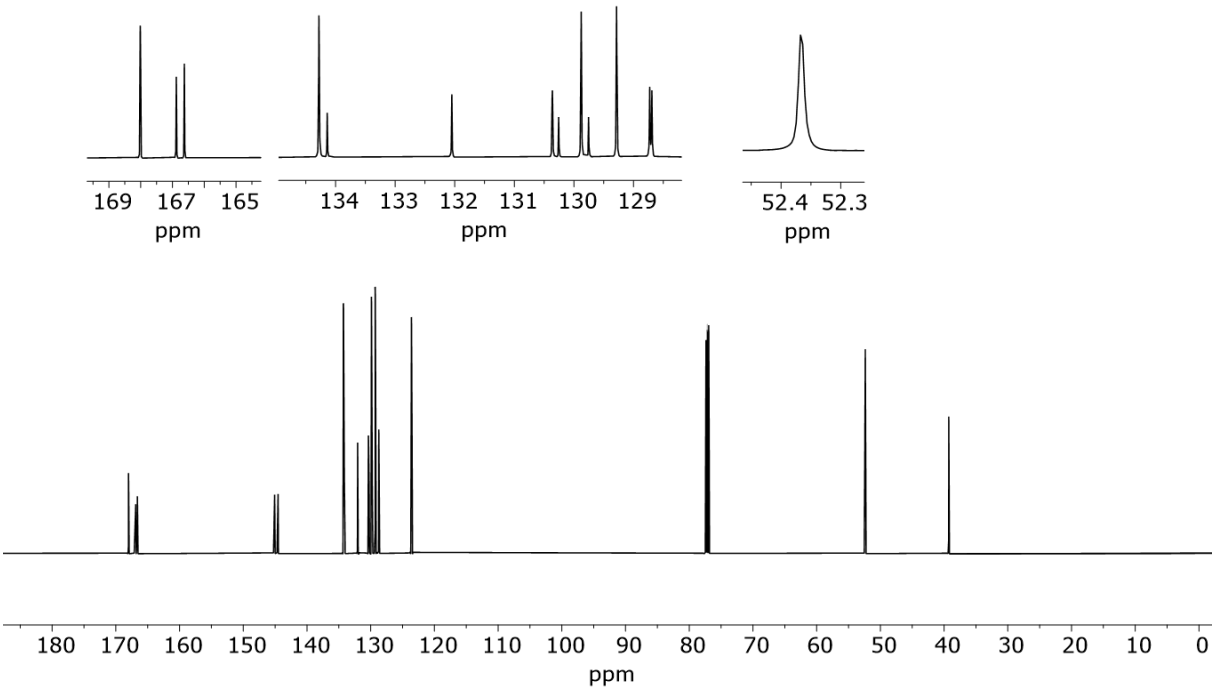

Figure 93: ^{13}C NMR (151 MHz, $CDCl_3$) spectrum of **3b**.

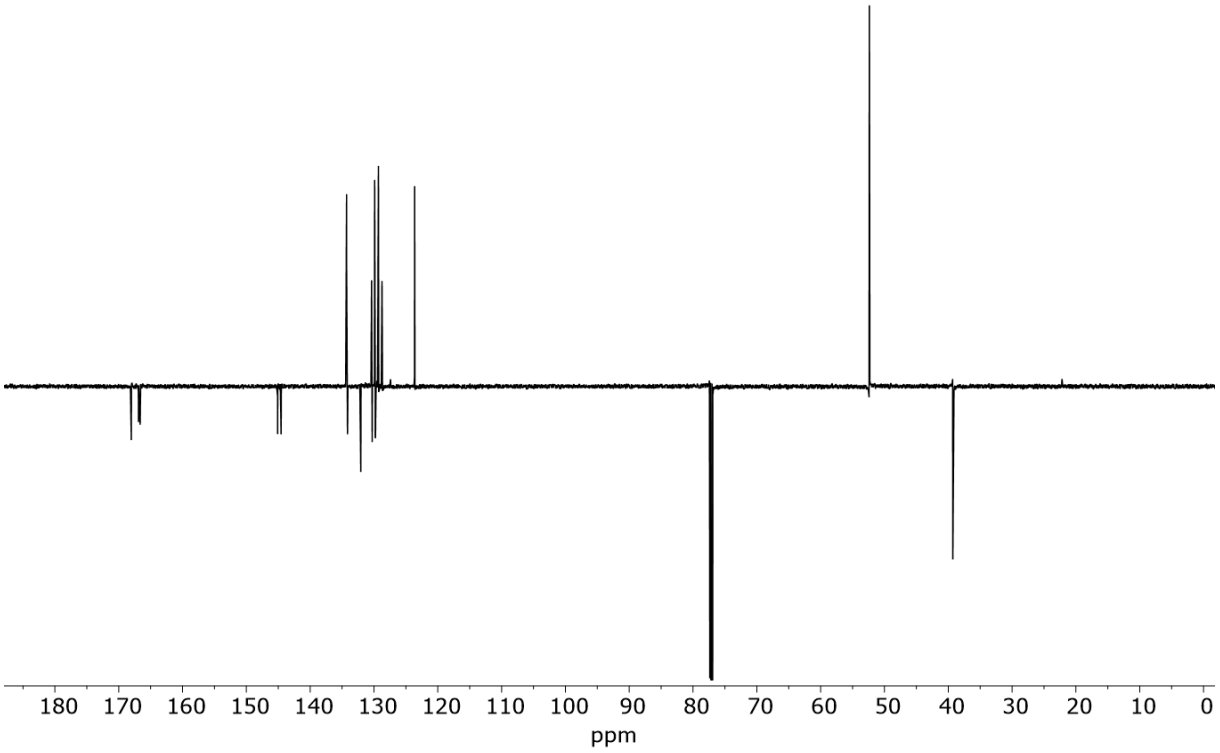

Figure 94: DEPT135Q (151 MHz, $CDCl_3$) spectrum of **3b**.

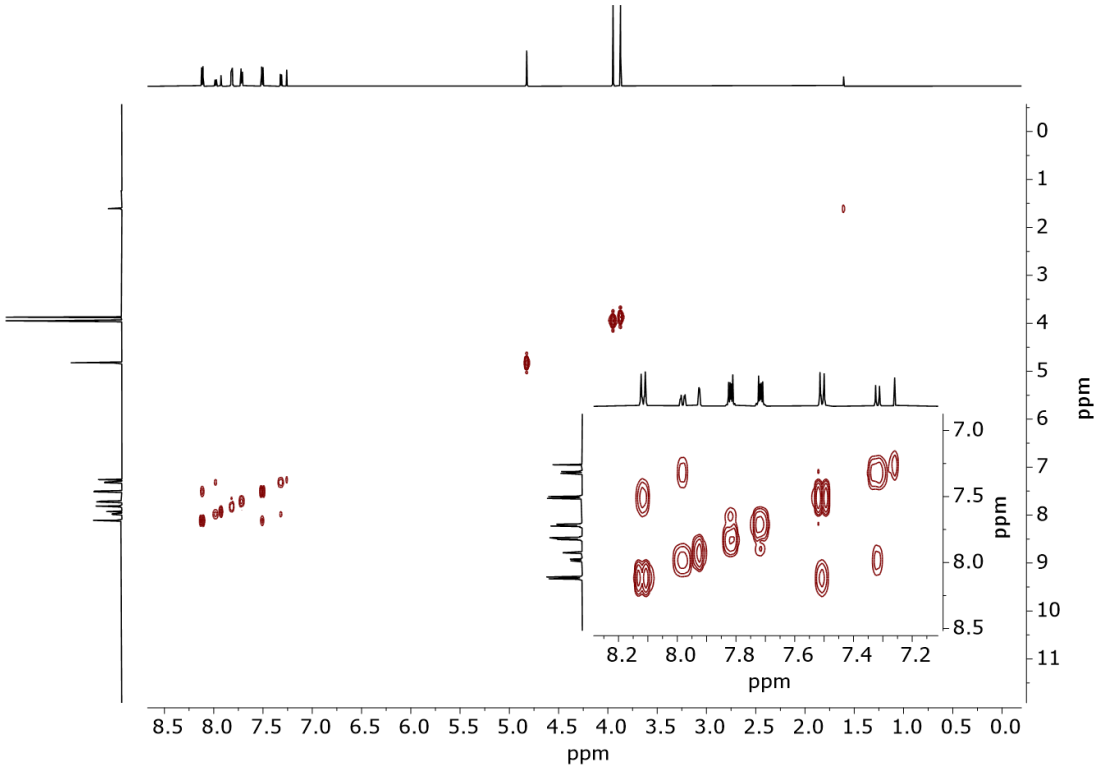

Figure 95: COSY (600 MHz, $CDCl_3$) spectrum of **3b**.

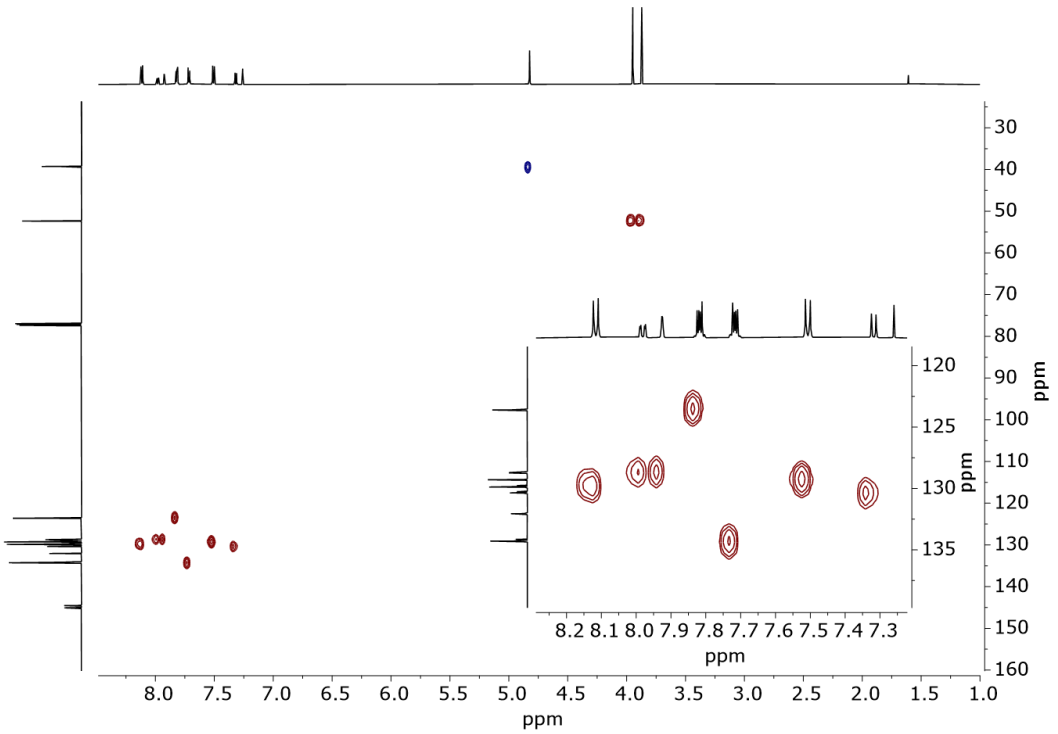

Figure 96: HSQC (600 MHz, $CDCl_3$) spectrum of **3b**.

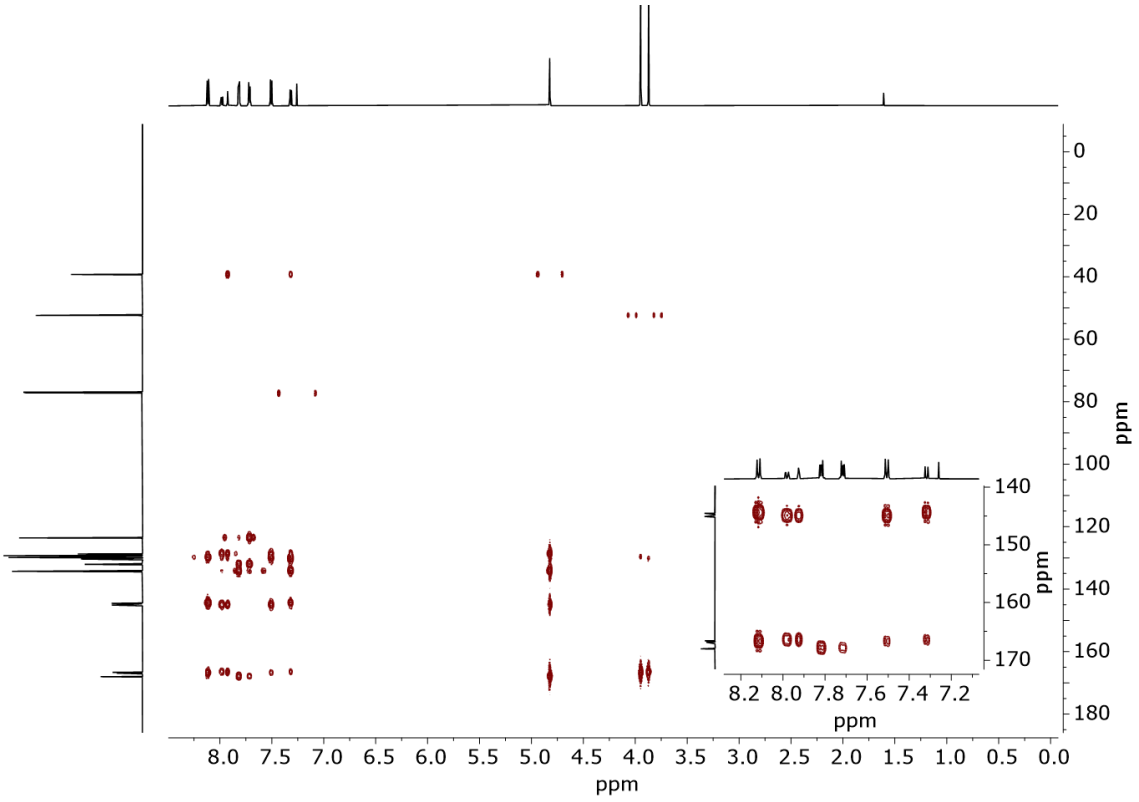

Figure 97: HMBC (600 MHz, $CDCl_3$) spectrum of **3b.**

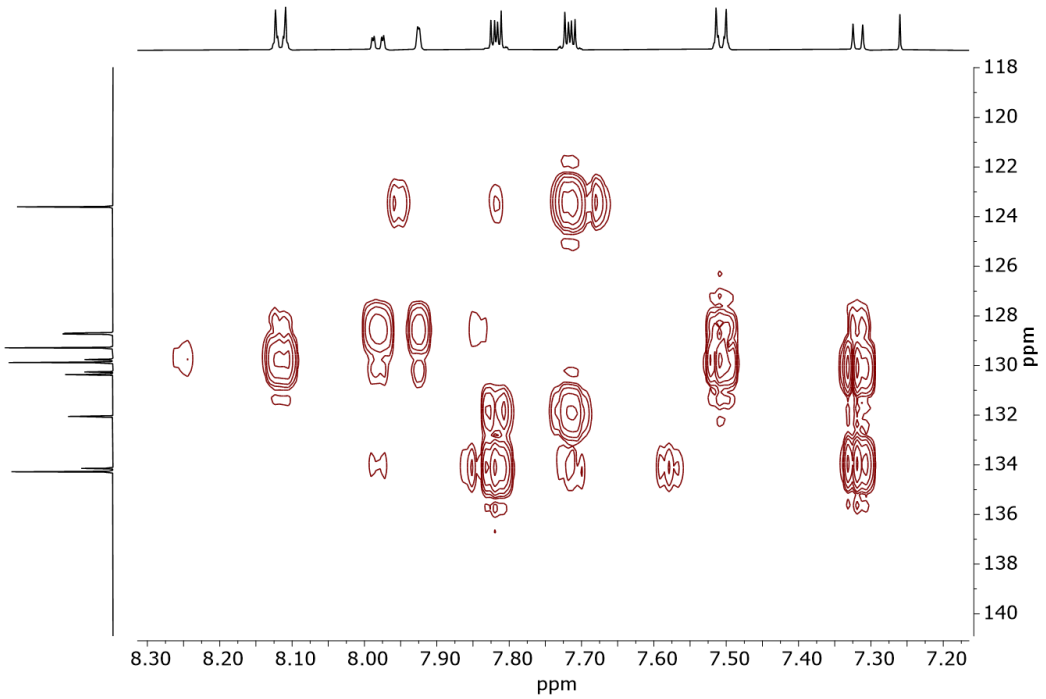

Figure 98: Zoom of HMBC (600 MHz, $CDCl_3$) spectrum of **3b**.

8.7 Compound 4b

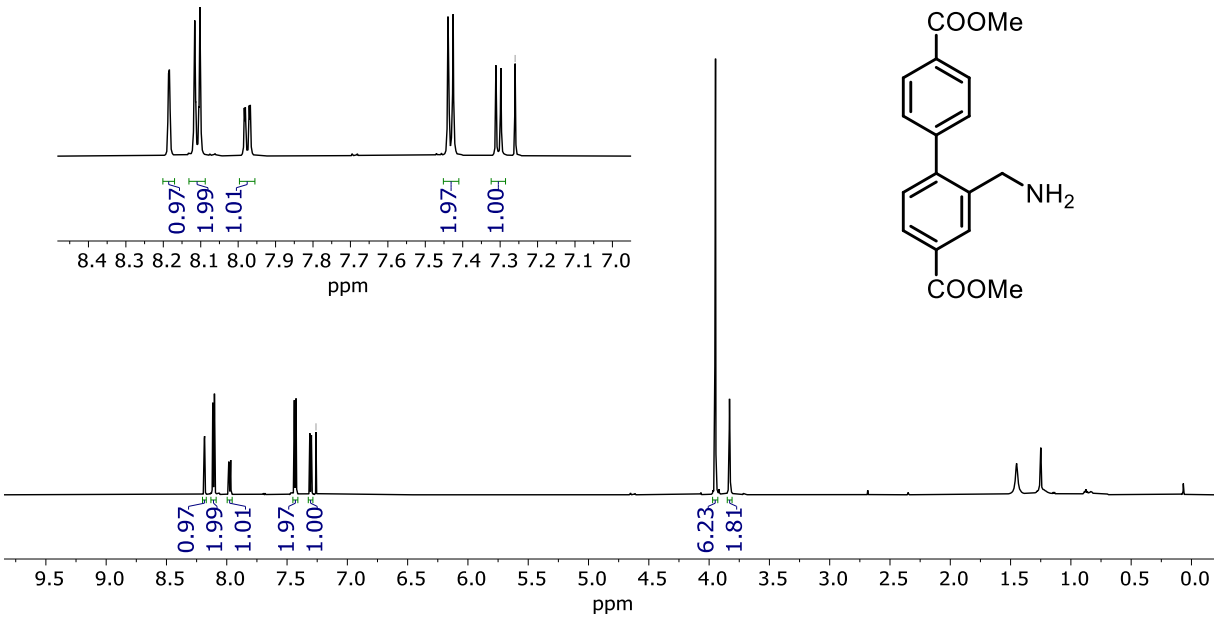

Figure 99: ^{1}H NMR (600 MHz, $CDCl_3$) spectrum of **4b**.

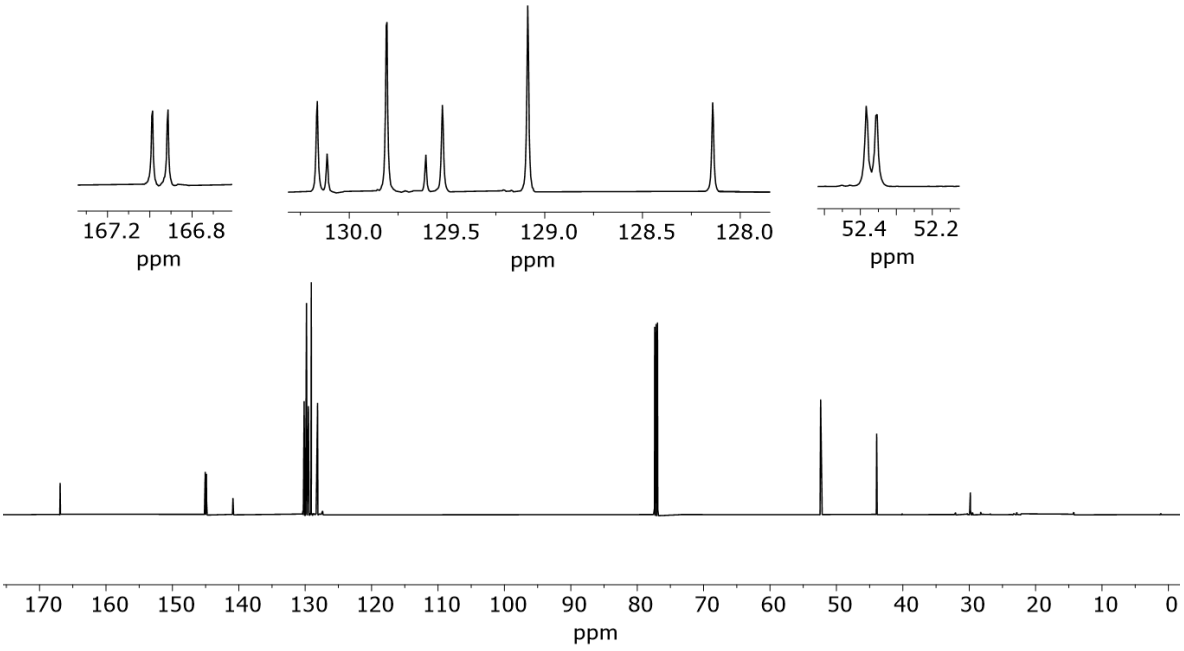

Figure 100: ^{13}C NMR (151 MHz, $CDCl_3$) spectrum of **4b.**

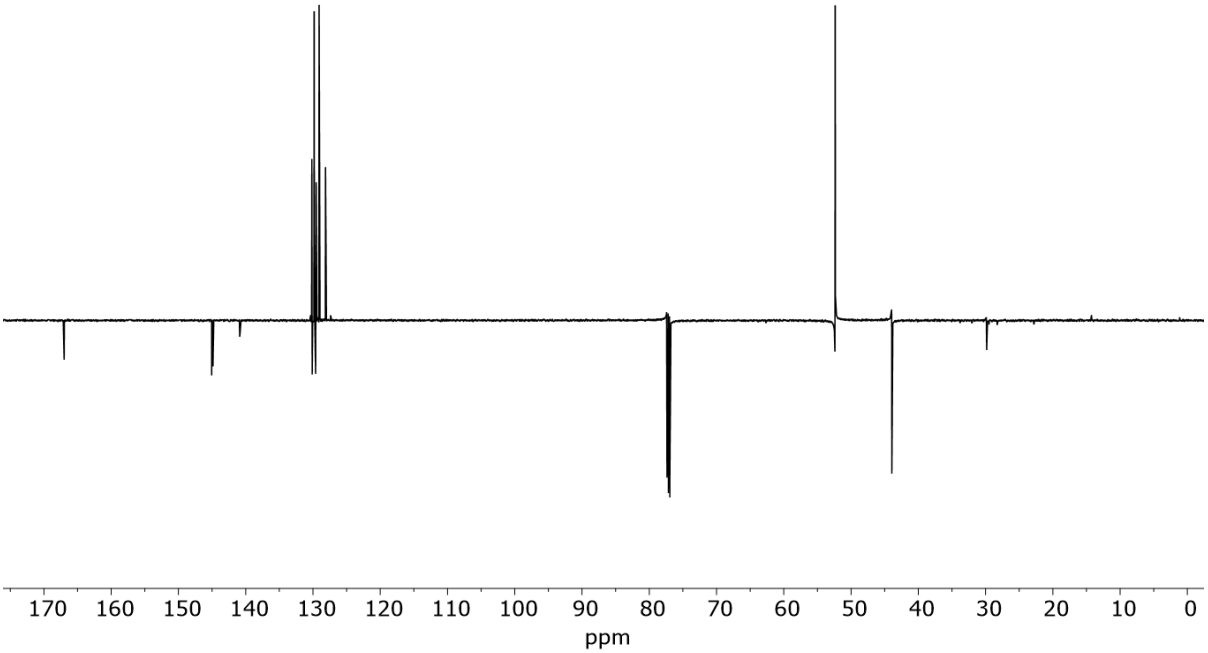

Figure 101: DEPT135Q (151 MHz, $CDCl_3$) spectrum of **4b**.

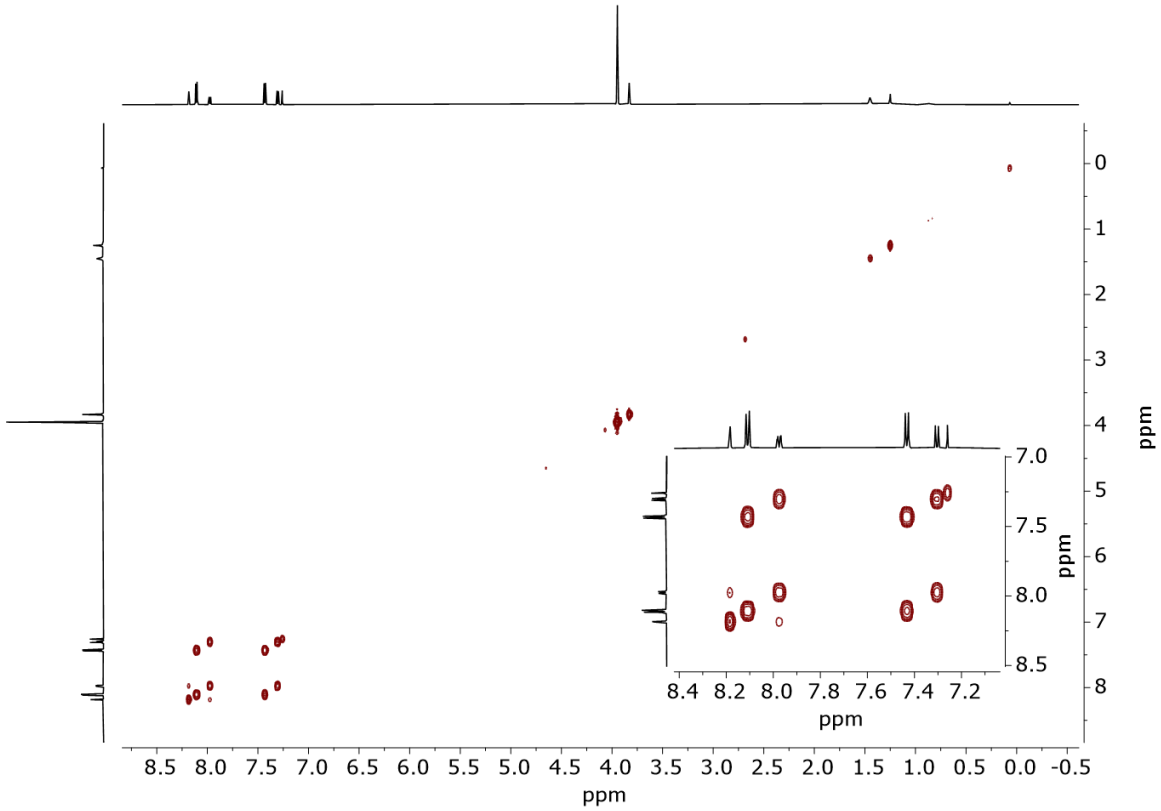

Figure 102: COSY (600 MHz, $CDCl_3$) spectrum of **4b**.

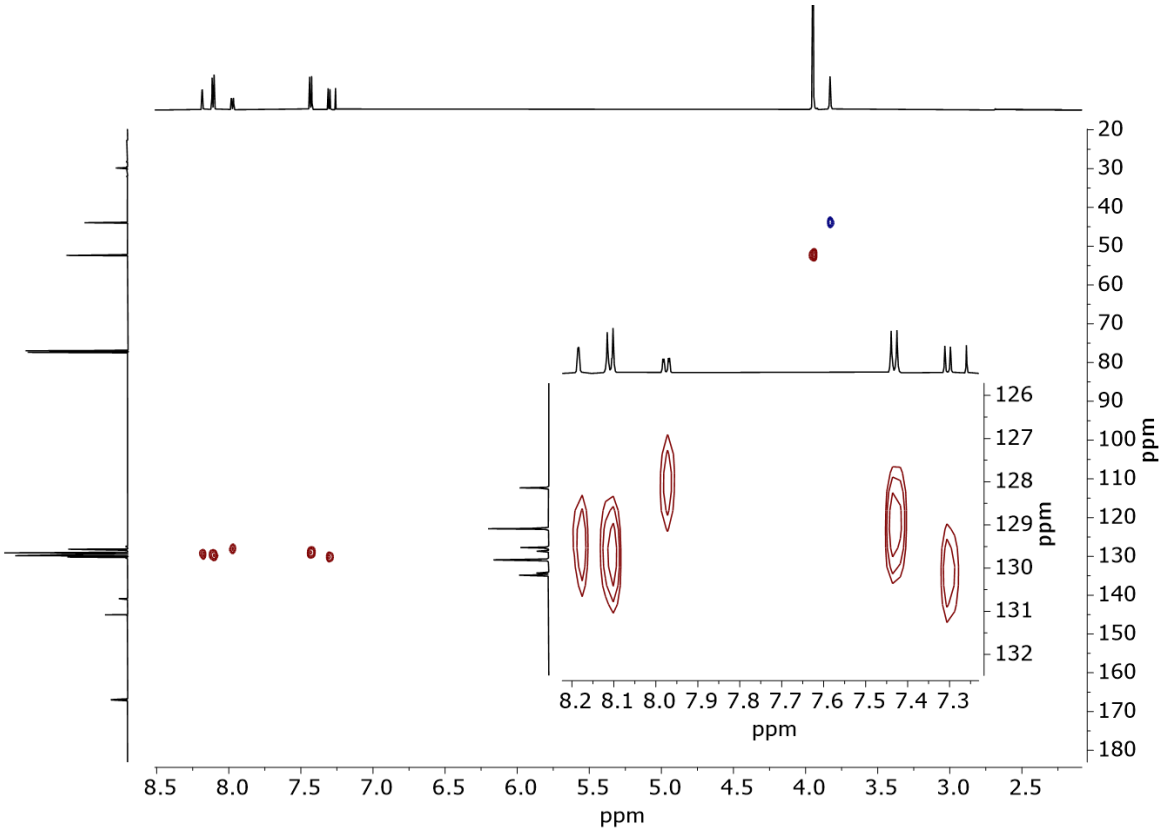

Figure 103: HSQC (600 MHz, $CDCl_3$) spectrum of **4b**.

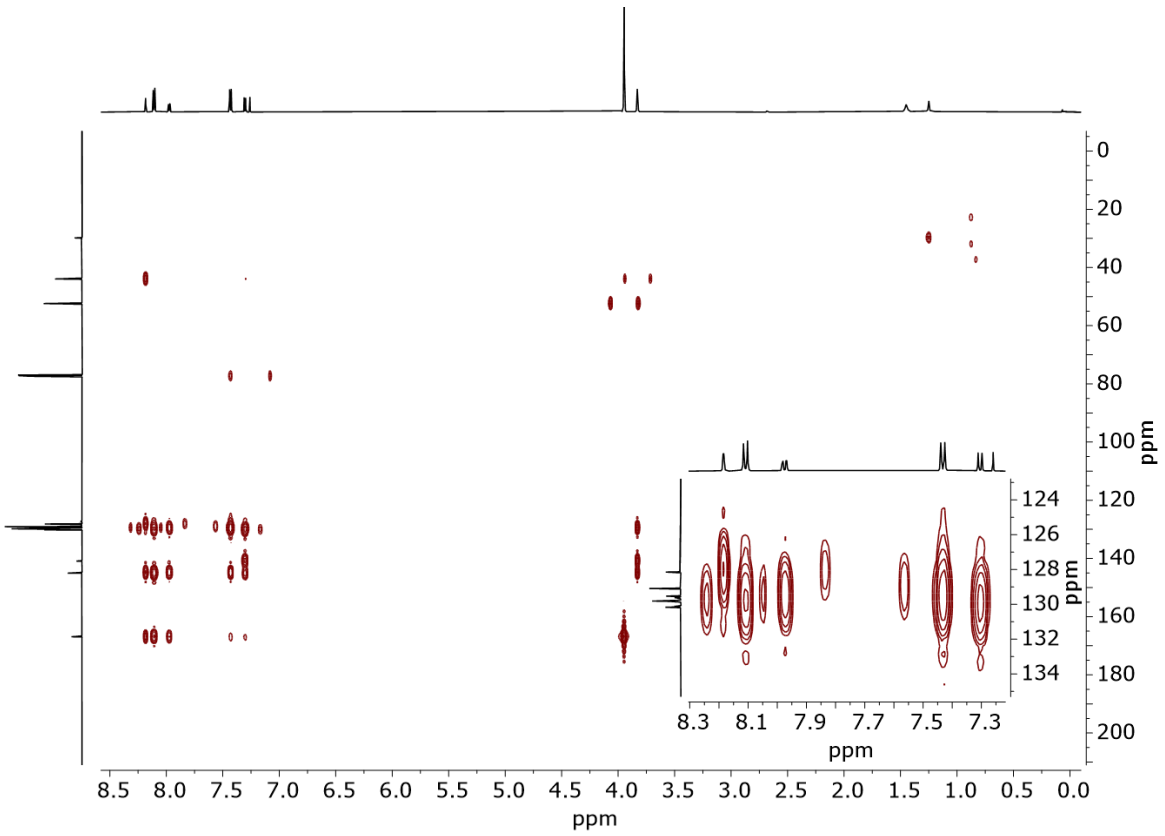

Figure 104: HMBC (600 MHz, $CDCl_3$) spectrum of **4b**.

8.8 Compound 10

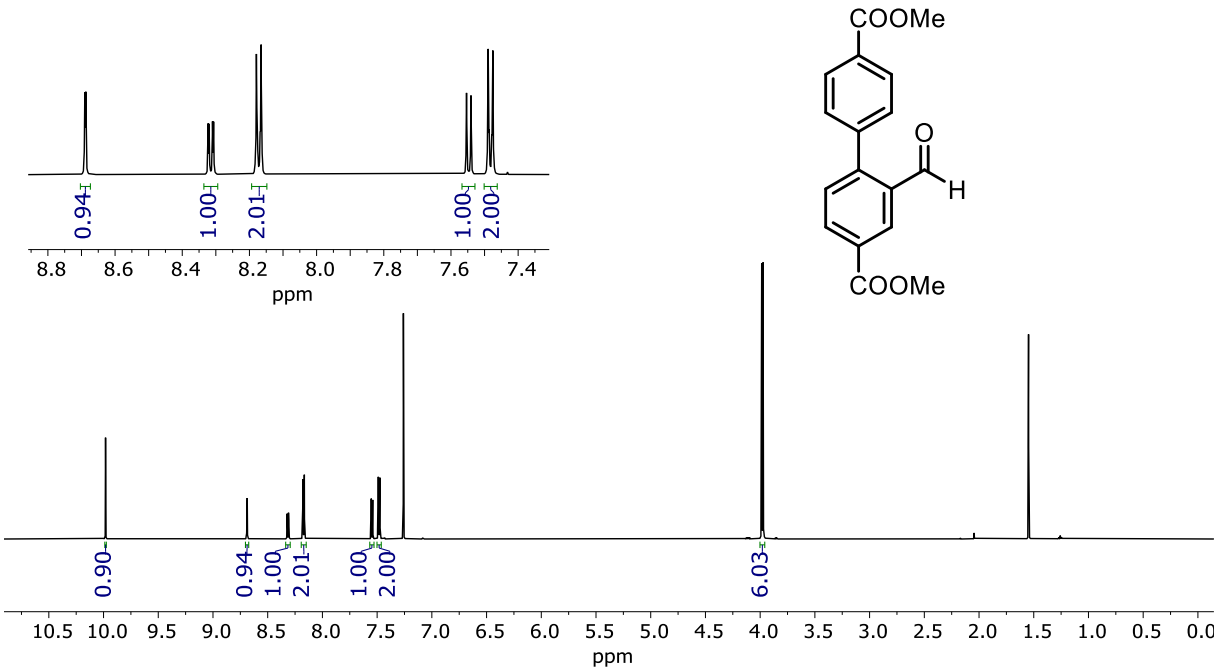

Figure 105: ^{1}H NMR (600 MHz, $CDCl_3$) spectrum of **10.**

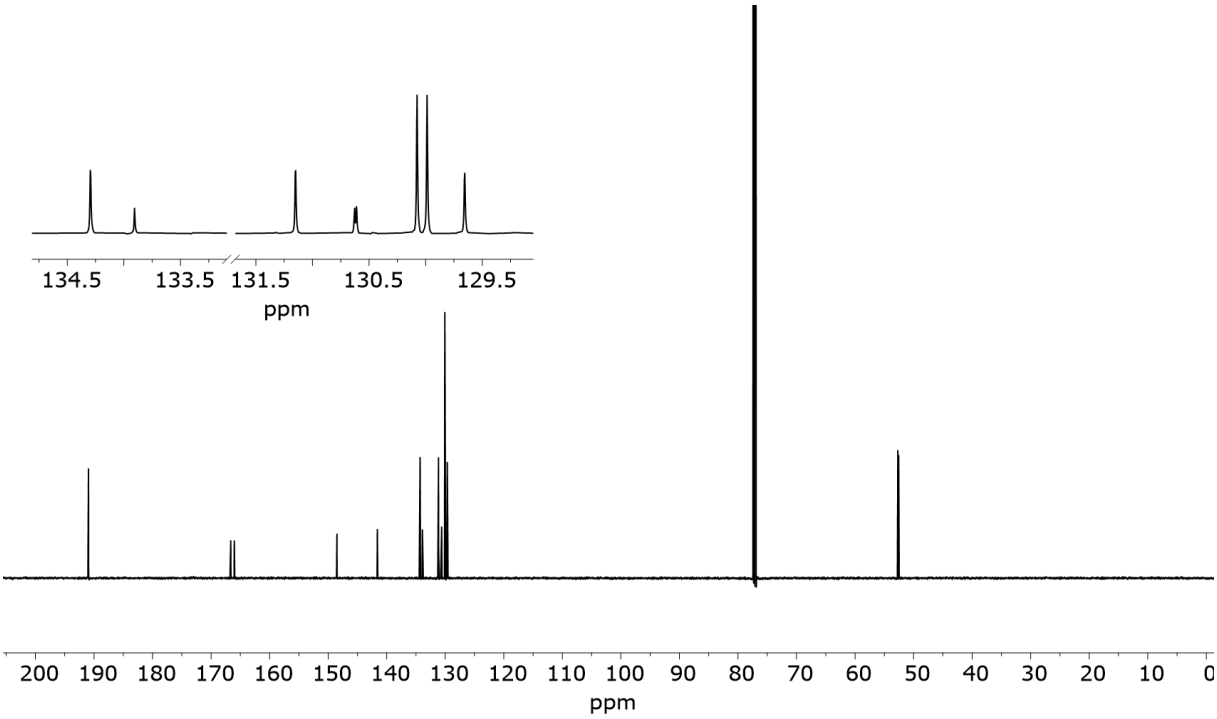

Figure 106: ^{13}C NMR (151 MHz, $CDCl_3$) spectrum of **10**.

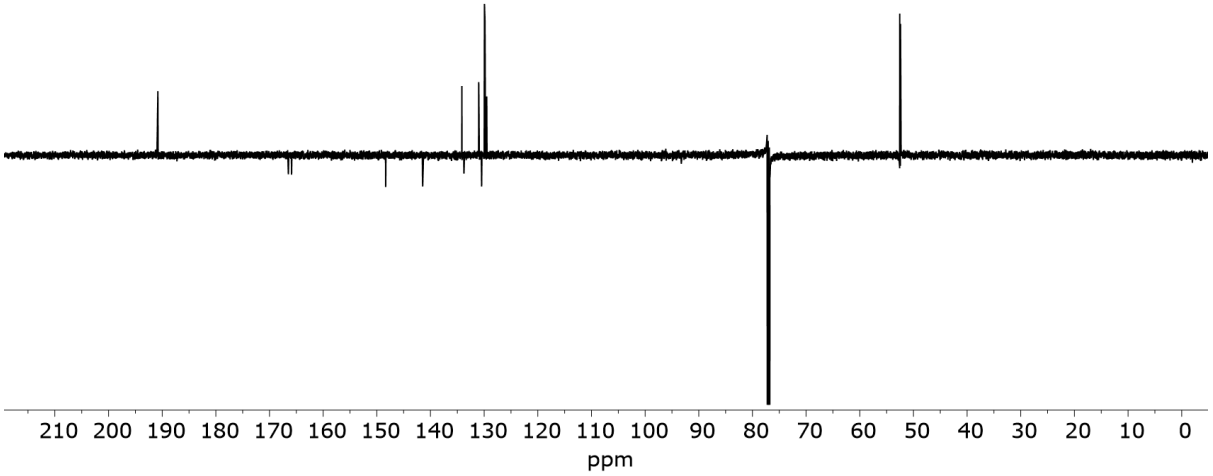

Figure 107: DEPT135Q (151 MHz, $CDCl_3$) spectrum of **10**.

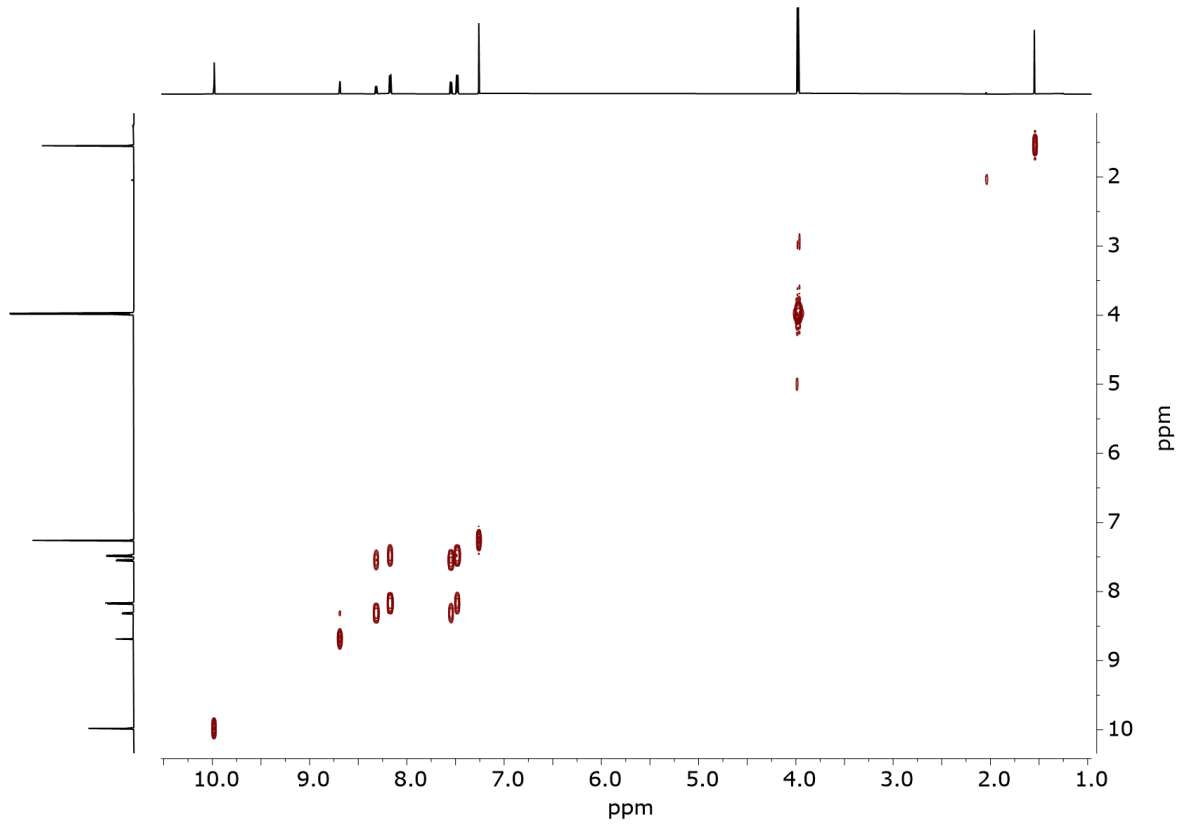

Figure 108: COSY (600 MHz, $CDCl_3$) spectrum of **10**.

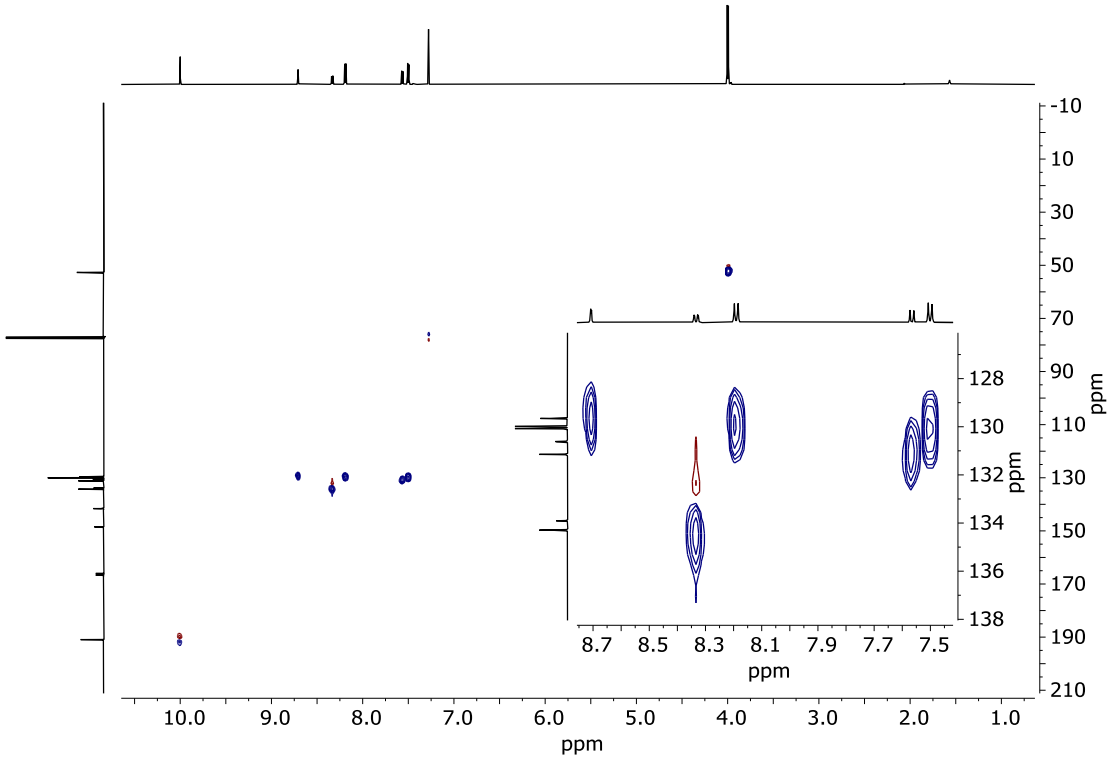

Figure 109: HSQC (600 MHz, $CDCl_3$) spectrum of **10**.

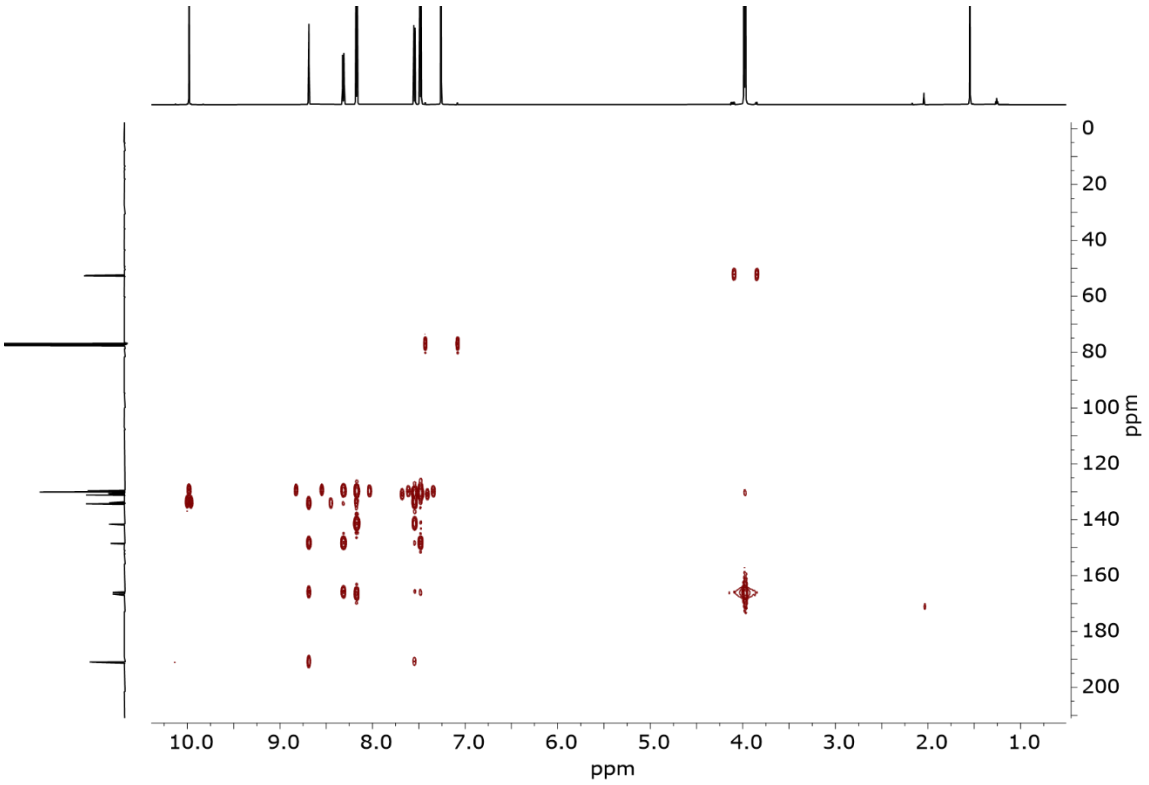

Figure 110: HMBC (600 MHz, $CDCl_3$) spectrum of **10**.

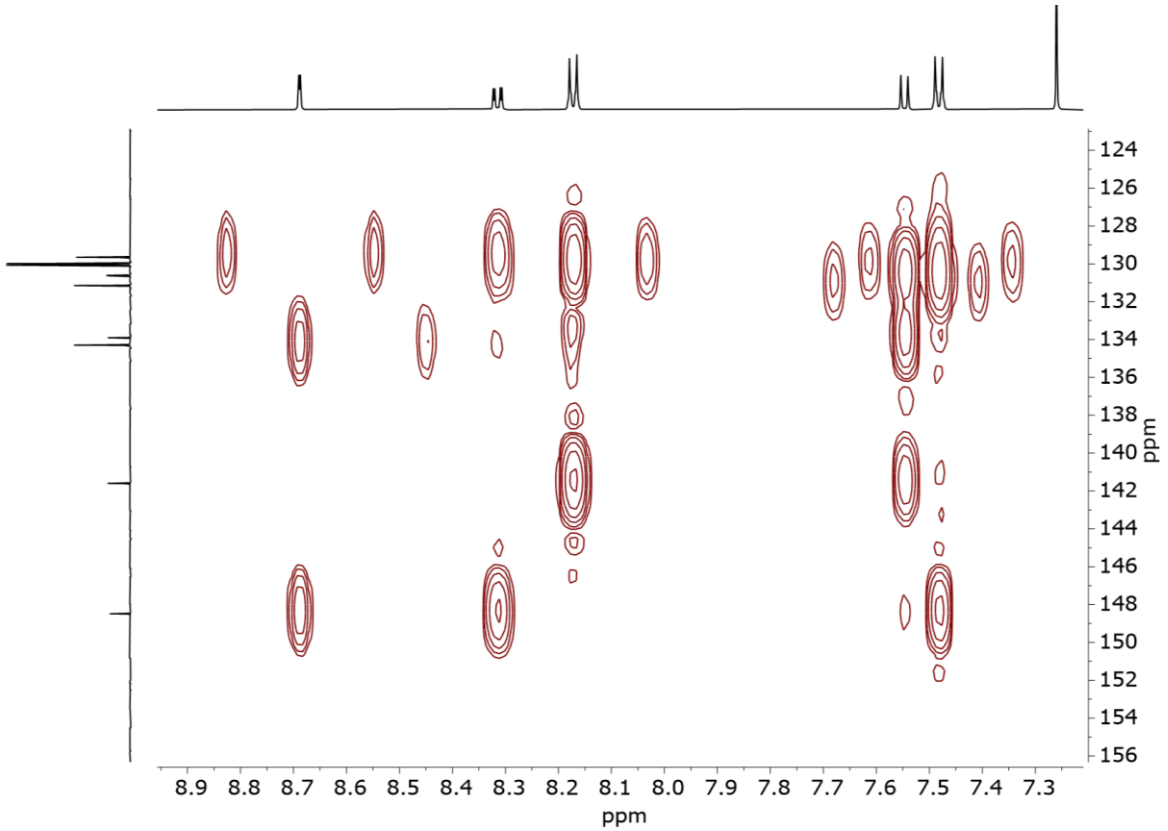

Figure 111: Zoom of HMBC (600 MHz, $CDCl_3$) spectrum of **10**.

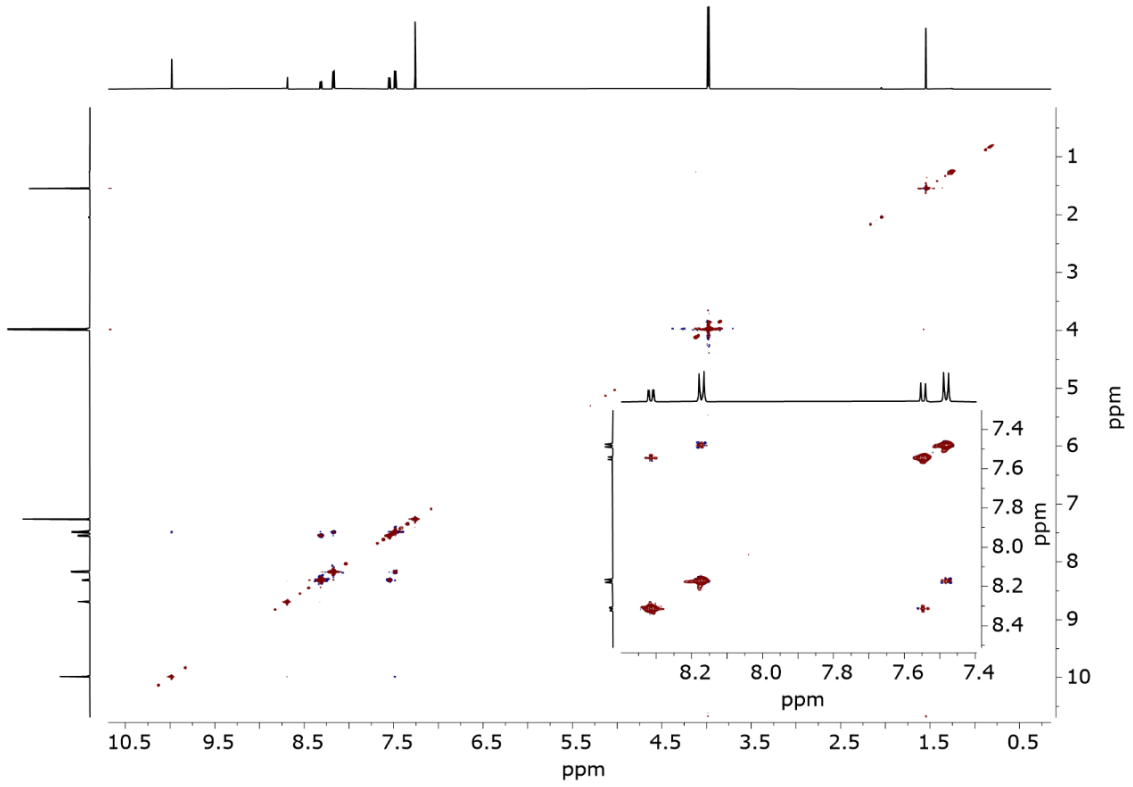

Figure 112: NOESY (600 MHz $CDCl_3$) spectrum of **10**.

7.9 Compound 11

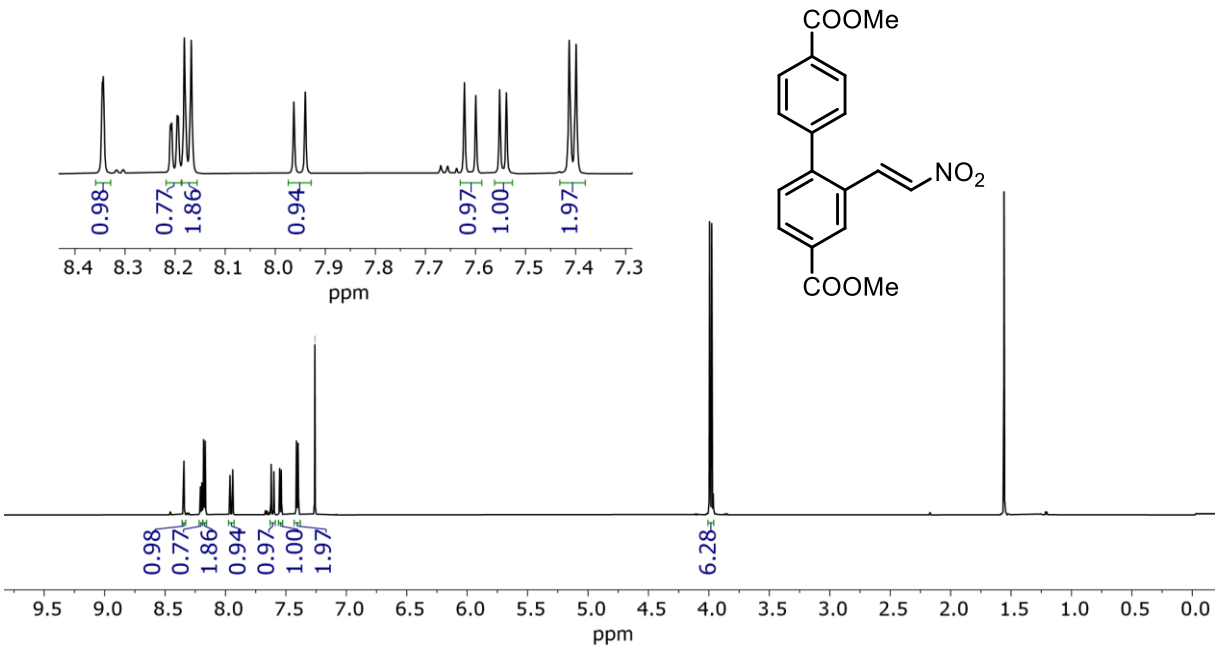

Figure 113: ^{1}H NMR (600 MHz, $CDCl_3$) spectrum of **11**.

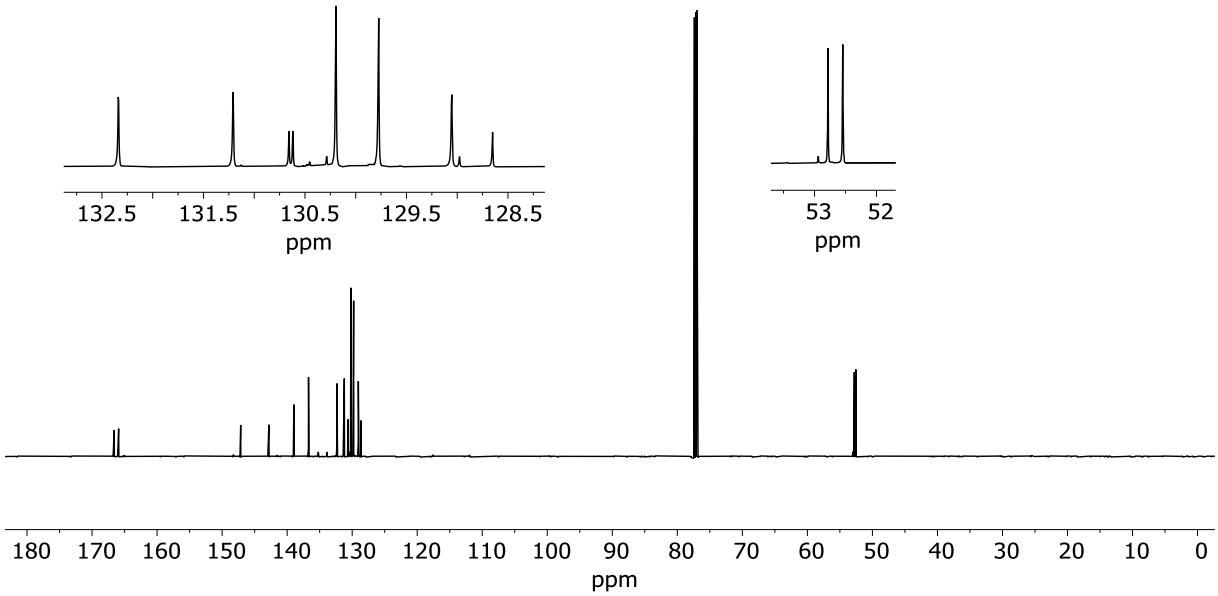

Figure 114: ^{13}C NMR (151 MHz, $CDCl_3$) spectrum of **11.**

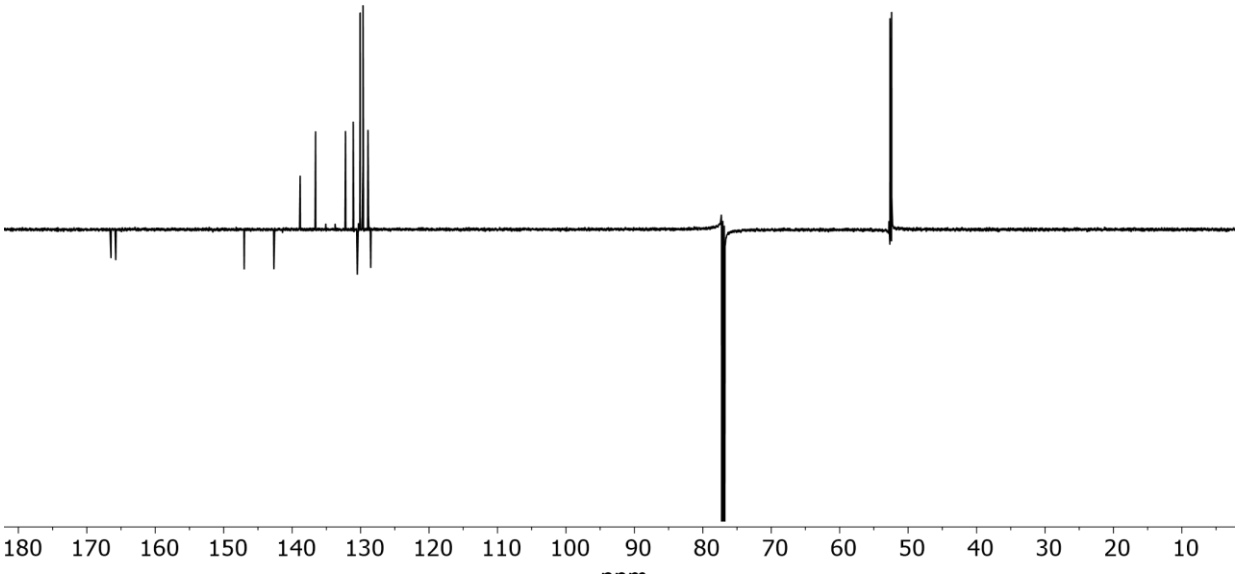

Figure 115: DEPT135Q (151 MHz, $CDCl_3$) spectrum of **11**.

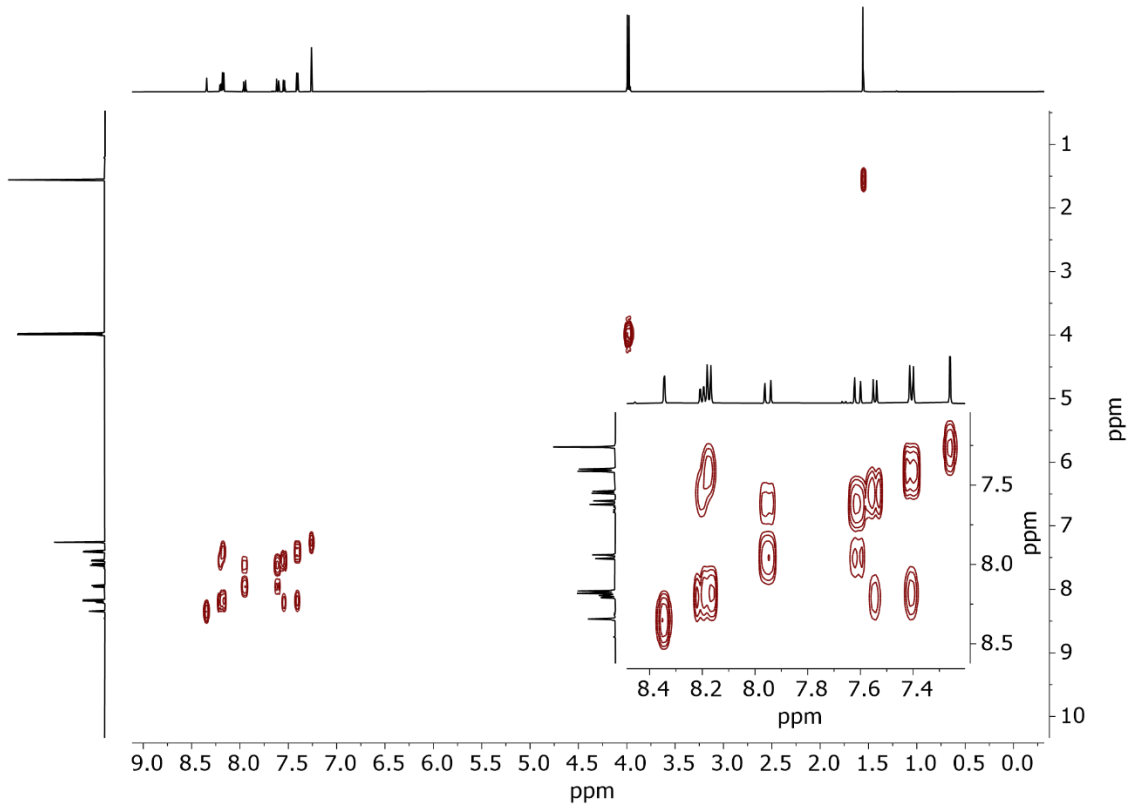

Figure 116: COSY (600 MHz, $CDCl_3$) spectrum of **11**.

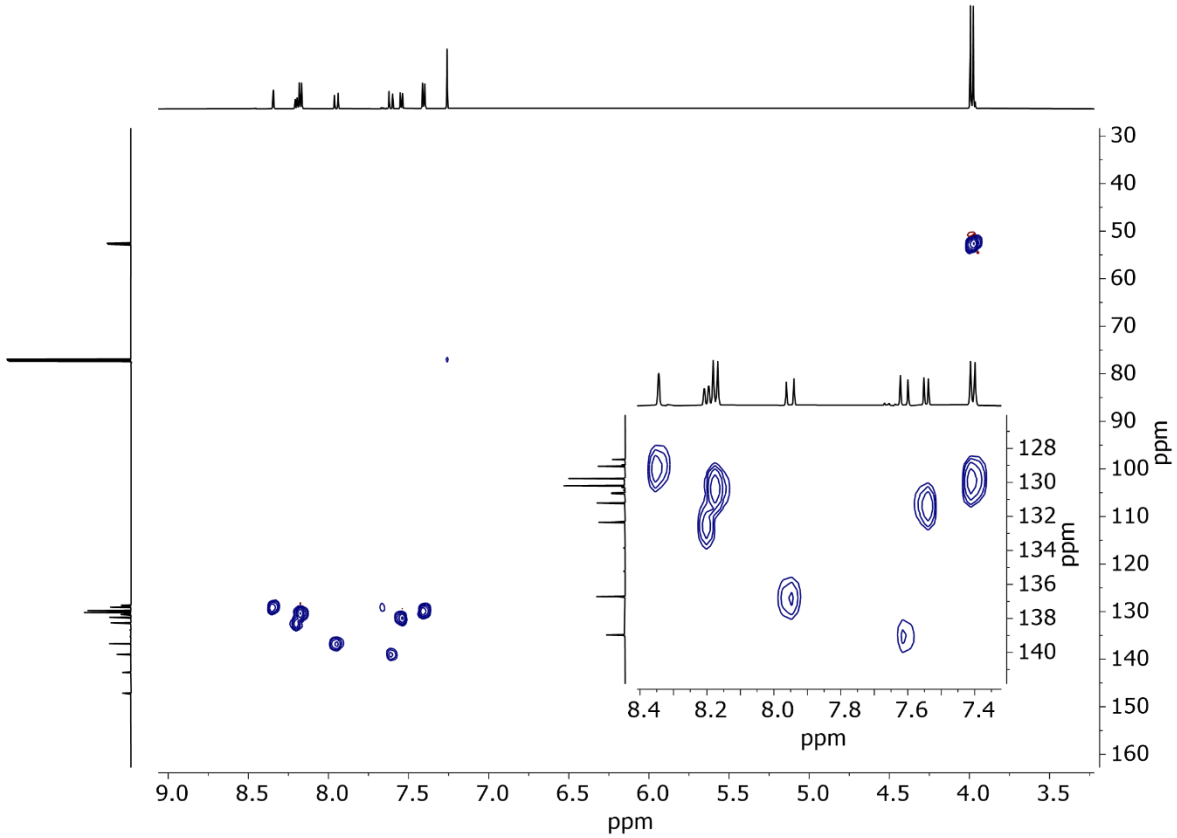

Figure 117: HSQC (600 MHz, $CDCl_3$) spectrum of **11**.

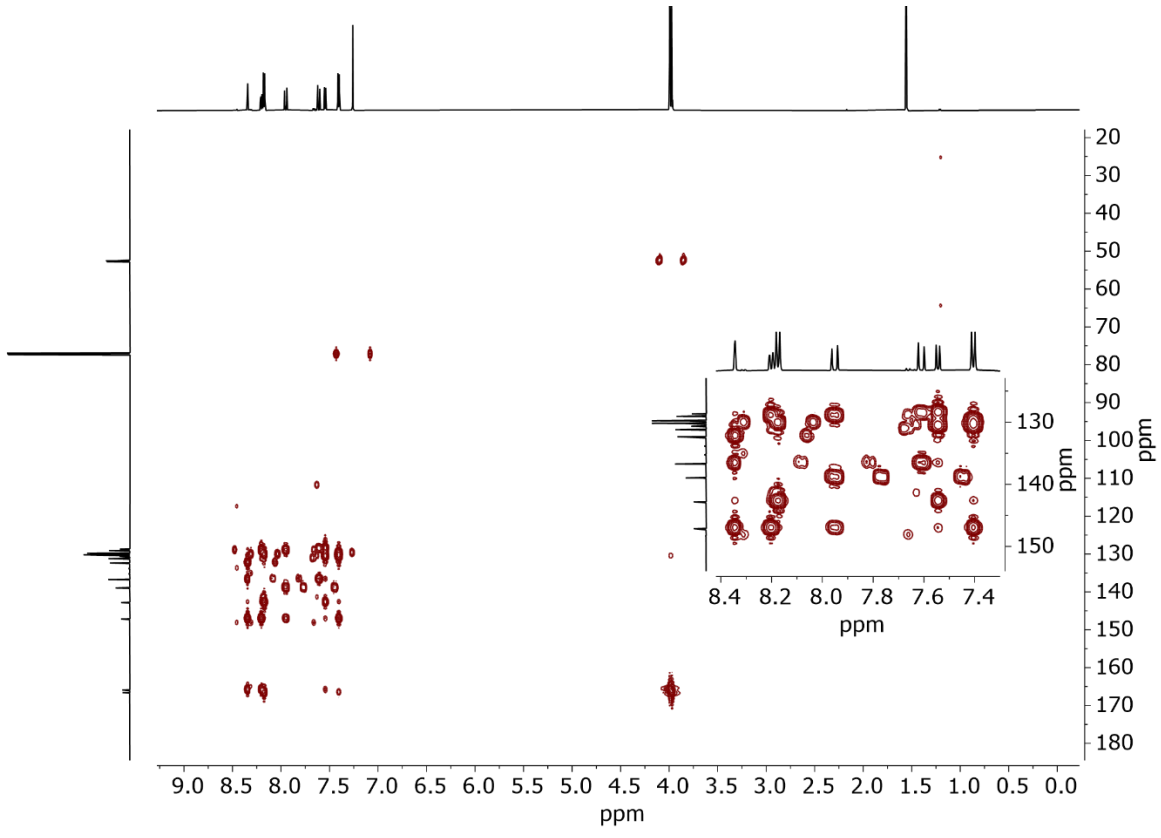

Figure 118: HMBC (600 MHz, $CDCl_3$) spectrum of **11**.

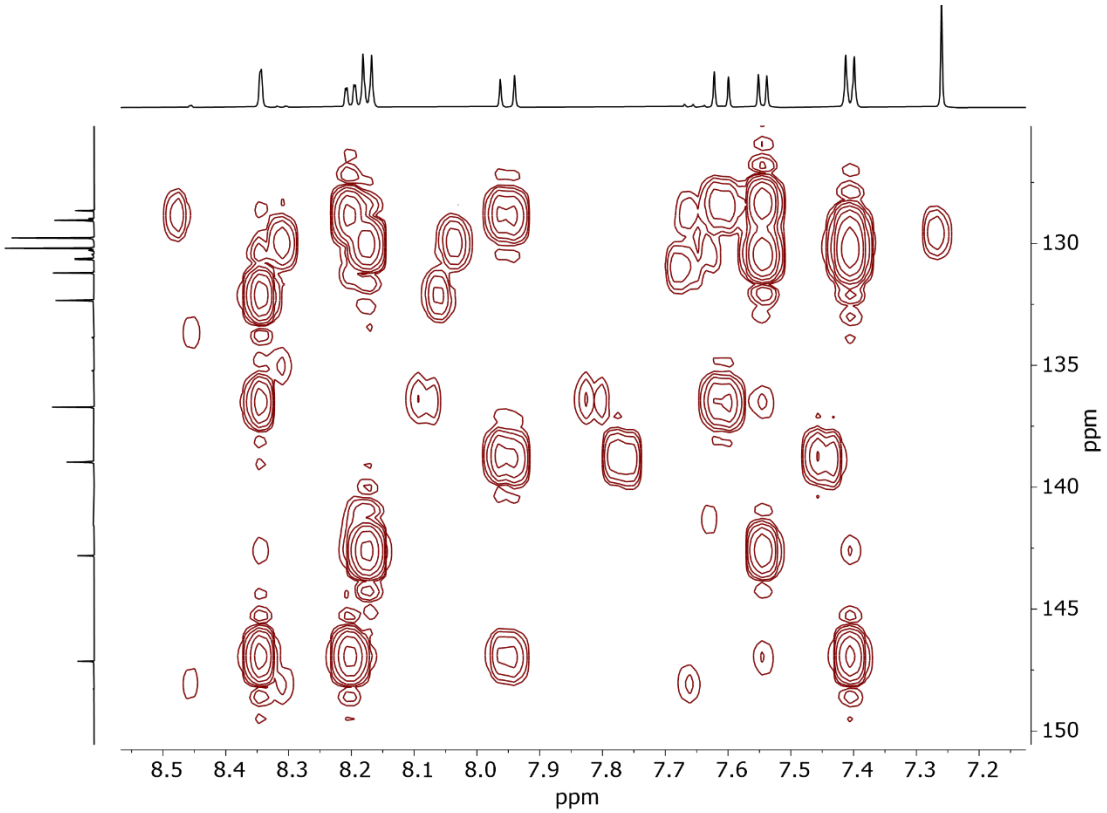

Figure 119: Zoom of HMBC (600 MHz, $CDCl_3$) spectrum of **11**.

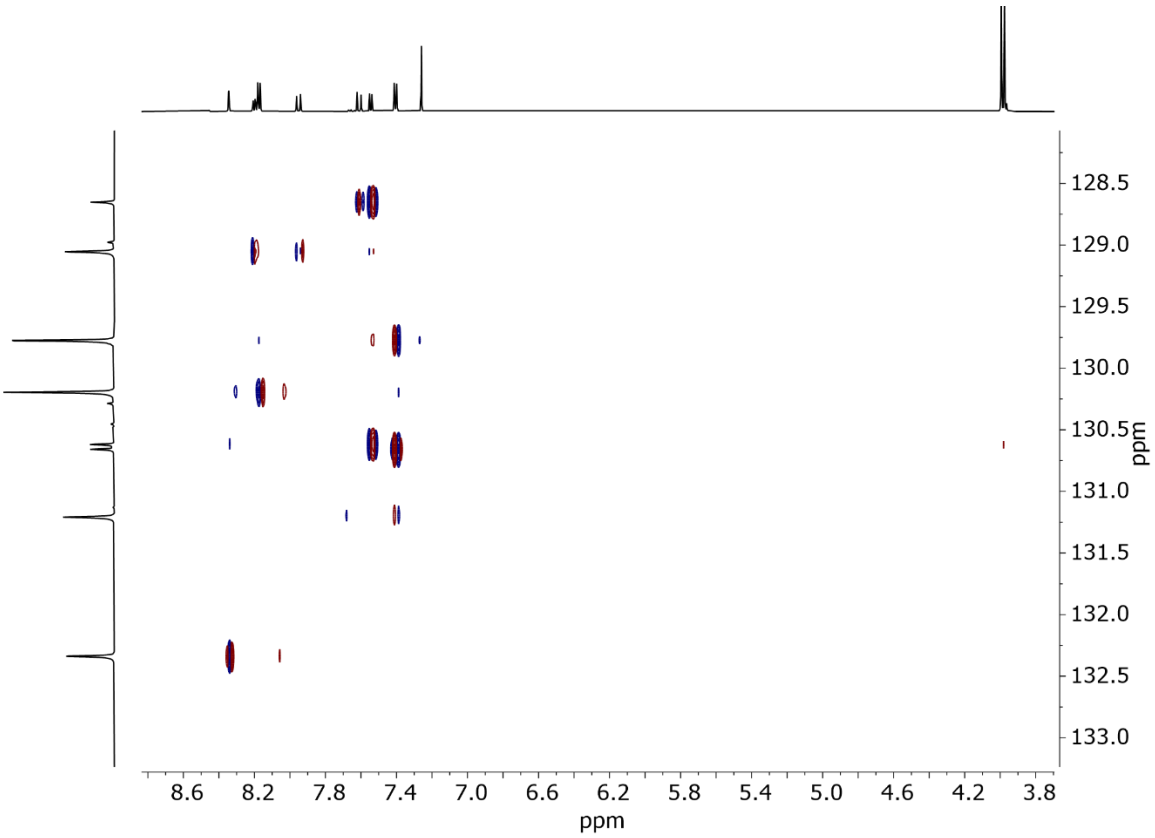

Figure 120: S HMBC (600 MHz, $CDCl_3$) spectrum of **11**.

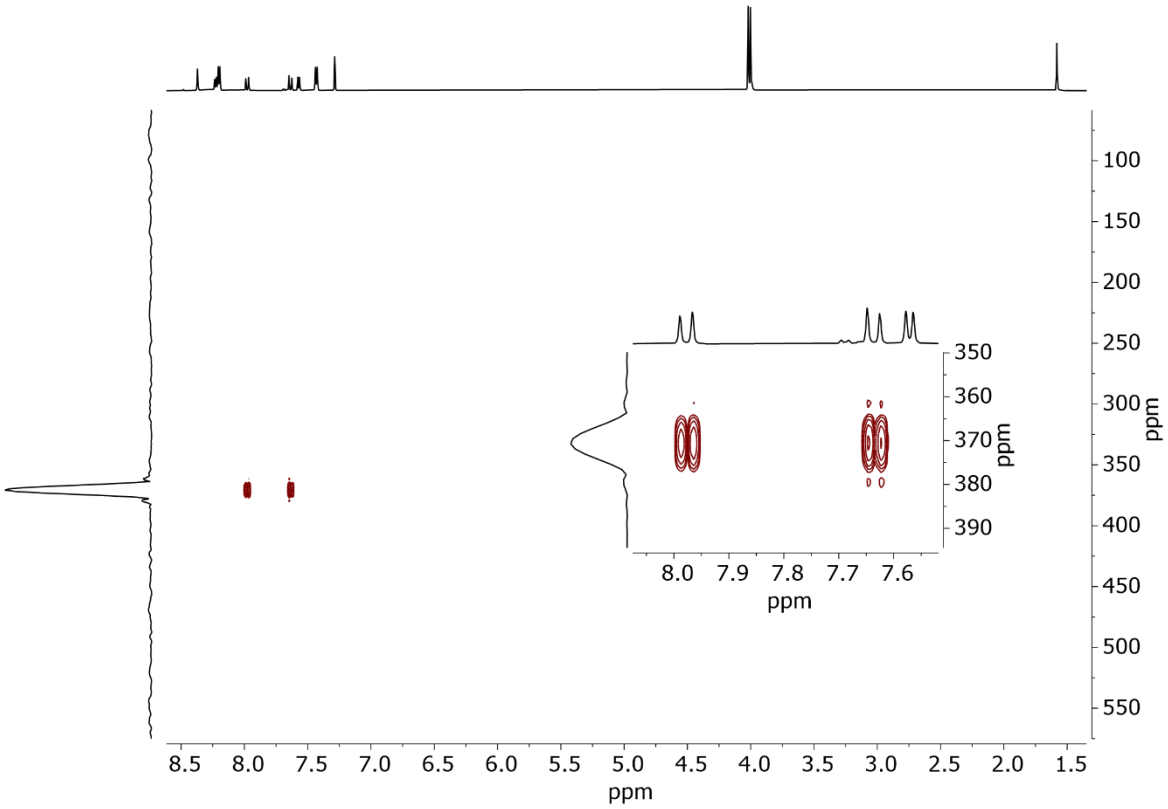

Figure 121: ^{1}H-^{15}N HMBC (600 MHz, $CDCl_3$) spectrum of **11**.

8.10 Compound 6

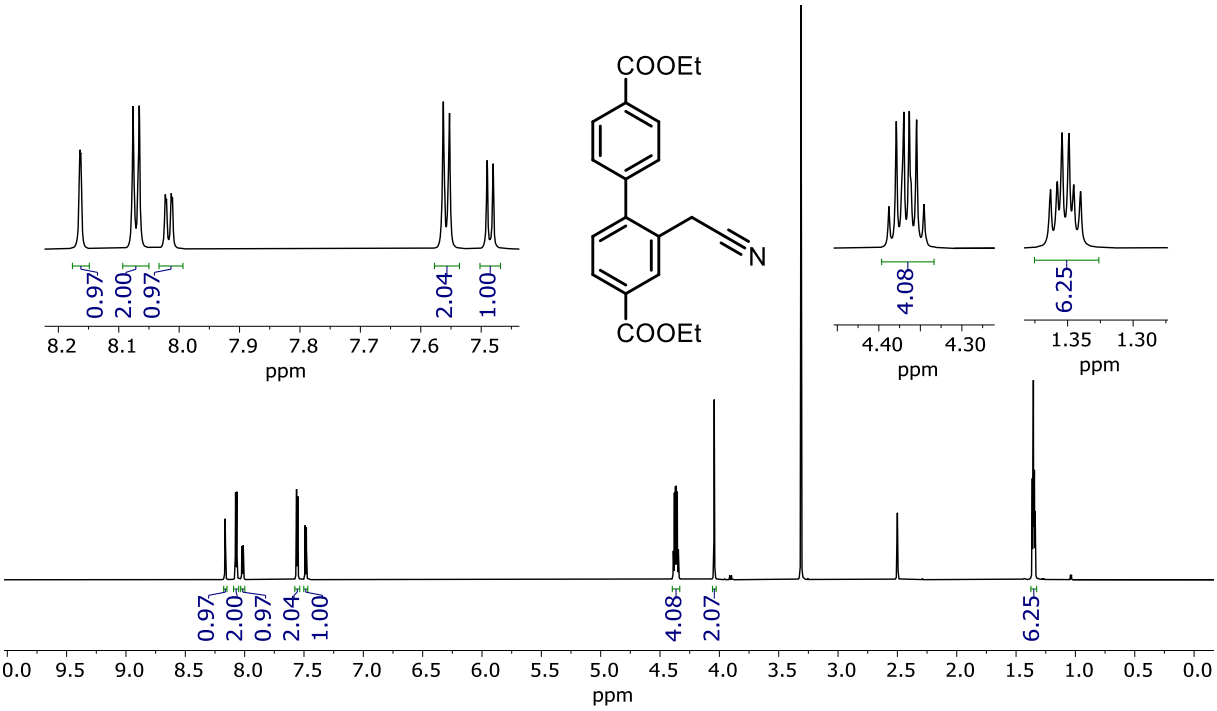

Figure 122: ^{1}H NMR (800 MHz, DMSO-d_6) spectrum of **6**.

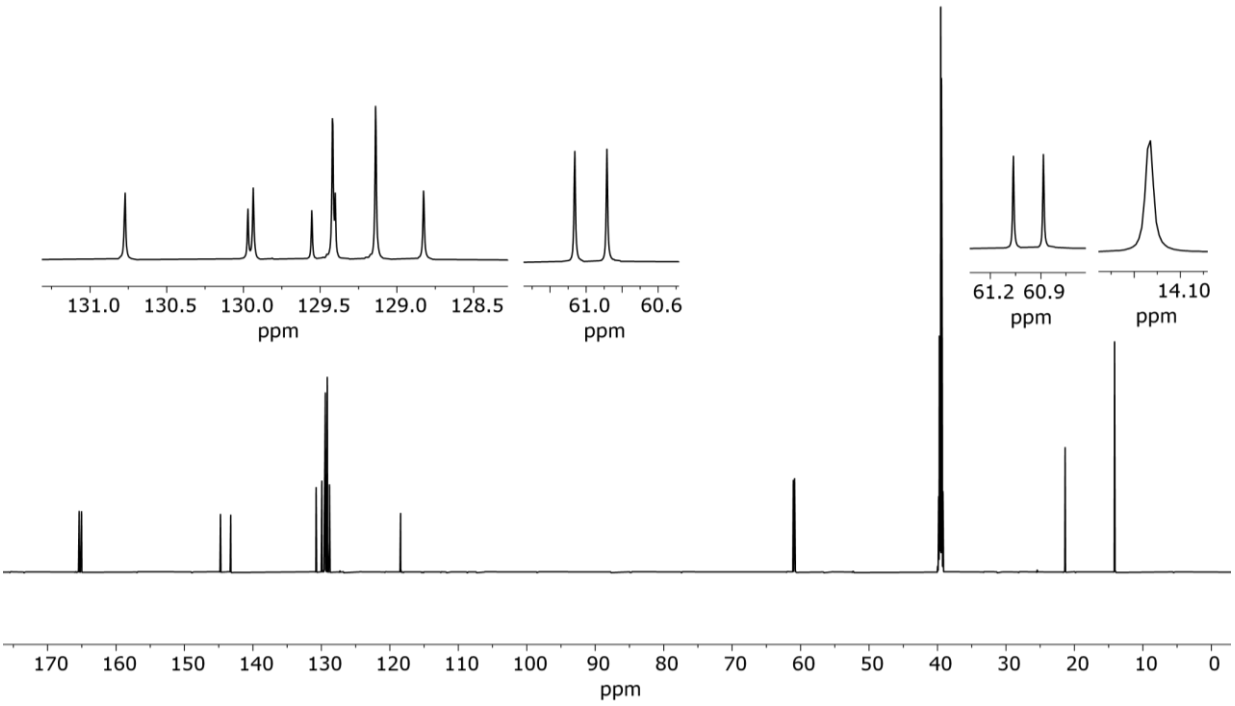

Figure 123: ^{13}C NMR (201 MHz, DMSO-d_6) spectrum of **6**.

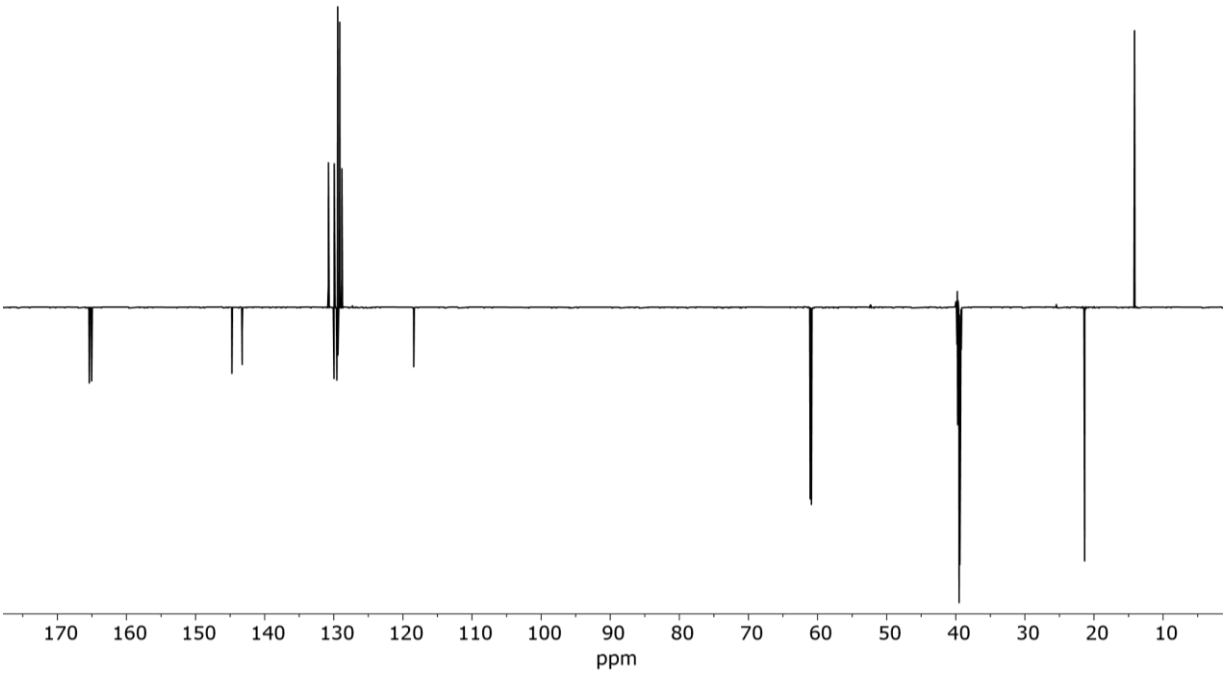

Figure 124: DEPT135Q (201 MHz, DMSO-d_6) spectrum of **6**.

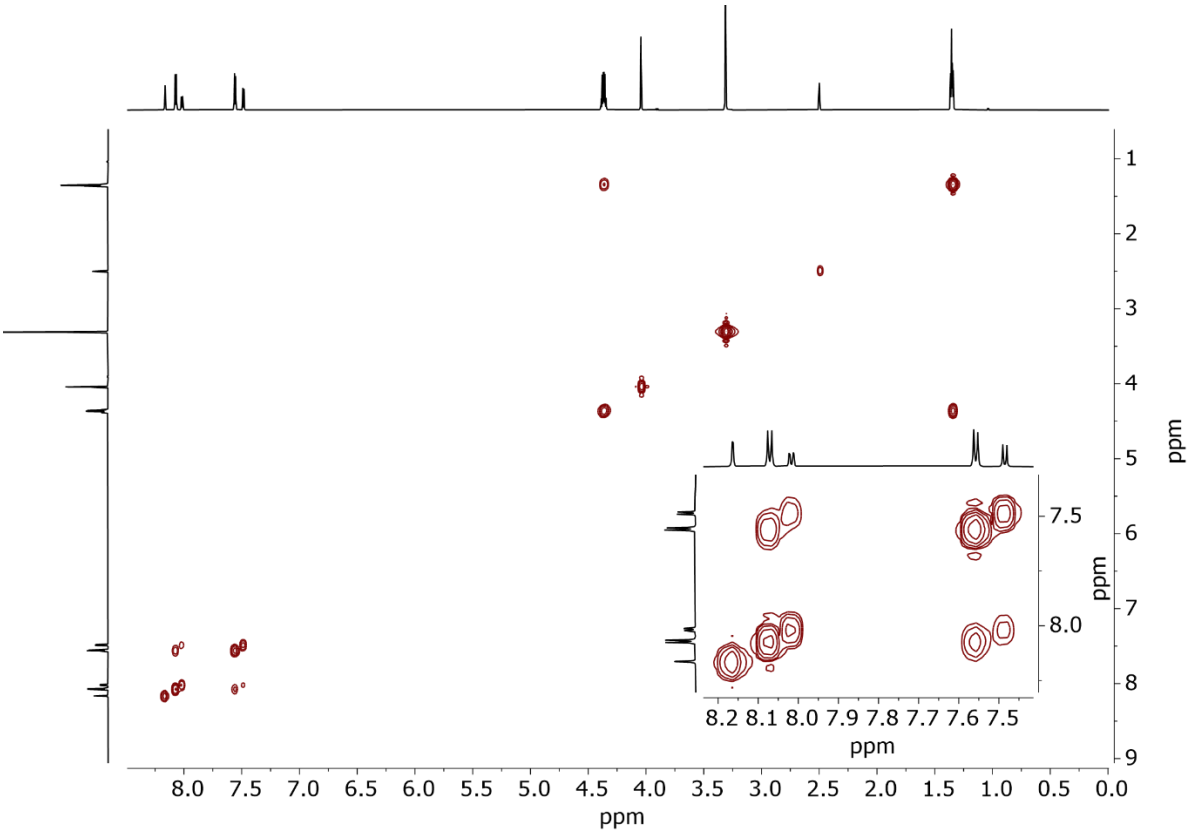

Figure 125: COSY (800 MHz, DMSO-d_6) spectrum of **6**.

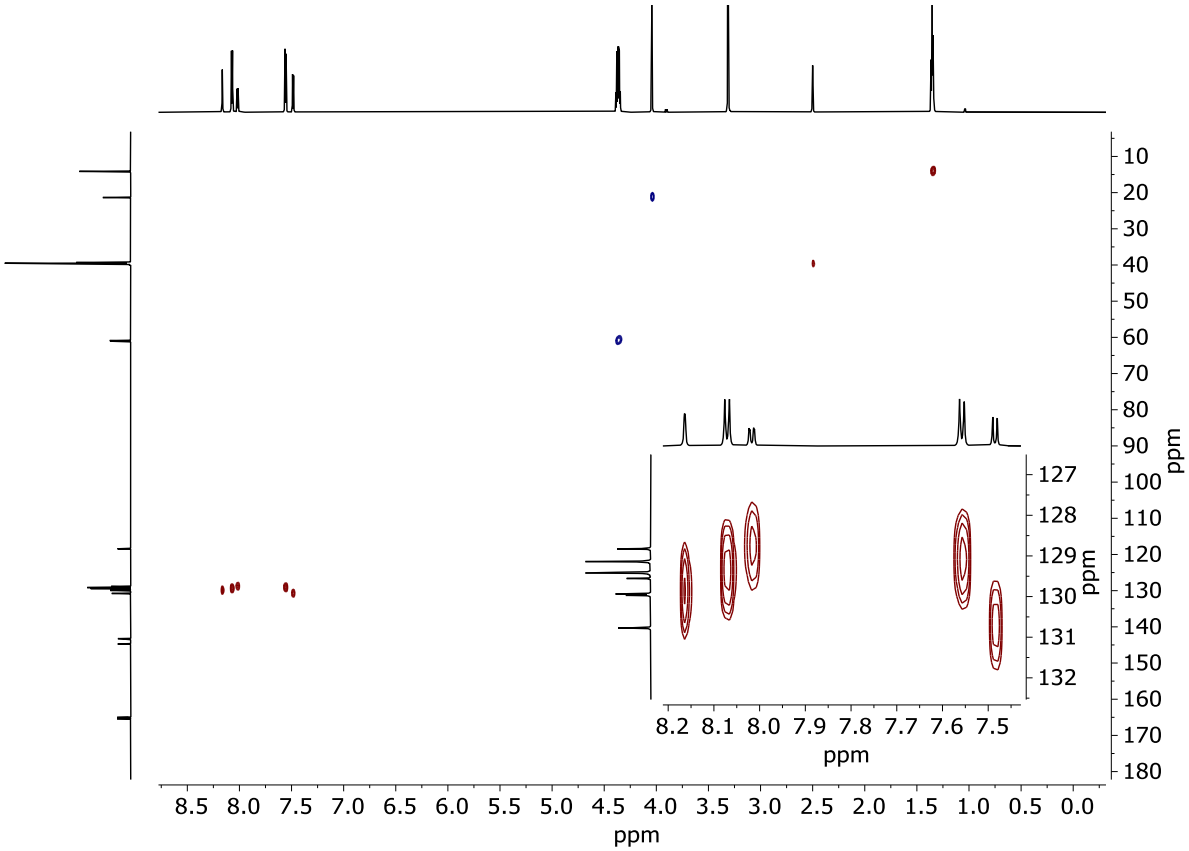

Figure 126: HSQC (800 MHz, DMSO-d_6) spectrum of **6**.

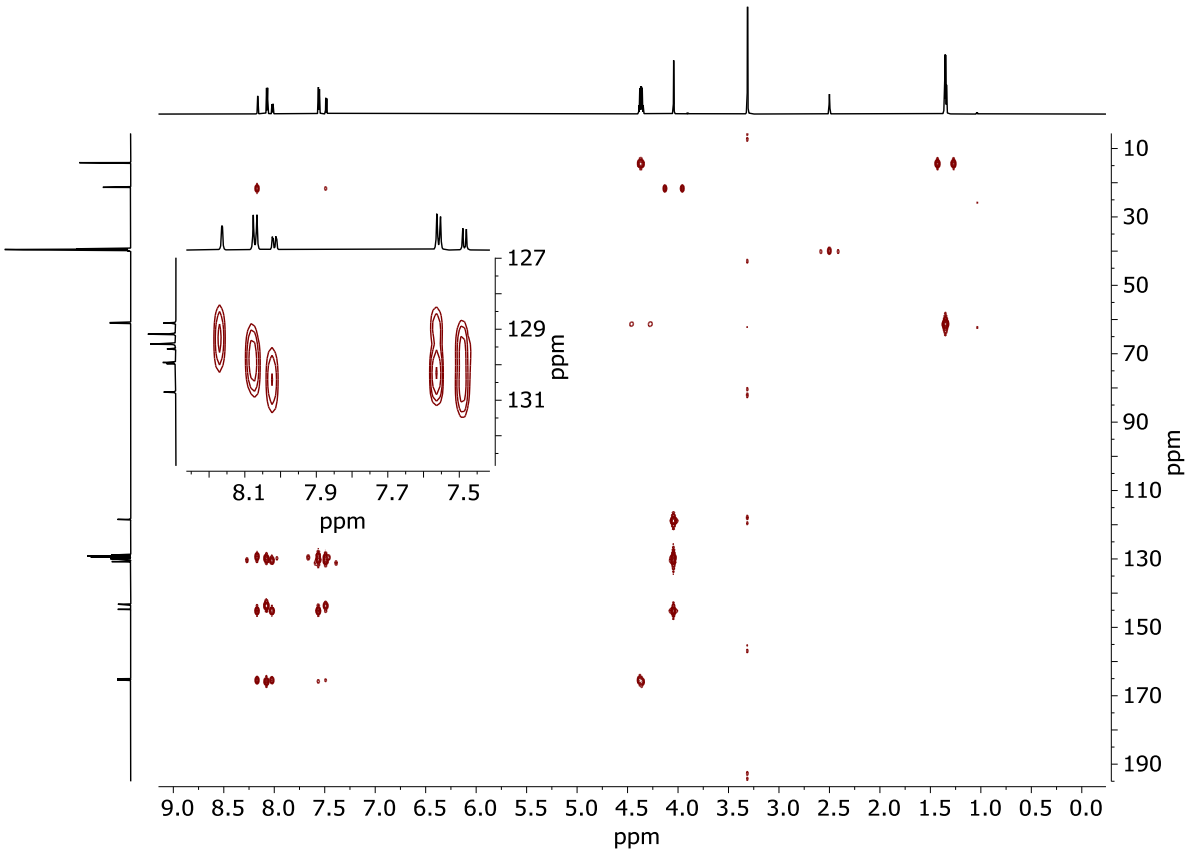

Figure 127: HMBC (800 MHz, DMSO-d_6) spectrum of **6**.

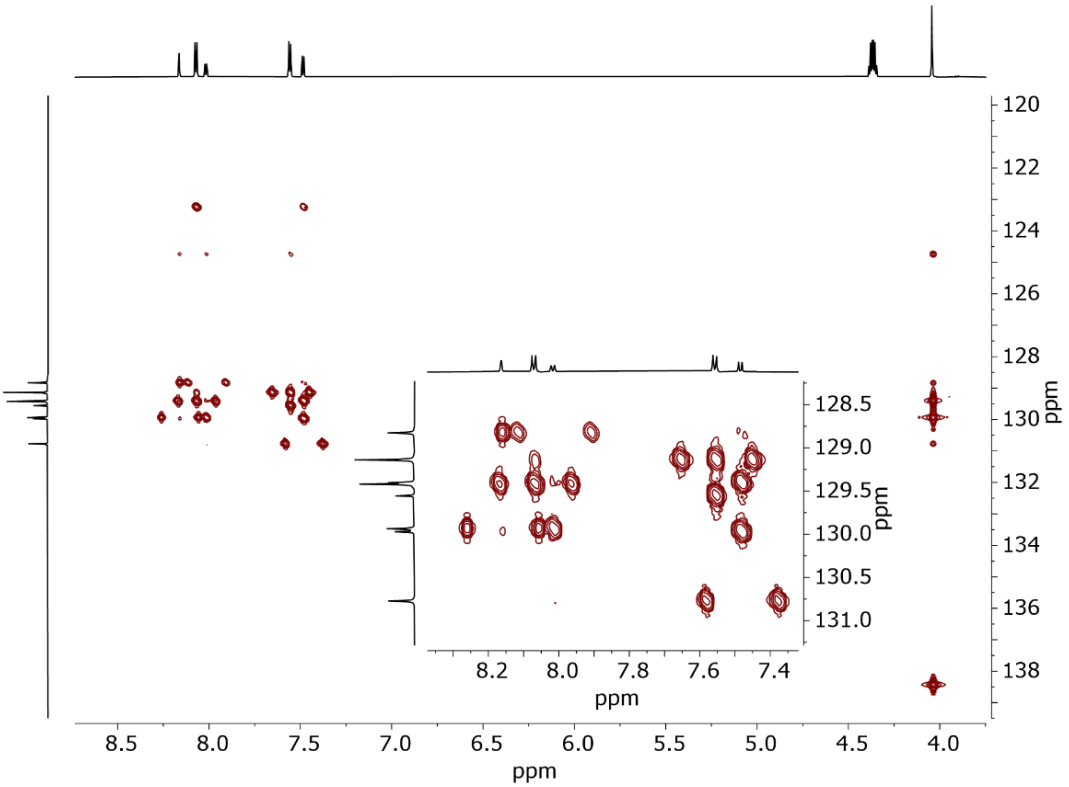

Figure 128: S HMBC (800 MHz, DMSO-d6) spectrum of **6**.

8.11 Compound 7

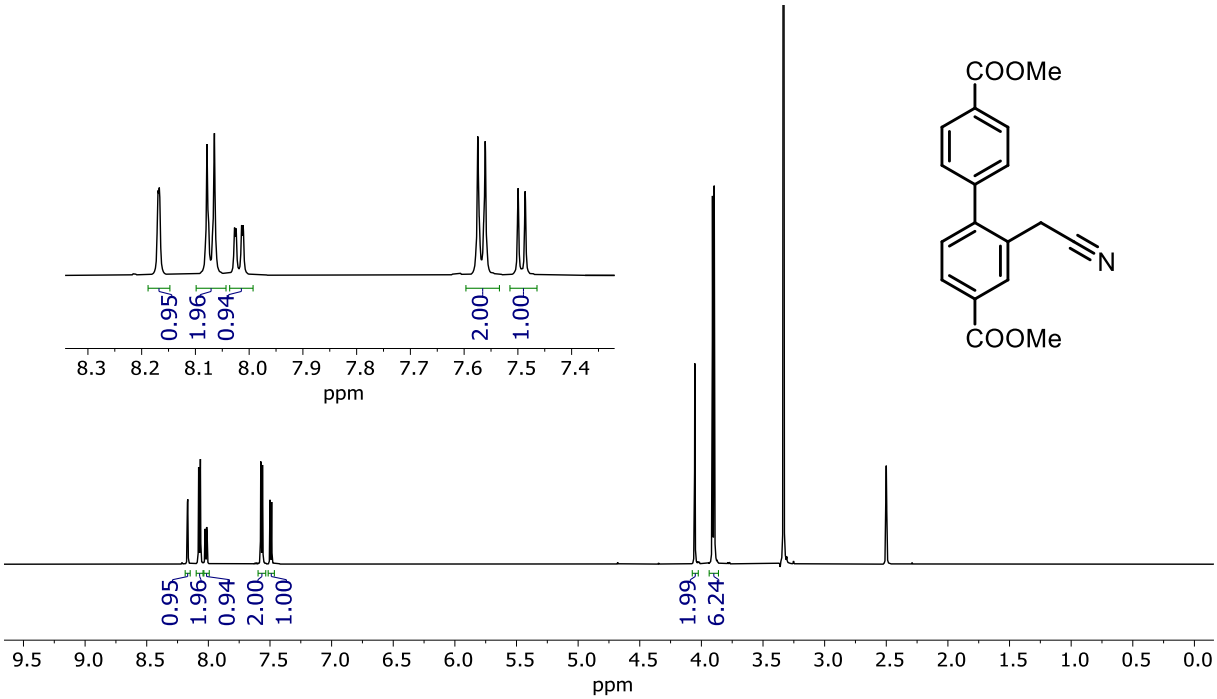

Figure 129: ^{1}H NMR (600 MHz, DMSO-d_6) spectrum of **7**.

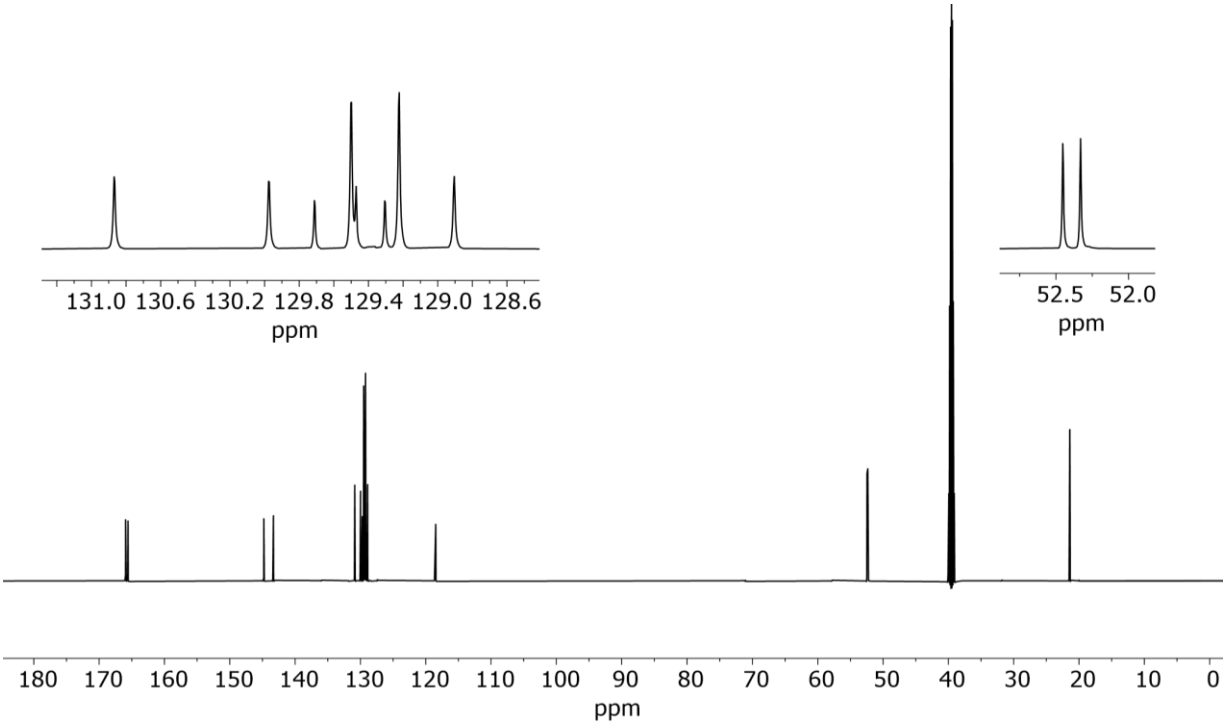

Figure 130: ^{13}C NMR (151 MHz, DMSO-d_6) spectrum of **7**.

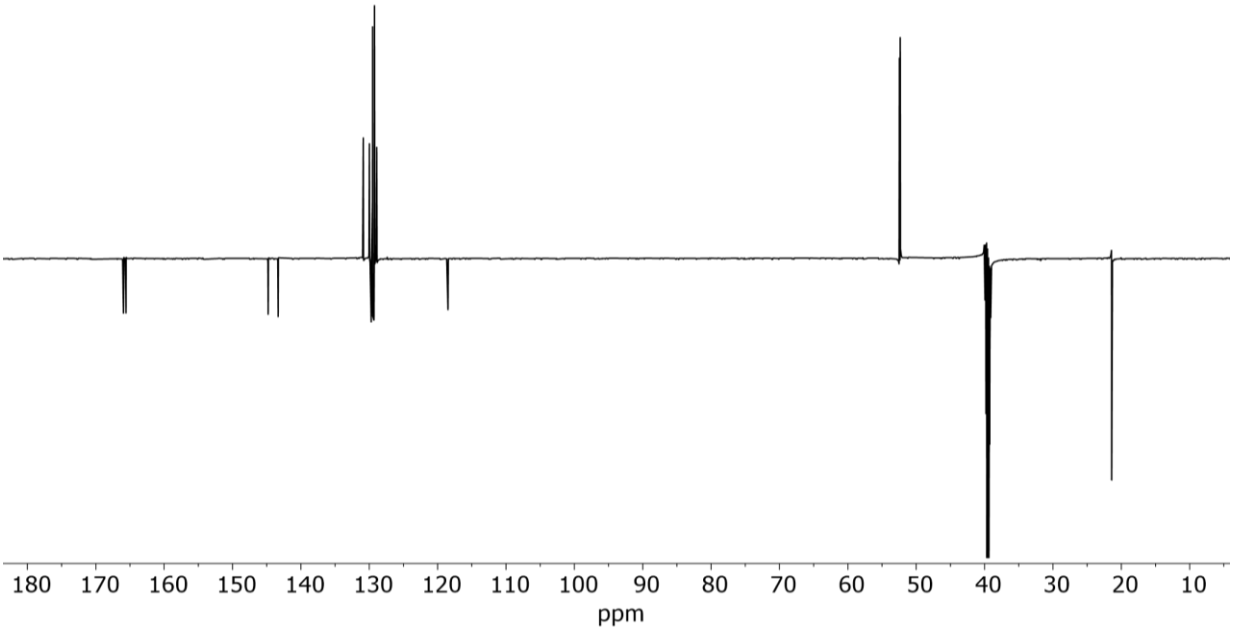

Figure 131: DEPT135Q (151 MHz, DMSO-d_6) spectrum of **7**.

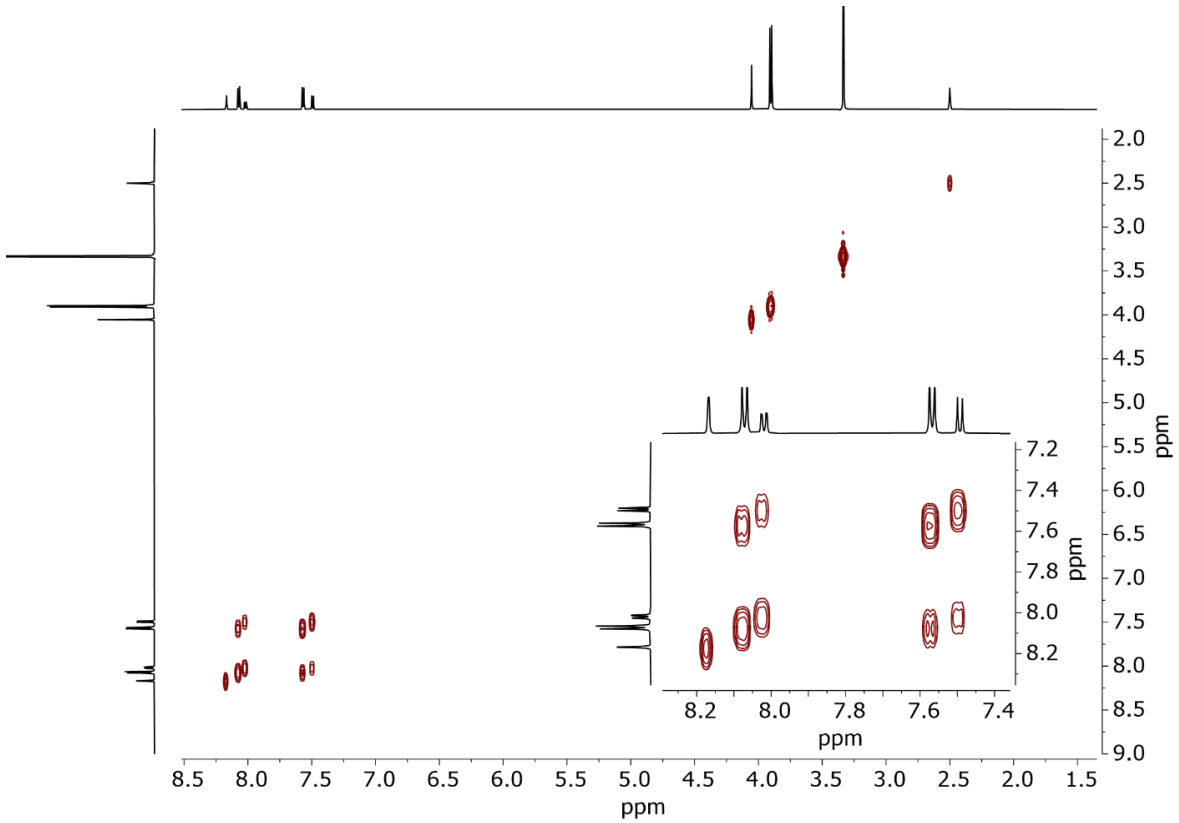

Figure 132: COSY (600 MHz, DMSO-d_6) spectrum of **7**.

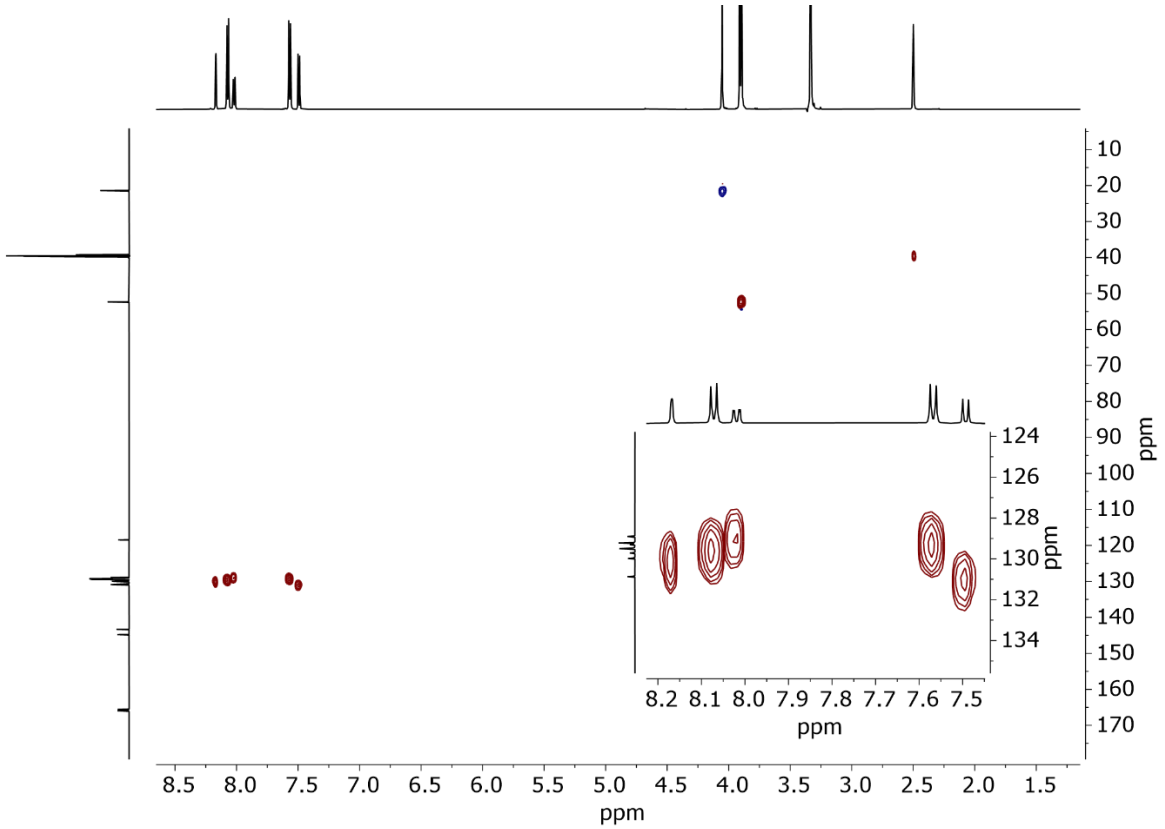

Figure 133: HSQC (600 MHz, DMSO-d_6) spectrum of **7**.

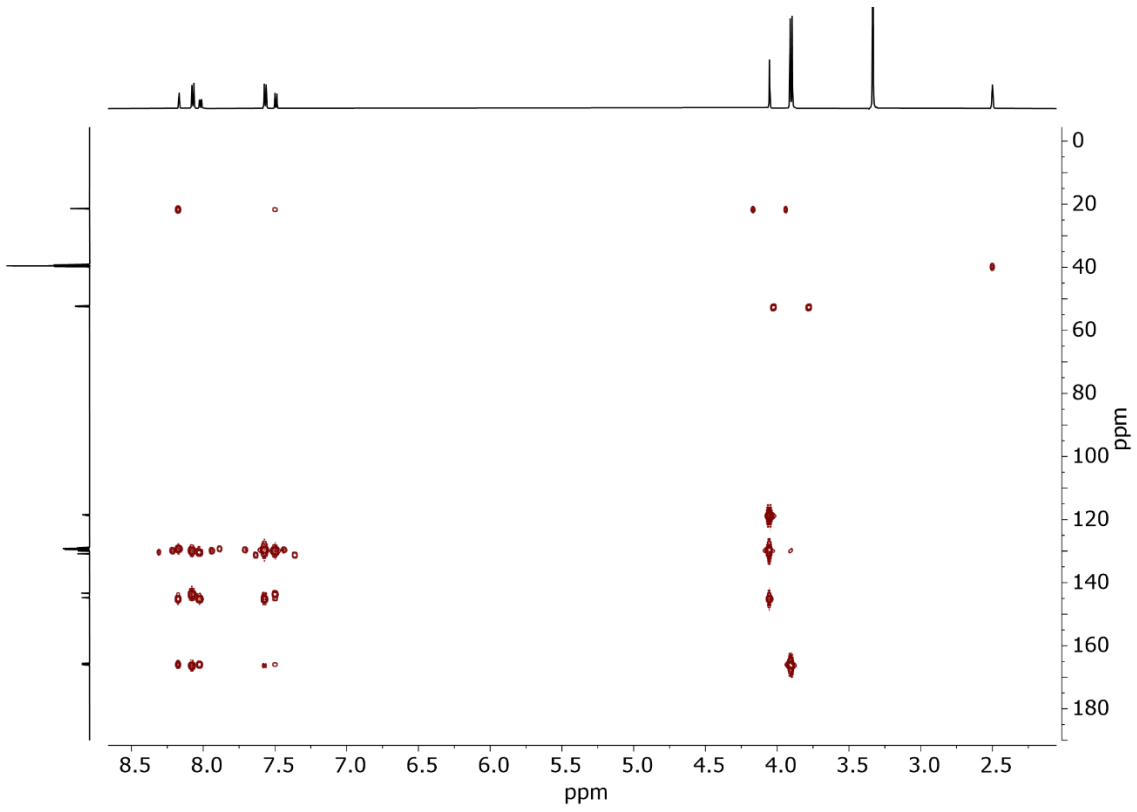

Figure 134: HMBC (600 MHz, DMSO-d_6) spectrum of **7**.

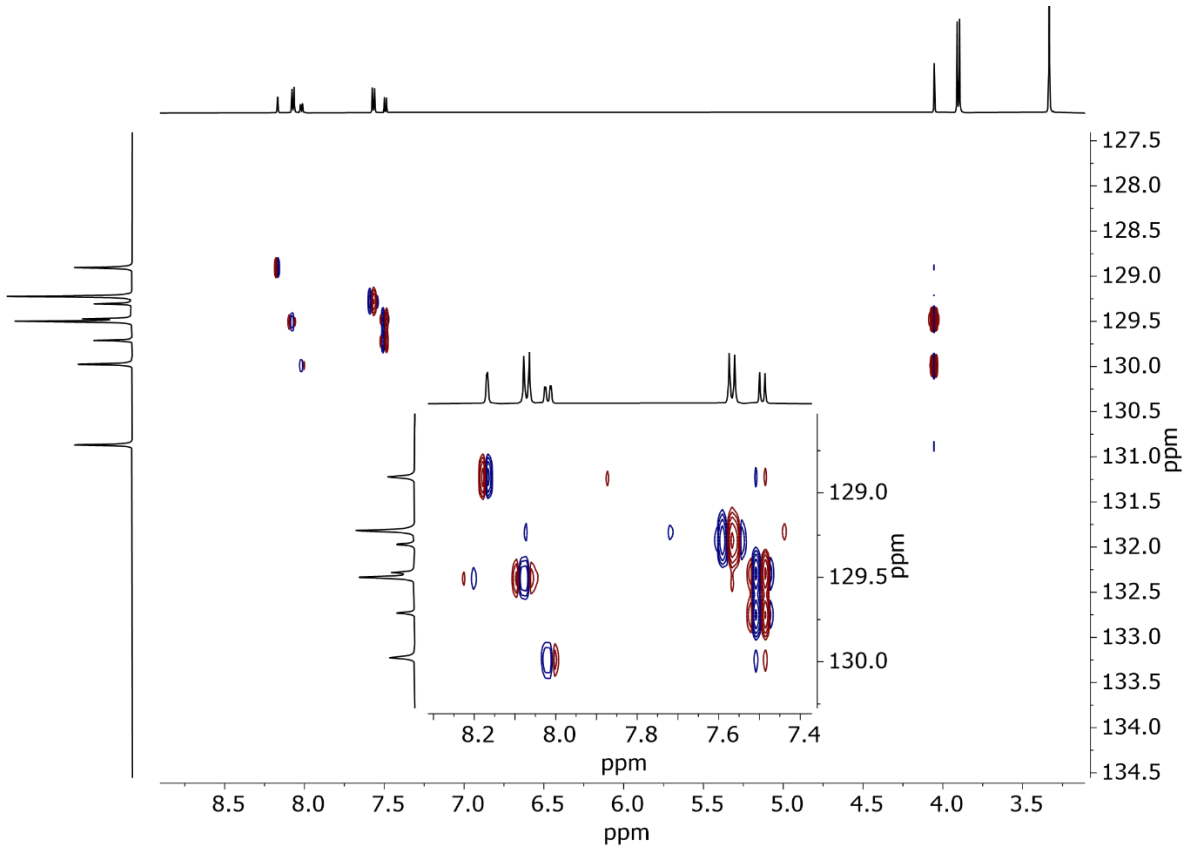

Figure 135: S HMBC (600 MHz, DMSO-d_6) spectrum of **7**.

8.12 Compound 8a

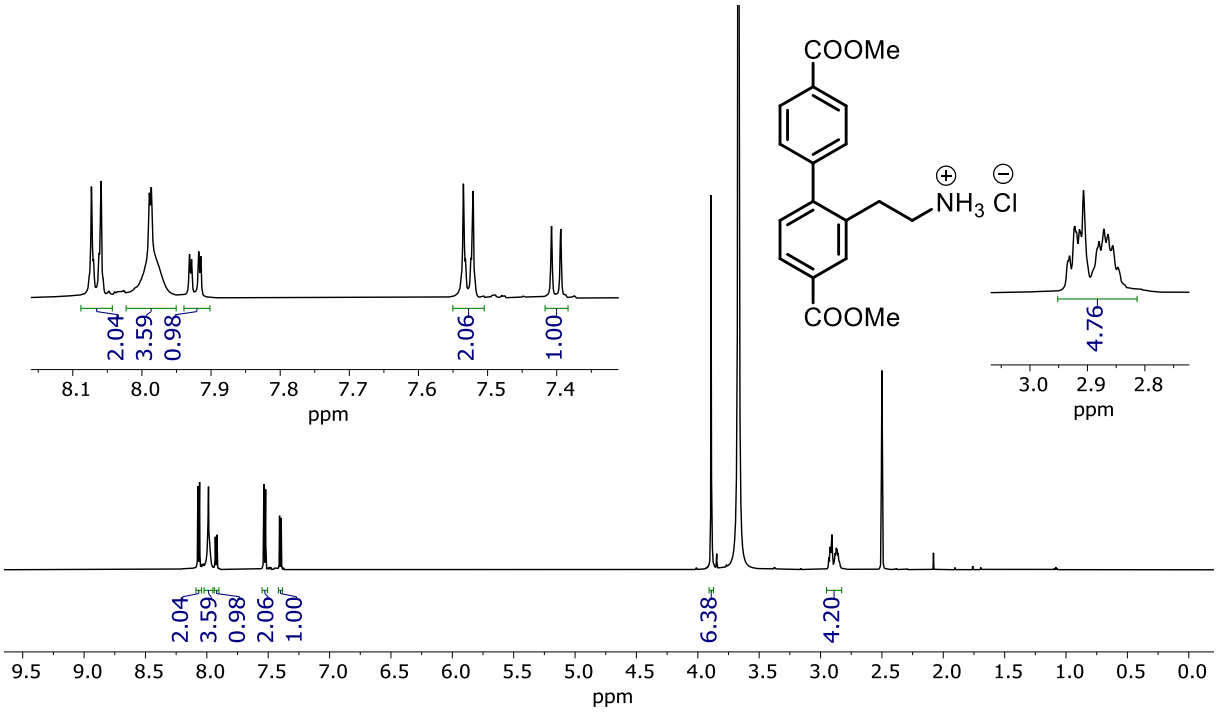

Figure 136: ^{1}H NMR (600 MHz, DMSO-d_6) spectrum of **8a**.

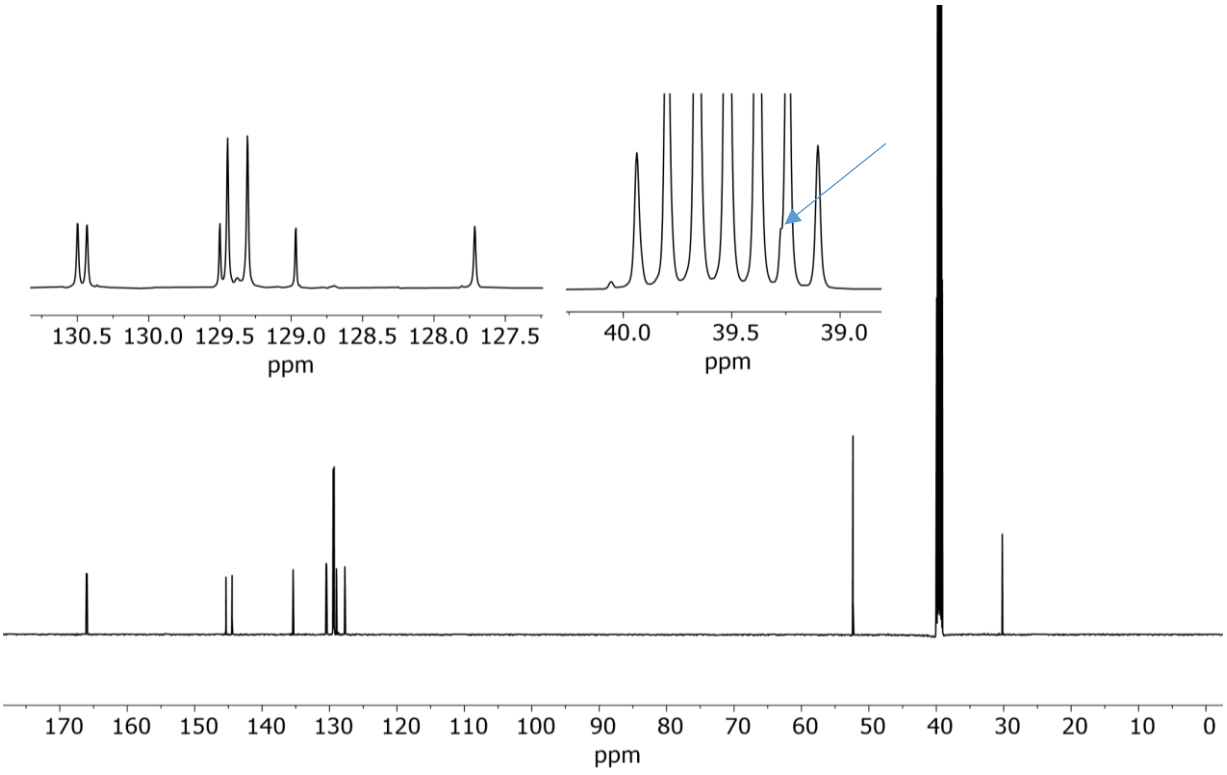

Figure 137: ^{13}C NMR (151 MHz, DMSO-d_6) spectrum of **8a**. Methylene carbon is marked with a blue arrow.

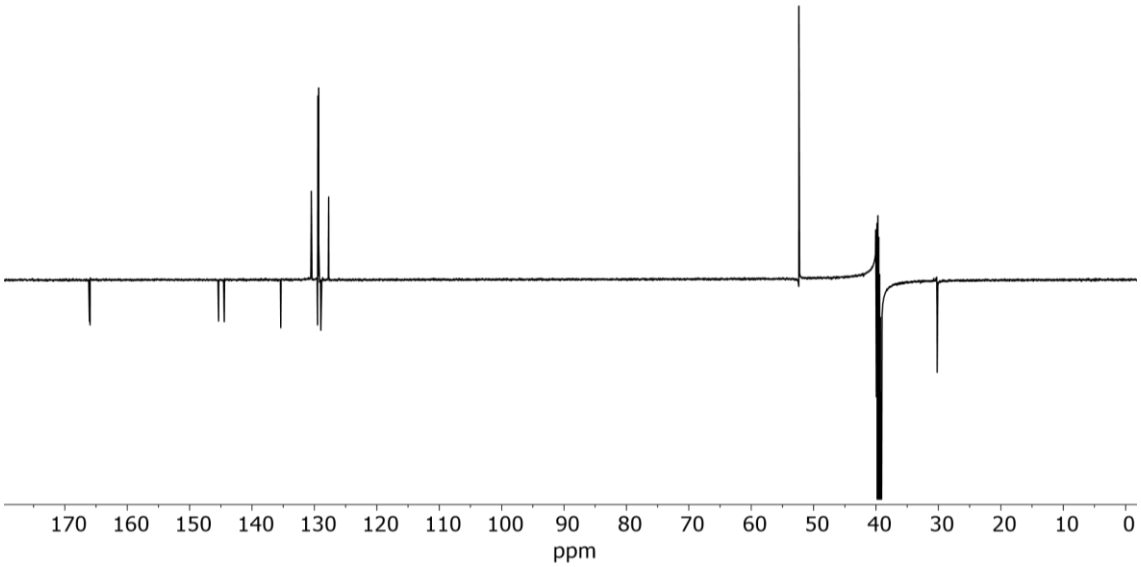

Figure 138: DEPT135Q (151 MHz, DMSO-d_6) spectrum of **8a**.

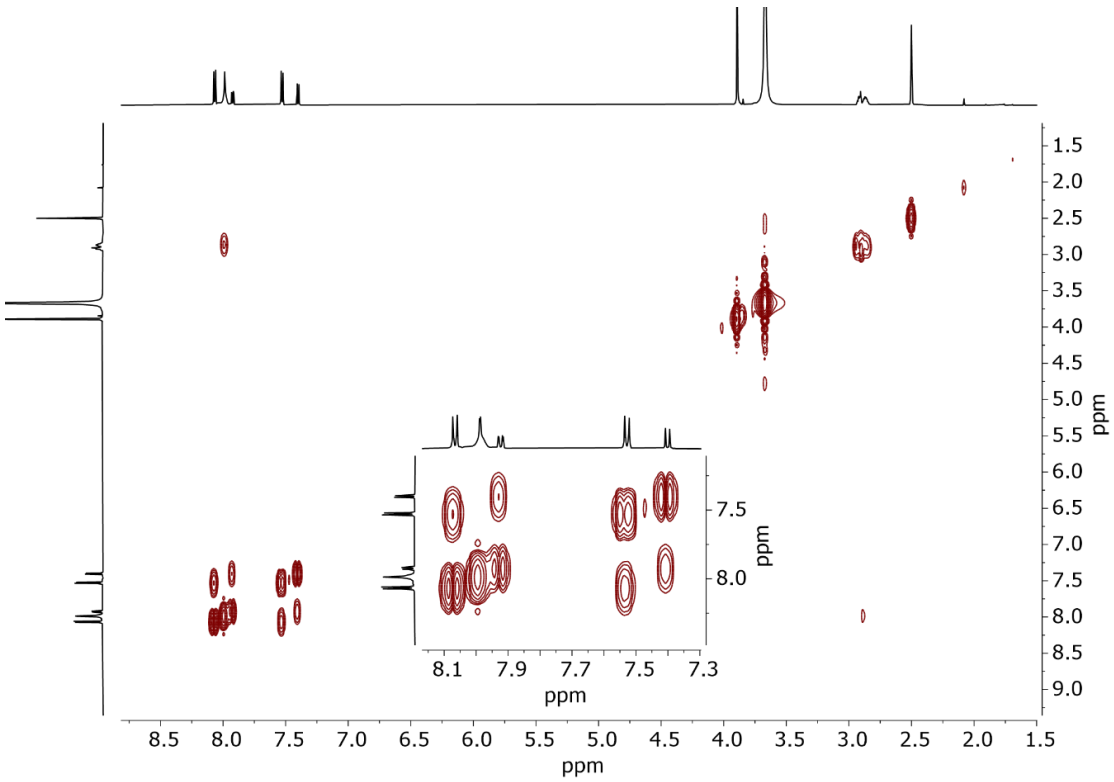

Figure 139: COSY (600 MHz, DMSO-d_6) spectrum of **8a**.

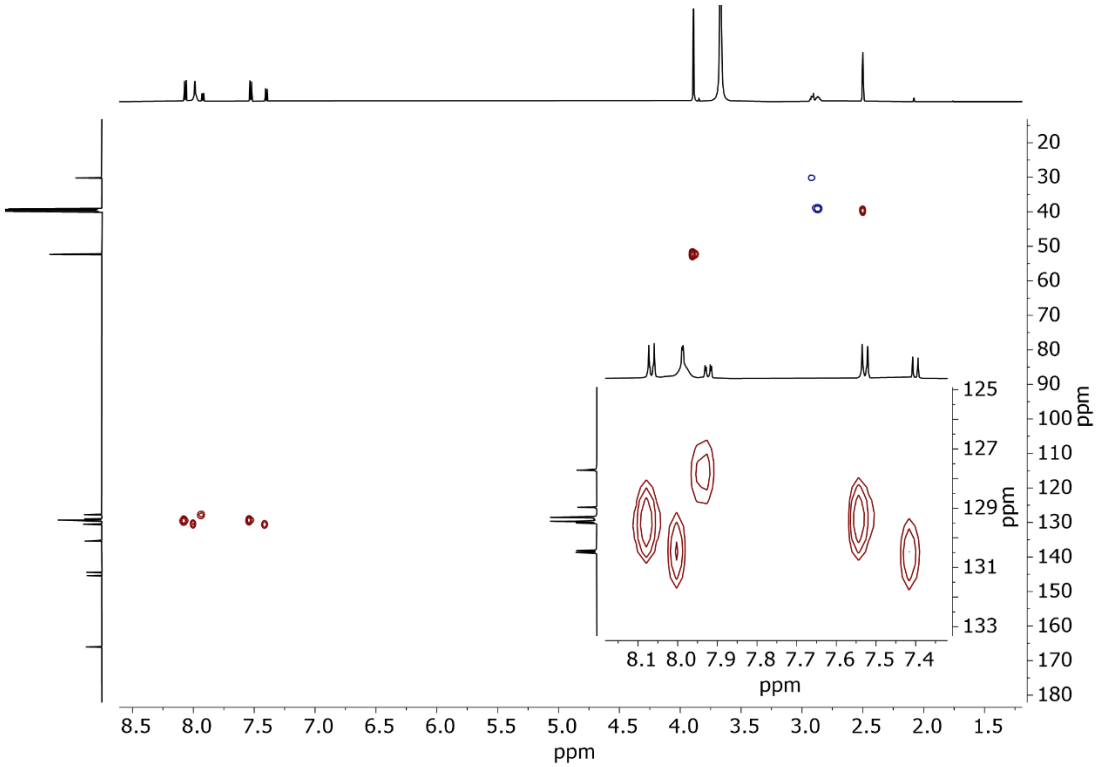

Figure 140: HSQC (600 MHz, DMSO-d_6) spectrum of **8a**.

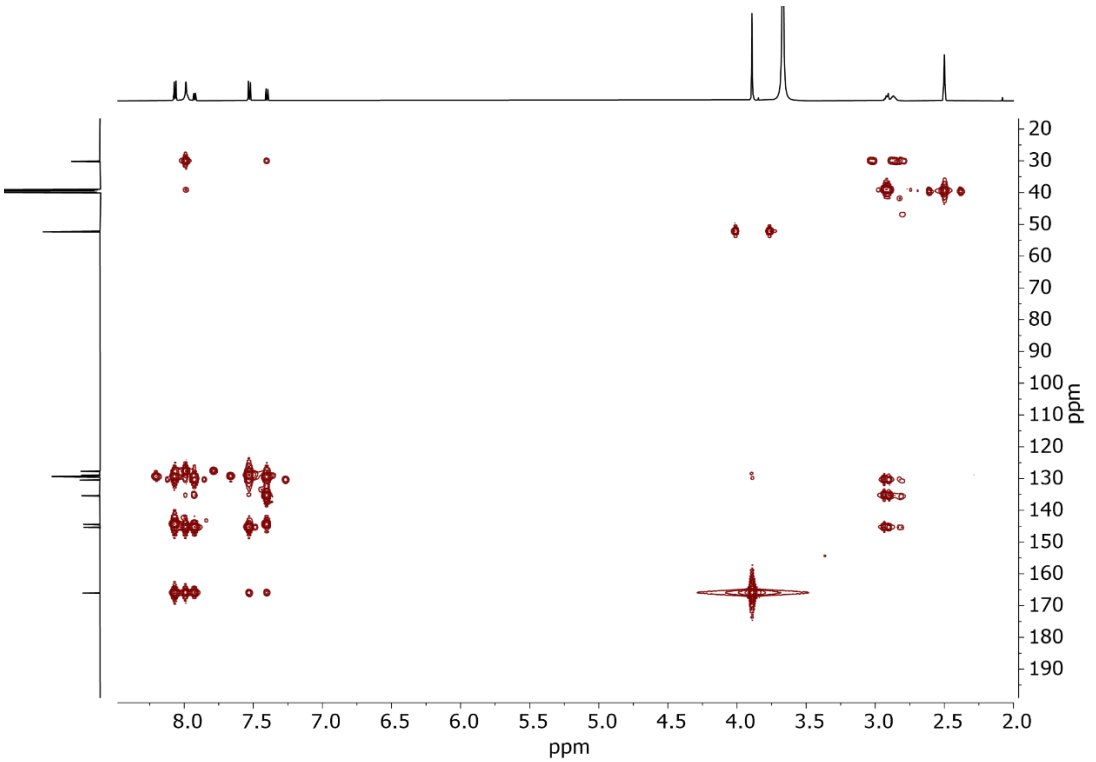

Figure 141: HMBC (600 MHz, DMSO-d_6) spectrum of **8a**.

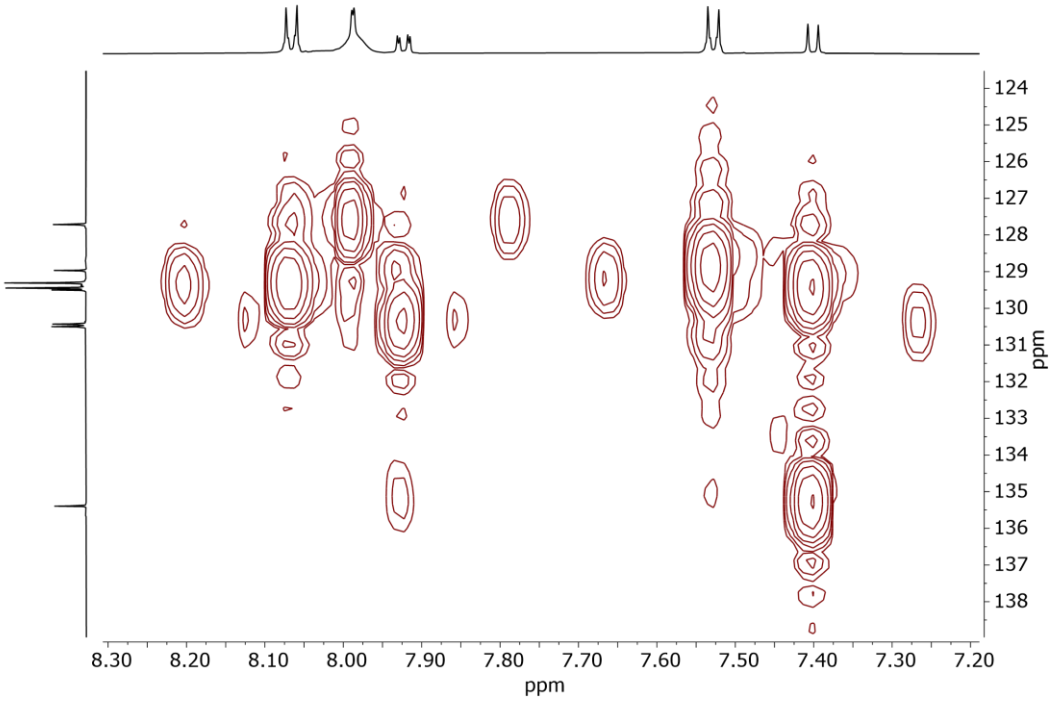

Figure 142: Zoom of HMBC (600 MHz, DMSO-d_6) spectrum of **8a**.

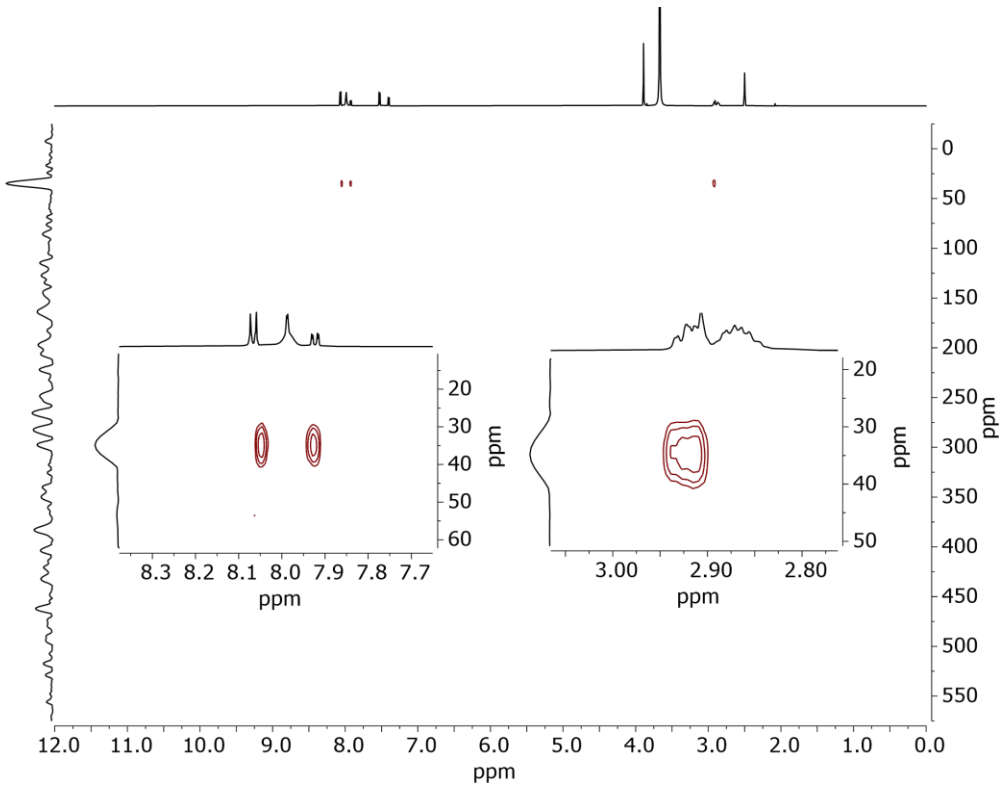

Figure 143: ^{1}H-^{15}N HMBC (600 MHz, DMSO-d_6) spectrum of **8a**.

8.13 Compound 8b

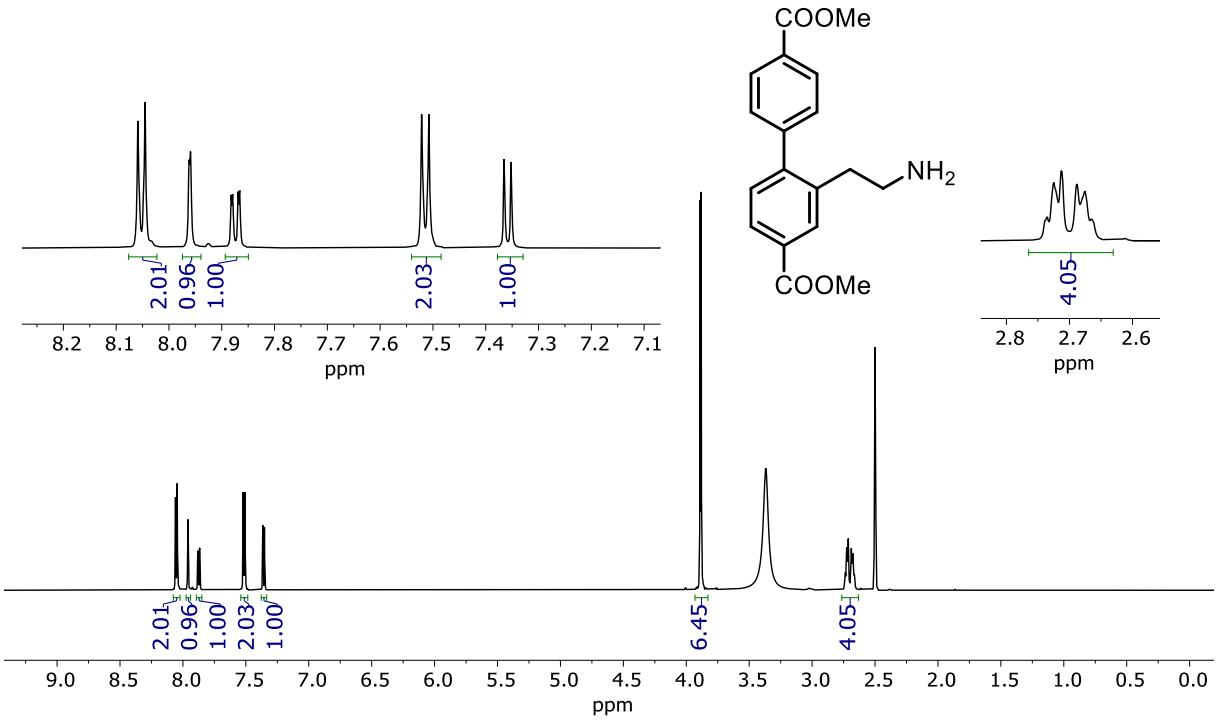

Figure 144: ^{1}H NMR (600 MHz, DMSO-d_6) spectrum of **8b**.

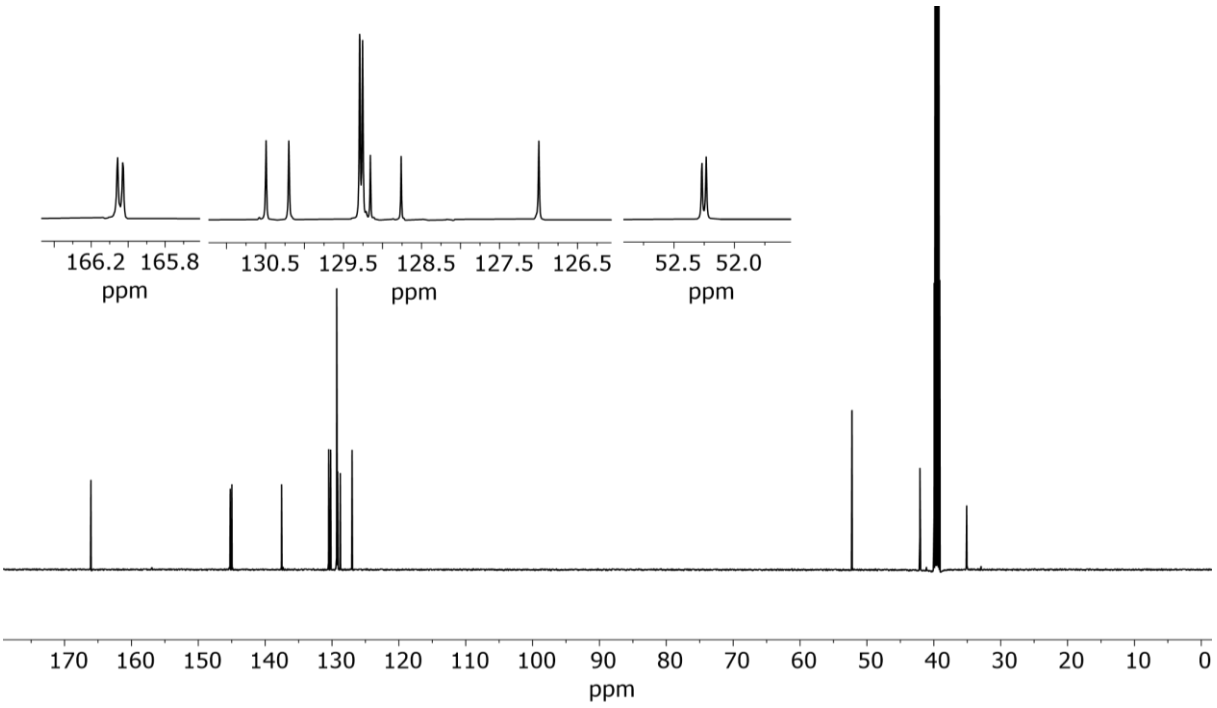

Figure 145: ^{13}C NMR (151 MHz, DMSO-d_6) spectrum of **8b**.

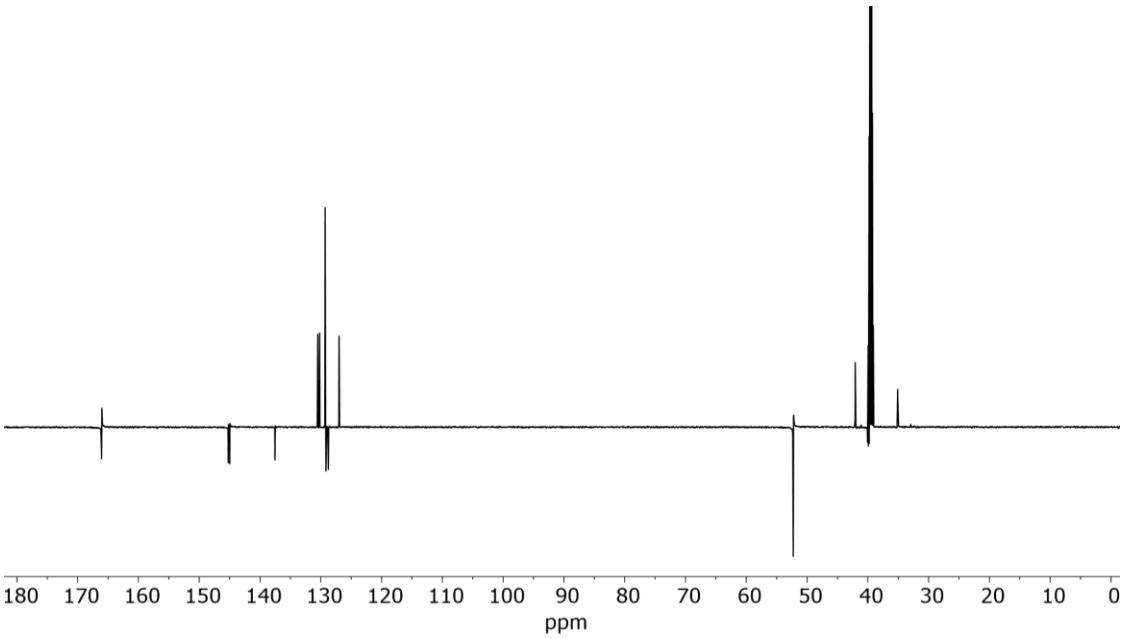

Figure 146: DEPT135Q (151 MHz, DMSO-d_6) spectrum of **8b**.

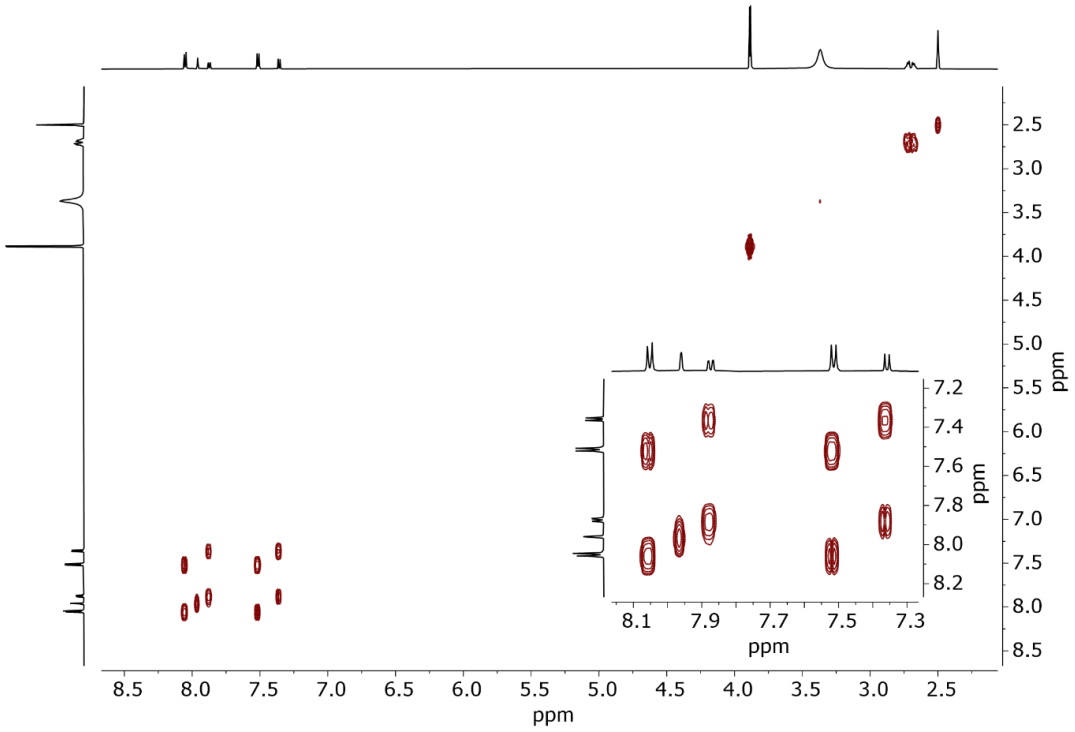

Figure 147: COSY (600 MHz, DMSO-d_6) spectrum of **8b**.

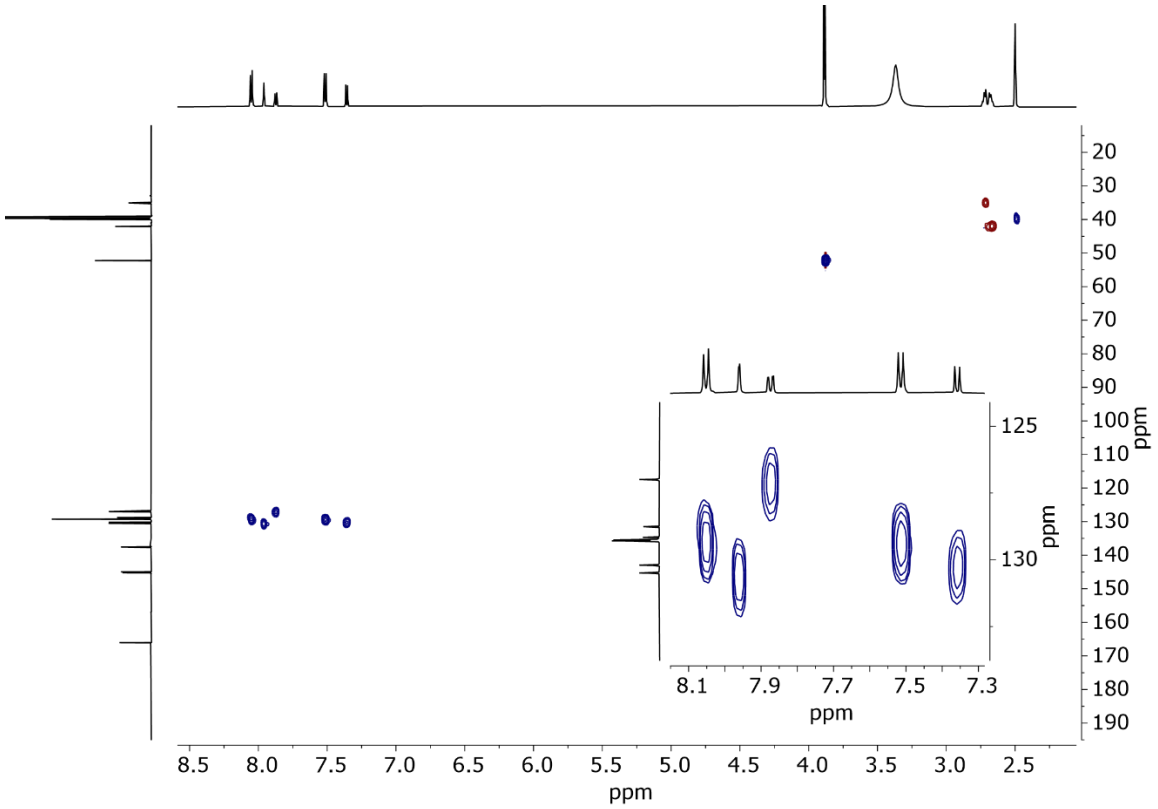

Figure 148: HSQC (600 MHz, DMSO-d_6) spectrum of **8b**.

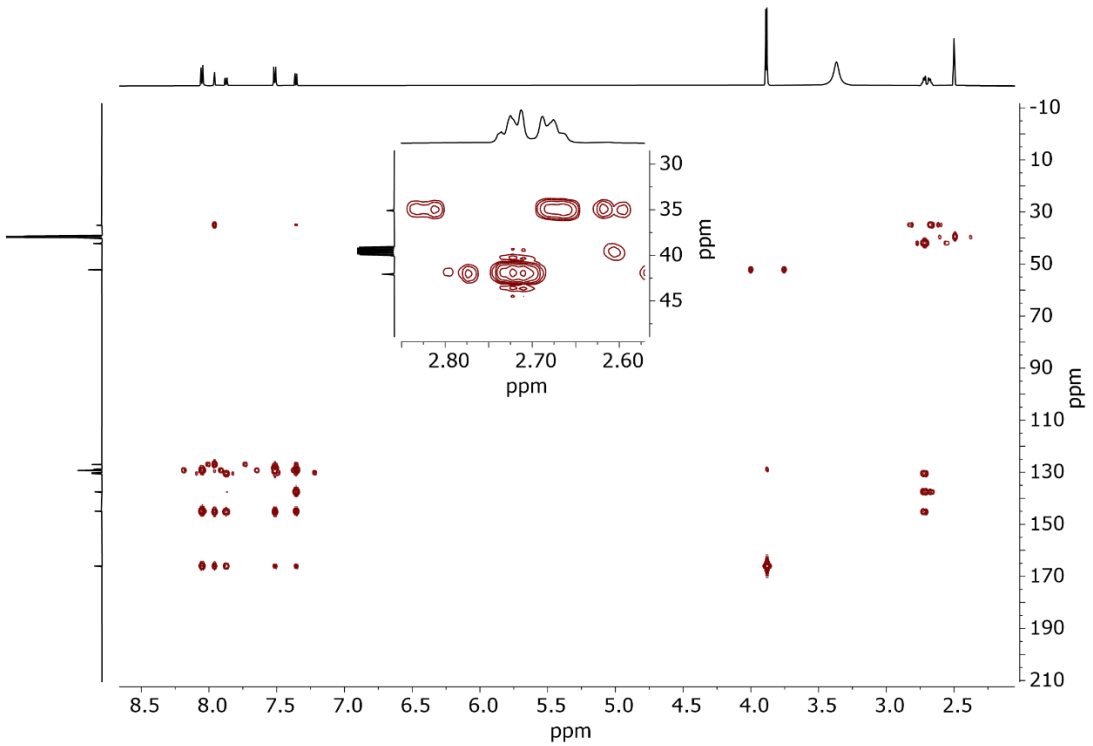

Figure 149: HMBC (600 MHz, DMSO-d_6) spectrum of **8b**.

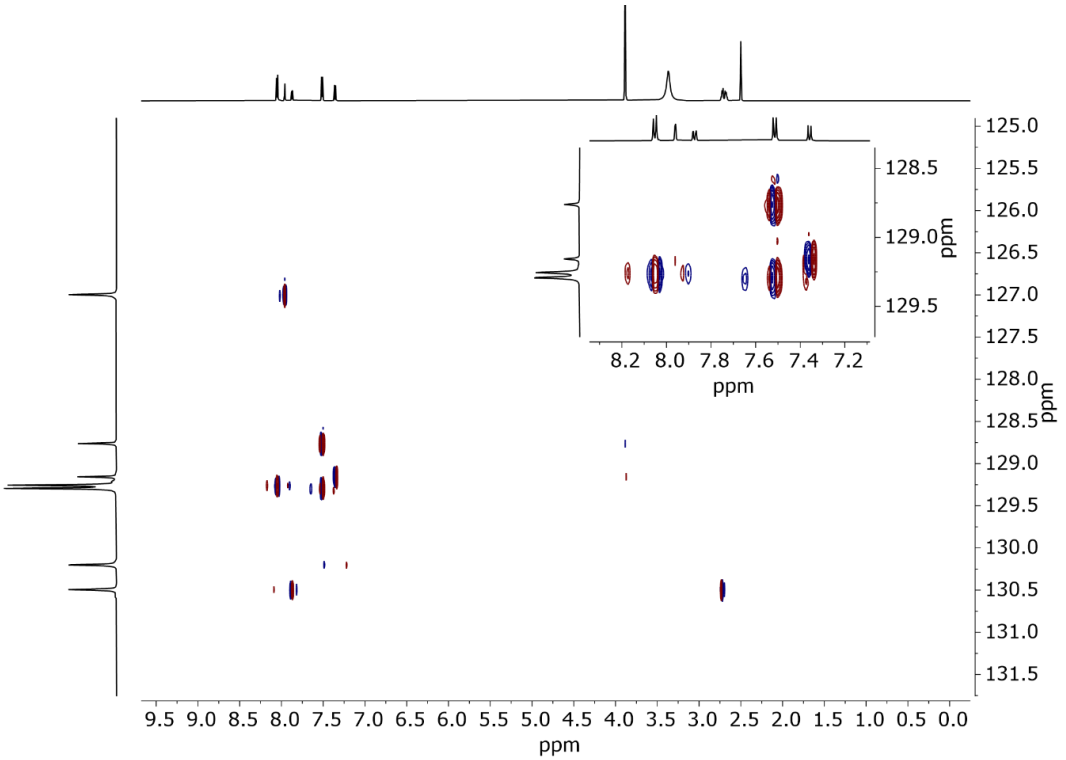

Figure 150: S HMBC (600 MHz, DMSO-d_6) spectrum of **8b**.

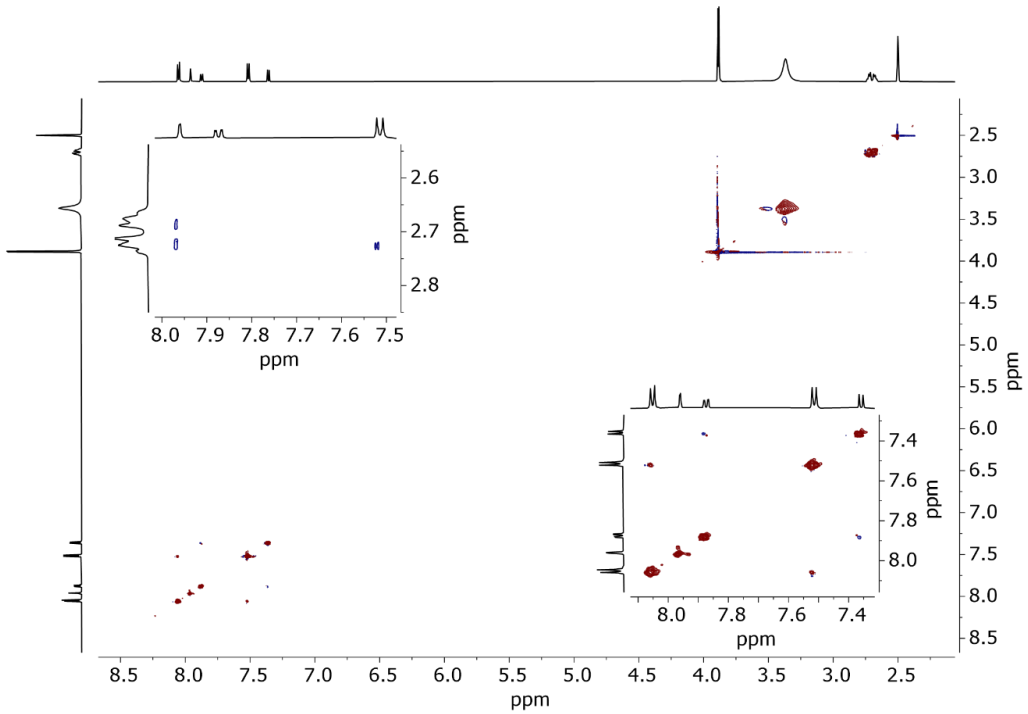

Figure 151: NOESY (600 MHz, DMSO-d_6) spectrum of **8b**.

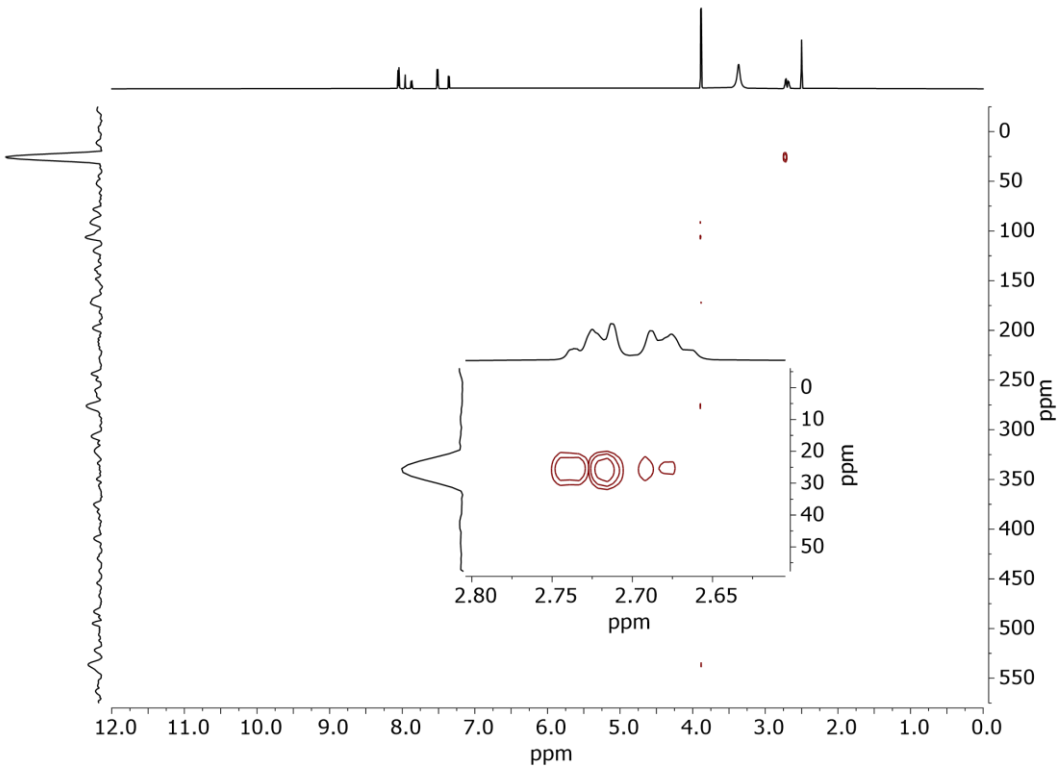

Figure 152: ^{1}H-^{15}N HMBC (600 MHz, DMSO-d_6) spectrum of **8b**.

8.14 Compound 9

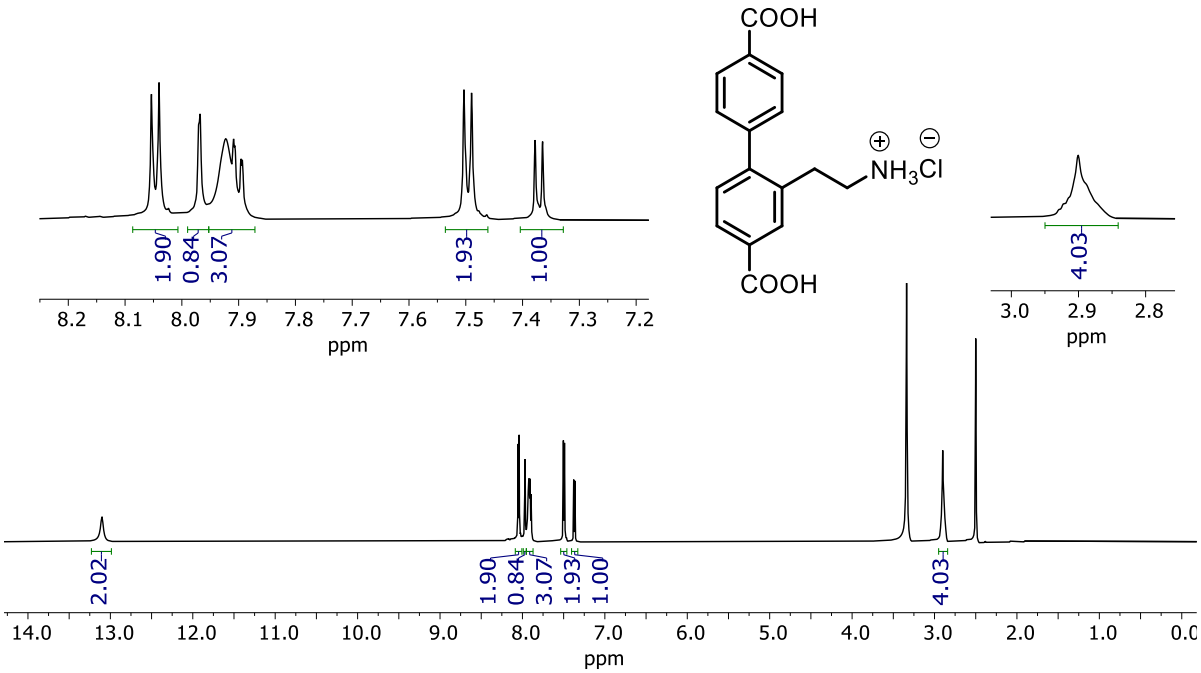

Figure 153: ^{1}H NMR (600 MHz, DMSO-d_6) spectrum of **9**.

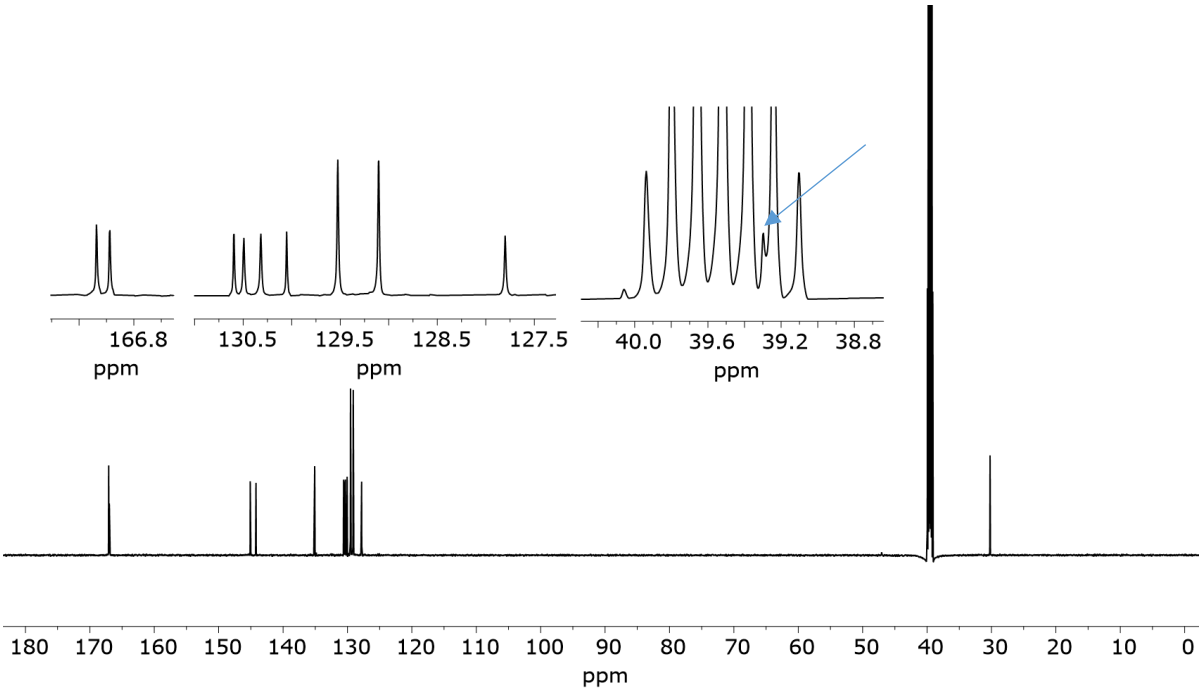

Figure 154: ^{13}C NMR (151 MHz, DMSO-d_6) spectrum of **9**.

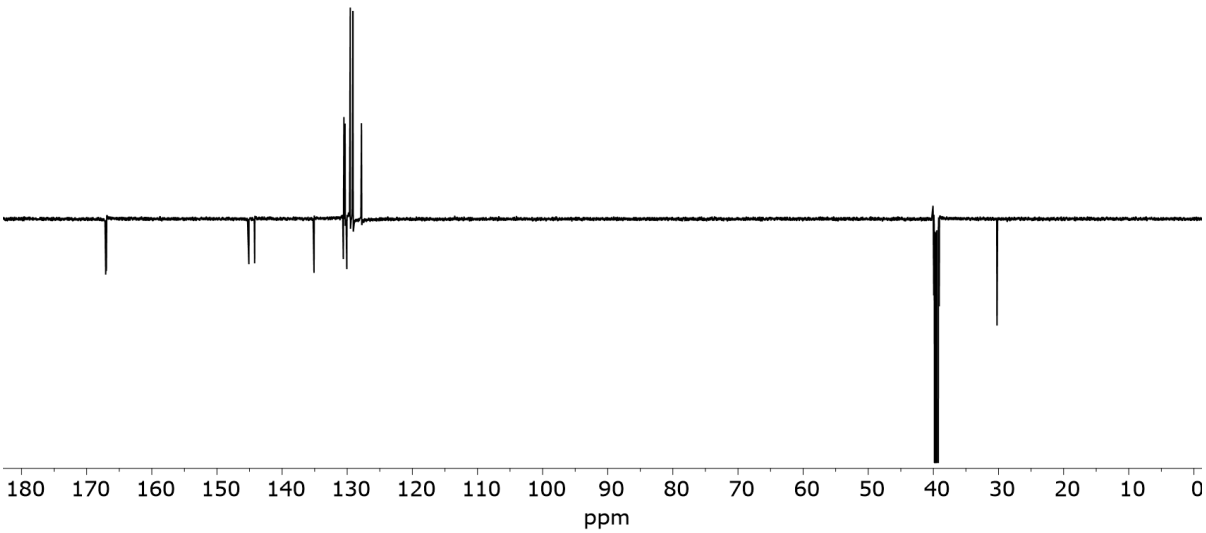

Figure 155: DEPT135Q (151 MHz, DMSO-d_6) spectrum of **9**.

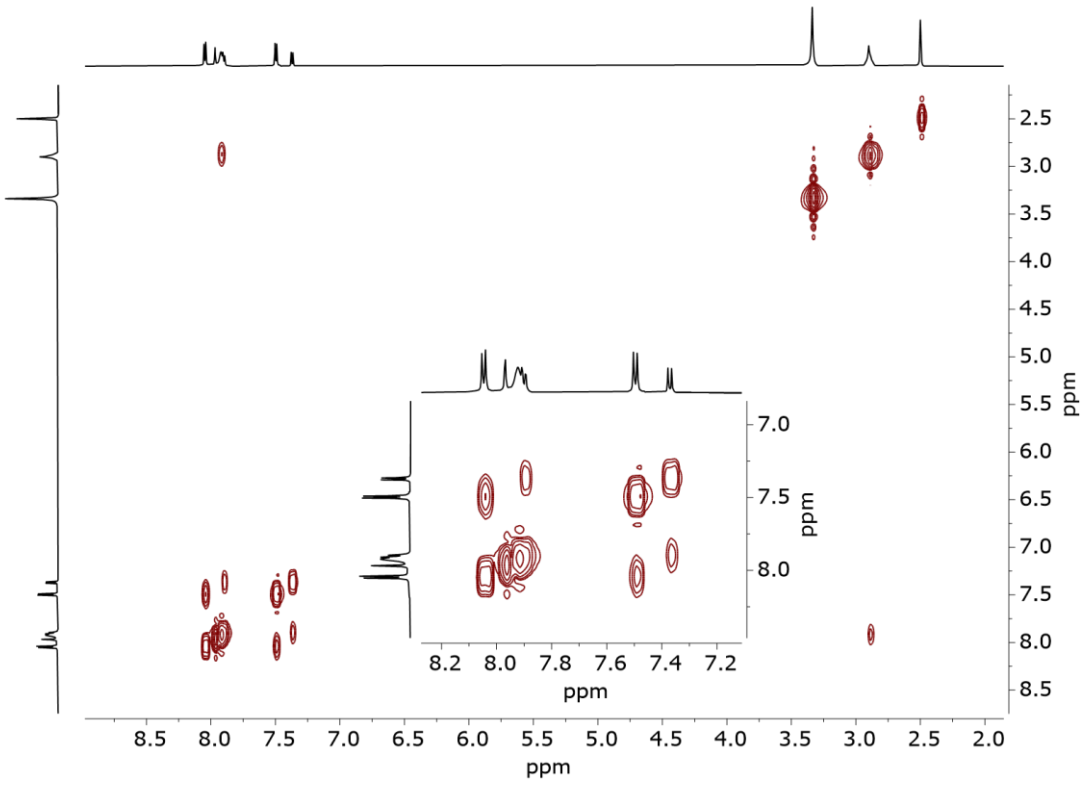

Figure 156: COSY (600 MHz, DMSO-d_6) spectrum of **9**.

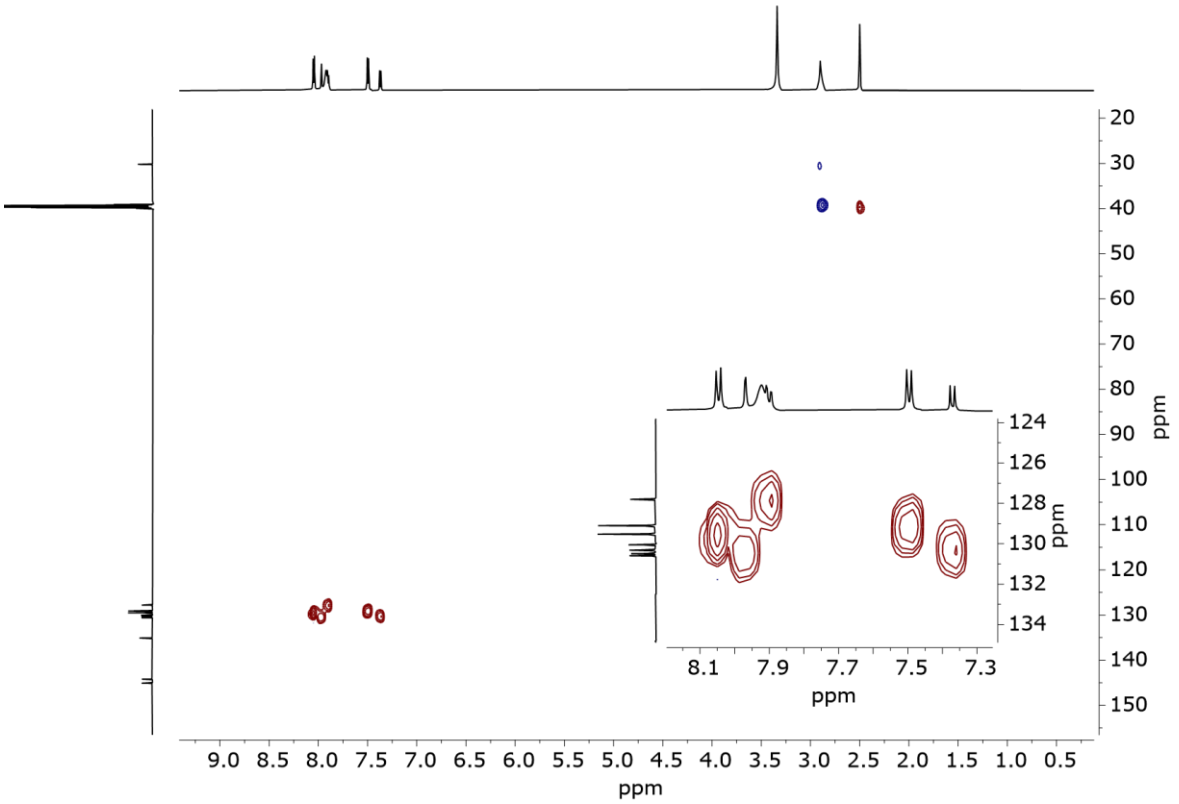

Figure 157: HSQC (600 MHz, DMSO-d_6) spectrum of **9**.

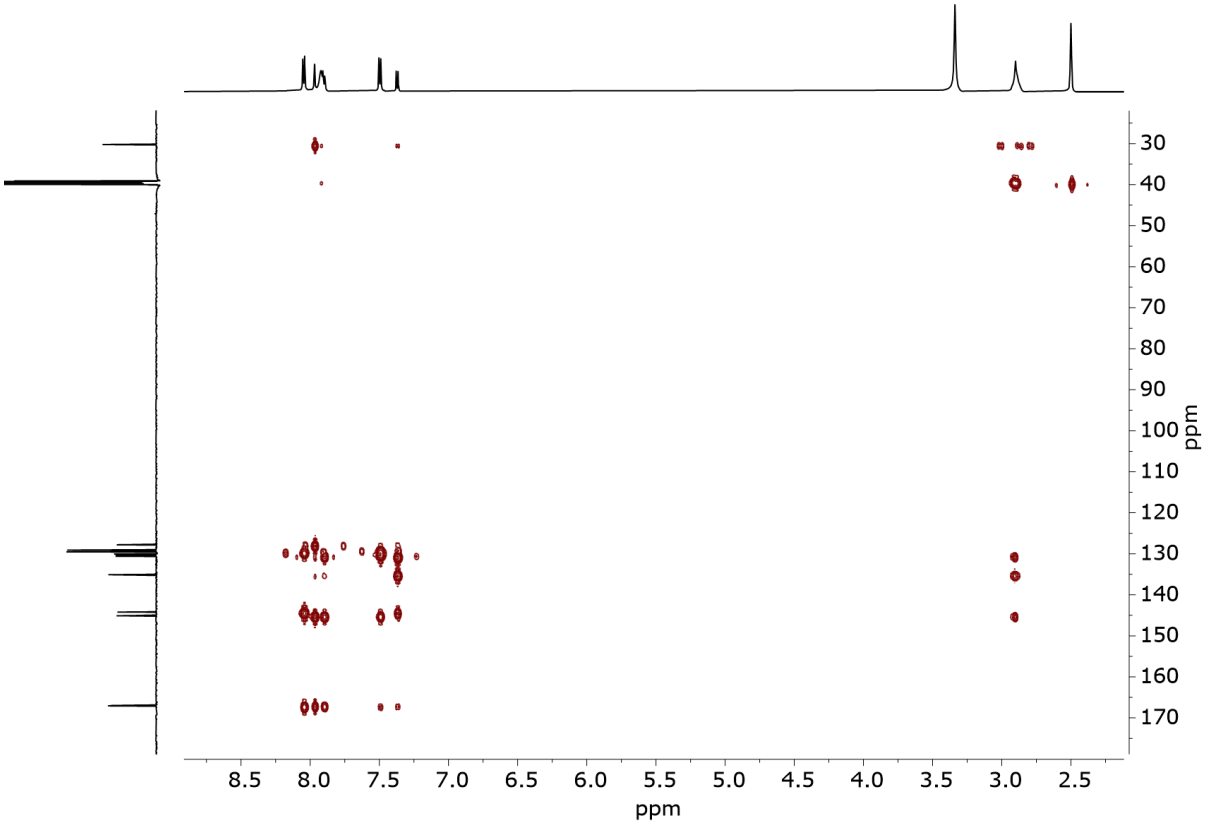

Figure 158: HMBC (600 MHz, DMSO-d_6) spectrum of **9**.

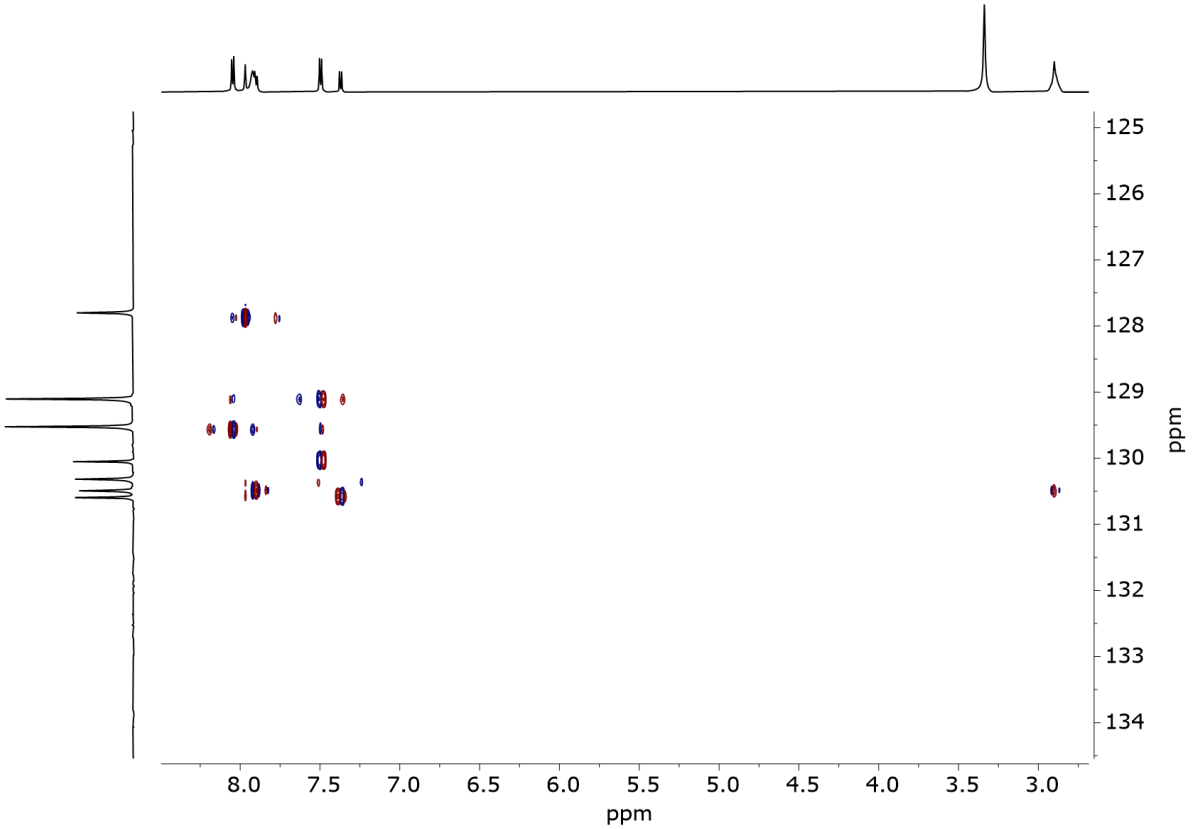

Figure 159: S HMBC (600 MHz, DMSO-d_6) spectrum of **9**.

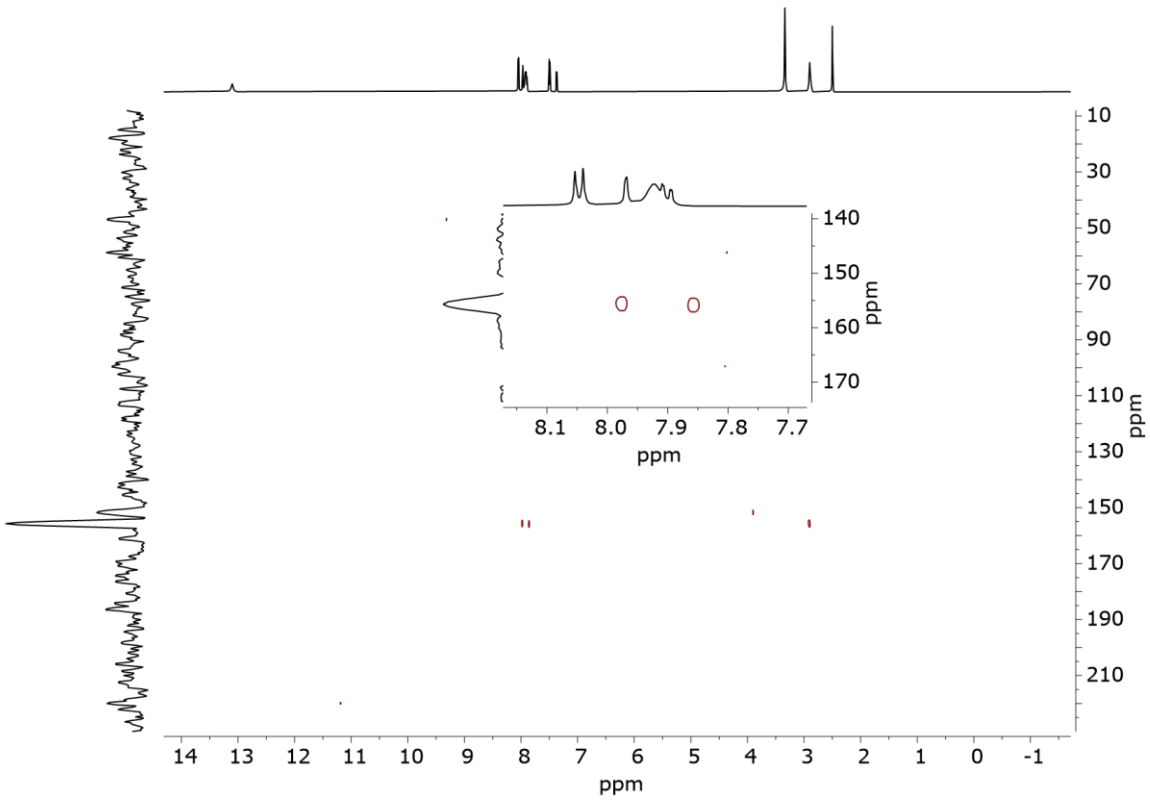

Figure 160: ^{1}H-^{15}N HMBC (600 MHz, DMSO-d_6) spectrum of **9**.

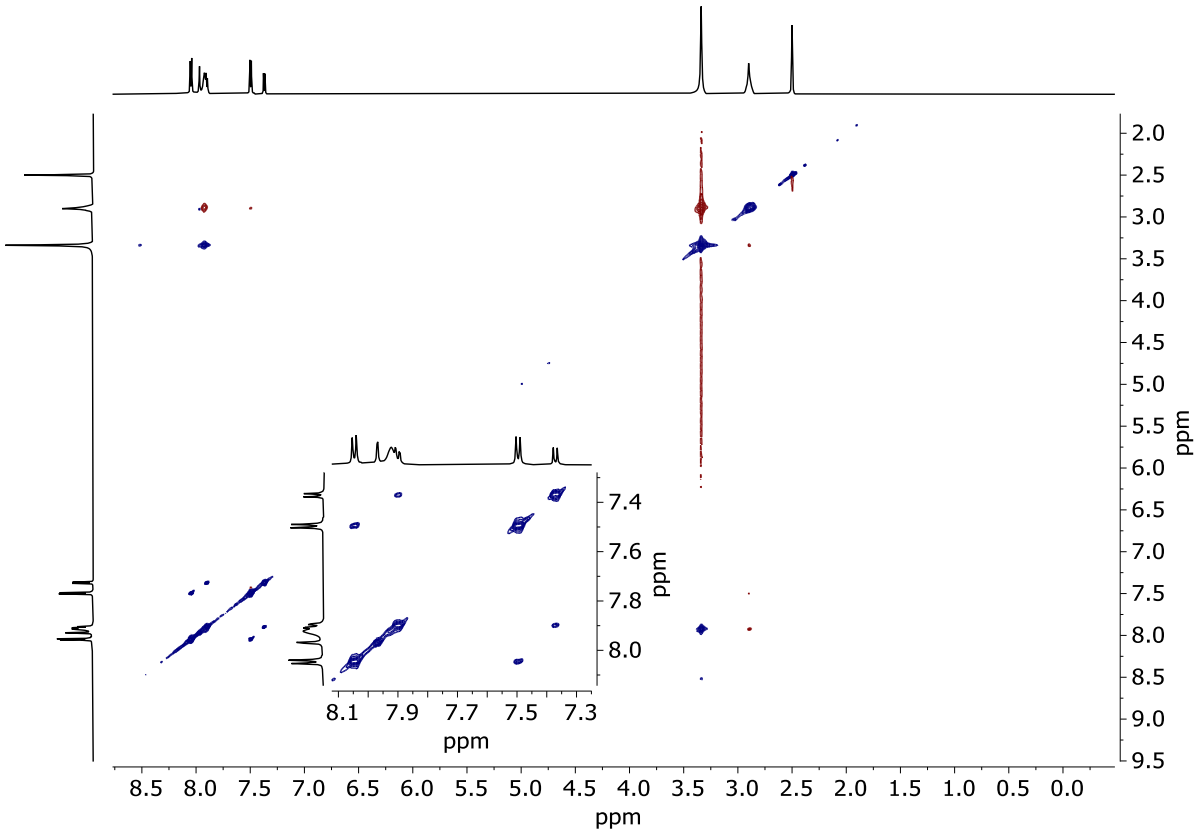

Figure 161: NOESY (600 MHz, DMSO-d_6) spectrum of **9**.

8.15 Compound 12

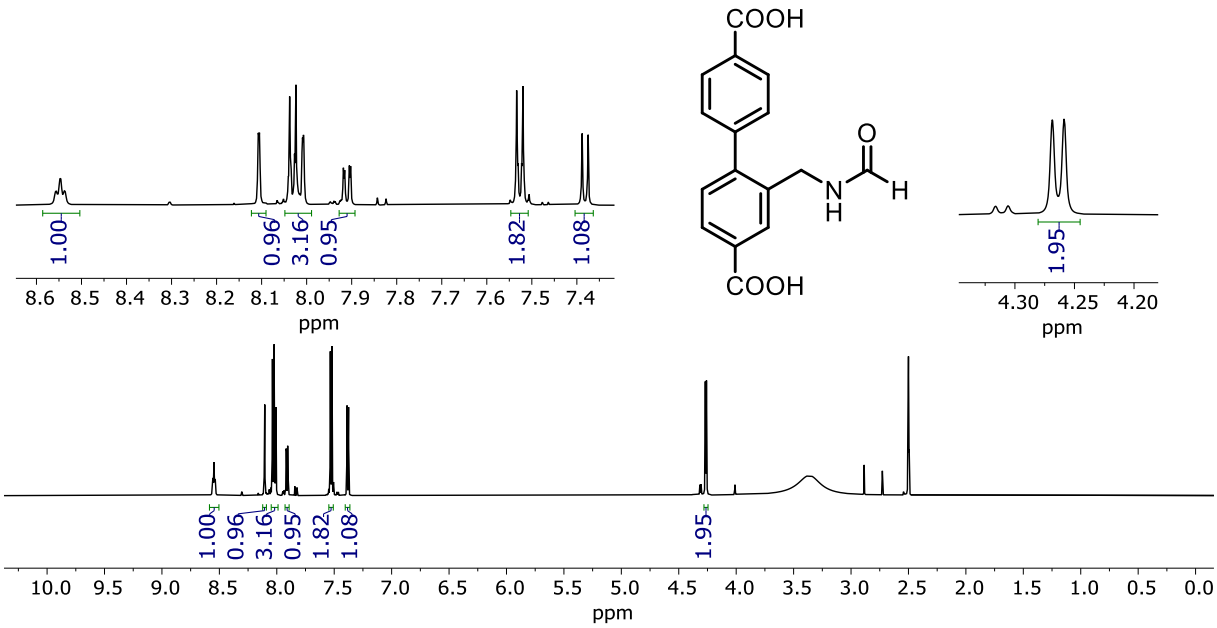

Figure 162: ^{1}H NMR (600 MHz, DMSO-d_6) spectrum of **12**.

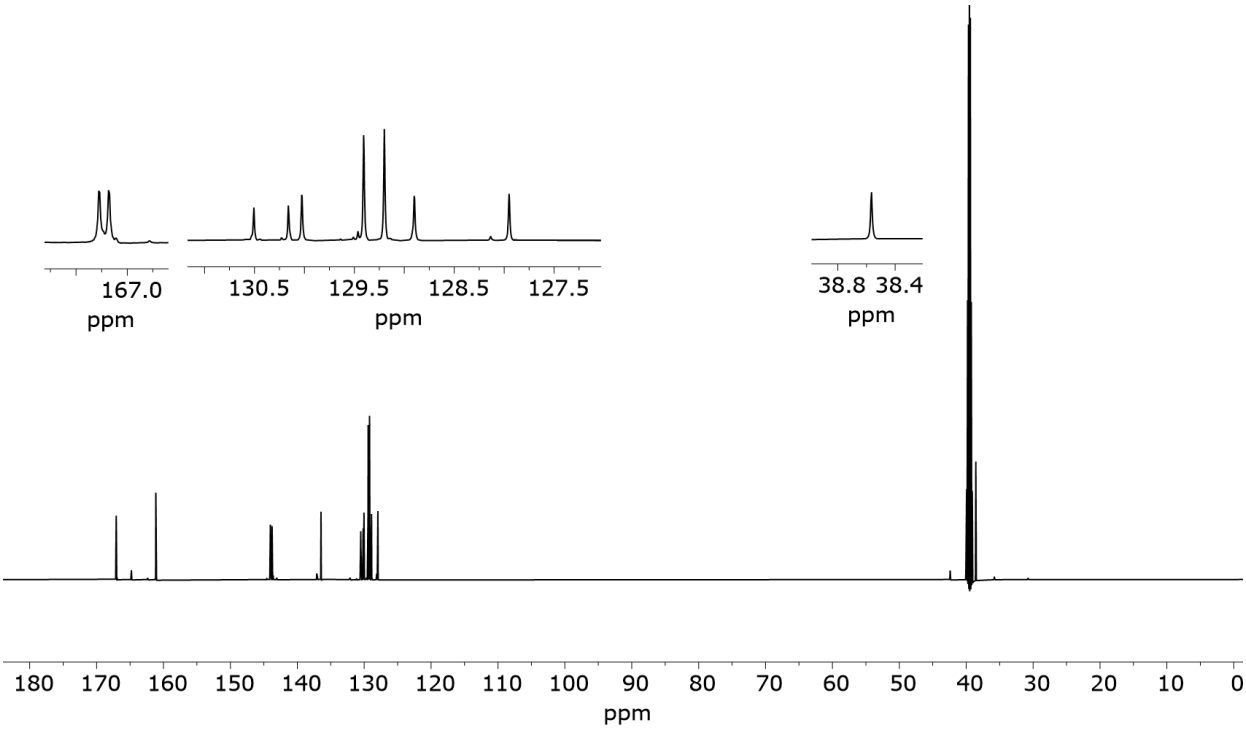

Figure 163: ^{13}C NMR (151 MHz, DMSO-d_6) spectrum of **12**.

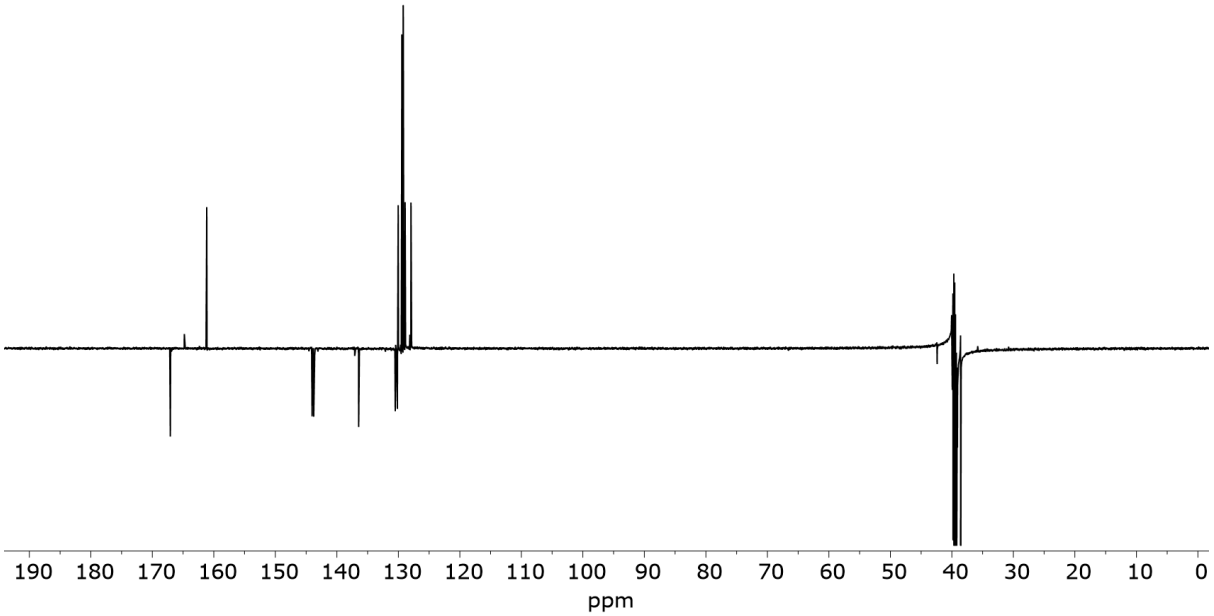

Figure 164: DEPT135Q (151 MHz, DMSO-d_6) spectrum of **12**

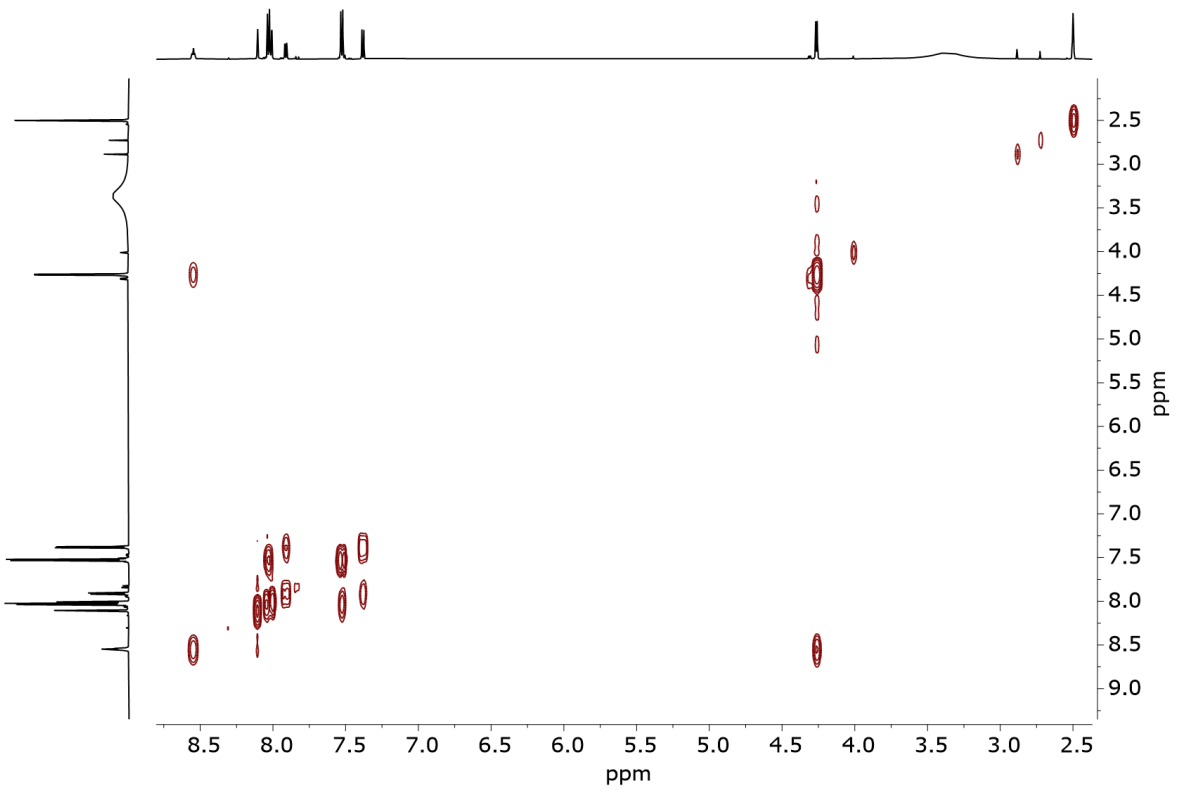

Figure 165: COSY (600 MHz, DMSO-d_6) spectrum of **12**.

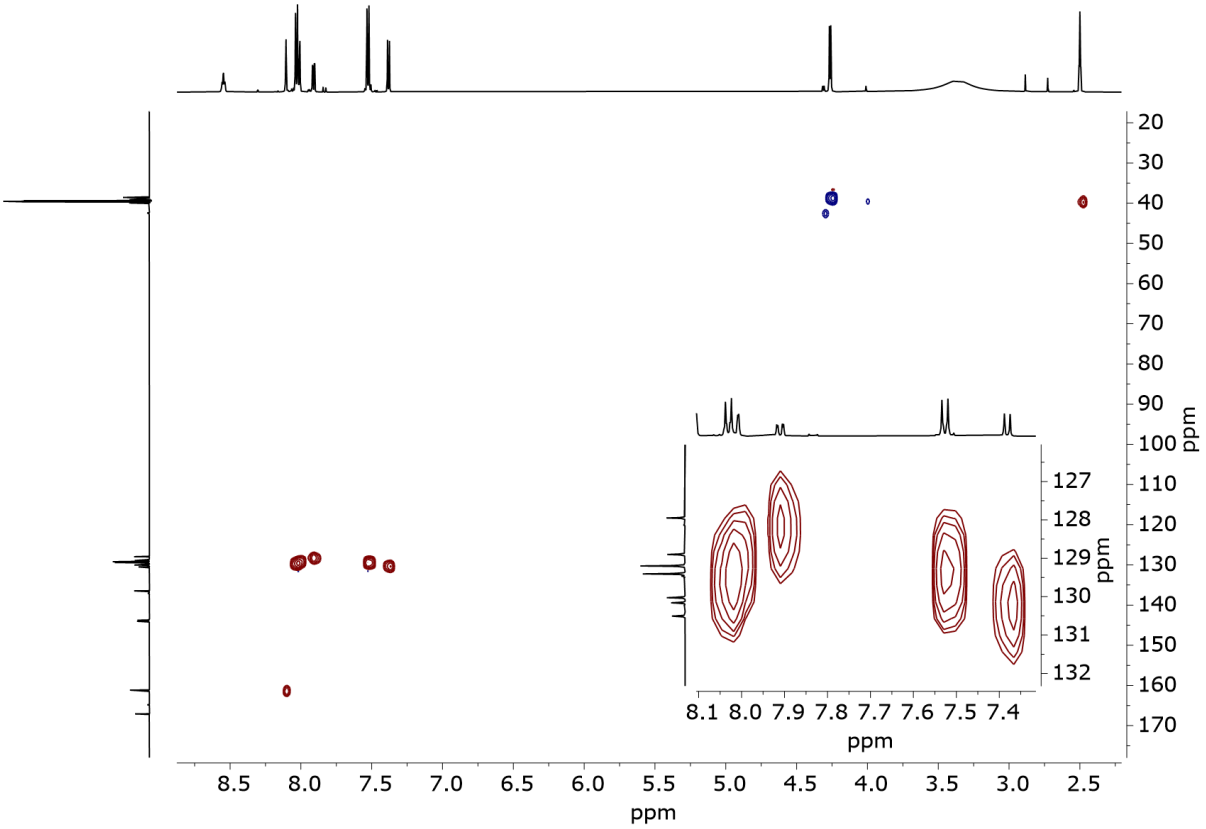

Figure 166: HSQC (600 MHz, DMSO-d_6) spectrum of **12**.

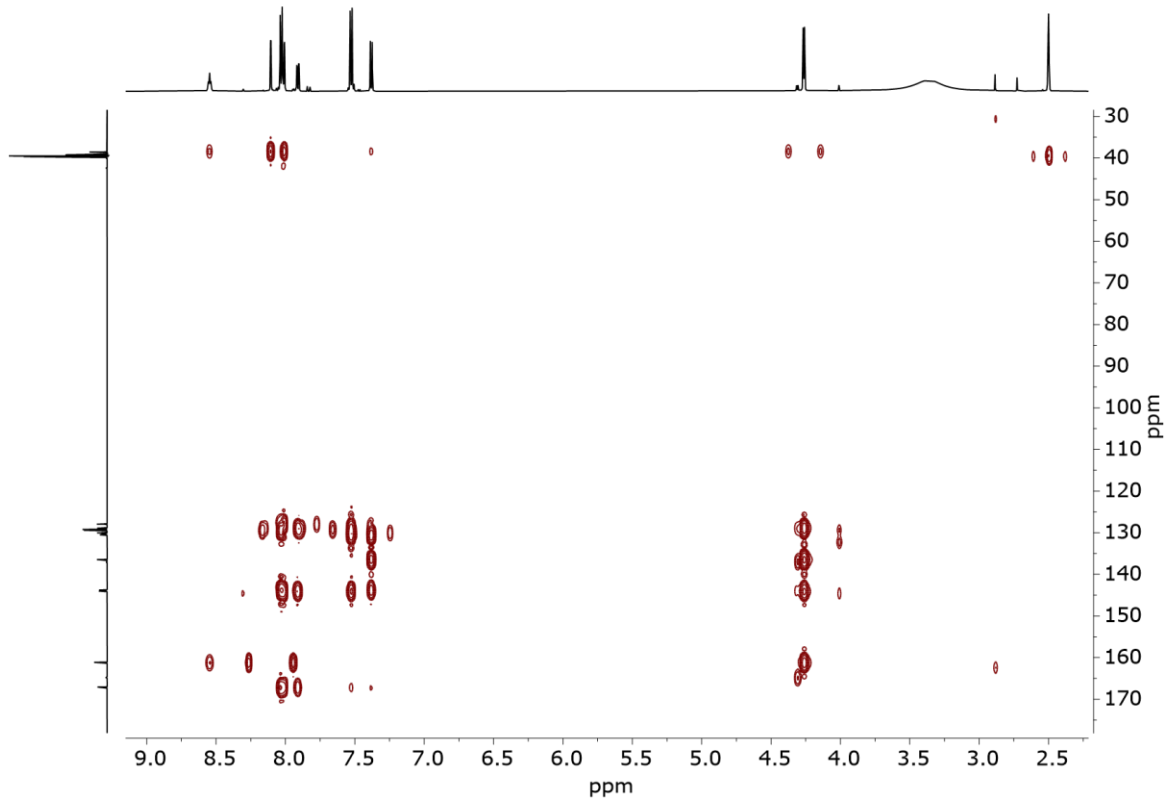

Figure 167: HMBC (600 MHz, DMSO-d_6) spectrum of **12**.

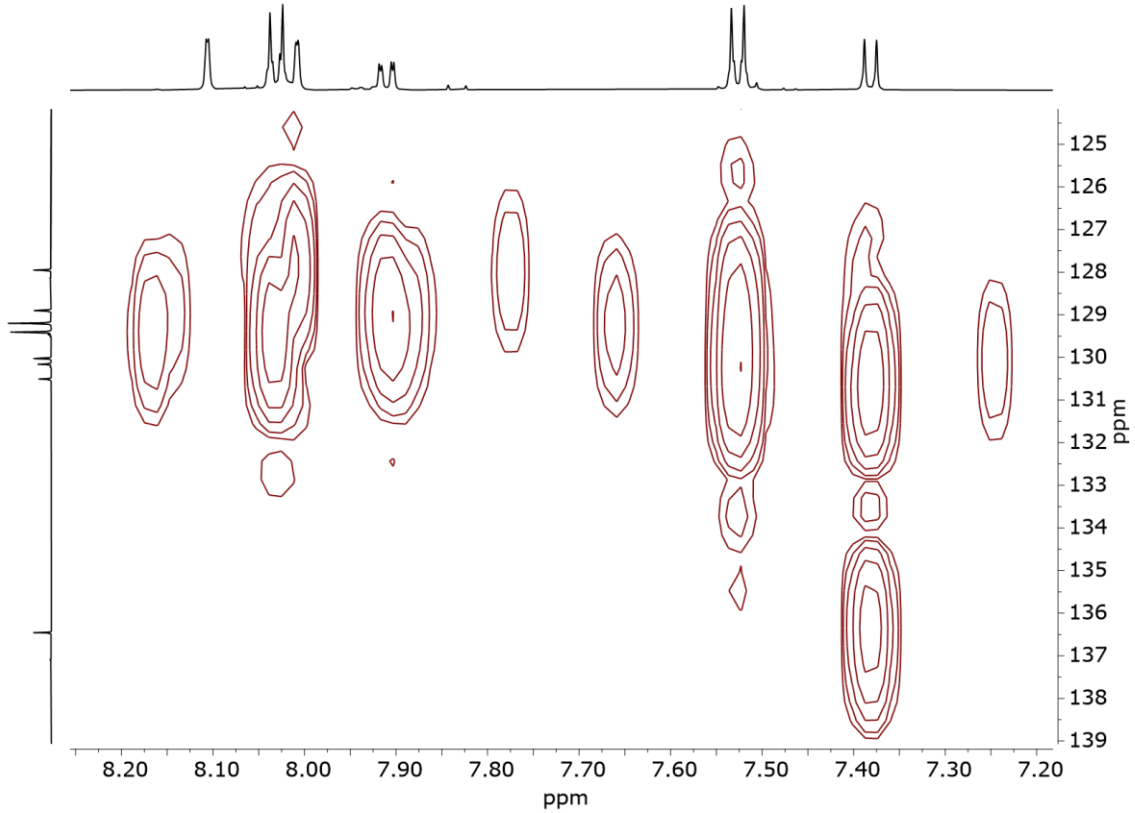

Figure 168: Zoom of HMBC (600 MHz, DMSO-d_6) spectrum of **12**.

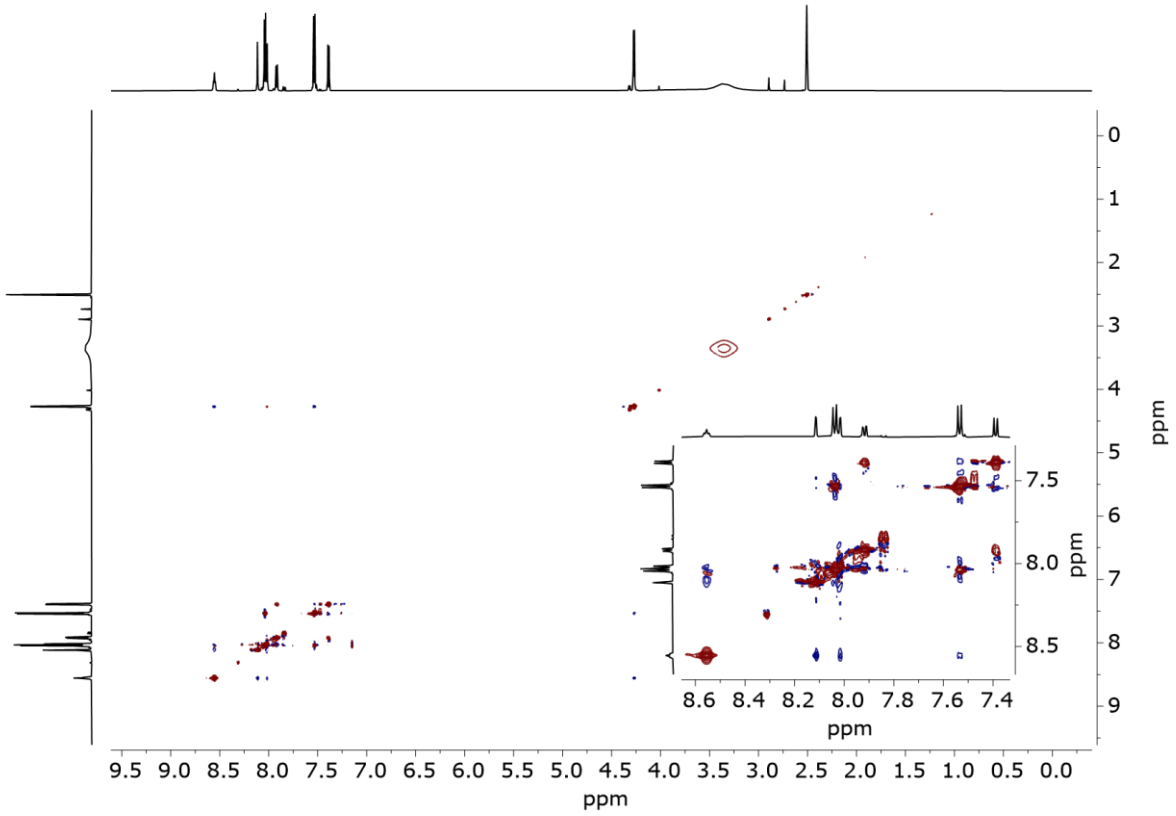

Figure 169: NOESY (600 MHz, DMSO-d_6) spectrum of **12**.

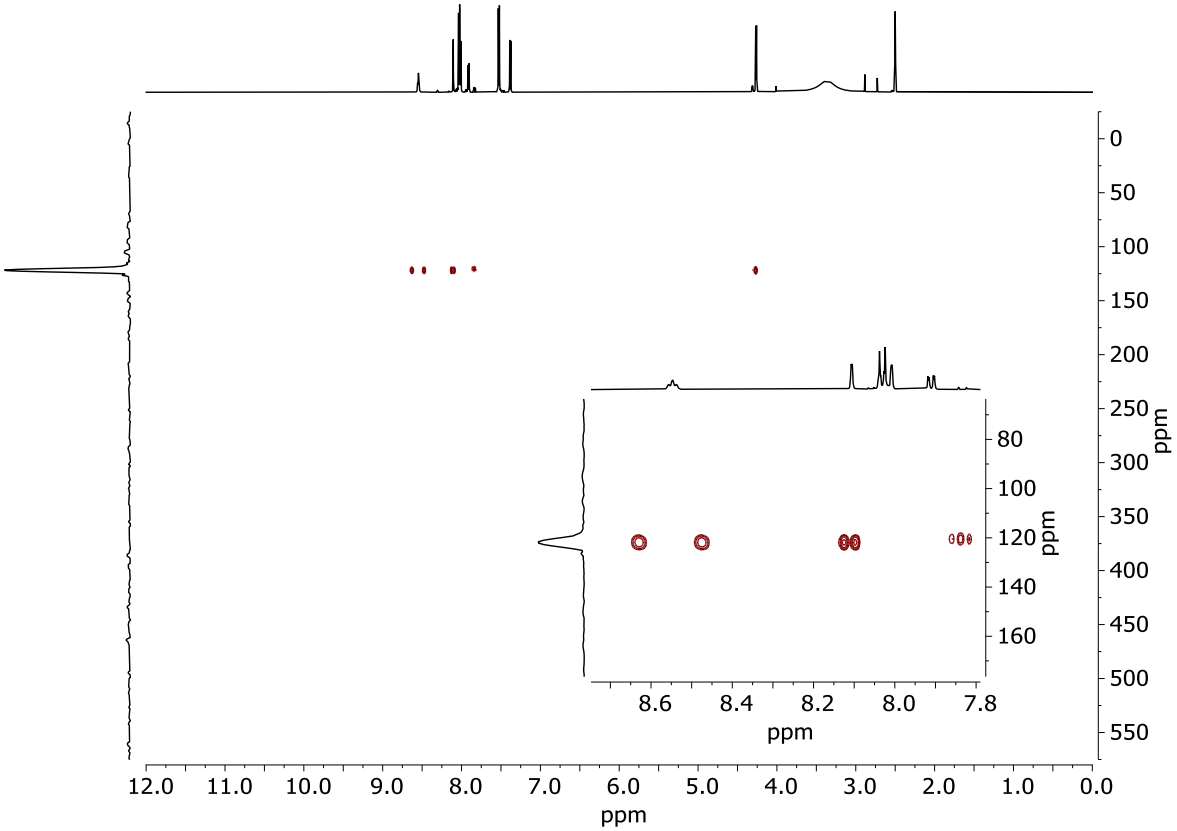

Figure 170: ^{1}H-^{15}N HMBC (600 MHz, DMSO-d_6) spectrum of **12**.

8.16 Compound 13

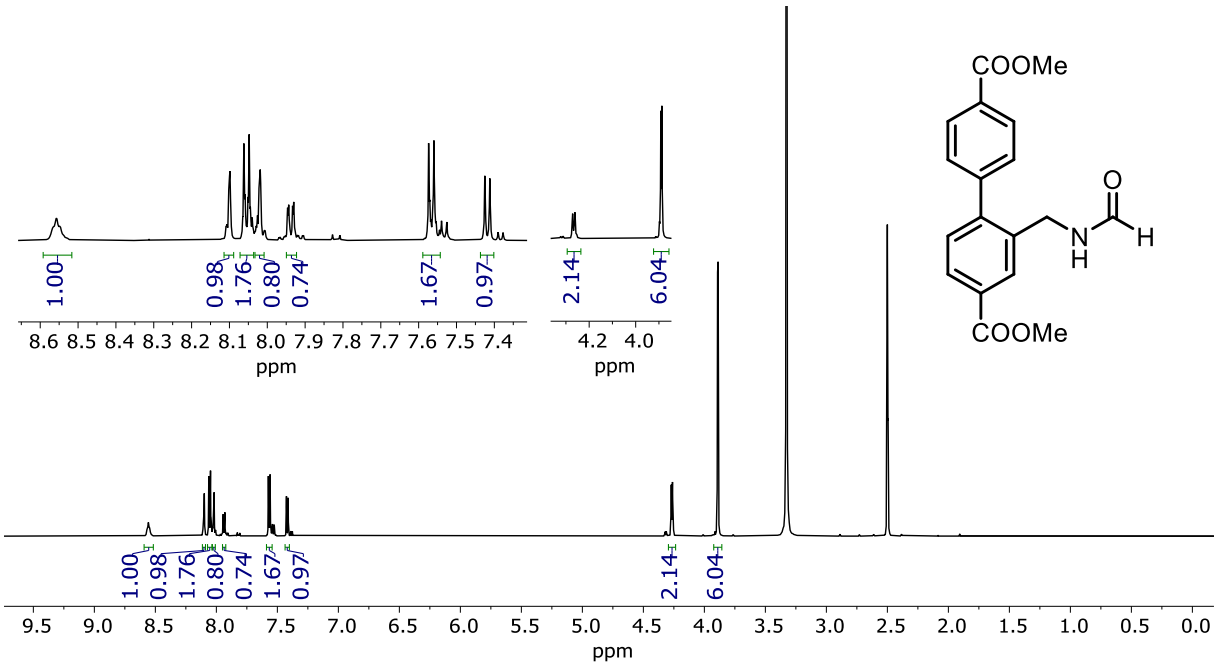

Figure 171: ^{1}H NMR (600 MHz, DMSO-d_6) spectrum of **13**.

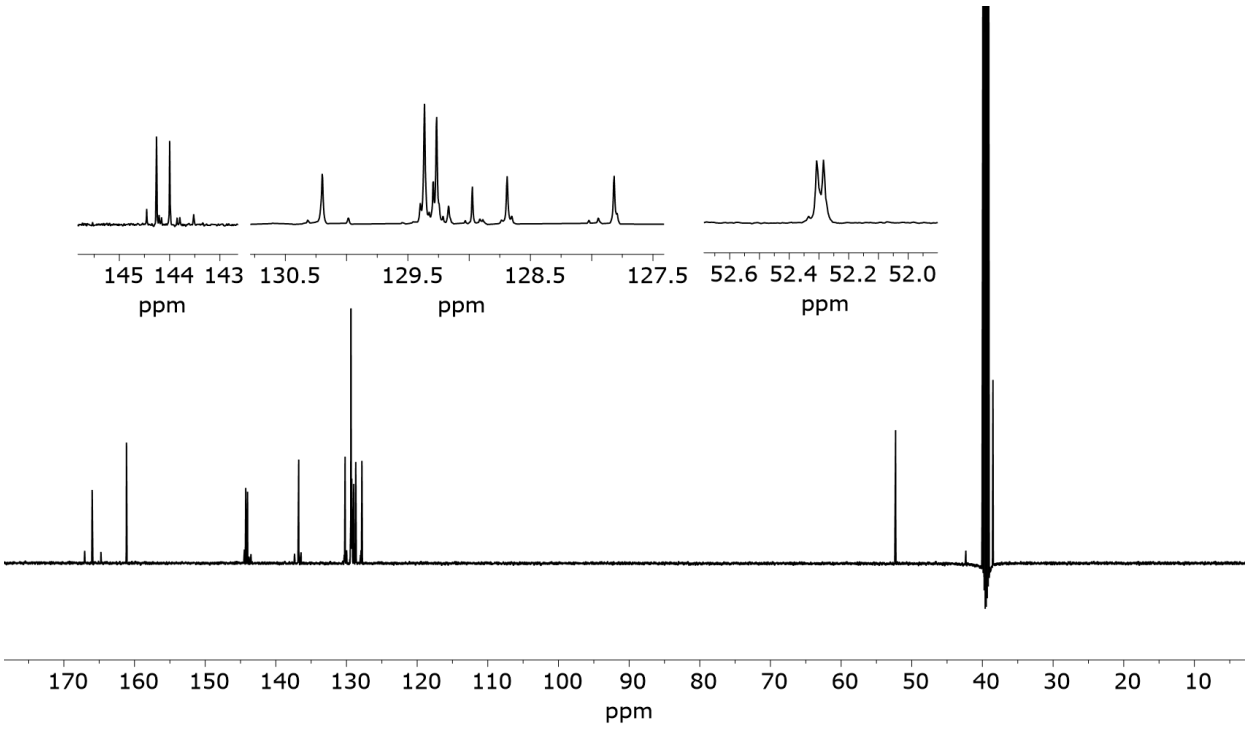

Figure 172: ^{13}C NMR (151 MHz, DMSO-d_6) spectrum of **13**.

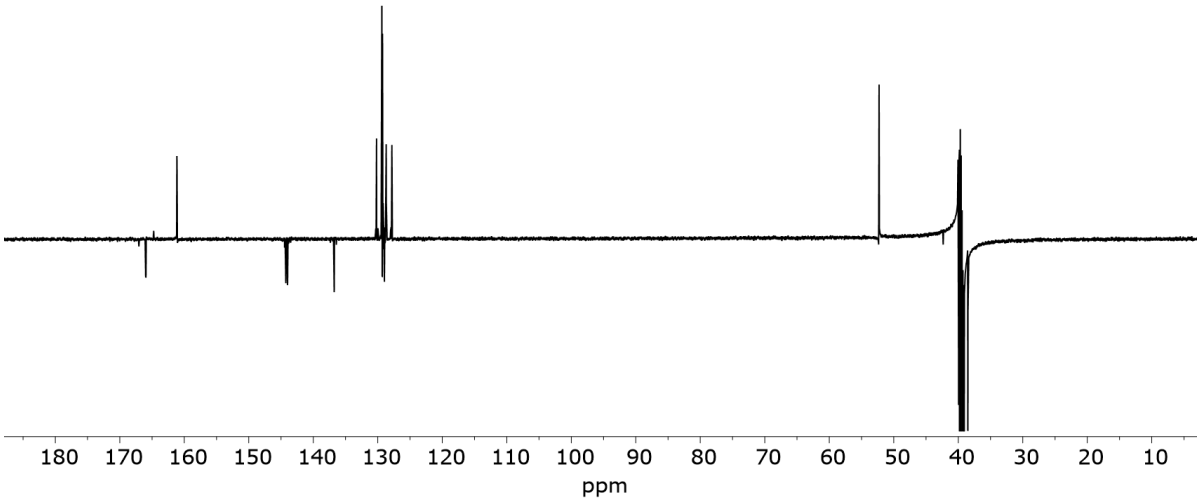

Figure 173: DEPT135Q (151 MHz, DMSO-d_6) spectrum of **13**.

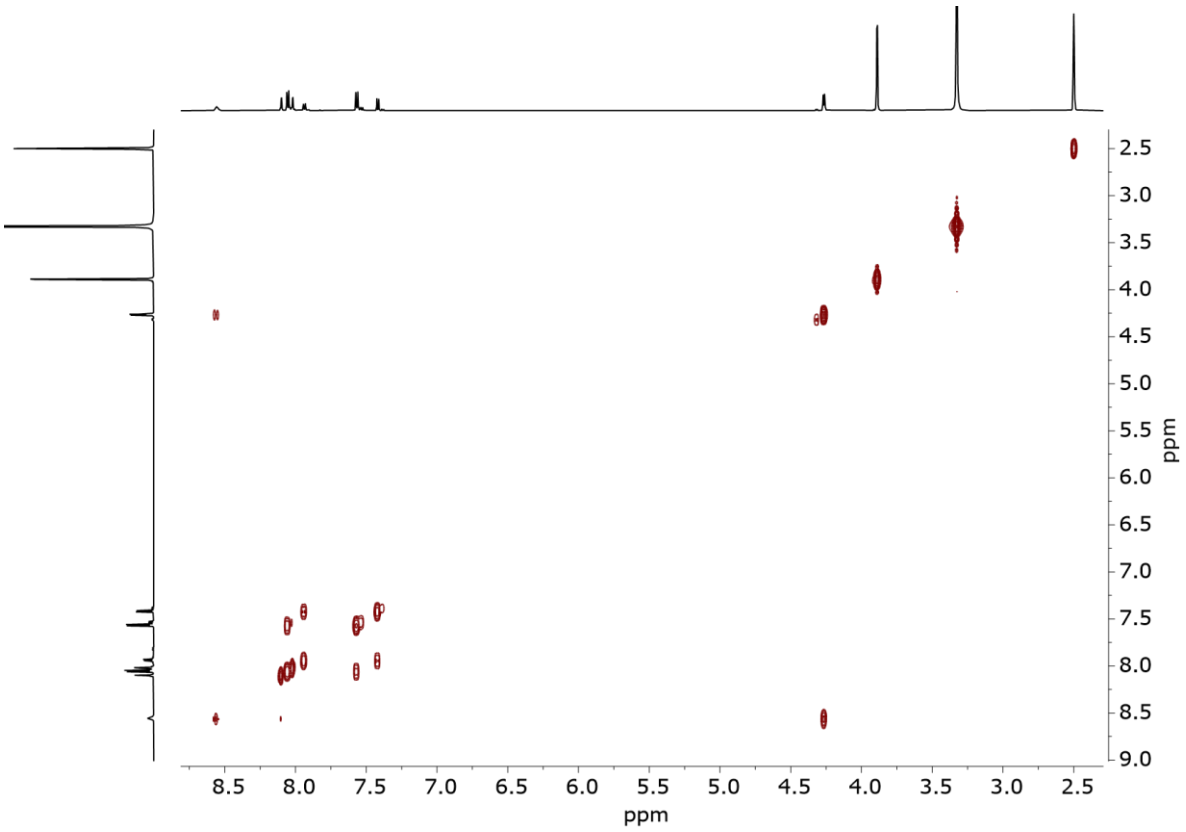

Figure 174: COSY (600 MHz, DMSO-d_6) spectrum of **13**.

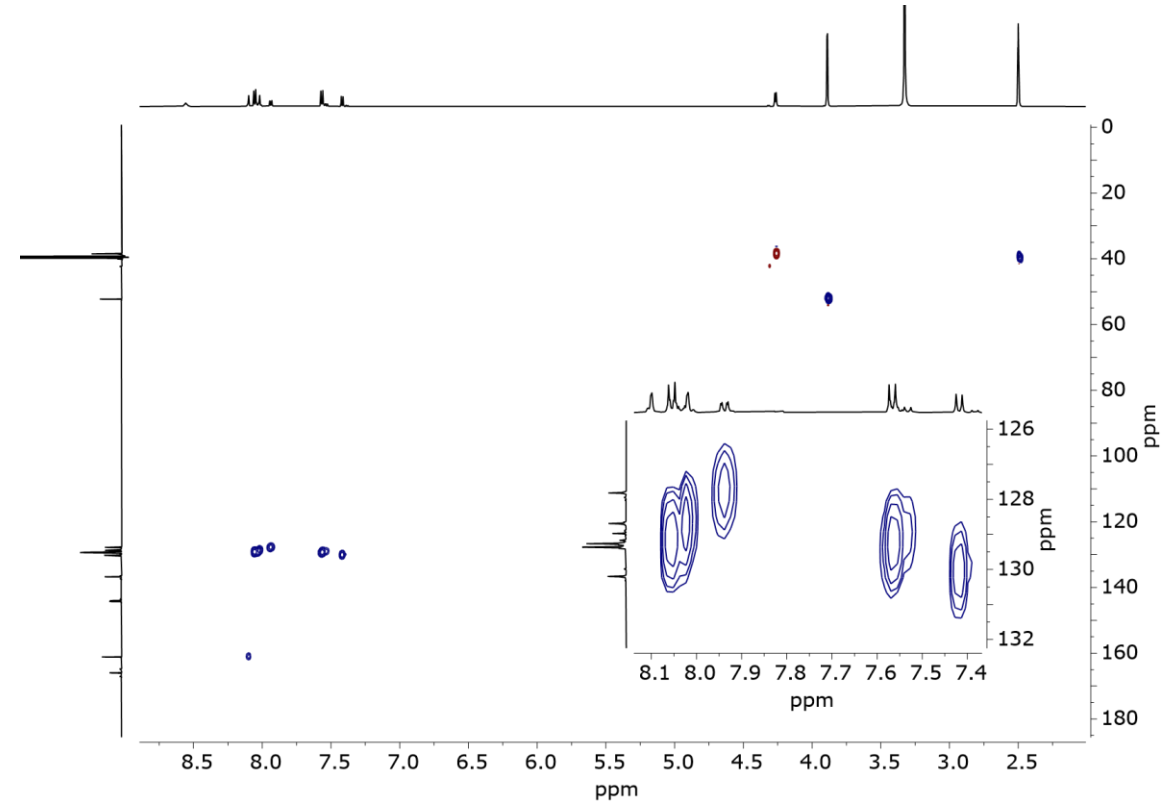

Figure 175: HSQC (600 MHz, DMSO-d_6) spectrum of **13**.

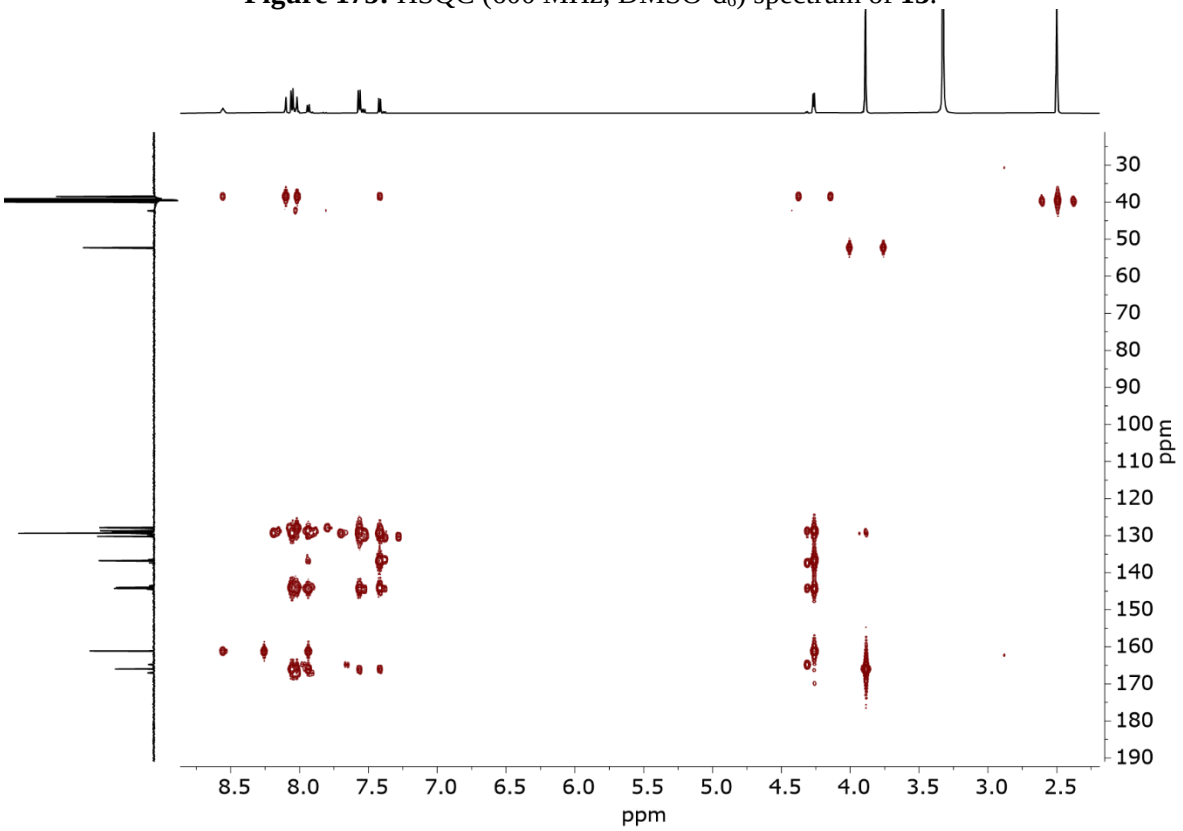

Figure 176: HMBC (600 MHz, DMSO-d6) spectrum of **13**.

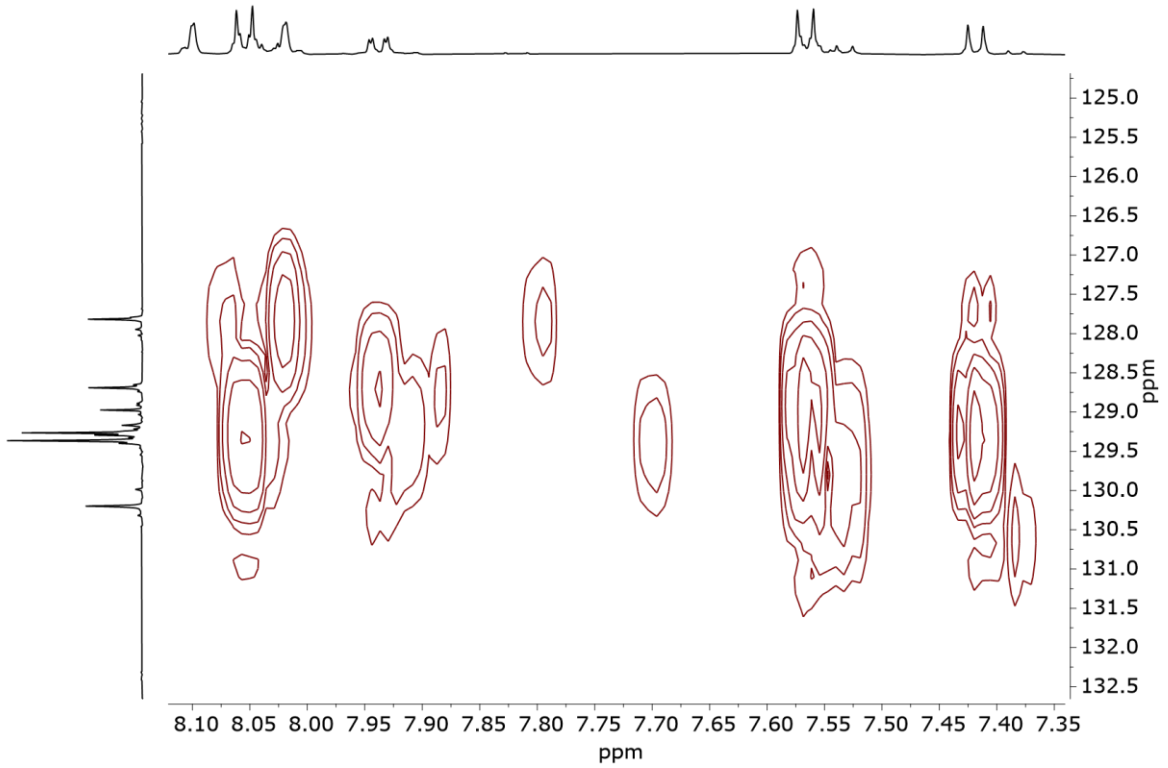

Figure 177: Zoom of HMBC (600 MHz, DMSO-d6) spectrum of **13**.

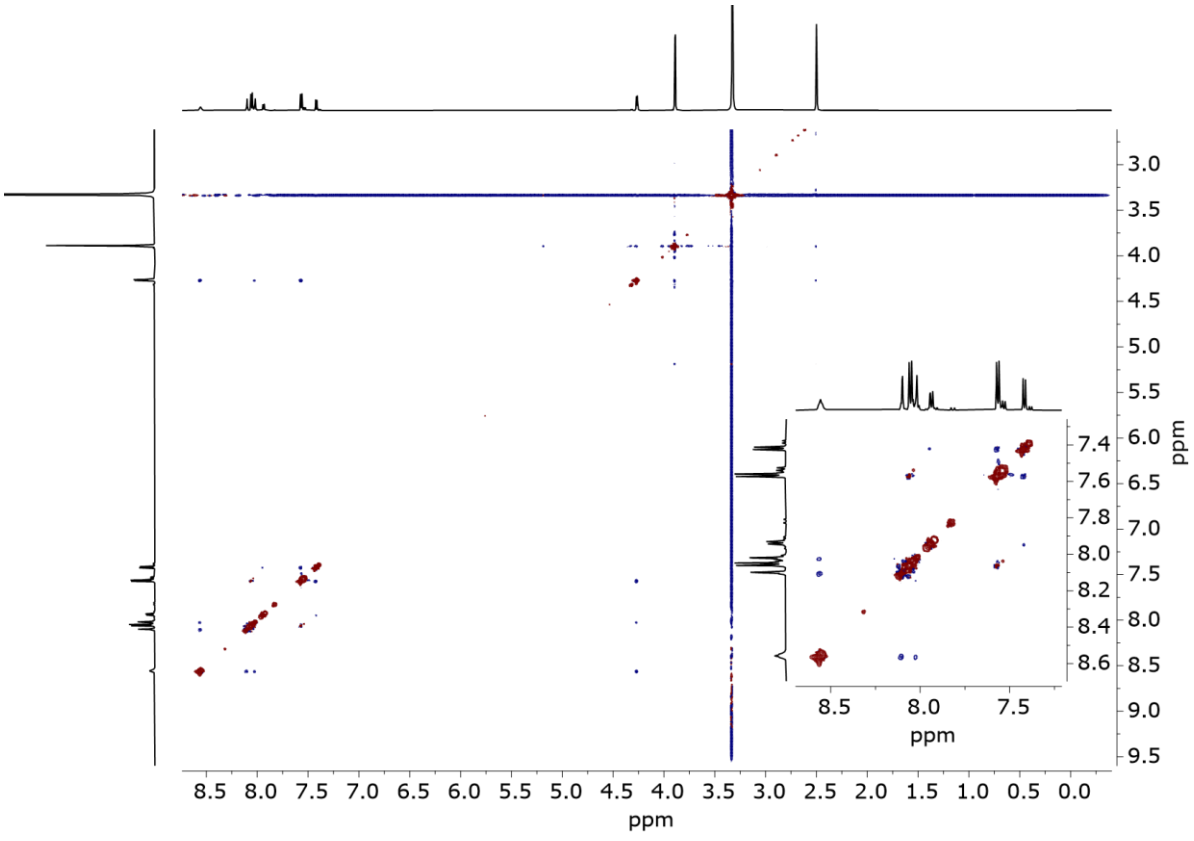

Figure 178: NOESY (600 MHz, DMSO-d6) spectrum of **13**.

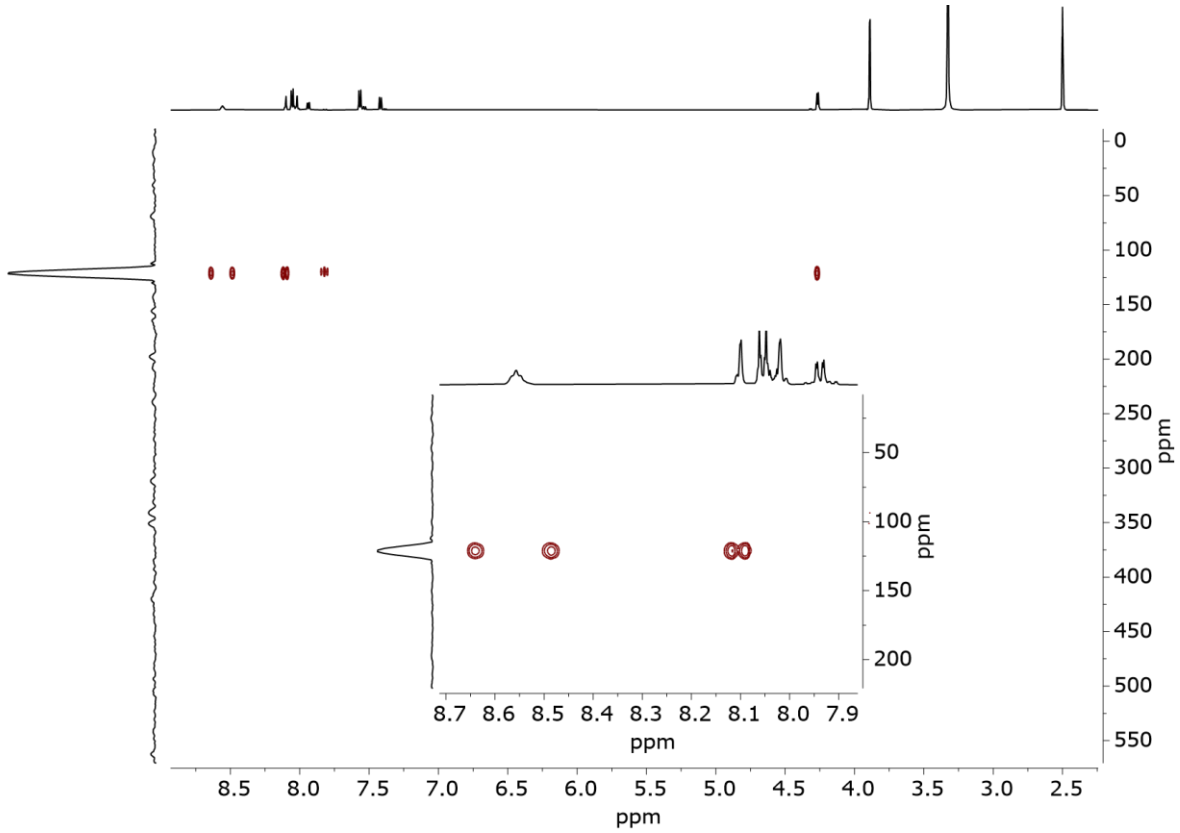

Figure 179: ^{1}H-^{15}N HMBC (600 MHz, DMSO-d_6) spectrum of **13**.

Additional data

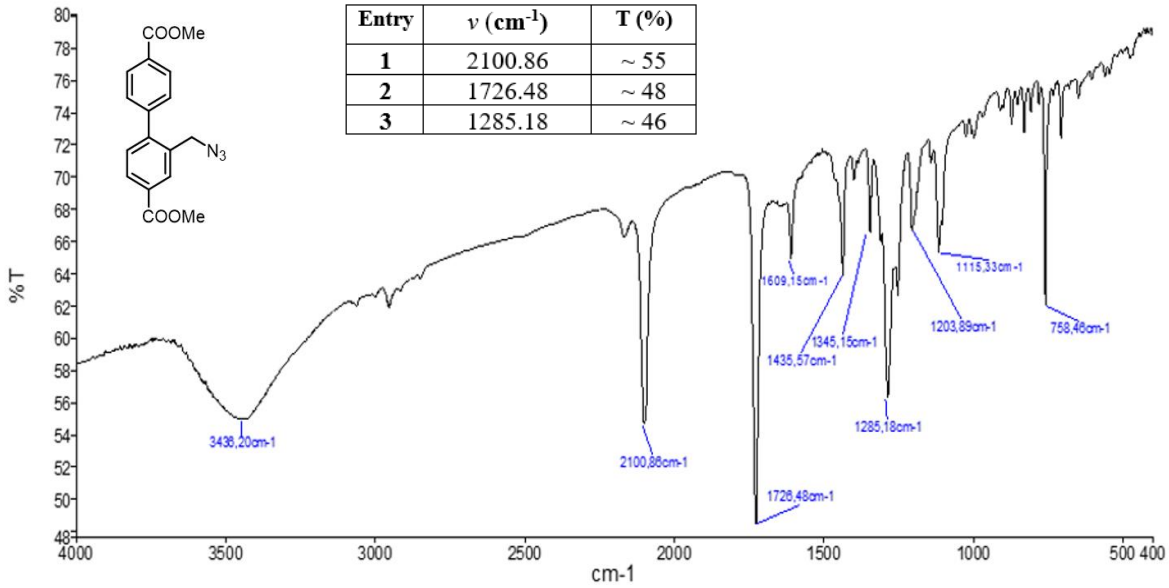

Entry	ν (cm^{-1})	T (%)
1	2100.86	~ 55
2	1726.48	~ 48
3	1285.18	~ 46

Figure 180: IR spectrum of **3a**.

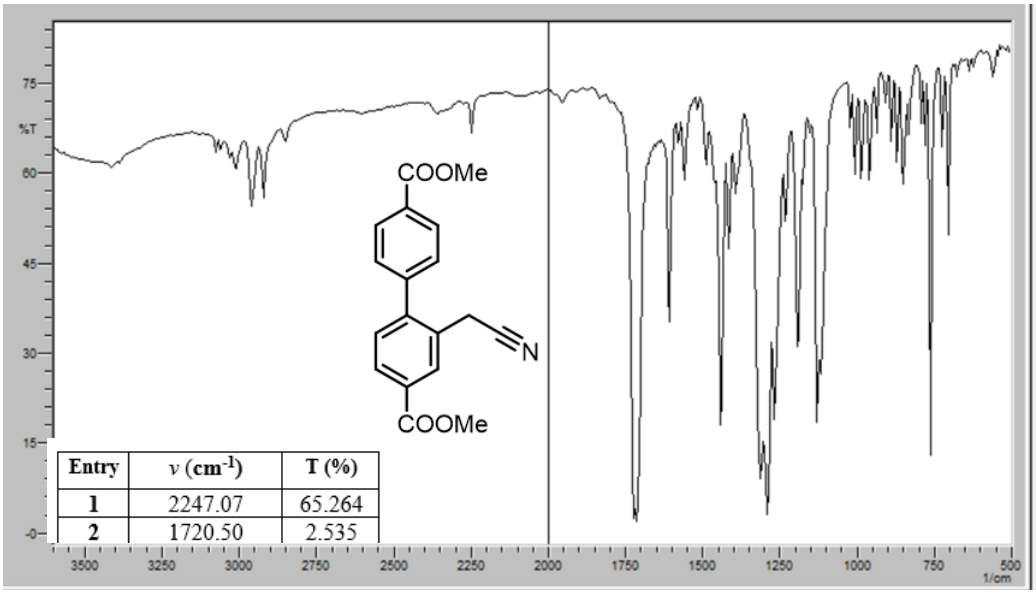

Entry	ν (cm^{-1})	T (%)
1	2247.07	65.264
2	1720.50	2.535

Figure 181: IR spectrum of **7**.

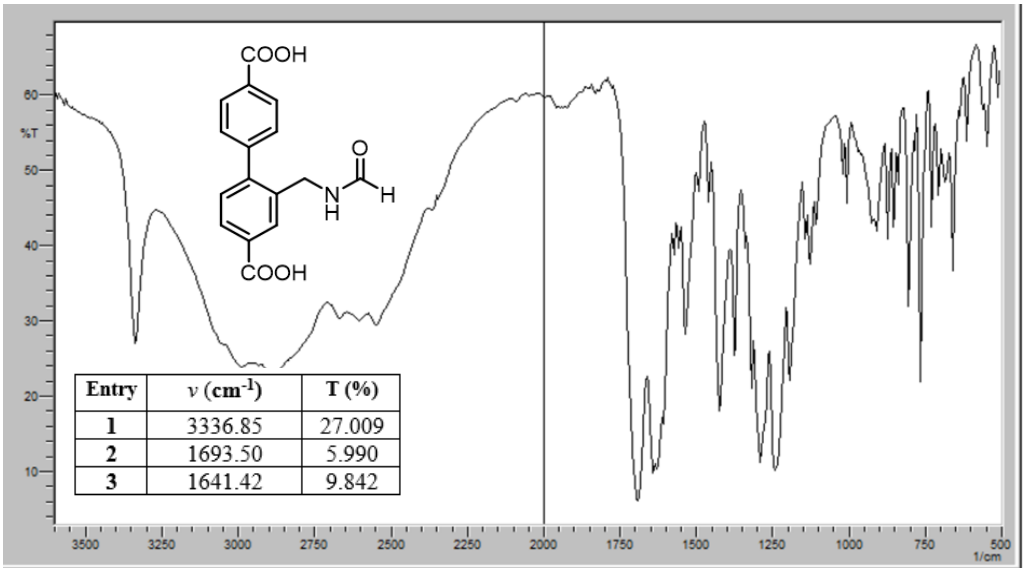

Entry	ν (cm^{-1})	T (%)
1	3336.85	27.009
2	1693.50	5.990
3	1641.42	9.842

Figure 182: IR spectrum of **12**.

Table 7: Crystallographic data for **4b.**

Crystal data	
Identification code	KMF_099D
Empirical formula	$C_{25}H_{19}N_3O_4$
Formula weight	425.43
Temperature/K	298(2)
Crystal system	monoclinic
Space group	$P2_1/c$
a/Å	22.349(5)
b/Å	4.5749(11)
c/Å	20.281(5)
α/°	90
β/°	100.674(7)
γ/°	90
Volume/Å^3	2037.7(8)
Z	4
ρ_{calc}g/cm^3	1.387
μ/mm^{-1}	0.096
F(000)	888.0
Crystal size/mm^3	0.350 × 0.080 × 0.050
Radiation	MoKα (λ = 0.71073)
2Θ range for data collection/°	3.004 to 49.93
Index ranges	$-26 \leq h \leq 26$, $-5 \leq k \leq 5$, $-23 \leq l \leq 23$
Reflections collected	48825
Independent reflections	3549 [R_{int} = 0.1836, R_{sigma} = 0.0892]
Data/restraints/parameters	3549/0/292
Goodness-of-fit on F^2	1.047
Final R indexes [I>=2σ (I)]	R_1 = 0.1041, wR_2 = 0.2950
Final R indexes [all data]	R_1 = 0.1676, wR_2 = 0.3362
Largest diff. peak/hole / e Å^{-3}	0.34/-0.33

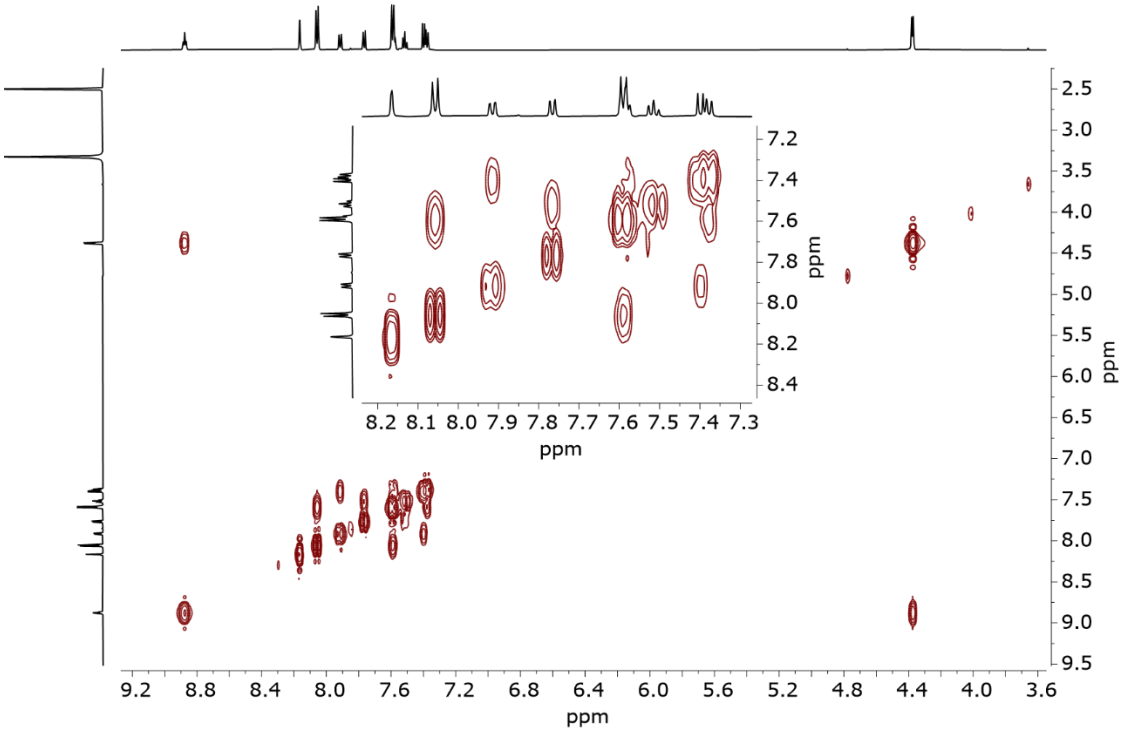

Figure 183: COSY (600 MHz, DMSO-d_6) spectrum of the isolated product from the attempted cleavage of the C-N bonds with LiOH.

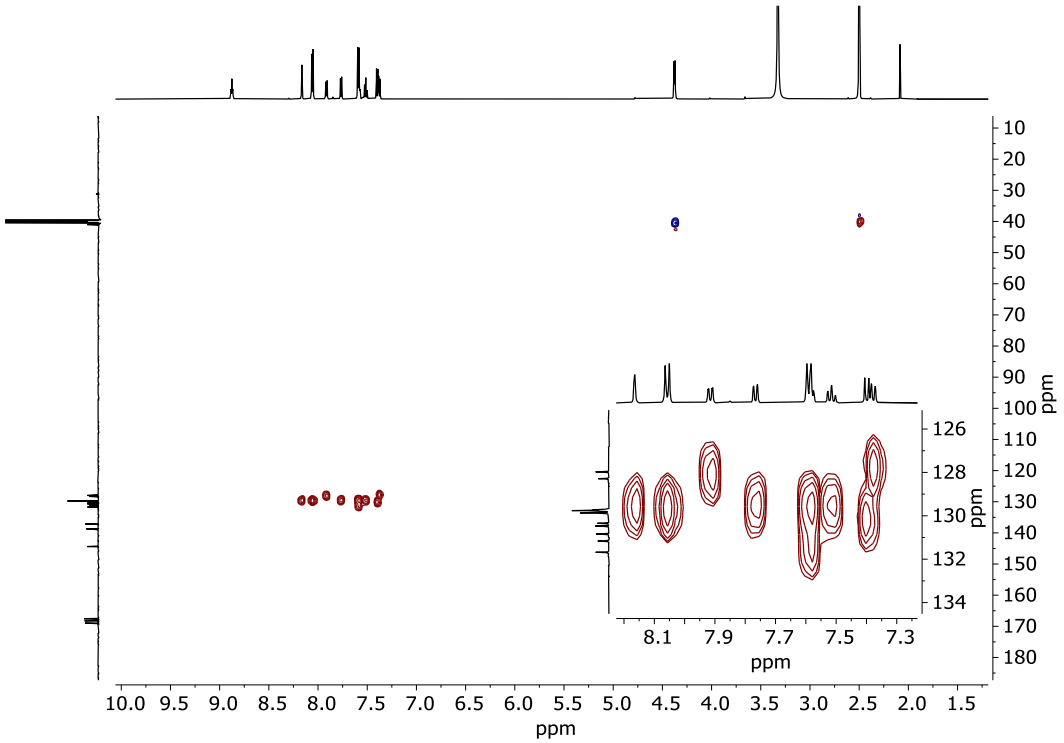

Figure 184: HSQC (600 MHz, DMSO-d_6) spectrum of the isolated product from the attempted cleavage of the C-N bonds with LiOH. The signal at 8.88 ppm (t, 1H) does not show any correlation to any carbon signal. This indicates that the proton might be positioned at a nitrogen atom.

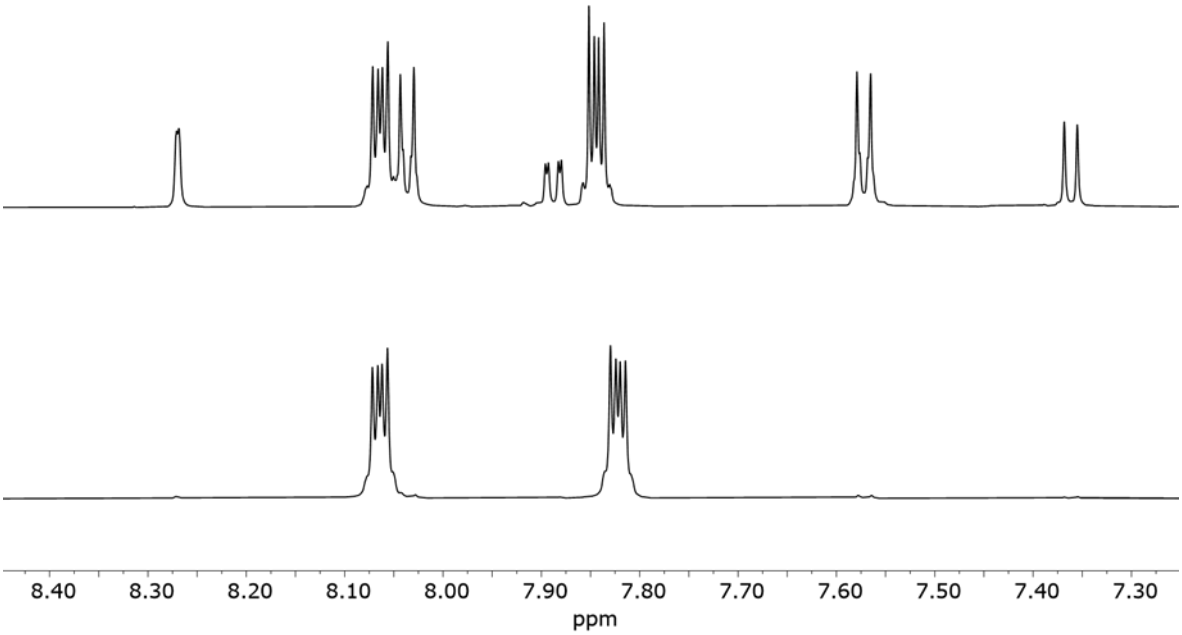

Figure 185: Stacked ^{1}H NMR (DMSO-d_6) spectra of the reaction mixture after two hours of reflux (top) and the precipitated phthalhydrazide.

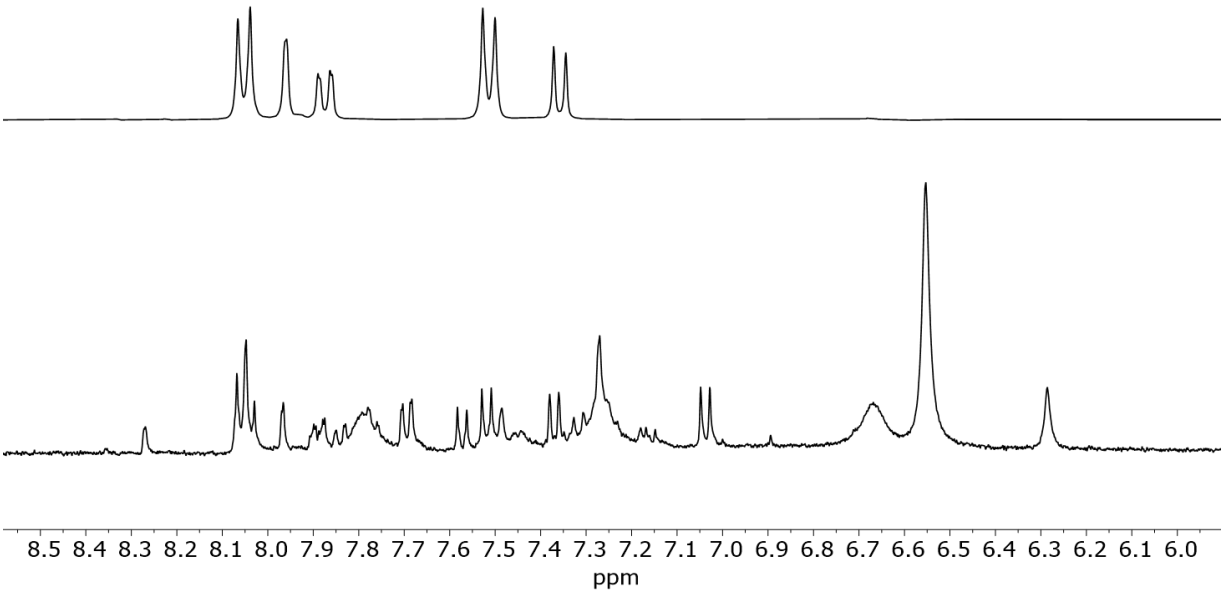

Figure 186: ^{1}H NMR (300 MHz, DMSO-d_6) spectrum of the desired product **8b** (top), and the reaction mixture from the attempted reduction of **11** with $CoCl_2 \cdot 6H_2O$ and $NaBH_4$ in THF/methanol (300 MHz, DMSO-d_6)

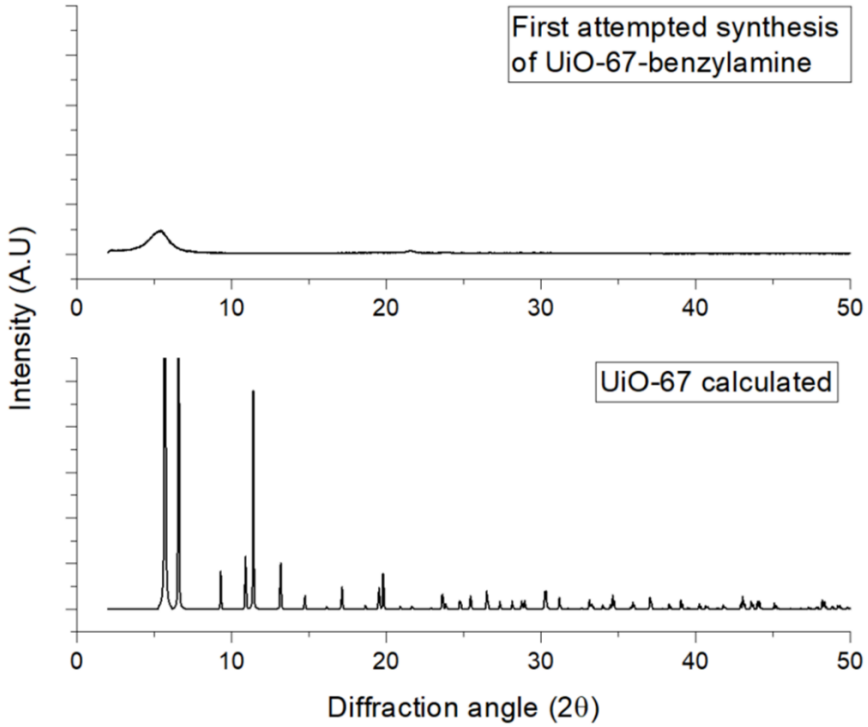

Figure 187: X-ray diffraction pattern of the amorphous material from the first attempt of synthesizing UiO-67-benzylamine (top), and X-ray diffraction pattern of calculated UiO-67 (bottom).

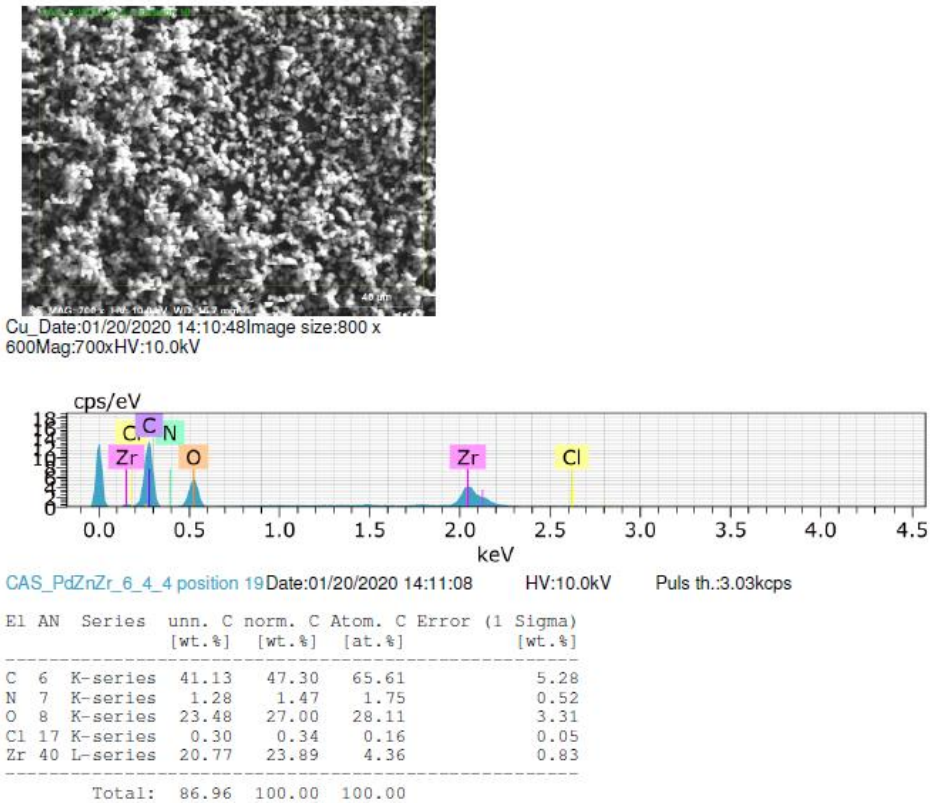

El	AN	Series	unn. C [wt.%]	norm. C [wt.%]	Atom. C [at.%]	Error (1 Sigma) [wt.%]
C	6	K-series	41.13	47.30	65.61	5.28
N	7	K-series	1.28	1.47	1.75	0.52
O	8	K-series	23.48	27.00	28.11	3.31
Cl	17	K-series	0.30	0.34	0.16	0.05
Zr	40	L-series	20.77	23.89	4.36	0.83
		Total:	86.96	100.00	100.00	

Figure 188: EDX analysis of the synthesized UiO-67.

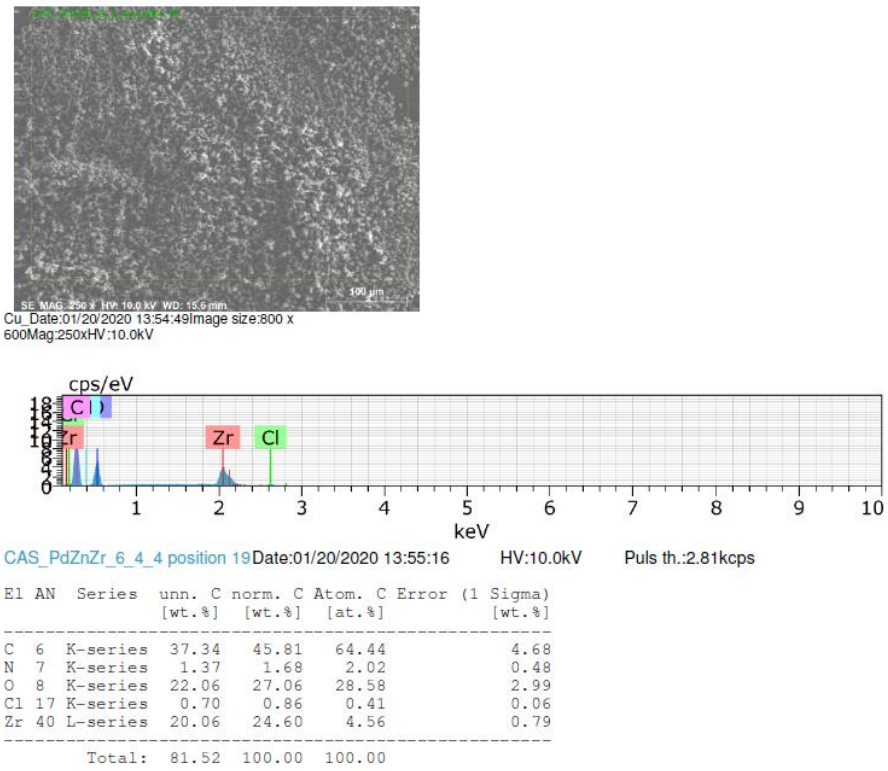

El	AN	Series	unn. C [wt.%]	norm. C [wt.%]	Atom. C [at.%]	Error (1 Sigma) [wt.%]
C	6	K-series	37.34	45.81	64.44	4.68
N	7	K-series	1.37	1.68	2.02	0.48
O	8	K-series	22.06	27.06	28.58	2.99
Cl	17	K-series	0.70	0.86	0.41	0.06
Zr	40	L-series	20.06	24.60	4.56	0.79
		Total:	81.52	100.00	100.00	

Figure 189: EDX analysis of UiO-67-benzylamine.

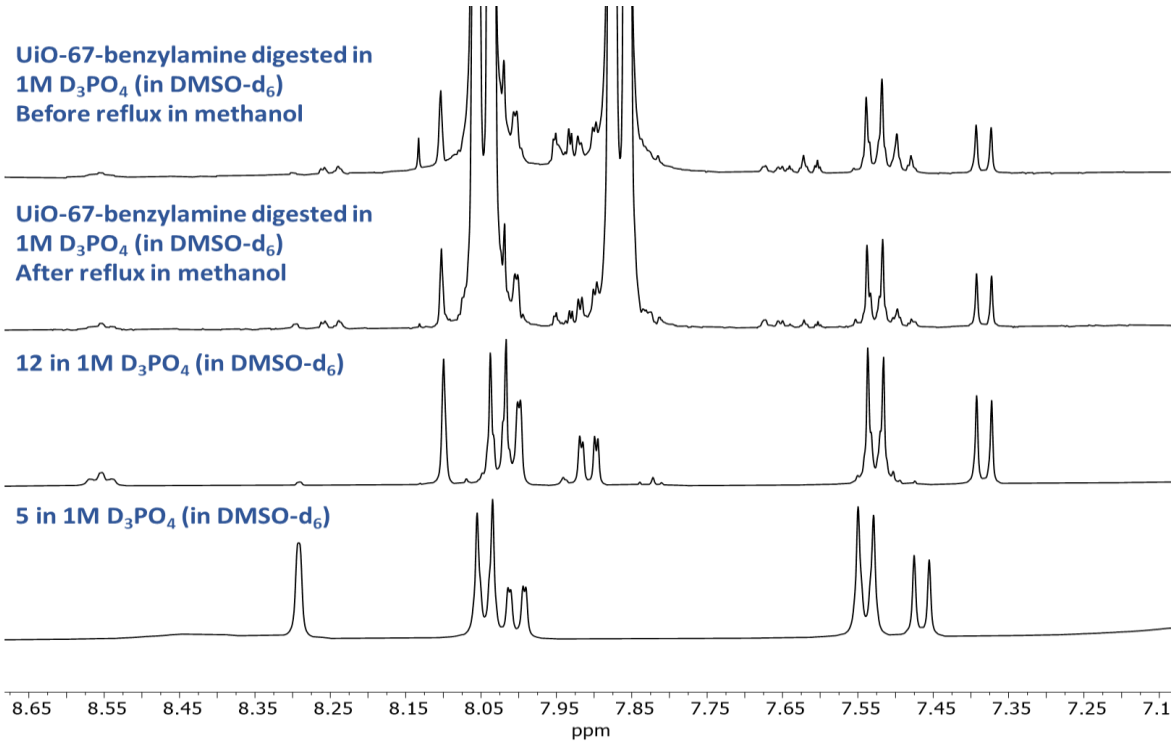

Figure 190: Stacked aromatic regions of ^{1}H NMR (400 MHz, 1M D_3PO_4 in DMSO-d_6) spectra of digested UiO-67-benzylamine before and after reflux in methanol, **12** and **5**.

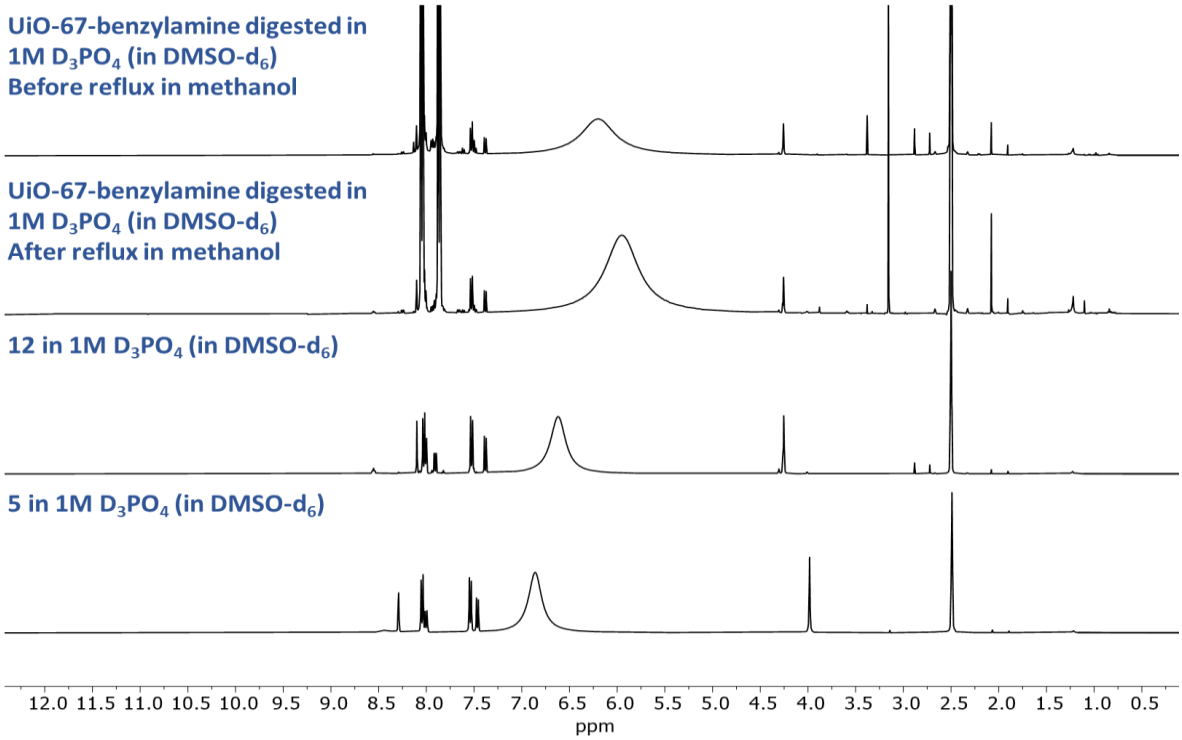

Figure 191: Stacked ^{1}H NMR (400 MHz, 1M D_3PO_4 in DMSO-d_6) spectra of digested UiO-67-benzylamine before and after reflux in methanol, **12** and **5**.

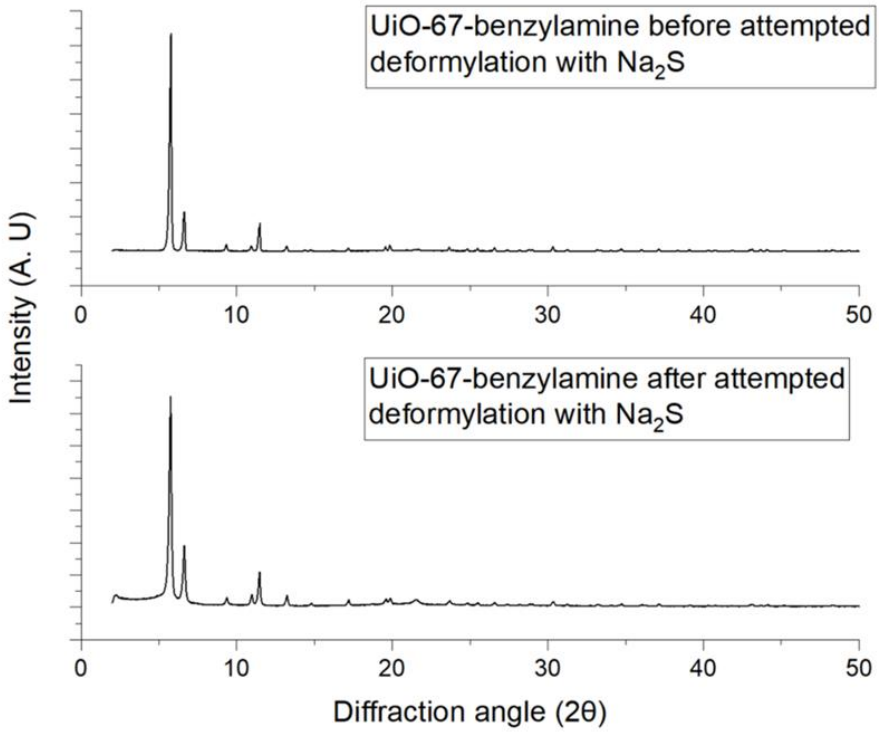

Figure 192: X-ray diffraction pattern of UiO-67-benzylamine before (top) and after (bottom) attempted deformylation of the MOF with sodium sulfide.

Bibliography

1. Cavka, J. H.; Jakobsen, S.; Olsbye, U.; Guillou, N.; Lamberti, C.; Bordiga, S.; Lillerud, K. P., A New Zirconium Inorganic Building Brick Forming Metal Organic Frameworks with Exceptional Stability. *J. Am. Chem. Soc.* **2008,** *130*, 13850-13851.
2. McMurry, J., *Organic Chemistry*. Brooks/Cole Cengage Learning: 2011.
3. Batten, S.; Champness, N.; Chen, X.-M.; García-Martínez, J.; Kitagawa, S.; Öhrström, L.; O Keeffe, M.; Suh, M.; Reedijk, J., Terminology of metal–organic frameworks and coordination polymers (IUPAC Recommendations 2013)*. *Pure Appl. Chem.* **2013,** *85*, 1715-1724.
4. Li, H.; Eddaoudi, M.; O'Keeffe, M.; Yaghi, O. M., Design and synthesis of an exceptionally stable and highly porous metal-organic framework. *Nature* **1999,** *402*, 276-279.
5. Serre, C.; Millange, F.; Surblé, S.; Férey, G., A Route to the Synthesis of Trivalent Transition-Metal Porous Carboxylates with Trimeric Secondary Building Units. *Angew. Chem. Int. Ed.* **2004,** *43*, 6285-6289.
6. MacGillivray, L. R.; Subramanian, S.; Zaworotko, M. J., Interwoven two- and three-dimensional coordination polymers through self-assembly of Cu cations with linear bidentate ligands. *J. Chem. Soc., Chem. Commun.* **1994**, 1325-1326.
7. Kandiah, M.; Nilsen, M. H.; Usseglio, S.; Jakobsen, S.; Olsbye, U.; Tilset, M.; Larabi, C.; Quadrelli, E. A.; Bonino, F.; Lillerud, K. P., Synthesis and Stability of Tagged UiO-66 Zr-MOFs. *Chem. Mater.* **2010,** *22*, 6632-6640.
8. Lu, W.; Wei, Z.; Gu, Z.-Y.; Liu, T.-F.; Park, J.; Park, J.; Tian, J.; Zhang, M.; Zhang, Q.; Gentle Iii, T.; Bosch, M.; Zhou, H.-C., Tuning the structure and function of metal–organic frameworks via linker design. *Chem. Soc. Rev.* **2014,** *43*, 5561-5593.
9. Furukawa, H.; Cordova, K. E.; O'Keeffe, M.; Yaghi, O. M., The Chemistry and Applications of Metal-Organic Frameworks. *Science* **2013,** *341*, 1230444.
10. Park, K. S.; Ni, Z.; Côté, A. P.; Choi, J. Y.; Huang, R.; Uribe-Romo, F. J.; Chae, H. K.; O'Keeffe, M.; Yaghi, O. M., Exceptional chemical and thermal stability of zeolitic imidazolate frameworks. *Proceedings of the National Academy of Sciences of the United States of America* **2006,** *103*, 10186-10191.
11. Huang, X. C.; Lin, Y. Y.; Zhang, J. P.; Chen, X. M., Ligand-directed strategy for zeolite-type metal-organic frameworks: zinc(II) imidazolates with unusual zeolitic topologies. *Angew. Chem. Int. Ed. Engl.* **2006,** *45*, 1557-9.
12. Tsuruoka, T.; Furukawa, S.; Takashima, Y.; Yoshida, K.; Isoda, S.; Kitagawa, S., Nanoporous Nanorods Fabricated by Coordination Modulation and Oriented Attachment Growth. *Angew. Chem. Int. Ed.* **2009,** *48*, 4739-4743.
13. Yaghi, O. M.; Li, H., Hydrothermal Synthesis of a Metal-Organic Framework Containing Large Rectangular Channels. *J. Am. Chem. Soc.* **1995,** *117*, 10401-10402.
14. Kinoshita, Y.; Matsubara, I.; Higuchi, T.; Saito, Y., The Crystal Structure of Bis(adiponitrilo)copper(I) Nitrate. *Bull. Chem. Soc. Jpn.* **1959,** *32*, 1221-1226.
15. Chui, S. S. Y.; Lo, S. M. F.; Charmant, J. P. H.; Orpen, A. G.; Williams, I. D., A Chemically Functionalizable Nanoporous Material [Cu3(TMA)2(H2O)3]n. *Science* **1999,** *283*, 1148.
16. Eddaoudi, M.; Moler, D. B.; Li, H.; Chen, B.; Reineke, T. M.; O'Keeffe, M.; Yaghi, O. M., Modular Chemistry: Secondary Building Units as a Basis for the Design of Highly Porous and Robust Metal−Organic Carboxylate Frameworks. *Acc. Chem. Res.* **2001,** *34*, 319-330.
17. Trotta, F.; Mele, A., *Nanosponges: Synthesis and Applications*. Wiley: 2019.
18. Zaworotko, M. J., Open season for solid frameworks. *Nature* **1999,** *402*, 242-243.

19. Eddaoudi, M.; Kim, J.; Rosi, N.; Vodak, D.; Wachter, J.; O'Keeffe, M.; Yaghi, O. M., Systematic design of pore size and functionality in isoreticular MOFs and their application in methane storage. *Science* **2002,** *295*, 469-72.
20. Kaur, G.; Øien-Ødegaard, S.; Lazzarini, A.; Chavan, S. M.; Bordiga, S.; Lillerud, K. P.; Olsbye, U., Controlling the Synthesis of Metal–Organic Framework UiO-67 by Tuning Its Kinetic Driving Force. *Cryst. Growth Des.* **2019,** *19*, 4246-4251.
21. Øien-Ødegaard, S.; Bouchevreau, B.; Hylland, K.; Wu, L.; Blom, R.; Grande, C.; Olsbye, U.; Tilset, M.; Lillerud, K. P., UiO-67-type Metal–Organic Frameworks with Enhanced Water Stability and Methane Adsorption Capacity. *Inorg. Chem.* **2016,** *55*, 1986-1991.
22. Schaate, A.; Roy, P.; Godt, A.; Lippke, J.; Waltz, F.; Wiebcke, M.; Behrens, P., Modulated Synthesis of Zr-Based Metal–Organic Frameworks: From Nano to Single Crystals. *Chemistry – A European Journal* **2011,** *17*, 6643-6651.
23. Dhakshinamoorthy, A.; Santiago-Portillo, A.; Asiri, A. M.; Garcia, H., Engineering UiO-66 Metal Organic Framework for Heterogeneous Catalysis. *ChemCatChem* **2019,** *11*, 899-923.
24. Introduction to Metal–Organic Frameworks. *Chem. Rev.* **2012,** *112*, 673-674.
25. Kazemi, S.; Safarifard, V., Carbon dioxide capture in MOFs: The effect of ligand functionalization. *Polyhedron* **2018,** *154*, 236-251.
26. Wu, H.; Gong, Q.; Olson, D. H.; Li, J., Commensurate Adsorption of Hydrocarbons and Alcohols in Microporous Metal Organic Frameworks. *Chem. Rev.* **2012,** *112*, 836-868.
27. Tan, K.; Nijem, N.; Canepa, P.; Gong, Q.; Li, J.; Thonhauser, T.; Chabal, Y. J., Stability and Hydrolyzation of Metal Organic Frameworks with Paddle-Wheel SBUs upon Hydration. *Chem. Mater.* **2012,** *24*, 3153-3167.
28. Wang, L.; Zheng, M.; Xie, Z., Nanoscale metal–organic frameworks for drug delivery: a conventional platform with new promise. *Journal of Materials Chemistry B* **2018,** *6*, 707-717.
29. Latifi, L.; Sohrabnezhad, S., Drug delivery by micro and meso metal-organic frameworks. *Polyhedron* **2020,** *180*, 114321.
30. Li, L.; Tang, S.; Wang, C.; Lv, X.; Jiang, M.; Wu, H.; Zhao, X., High gas storage capacities and stepwise adsorption in a UiO type metal-organic framework incorporating Lewis basic bipyridyl sites. *Chem Commun (Camb)* **2014,** *50*, 2304-2307.
31. Grissom, T. G.; Driscoll, D. M.; Troya, D.; Sapienza, N. S.; Usov, P. M.; Morris, A. J.; Morris, J. R., Molecular-Level Insight into CO2 Adsorption on the Zirconium-Based Metal–Organic Framework, UiO-66: A Combined Spectroscopic and Computational Approach. *The Journal of Physical Chemistry C* **2019,** *123*, 13731-13738.
32. Bae, Y.-S.; Snurr, R. Q., Development and Evaluation of Porous Materials for Carbon Dioxide Separation and Capture. *Angew. Chem. Int. Ed.* **2011,** *50*, 11586-11596.
33. Flaig, R. W.; Osborn Popp, T. M.; Fracaroli, A. M.; Kapustin, E. A.; Kalmutzki, M. J.; Altamimi, R. M.; Fathieh, F.; Reimer, J. A.; Yaghi, O. M., The Chemistry of CO2 Capture in an Amine-Functionalized Metal–Organic Framework under Dry and Humid Conditions. *J. Am. Chem. Soc.* **2017,** *139*, 12125-12128.
34. Fu, Q.; Ding, J.; Wang, W.; Lu, J.; Huang, Q., Carbon Dioxide Adsorption over Amine-Functionalized MOFs. *Energy Procedia* **2017,** *142*, 2152-2157.
35. Chavan, S. M.; Shearer, G. C.; Svelle, S.; Olsbye, U.; Bonino, F.; Ethiraj, J.; Lillerud, K. P.; Bordiga, S., Synthesis and Characterization of Amine-Functionalized Mixed-Ligand Metal–Organic Frameworks of UiO-66 Topology. *Inorg. Chem.* **2014,** *53*, 9509-9515.
36. Couck, S.; Denayer, J. F. M.; Baron, G. V.; Rémy, T.; Gascon, J.; Kapteijn, F., An Amine-Functionalized MIL-53 Metal−Organic Framework with Large Separation Power for CO2 and CH4. *J. Am. Chem. Soc.* **2009,** *131*, 6326-6327.
37. Chen, D.-M.; Xu, N.; Qiu, X.-H.; Cheng, P., Functionalization of Metal–Organic Framework via Mixed-Ligand Strategy for Selective CO2 Sorption at Ambient Conditions. *Cryst. Growth Des.* **2015,** *15*, 961-965.

38. Hooshmand, S. E.; Heidari, B.; Sedghi, R.; Varma, R. S., Recent advances in the Suzuki–Miyaura cross-coupling reaction using efficient catalysts in eco-friendly media. *Green Chemistry* **2019,** *21*, 381-405.
39. Taheri Kal Koshvandi, A.; Heravi, M. M.; Momeni, T., Current Applications of Suzuki–Miyaura Coupling Reaction in The Total Synthesis of Natural Products: An update. *Appl. Organomet. Chem.* **2018,** *32*, e4210.
40. Spessard, G. O.; Miessler, G. L., *Organometallic Chemistry*. Oxford University Press: 2016.
41. Clayden, J.; Greeves, N.; Warren, S., *Organic Chemistry*. OUP Oxford: 2012.
42. Hylland, K. T.; Øien-Ødegaard, S.; Tilset, M., The Suzuki–Miyaura Cross-Coupling as the Key Step in the Synthesis of 2-Aminobiphenyls and 2,2'-Diaminobiphenyls: Application in the Synthesis of Schiff Base Complexes of Zn. *Eur. J. Org. Chem.* **2020,** *n/a*.
43. Kurti, L.; Czako, B., *Strategic Applications of Named Reactions in Organic Synthesis*. Elsevier Science: 2005.
44. Magano, J.; Dunetz, J. R., Large-Scale Applications of Transition Metal-Catalyzed Couplings for the Synthesis of Pharmaceuticals. *Chem. Rev.* **2011,** *111*, 2177-2250.
45. Schneider, N.; Lowe, D. M.; Sayle, R. A.; Tarselli, M. A.; Landrum, G. A., Big Data from Pharmaceutical Patents: A Computational Analysis of Medicinal Chemists' Bread and Butter. *J. Med. Chem.* **2016,** *59*, 4385-4402.
46. Li, B.; Seth, K.; Niu, B.; Pan, L.; Yang, H.; Ge, H., Transient-Ligand-Enabled ortho-Arylation of Five-Membered Heterocycles: Facile Access to Mechanochromic Materials. *Angew. Chem. Int. Ed.* **2018,** *57*, 3401-3405.
47. Slyusarchuk, V. D.; Kruger, P. E.; Hawes, C. S., Cyclic Aliphatic Hydrocarbons as Linkers in Metal-Organic Frameworks: New Frontiers for Ligand Design. *ChemPlusChem* **2020,** *85*, 845-854.
48. Rehman, A.; Farrukh, S.; Hussain, A.; Fan, X.; Pervaiz, E., Adsorption of CO2 on amine-functionalized green metal-organic framework: an interaction between amine and CO2 molecules. *Environ. Sci. Pollut. Res.* **2019,** *26*, 36214-36225.
49. Zhang, Z.; Zhao, Y.; Gong, Q.; Li, Z.; Li, J., MOFs for CO2 capture and separation from flue gas mixtures: the effect of multifunctional sites on their adsorption capacity and selectivity. *Chem. Commun.* **2013,** *49*, 653-661.
50. Dmello, M. E.; Sundaram, N. G.; Singh, A.; Singh, A. K.; Kalidindi, S. B., An amine functionalized zirconium metal–organic framework as an effective chemiresistive sensor for acidic gases. *Chem. Commun.* **2019,** *55*, 349-352.
51. Levchenko, V.; Glessi, C.; Øien-Ødegaard, S.; Tilset, M., Organometallic chemistry in aqua regia: metal and ligand based oxidations of (NHC)AuCl complexes. *Dalton Trans.* **2020,** *49*, 3473-3479.
52. Hu, Y.-H.; Wang, J.-C.; Yang, S.; Li, Y.-A.; Dong, Y.-B., CuI@UiO-67-IM: A MOF-Based Bifunctional Composite Triphase-Transfer Catalyst for Sequential One-Pot Azide–Alkyne Cycloaddition in Water. *Inorg. Chem.* **2017,** *56*, 8341-8347.
53. Schumacher, W. T.; Mathews, M. J.; Larson, S. A.; Lemmon, C. E.; Campbell, K. A.; Crabb, B. T.; Chicoine, B. J. A.; Beauvais, L. G.; Perry, M. C., Organocatalysis by site-isolated N-heterocyclic carbenes doped into the UIO-67 framework. *Polyhedron* **2016,** *114*, 422-427.
54. Ding, L.-G.; Yao, B.-J.; Jiang, W.-L.; Li, J.-T.; Fu, Q.-J.; Li, Y.-A.; Liu, Z.-H.; Ma, J.-P.; Dong, Y.-B., Bifunctional Imidazolium-Based Ionic Liquid Decorated UiO-67 Type MOF for Selective CO2 Adsorption and Catalytic Property for CO2 Cycloaddition with Epoxides. *Inorg. Chem.* **2017,** *56*, 2337-2344.
55. Clark, H. C.; Goel, A. B.; Goel, R. G.; Goel, S.; Ogini, W. O., Solvent effects on the metalation of Tri,-tert-butylphosphine.Preparation and characterization of [PtPBut2C(CH3)2CH2Cl]2 and [PdPBut2C(CH3)2)CH2Cl]2. *Inorg. Chim. Acta* **1978,** *31*, L441-L442.
56. Clawson, G. A., Mechanisms of carbon tetrachloride hepatotoxicity. *Pathol Immunopathol Res* **1989,** *8*, 104-112.
57. Manibusan, M. K.; Odin, M.; Eastmond, D. A., Postulated Carbon Tetrachloride Mode of Action: A Review. *Journal of Environmental Science and Health, Part C* **2007,** *25*, 185-209.

58. Smith, M. B.; March, J., *March's Advanced Organic Chemistry: Reactions, Mechanisms, and Structure*. Wiley: 2007.
59. Babu, J.; Ganesan, S.; Kumar, K. A.; Karuppusamy, M.; Pandurangan, A.; Rajakumar, P., Cyclohexadienone core 3,6-di-tert-butylcarbazole decorated triazole bridged dendrimers: synthesis, photophysical and electrochemical properties and application as an additive in dye-sensitized solar cells. *New J. Chem.* **2019,** *43*, 4036-4048.
60. Ke, Y.; Wang, W.; Zhao, L.-F.; Liang, J.-J.; Liu, Y.; Zhang, X.; Feng, K.; Liu, H.-M., Design, synthesis and biological mechanisms research on 1,2,3-triazole derivatives of Jiyuan Oridonin A. *Biorg. Med. Chem.* **2018,** *26*, 4761-4773.
61. Lenstra, D. C.; Wolf, J. J.; Mecinović, J., Catalytic Staudinger Reduction at Room Temperature. *J. Org. Chem.* **2019,** *84*, 6536-6545.
62. Loughlin, W. A.; Jenkins, I. D.; Karis, N. D.; Healy, P. C., Discovery of new nanomolar inhibitors of GPa: Extension of 2-oxo-1,2-dihydropyridinyl-3-yl amide-based GPa inhibitors. *Eur. J. Med. Chem.* **2017,** *127*, 341-356.
63. Swetha, M.; Ramana, P. V.; Shirodkar, S. G., Simple and Efficient Method for the Synthesis of Azides in Water-THF Solvent System. *Org. Prep. Proced. Int.* **2011,** *43*, 348-353.
64. Tseng, M.-C.; Chu, Y.-H., Reaction-Based Azide Gas Sensing with Tailored Ionic Liquids Measured by Quartz Crystal Microbalance. *Anal. Chem.* **2014,** *86*, 1949-1952.
65. Zanato, C.; Cascio, M. G.; Lazzari, P.; Pertwee, R.; Testa, A.; Zanda, M., ChemInform Abstract: Tricyclic Fused Pyrazoles with a 'Click' 1,2,3-Triazole Substituent in Position 3 are Nanomolar CB1 Receptor Ligands. *ChemInform* **2015,** *46*.
66. Sander, K.; Kottke, T.; Tanrikulu, Y.; Proschak, E.; Weizel, L.; Schneider, E. H.; Seifert, R.; Schneider, G.; Stark, H., 2,4-Diaminopyrimidines as histamine H4 receptor ligands—Scaffold optimization and pharmacological characterization. *Biorg. Med. Chem.* **2009,** *17*, 7186-7196.
67. Dobrovolný, K.; Ulbrich, P.; Švecová, M.; Rimpelová, S.; Malinčík, J.; Kohout, M.; Svoboda, J.; Bartůněk, V., Copper nanoparticles in glycerol-polyvinyl alcohol matrix: In situ preparation, stabilisation and antimicrobial activity. *J. Alloys Compd.* **2017,** *697*, 147-155.
68. Lieber, E.; Rao, C. N. R.; Thomas, A. E.; Oftedahl, E.; Minnis, R.; Nambury, C. V. N., Infrared spectra of acid azides, carbamyl azides and other azido derivatives: Anomalous splittings of the N3 stretching bands. *Spectrochim. Acta* **1963,** *19*, 1135-1144.
69. Pramanik, S.; Ghorai, P., Chemoselective three-component synthesis of homoallylic azides using an FeCl3 catalyst. *RSC Advances* **2013,** *3*, 23157-23165.
70. Li, W.-Y.; Wang, Q.-Q.; Yang, L., Fe-Catalyzed radical-type difunctionalization of styrenes with aliphatic aldehydes and trimethylsilyl azide via a decarbonylative alkylation–azidation cascade. *Organic & Biomolecular Chemistry* **2017,** *15*, 9987-9991.
71. Pal, B.; Jaisankar, P.; Giri, V. S., Versatile Reagent for Reduction of Azides to Amines. *Synth. Commun.* **2004,** *34*, 1317-1323.
72. Lin, W.; Zhang, X.; He, Z.; Jin, Y.; Gong, L.; Mi, A., Reduction of azides to amines or amides with zinc and ammonium chloride as reducing agent. *Synth. Commun.* **2002,** *32*, 3279-3284.
73. Allport, N. L., A new method for detecting decomposition products in anaesthetic chloroform. *Analyst* **1931,** *56*, 706-710.
74. Peerlings, H. W. I.; Meijer, E. W., A mild and convenient method for the preparation of multi-isocyanates starting from primary amines. *Tetrahedron Lett.* **1999,** *40*, 1021-1024.
75. Gibson, M. S.; Bradshaw, R. W., The Gabriel Synthesis of Primary Amines. *Angewandte Chemie International Edition in English* **1968,** *7*, 919-930.
76. Ing, H. R.; Manske, R. H. F., CCCXII.—A modification of the Gabriel synthesis of amines. *Journal of the Chemical Society (Resumed)* **1926,** *129*, 2348-2351.
77. Yuan, Y.-C.; Kamaraj, R.; Bruneau, C.; Labasque, T.; Roisnel, T.; Gramage-Doria, R., Unmasking Amides: Ruthenium-Catalyzed Protodecarbonylation of N-Substituted Phthalimide Derivatives. *Org. Lett.* **2017,** *19*, 6404-6407.
78. Janiak, C., A critical account on π–π stacking in metal complexes with aromatic nitrogen-containing ligands. *J. Chem. Soc., Dalton Trans.* **2000**, 3885-3896.

79. Pavia, D.; Lampman, G.; Kriz, G.; Vyvyan, J., *Introduction to spectroscopy/ Donald L. Pavia, Gary M. Lampman, George S. Kriz, and James R. Vyvyan*. 2015.
80. Barnes, R. A.; Godfrey, J. C., Syntheses of N-Substituted Isoindolines. I. Derivatives of Phthalimide. *J. Org. Chem.* **1957,** *22*, 1038-1043.
81. Hylland, K. T.; Øien-Ødegaard, S.; Lillerud, K. P.; Tilset, M., Efficient, Scalable Syntheses of Linker Molecules for Metal-Organic Frameworks. *Synlett* **2015,** *26*, 1480-1485.
82. Li, C.-J.; Trost, B. M., Green chemistry for chemical synthesis. *Proceedings of the National Academy of Sciences* **2008,** *105*, 13197.
83. Tanimoto, H.; Kakiuchi, K., Recent Applications and Developments of Organic Azides in Total Synthesis of Natural Products. *Natural Product Communications* **2013,** *8*, 1934578X1300800730.
84. Winterton, S. E.; Capota, E.; Wang, X.; Chen, H.; Mallipeddi, P. L.; Williams, N. S.; Posner, B. A.; Nijhawan, D.; Ready, J. M., Discovery of Cytochrome P450 4F11 Activated Inhibitors of Stearoyl Coenzyme A Desaturase. *J. Med. Chem.* **2018,** *61*, 5199-5221.
85. Zhang, W.; Zhao, Q.; Liu, T.; Gao, Y.; Li, Y.; Zhang, G.; Zhang, F.; Fan, X., Phosphotungstic Acid Immobilized on Amine-Grafted Graphene Oxide as Acid/Base Bifunctional Catalyst for One-Pot Tandem Reaction. *Ind. Eng. Chem. Res.* **2014,** *53*, 1437-1441.
86. Rani, D.; Bhargava, M.; Agarwal, J., Asymmetric Michael Addition of Unactivated Ketones with β-Nitrostyrenes Mediated by Bifunctional L-Prolinamide Organocatalysts. *ChemistrySelect* **2020,** *5*, 2435-2440.
87. Padilha, G.; Iglesias, B. A.; Back, D. F.; Kaufman, T. S.; Silveira, C. C., Synthesis of Chromeno[4,3-b]pyrrol-4(1H)-ones, from β-Nitroalkenes and 4-Phenylaminocoumarins, under Solvent–free Conditions. *ChemistrySelect* **2017,** *2*, 1297-1304.
88. Nugent, T. C.; Hussein, H. A. E. D.; Ahmed, S.; Najafian, F. T.; Hussain, I.; Georgiev, T.; Aljoumhawy, M. K., Carboxylate Salt Bridge-Mediated Enamine Catalysis: Expanded Michael Reaction Substrate Scope and Facile Access to Antidepressant (R)-Pristiq. *Adv. Synth. Catal.* **2017,** *359*, 2824-2831.
89. Fujino, S.; Yamaji, M.; Okamoto, H.; Mutai, T.; Yoshikawa, I.; Houjou, H.; Tani, F., Systematic investigations on fused π-system compounds of seven benzene rings prepared by photocyclization of diphenanthrylethenes. *Photochem. Photobiol. Sci.* **2017,** *16*, 925-934.
90. Bolli, M. H.; Abele, S.; Birker, M.; Bravo, R.; Bur, D.; de Kanter, R.; Kohl, C.; Grimont, J.; Hess, P.; Lescop, C.; Mathys, B.; Müller, C.; Nayler, O.; Rey, M.; Scherz, M.; Schmidt, G.; Seifert, J.; Steiner, B.; Velker, J.; Weller, T., Novel S1P1 Receptor Agonists − Part 3: From Thiophenes to Pyridines. *J. Med. Chem.* **2014,** *57*, 110-130.
91. Wood, J. H.; Tung, C. C.; Perry, M. A.; Gibson, R. E., The Sommelet Reaction in the Synthesis of Aromatic Dialdehydes1. *J. Am. Chem. Soc.* **1950,** *72*, 2992-2993.
92. Kornblum, N.; Jones, W. J.; Anderson, G. J., A NEW AND SELECTIVE METHOD OF OXIDATION. THE CONVERSION OF ALKYL HALIDES AND ALKYL TOSYLATES TO ALDEHYDES. *J. Am. Chem. Soc.* **1959,** *81*, 4113-4114.
93. Bratulescu, G., Synthesis of Aromatic Aldehydes by a Fast Method Involving Kornblum's Reaction. *Synth. Commun.* **2008,** *38*, 2748-2752.
94. Xu, G.; Wu, J. P.; Ai, X. M.; Yang, L. R., Microwave-assisted Kornblum oxidation of organic halides. *Chin. Chem. Lett.* **2007,** *18*, 643-646.
95. Bach, R. D.; Su, M.-D.; Schlegel, H. B., Oxidation of Amines and Sulfides with Hydrogen Peroxide and Alkyl Hydrogen Peroxide. The Nature of the Oxygen-Transfer Step. *J. Am. Chem. Soc.* **1994,** *116*, 5379-5391.
96. Tang, J.; Zhu, J.; Shen, Z.; Zhang, Y., Efficient and convenient oxidation of organic halides to carbonyl compounds by H2O2 in ethanol. *Tetrahedron Lett.* **2007,** *48*, 1919-1921.
97. Goswami, S.; Jana, S.; Dey, S.; Adak, A. K., A Simple and Convenient Manganese Dioxide Oxidation of Benzyl Halides to Aromatic Aldehydes under Neutral Condition. *Chem. Lett.* **2005,** *34*, 194-195.
98. Chen, D. X.; Ho, C. M.; Rudy Wu, Q. Y.; Wu, P. R.; Wong, F. M.; Wu, W., Convenient oxidation of benzylic and allylic halides to aldehydes and ketones. *Tetrahedron Lett.* **2008,** *49*, 4147-4148.

99. Letort, S.; Lejeune, M.; Kardos, N.; Métay, E.; Popowycz, F.; Lemaire, M.; Draye, M., New insights into the catalytic reduction of aliphatic nitro compounds with hypophosphites under ultrasonic irradiation. *Green Chemistry* **2017,** *19*, 4583-4590.
100. Xi, F.-G.; Liu, H.; Yang, N.-N.; Gao, E.-Q., Aldehyde-Tagged Zirconium Metal–Organic Frameworks: a Versatile Platform for Postsynthetic Modification. *Inorg. Chem.* **2016,** *55*, 4701-4703.
101. Liu, X.-H.; Park, H.; Hu, J.-H.; Hu, Y.; Zhang, Q.-L.; Wang, B.-L.; Sun, B.; Yeung, K.-S.; Zhang, F.-L.; Yu, J.-Q., Diverse ortho-C(sp2)–H Functionalization of Benzaldehydes Using Transient Directing Groups. *J. Am. Chem. Soc.* **2017,** *139*, 888-896.
102. Liu, C.; Luo, T.-Y.; Feura, E. S.; Zhang, C.; Rosi, N. L., Orthogonal Ternary Functionalization of a Mesoporous Metal–Organic Framework via Sequential Postsynthetic Ligand Exchange. *J. Am. Chem. Soc.* **2015,** *137*, 10508-10511.
103. abcr Webshop. https://www.abcr.de/shop/en/catalogsearch/advanced/result/?q=4-bromo-3-formylbenzoate (accessed 18.06.20).
104. Chen, H.; Han, X.; Qin, N.; Wei, L.; Yang, Y.; Rao, L.; Chi, B.; Feng, L.; Ren, Y.; Wan, J., Synthesis and biological evaluation of novel inhibitors against 1,3,8-trihydroxynaphthalene reductase from Magnaporthe grisea. *Biorg. Med. Chem.* **2016,** *24*, 1225-1230.
105. Satoh, T.; Suzuki, S.; Suzuki, Y.; Miyaji, Y.; Imai, Z., Reduction of organic compounds with sodium borohydride-transition metal salt systems: Reduction of organic nitrile, nitro and amide compounds to primary amines. *Tetrahedron Lett.* **1969,** *10*, 4555-4558.
106. Moore, G.; McMaster, D., REMOVAL OF PROTECTED PEPTIDES FROM THE MERRIFIELD RESIN BY POTASSIUM CYANIDE CATALYZED TRANSESTERIFICATION. *Int. J. Pept. Protein Res.* **1978,** *11*, 140-148.
107. Zwoliński, K. M.; Nowak, P.; Chmielewski, M. J., Towards multifunctional MOFs – transforming a side reaction into a post-synthetic protection/deprotection method. *Chem. Commun.* **2015,** *51*, 10030-10033.
108. Li, C.; Wang, M.; Lu, X.; Zhang, L.; Jiang, J.; Zhang, L., Reusable Brønsted Acidic Ionic Liquid Efficiently Catalyzed N-Formylation and N-Acylation of Amines. *ACS Sustain. Chem. Eng.* **2020,** *8*, 4353-4361.
109. Ma, J.; Zhang, J.; Zhou, X.; Wang, J.; Gong, H., N-formylation of amine using graphene oxide as a sole recyclable metal-free carbocatalyst. *J. Iran. Chem. Soc.* **2018,** *15*, 2851-2860.
110. Wei, J.; Li, Y.; Jiang, X., Aqueous Compatible Protocol to Both Alkyl and Aryl Thioamide Synthesis. *Org. Lett.* **2016,** *18*, 340-343.
111. Bai, Y.; Dou, Y.; Xie, L.-H.; Rutledge, W.; Li, J.-R.; Zhou, H.-C., Zr-based metal–organic frameworks: design, synthesis, structure, and applications. *Chem. Soc. Rev.* **2016,** *45*, 2327-2367.
112. Burrows, A. D.; Frost, C. G.; Mahon, M. F.; Richardson, C., Sulfur-tagged metal–organic frameworks and their post-synthetic oxidation. *Chem. Commun.* **2009**, 4218-4220.
113. Zhu, L.; Duquette, J.; Zhang, M., An Improved Preparation of Arylboronates: Application in One-Pot Suzuki Biaryl Synthesis†. *J. Org. Chem.* **2003,** *68*, 3729-3732.